

Dissertation zur Erlangung des Doktorgrades der Fakultät für
Chemie und Pharmazie der Ludwig-Maximilians-Universität
München

Development, characterization and stability of therapeutic protein co-formulations



Dennis Krieg

aus

Gernsbach, Deutschland

2021

Erklärung

Diese Dissertation wurde im Sinne von § 7 der Promotionsordnung vom 28. November 2011 von Herrn Prof. Dr. Gerhard Winter betreut.

Eidesstattliche Versicherung

Diese Dissertation wurde eigenständig und ohne unerlaubte Hilfe erarbeitet.

München, 07.02.2021

Dennis Krieg

| | |
|-----------------------------|--------------------------|
| Dissertation eingereicht am | 08.02.2021 |
| 1. Gutachter: | Prof. Dr. Gerhard Winter |
| 2. Gutachter: | Prof. Dr. Wolfgang Frieß |
| Mündliche Prüfung am | 11.03.2021 |

To my family

Acknowledgements

This thesis would not have been possible without the outstanding support of my supervisors, team members, family and friends, and I want to express my deepest gratitude to all of you.

First, thank you Prof. Dr. Gerhard Winter for welcoming me in your team and giving me the opportunity to work on this fascinating and challenging project. Thanks for your “gut feeling” and advice in critical questions, your trust in my work and for your motivation during the rocky stages of this project. I appreciated your scientific guidance that provided freedom wherever possible and support wherever necessary, and I will never forget your little story about the hunter and the hound. Thank you also for the great working atmosphere you created and also for the opportunity to share our results with scientists at conferences worldwide.

Second, thank you Dr. Hristo Svilenov for being such an excellent co-supervisor of this thesis, for your support and advice to shape the project, the valuable discussions on the challenges we faced throughout this project, and the review of this work. Thank you for everything, my friend!

Further, thank you Prof. Dr. Wolfgang Frieß not only for being the co-referee of this thesis, but also for the scientific discussions and your great sense of humour. I also enjoyed our collaboration to organize the seminars and the practical course in biopharmaceutics.

I also want to thank Prof. Dr. Franz Bracher, Prof. Dr. Martin Biel, Prof. Dr. Ernst Wagner and PD Dr. Simone Braig for joining the examination board.

Thanks to all members of AK Winter, Frieß & Merkel and associates for the countless scientific and social activities inside and outside the LMU, such as the legendary trips to Granada and Breckenridge, summer festivals, barbecues, Oktoberfeste, Starkbierfeste, concerts, wine-, beer-, gin- and whisky-tastings, carneval events, motorbike-, paintball-, hiking-, canyoning- and ski-trips (Yes, I admit that I even enjoyed the freezing cold mountains with you people. Still, we should have gone to the beach!). Thank you Friederike Adams, Regine Bahr, Domizia Baldassi, Carolin Berner, Oliver Blümel, Michaela Breitsamer, Natalie Deiringer, Martin Domnowski, Simon Eisele, Inas El Bialy, Katharina Geh, Lorenzo Gentiluomo, Julian Gitter, Nina Grilc, Sebastian Groël, Christian Haase, Natascha Hartl, Bernard Haryadi, Nicole Hårdter, Alice Hirschmann, Lorenz Isert, Yao Jin, Rima Kandil, Tobias Keil, Sabine Kohler, Katharina Kopp, Teresa Kraus, Imke Leitner, Weiwei Liu, Christoph Marschall, Aditi Mehta, Robina Meyer, Fabian Moll, Alexandra Mösslang, Susanne Petzel, Ruth Rieser, Ute Rockinger, Leticia Rodrigues Neibecker, Bettina Schwarz,

Yvonne Seifert, Gerhard Simon, Andreas Stelzl, Hristo Svilenov, Andreas Tosstorff, Eduard Trenkenschuh, Ben Werner, Markus Zang and Christoph Zimmermann – Thank you all for making these years unforgettable, for the sometimes more, sometimes less scientific discussions, your support in teaching, administrative tasks and practical work, and also for the after-work beers in both good and bad times!

Finally, I want to thank my family and friends. Infinite thanks to my parents Ernst and Sabine, my sister Tatjana with Niko and Noah, my sister Jennifer with Marcel, and my aunt Natalie for their unlimited support and for giving me a home that I am always happy to visit! I am also very grateful that I could always count on my friends that have crossed my way from Gaggenau to Freiburg, Munich and Berlin. Thank you so much for your unconditional support in tough times (such as the spontaneous setup of the amazing all-inclusive thesis defense hotel) and for the truckloads of good times we shared together in the course of this thesis! We may see each other not often nowadays, but I am proud and thankful that we still manage to keep our friendships alive – some of them already for decades, and hopefully all of them for life!

*Everyone talks about rock these days;
the problem is they forget about the roll
- Keith Richards*

Table of Content

| | | |
|-------------------|---|----|
| Chapter I | Challenges for the pharmaceutical development of protein co-formulations | 1 |
| I.1 | Introduction | 1 |
| I.2 | Clinical and regulatory challenges | 2 |
| I.3 | Analytical challenges | 6 |
| I.3.1 | General considerations for the analysis of protein co-formulations | 6 |
| I.3.2 | Structural analysis and conformational stability of proteins in co-formulations | 8 |
| I.3.3 | Analysis of chemical stability in protein co-formulations | 11 |
| I.3.4 | Analysis of protein interactions and colloidal stability in protein co-formulations | 13 |
| I.3.5 | Analysis of protein aggregates in co-formulations | 22 |
| I.3.6 | Functional analysis of proteins in co-formulations | 24 |
| I.4 | Formulation challenges | 25 |
| I.5 | Aim of the thesis | 30 |
| I.6 | References | 31 |
| Chapter II | Rational development of a stable co-formulation for EPO and G-CSF | 44 |
| II.1 | Introduction | 44 |
| II.2 | Materials and Methods | 46 |
| II.2.1 | Materials | 46 |
| II.2.2 | Preparation of co-formulations | 46 |
| II.2.3 | Lyophilization | 46 |
| II.2.4 | High-throughput fluorimetric analysis of thermal protein unfolding with nanoDSF | 47 |
| II.2.5 | Circular dichroism (CD) | 48 |
| II.2.6 | Flow Imaging Microscopy | 48 |
| II.2.7 | High-Performance Size Exclusion Chromatography (HP-SEC) | 48 |
| II.2.8 | Reversed-Phase High-Performance Liquid Chromatography (RP-HPLC) | 49 |
| II.2.9 | Differential Scanning Calorimetry (DSC) | 49 |
| II.2.10 | Gas adsorption (BET) | 49 |
| II.2.11 | Karl Fischer Titration | 50 |
| II.2.12 | X-ray Powder Diffraction (XRD) | 50 |
| II.3 | Results and Discussion | 50 |
| II.3.1 | Screen for optimal pH | 50 |
| II.3.2 | Liquid co-formulations pH 7.5 | 52 |
| II.3.3 | Lyophilized co-formulations pH 7.5 | 55 |
| II.3.4 | Lyophilized co-formulations pH 4.0 | 57 |
| II.3.5 | Lyophilized co-formulations pH 4.0 with optimized reconstitution medium | 57 |
| II.3.6 | Final co-formulation of EPO and G-CSF | 58 |
| II.4 | Conclusion | 65 |

| | |
|---|-----------|
| II.5 References | 65 |
| II.6 Supplementary data | 69 |
| Chapter III Studies on pH- and salt-dependent protein aggregation of EPO and G-CSF in binary mixtures | 70 |
| III.1 Introduction | 70 |
| III.2 Materials and Methods | 71 |
| III.2.1 Materials | 71 |
| III.2.2 Preparation of protein formulations | 71 |
| III.2.3 Analysis of thermal protein aggregation with nanoDSF backscattering | 72 |
| III.2.4 Dynamic light scattering | 72 |
| III.2.5 Zeta potential measurements | 73 |
| III.2.6 High-Performance Size Exclusion Chromatography (HP-SEC) | 73 |
| III.3 Results & Discussion | 73 |
| III.3.1 Comparative analysis of protein aggregation of G-CSF in single and co-formulations by nanoDSF backscattering | 73 |
| III.3.2 Comparative analysis of protein aggregation of EPO and G-CSF in single and co-formulations by DLS | 80 |
| III.3.3 Comparative analysis of protein interactions of EPO and G-CSF in single and co-formulations by the apparent diffusion interaction parameter (Apparent k_D) | 83 |
| III.3.4 Forced degradation studies by HP-SEC | 85 |
| III.4 Conclusion | 88 |
| III.5 References | 90 |
| Chapter IV Biophysical characterization of binary therapeutic monoclonal antibody mixtures | 92 |
| IV.1 Introduction | 92 |
| IV.2 Materials and Methods | 93 |
| IV.2.1 Materials | 93 |
| IV.2.2 <i>In silico</i> comparison of mAb properties and selection of model proteins | 93 |
| IV.2.3 Preparation of mAb formulations | 95 |
| IV.2.4 High-throughput fluorimetric analysis of thermal protein unfolding with nanoDSF | 96 |
| IV.2.5 Dynamic light scattering | 96 |
| IV.3 Results | 97 |
| IV.3.1 Results Overview | 97 |
| IV.3.2 <i>In silico</i> comparison of the model mAbs | 97 |
| IV.3.3 Aggregation during heating determined with DLS | 103 |
| IV.3.4 Thermal unfolding with nanoDSF | 104 |
| IV.3.5 Aggregation during heating determined with nanoDSF backscattering | 106 |
| IV.3.6 Analysis of the diffusion interaction parameter (k_D) | 109 |
| IV.3.7 Results for high protein concentrations | 110 |
| IV.4 Discussion | 115 |
| IV.5 Conclusion | 118 |

| | | |
|-------------------|--|------------|
| IV.6 | References..... | 118 |
| IV.7 | Supplementary data..... | 121 |
| IV.7.1 | Primary sequences used in this work..... | 122 |
| IV.7.2 | Sequence identity in % from BLAST alignment..... | 128 |
| IV.7.3 | Surface charge and hydrophobicity of Fab regions | 129 |
| IV.7.4 | DLS data for the Aggregation Onset Temperature (T_{on}) | 130 |
| IV.7.5 | Thermal unfolding traces for inflection points of thermal unfolding transitions (IP1 and IP2)..... | 132 |
| IV.7.6 | nanoDSF backscattering data for Aggregation Onset Temperature (T_{agg}) | 134 |
| IV.7.7 | DLS data for diffusion interaction parameter (k_D)..... | 136 |
| IV.7.8 | Results for high protein concentrations | 138 |
| IV.7.9 | Analysis of stressed mAb solutions..... | 142 |
| Chapter V | Further studies on binary mAb mixtures of trastuzumab and rituxumab | 143 |
| V.1 | Introduction..... | 143 |
| V.2 | Materials and Methods..... | 143 |
| V.2.1 | Materials | 143 |
| V.2.2 | Preparation of protein formulations and binary mixtures | 144 |
| V.2.3 | DLS and nanoDSF backscattering..... | 144 |
| V.2.4 | High performance size exclusion chromatography (HP-SEC) | 144 |
| V.2.5 | Weak cation exchange high performance chromatography (WCX-HPLC) | 144 |
| V.2.6 | Viscosity measurements | 145 |
| V.3 | Results and Discussion..... | 145 |
| V.3.1 | DLS and nanoDSF..... | 145 |
| V.3.2 | Forced degradation studies by HP-SEC and WCX-HPLC | 148 |
| V.3.3 | Viscosity measurements | 151 |
| V.4 | Conclusion | 152 |
| V.5 | References..... | 153 |
| Chapter VI | Short-time and in-use stability of binary mixtures of DNase and r-tPa..... | 154 |
| VI.1 | Introduction..... | 154 |
| VI.2 | Material and Methods | 156 |
| VI.2.1 | Materials..... | 156 |
| VI.2.2 | Preparation of protein formulations..... | 156 |
| VI.2.3 | DNase activity assay..... | 156 |
| VI.2.4 | r-tPa activity assay..... | 157 |
| VI.2.5 | Near-UV CD spectroscopy..... | 157 |
| VI.2.6 | Reversed-Phase High-Performance Liquid Chromatography (RP-HPLC) | 158 |
| VI.2.7 | High-Performance Size Exclusion Chromatography (HP-SEC) | 158 |
| VI.2.8 | Flow Imaging Microscopy | 158 |
| VI.3 | Results & Discussion..... | 159 |
| VI.3.1 | DNase activity assay..... | 159 |
| VI.3.2 | r-tPa activity assay..... | 160 |

| | |
|--|------------|
| VI.3.3 Near-UV CD spectroscopy | 162 |
| VI.3.4 Reversed-Phase High-Performance Liquid Chromatography (RP-HPLC) | 163 |
| VI.3.5 High-Performance Size Exclusion Chromatography (HP-SEC) | 164 |
| VI.3.6 Flow Imaging Microscopy | 167 |
| VI.4 Conclusion | 169 |
| VI.5 References..... | 169 |
| Chapter VII Summary of the thesis | 172 |
| Appendix..... | 176 |

Chapter I Challenges for the pharmaceutical development of protein co-formulations

I.1 Introduction

Protein therapeutics have steadily gained importance for the targeted pharmacotherapy of severe diseases in the last decades. Until 2019, 79 therapeutic monoclonal antibodies (mAbs), which represent one of the most dominant subclasses of protein drugs, have been approved by the U.S. Food and Drug Administration (FDA).¹ One reason for the advent of protein drugs is their high specificity against a single therapeutic target,² that enables high therapeutic efficacy and safety. The specific targeting of a single antigen has proven to be a successful therapeutic concept and the combination of multiple antibodies in one drug product to target multiple antigens by one medication has gained increasing interest in the last years.

For small molecule drugs, fixed-dose combinations of drugs have been long established and offer at least five possible strategies to improve pharmacotherapy: First, the clinical efficacy can be improved by synergistic pharmacodynamic interactions, for example the fixed-dose combinations of fluticasone and salmeterol for the treatment of asthma. Second, pharmacokinetic interactions can be triggered to improve clinical efficacy, for example in the treatment of human immunodeficiency virus (HIV) infections, where anti-retroviral drugs such as lopinavir and ritonavir are combined. Third, side effects of single drugs can be reduced, for example by combination of ethinylestradiol and levonorgestrel in oral contraceptive pills. Fourth, chemotherapeutic resistances in antibiotic treatments can be overcome as in fixed-dose combinations of sulbactam and ampicillin. Finally, it is even possible to improve the drug delivery to the target, which is clinically applied in the treatment of Parkinson's disease. Fixed-dose combinations of levodopa and benserazid are used to reduce the peripheral decarboxylation of levodopa in order to provide the specific transport of levodopa across the blood-brain-barrier. Overall, fixed-dose combinations of small molecule drugs are frequently applied in the treatment of a wide range of severe diseases such as HIV infections, hypertension, diabetes or cancer.

Despite the high number of available fixed-dose co-formulations containing small molecule drugs, and despite the clinical use of binary mixtures of fast-releasing insulins and sustained-releasing neutral protamine hagedorn (NPH) insulins,³⁻⁵ only a small number of fixed-dose combinations of different protein drugs has gained access to the market: In 2015, the FDA approved Ryzodeg[®], the first co-formulation of two different protein drugs (Insulin degludec + insulin aspart). With Xultophy[®] (insulin degludec + liraglutide) and Soliqua[®]

(insulin glargine + lixisenatide), two additional protein co-formulations were approved by the FDA in 2016. Finally, in 2020 the first mAb co-formulations Phesgo[®] (trastuzumab + pertuzumab) and Inmazeb[®] (atoltivimab + maftivimab + odesivimab) were approved by the FDA – 13 years after antibody cocktails were described as the next-generation biopharmaceuticals due to their potential to recruit pharmacological effects in combination.⁶ This is already indicative for the clinical, regulatory, analytical and technological challenges that can arise during the development of protein co-formulations, which have been previously reviewed,^{7,8} and which will be presented in this chapter. First, the medical benefits of protein co-formulations will be discussed together with the respective clinical and regulatory challenges. Second, the analytical and technological challenges to produce fixed-dose-combinations of protein therapeutics will be presented. Finally, the objectives of this thesis will be derived from the analytical and technological challenges of protein co-formulations.

I.2 Clinical and regulatory challenges

Like fixed-dose combinations of small molecule drugs, protein co-formulations can offer multiple possibilities to improve pharmacotherapy in different indications, such as the synergistic activation of multiple pharmacologic pathways in oncology. A wide range of therapeutic mAbs is available in clinical oncology, and several clinical studies evaluated the synergistic clinical effects of combined administrations of mAbs based on the targeting of multiple signal transduction pathways to impede the activation of alternative growth signal pathways.^{9,10} Some of these mAb combinations improved the clinical therapy significantly, such as pertuzumab plus trastuzumab against HER2-positive metastatic breast cancer,¹¹ nivolumab plus ipilimumab as first-line therapy against advanced renal cell carcinoma,¹² and atezolizumab plus bevacizumab against hepatocellular carcinoma.¹³

Synergistic pharmacological effects of protein combinations have not only been demonstrated in oncology, but also in clinical trials for the treatment of infections. For example, a phase 1 study has been conducted to assess the safety profile of a co-formulated cocktail of three human mAbs, where each mAb targets a different epitope of the viral glycoprotein of the Ebola virus.¹⁴ In addition, the use of antibody cocktails has been studied to achieve a synergistic drug effect for the treatment of COVID-19 through the targeting of different viral epitopes and avoidance of the mutational escape of SARS-CoV2.^{15,16} The FDA even issued an emergency authorization in 2020 for a combined administration of casirivimab and imdevimab for the treatment of mild to moderate COVID-19.¹⁷

Moreover, the use of protein combinations in pharmacotherapy is not only limited to mAb combinations. First, combinations of mAbs and cytokines improved the clinical outcome in the targeted indications, such as bevacizumab plus interferon alpha-2a against metastatic renal cell carcinoma,^{18,19} or natalizumab plus interferon beta-1a against multiple sclerosis.²⁰ Second, combinations of cytokines were successfully used to improve pharmacotherapy, such as interferon alpha-2b and interferon gamma against different types of cancer like non-melanoma skin cancer or glioblastoma,²¹⁻²³ or erythropoietin (EPO) plus granulocyte-colony stimulating factor (G-CSF) against the myelodysplastic syndrome.²⁴ Also combinations of enzymes such as dornase alfa and recombinant tissue plasminogen activator (r-tPa) showed a synergistic effect on the treatment of pleural infections, whereas the single components did not improve the clinical outcome.²⁵ Finally, combinations of hormone derivatives such as insulin degludec and liraglutide improved efficacy, safety and tolerability of the therapy compared to the application of the single components.²⁶

Despite the high number of reports on the successful application of combination therapies in pharmacotherapy, only a small number of co-formulations of protein drugs were approved until 2020 (See I.1). In addition to the synergistic pharmacologic effects, protein co-formulations could also facilitate pharmacotherapy in both the clinical and ambulant environment by a reduced number of intravenous infusions or (subcutaneous) injections for the administration of both drugs. This would reduce the workload for healthcare professionals in the clinics and improve patient compliance in ambulant pharmacotherapy. The discrepancy between the steadily increasing interest for drug combinations in pharmacotherapy and the low number of available protein co-formulations can partially be explained with the clinical and regulatory requirements.

First, some protein combinations failed to improve the clinical outcome despite an anticipated synergistic pharmacological effect, such as bevacizumab plus cetuximab against metastatic colorectal cancer,²⁷ or aflibercept plus ranibizumab against neovascular age-related macular degeneration.²⁸ Anticipated synergistic pharmacological effects that have been reported in pre-clinical studies are not necessarily confirmed in clinical studies on the efficacy and safety of the fixed-dose combination, for example due to exceeding side effects compared to the monotherapy. This potential risk for the clinical failure of the drug combination has to be balanced against the potential benefit of the fixed-dose combination. A critical evaluation on the anticipated efficacy and safety of the combination is required before the co-formulation development is initiated to avoid expensive project failures in drug product development.

Second, compatible pharmacokinetic profiles of the individual drugs are required for a fixed-dose combination. Different dosing intervals may exclude each other and impede a co-formulation of both drugs. For example, a co-formulation of bevacizumab plus interferon α -2a against metastatic renal cell carcinoma is not feasible because bevacizumab is administered every two weeks, while interferon α -2a is administered three times per week.¹⁸ Furthermore, fixed-dose combinations of biologics are not a rationale development option if the drugs have to be titrated individually to achieve the desired clinical effect. A fixed-dose combination has to offer a reasonable dosing ratio which is applicable to a high number of patients without decreasing the clinical efficacy and safety compared to a flexible co-administration of the single drug products. This can require additional pharmacokinetic studies and also inherits the risk that the fixed-dose combination is only beneficial for a small number of patients at the given drug-ratio. The identification of a dosing ratio that fits to a large patient population can become challenging based on the differences in the pharmacokinetic profile of the individual drugs. Although it has been stated that the fixed-dosing could be a viable option in oncology due to the wide therapeutic windows and flat dose-response curves of the used mAbs,²⁹ many biologicals still require a flexible dosing scheme based on body weight or body volume. Further, the co-formulated drugs have to maintain their individual pharmacokinetic profile in the mixture to obtain the desired clinical effect. For example, the mixing of two different insulin analogues in the same syringe in order to reduce the number of injections altered the pharmacokinetic parameters of the individual components.^{30,31} In some cases, changes in the pharmacokinetic profiles can be prevented by a rationale co-formulation, such as the combination of insulin degludec and insulin aspart. The individual pharmacokinetic profiles were preserved by high concentrations of zinc to avoid the formation of mixed hexamers of the individual drugs.^{32,33} In other cases, small changes of pharmacokinetic parameters, such as the reduced maximal plasma concentration of liraglutide in combination with insulin degludec,³⁴ do not necessarily compromise the clinical effect and can be accepted for the targeted indication. In any case, the pharmacokinetic profile of the co-formulated drugs has to be compared to the individual components and critically evaluated.

Third, pharmacoeconomic reasons can impede the development of protein co-formulations. While multiple rationale fixed-dose combinations of small molecule drugs have been established for decades, the clinical value of some combinations has been critically assessed with regard to the additional costs compared to the single drug products.^{35,36} Therefore, co-formulations of expensive biological drugs have to present a clear clinical benefit to justify both the development costs for the company and the targeted market price for the clinics.

Even if co-administrations of biologicals such as atezolizumab and bevacizumab improve the clinical outcome,³⁷ the additional clinical benefit has to be evaluated against the medication costs compared to alternative reference medications.³⁸ Still, a co-formulation of two active biologic drugs can reduce the costs for the clinical treatment compared to the concurrent administration of the single drug products and also reduce the costs for logistics and distribution of the medication.³⁹ For example, the FDA approved a co-formulation of pertuzumab and trastuzumab based on the non-inferior safety and efficacy of the subcutaneously administered fixed-dose combination compared to the separate intravenous administration of pertuzumab and trastuzumab.⁴⁰ The ambulant subcutaneous administration presents a clear benefit for patients and healthcare professionals that cannot be provided by the individual drug products. Moreover, the emerging market of biosimilars will certainly decrease the purchasing costs for biological drugs in the future,⁴¹ and the ongoing discussion on the similarity between originator drugs and biosimilars impedes the change from the originator drugs to biosimilars in ongoing clinical treatments.⁴² Therefore, the clinical trend towards the administration of drug combinations becomes interesting for the lifecycle management (LCM) of approved biological drugs. Clinical data on the efficacy and safety on the use of the respective drugs in combination therapy provide strong arguments to initiate a therapy with these drugs compared to competitor products which cannot provide such data. Subsequently, the development of a protein co-formulation for an originator drug with a second drug can become a viable strategy to provide such combination therapies and secure market shares that were established with the originator drug. Although the pharmaceutical development of such protein co-formulations can become challenging (See I.3 and I.4), the analytical and technological knowledge on the originator drug(s) can accelerate the development and approval of the protein co-formulation compared to competitor companies. The available pre-clinical and clinical data on the stability, efficacy and safety of the originator drug(s) can set the basis for further tailor-made studies to approve the co-formulation.

Finally, there is no singular regulatory strategy for the successful approval due to the variety of subtypes of fixed-dose combinations: A binary fixed-dose combination can consist of (a) two already approved drugs, (b) one already approved drug and one new chemical entity, (c) two new entities.⁷ As pointed out by Kwon *et al.* the regulatory requirements for approval of fixed-dose combinations are flexible and can include data about the justification for the drug combination, benefit-to-risk ratios, individual contribution of the single drugs to a combined effect and clinical experience with the drug combination.⁴³ Several guidelines on

the development of fixed-dose combinations were published by the World Health Organization (WHO) and the regulatory authorities.^{39,44,45} These guidelines describe the regulatory requirements for a fixed-dose combination such as the scientific discussion on its advantages, the identification of a patient population in need for this combination and the required non-clinical characterization of the combination compared to the single drugs. Short-term clinical studies to prove the significant therapeutic benefit of the combination compared to the single drugs can also be required. The type and quantity of data which is required to convince the regulatory authorities depends on the given drug combination, and it is important to closely shape and communicate the targeted approval strategy with the regulators. While some combinations of previously approved small molecule drugs such as *Contrave*[®] (naltrexon-HCl and bupropion-HCl) required additional clinical phase 3 trials,⁴⁶ other drug products such as *Juvisync*[®] (sitagliptin and simvastatin) were approved based on the analysis of the clinical data of the single drug products.⁴³ Overall, the available pre-clinical and clinical data on the individual protein drug products determines the need for additionally required studies to prove the preservation of the individual quality, efficacy and safety of the individual (protein) drugs in the co-formulation.

I.3 Analytical challenges

I.3.1 General considerations for the analysis of protein co-formulations

The European Pharmacopoeia (Ph. Eur.) demands an extensive drug product characterization already for single mAb drug products in terms of identity, content uniformity and purity testing.⁴⁷ The required analytical methods become even more complex for protein co-formulations due to the possible interference of the protein signals in chromatographic, spectroscopic and activity assays based on the individual protein properties. General considerations on the analytical challenges in the development of protein co-formulations are presented in the following:

First, the physicochemical properties of the proteins can be very similar and complicate the individual qualitative and quantitative analysis, especially if both drugs are humanized mAbs, where differences in the amino acid composition are mostly limited to the complementary-determining regions (CDRs). For example, chromatographic methods are frequently applied for the purification and analytical characterization of therapeutic proteins, based on different affinities of the individual compounds in a given mixture to the stationary phase. The affinities of two co-formulated protein drugs can become very similar based on the little differences in physical, chemical and conformational properties due to highly similar

amino acid compositions. A recently published study evaluated multiple analytical methods such as high performance size exclusion chromatography (HP-SEC), reversed phase high performance liquid chromatography (RP-HPLC), imaged capillary isoelectric focusing (iCIEF), weak cation exchange chromatography (WCX) and hydrophobic interaction chromatography (HIC) for their ability to achieve a baseline separation for a mixture of three mAbs.⁴⁸ Feasible separations were achieved only with WCX and HIC. However, Sharma *et al.* were able to develop several stability-indicating methods (HP-SEC, RP-HPLC and WCX) with feasible separation, linearity, precision and accuracy for both mAbs in a given co-formulation.⁴⁹ The optimal chromatographic conditions for the separation of a given protein mixture depend on the individual physical and chemical properties. The development of stability-indicating chromatographic methods that provide sufficient selectivity and sensitivity for both proteins and the respective degradation products is required for the pharmaceutical development of protein co-formulations. Acceptance limits for impurities have to be defined for drug product release according to the guidelines ICH Q6B and ICH Q5C, and co-elution of protein impurities such as aggregates can easily exceed reporting thresholds. Thus, it is crucial to define critical quality attributes for the stability of the co-formulation that are based on an intensive *in vitro* protein characterization of the individual proteins. The gained knowledge on stability-limiting properties of the single proteins accelerates the development of feasible analytical methods that can assess the stability of both proteins in the co-formulation.

However, not only mixtures of proteins with similar physical and chemical properties can become challenging for the development of chromatographic methods. Also proteins with very different physical and chemical properties can cause challenges for the analytical characterization, such as co-formulations of different cytokines. If the two proteins excessively differ in terms of solubility, size or hydrophobicity, it can become challenging to separate these proteins with a single chromatographic method that is (among other factors) defined by a mobile phase with a given pH and salt concentration and a limited working range of the applied column. The analysis of the hydrophilic cytokine EPO and hydrophobic cytokine G-CSF by a single RP-HPLC method will be presented in Chapter II of this thesis.⁵⁰

Further, excessively different protein concentrations can become problematic, for example if a high concentrated mAb is co-formulated with a low concentrated cytokine. The detector settings have to be properly adjusted to work above the detection limit of the low concentration drug without exceeding the detector limit by the strong signal of the higher concentrated drug. Excessively different mixing ratios can also cause difficulties to detect

both proteins in the protein mixture in several analytical assays because the analytical signal of the low concentrated protein in a 1:10 mixture can become negligible due to the excessive signal of the second protein.⁵¹

Moreover, even if an analytical method can be optimized to selectively study each protein in the mixture, it is important to compare the analytical results of the co-formulation to the respective single protein formulations. Changes in analytical parameters such as the chromatographic retention time or peak area for a given drug alone and in mixture can already indicate protein cross-interactions, that could potentially limit the stability of the co-formulation (See I.4). In this respect, it is important to control the protein concentrations in the single and co-formulations to avoid the generation of analytical artefacts due to differences in the respective protein concentrations.

Several analytical challenges will be described in the following for a selection of methods that can be applied to study the protein stability in co-formulations. The development of a stable protein co-formulation requires analytical tools to characterize the conformational, colloidal, and chemical stability as well as the functionality of all proteins in the given co-formulation. Based on their clinical relevance and domination on the biopharmaceutical drug product landscape, the co-formulation research has a strong focus on combinations of mAbs, and many available reports on analytical characterization of protein co-formulations are focused on mAb mixtures.

I.3.2 Structural analysis and conformational stability of proteins in co-formulations

The conformational stability of the native folded state of a protein is defined by a balance between the stabilizing electrostatic attraction, hydrophobic interactions, van der Waals forces and hydrogen bonds on the one hand, and the destabilizing unfavorable entropy and electrostatic repulsion on the other hand.⁵² The conformational stability depends on formulation parameters like pH and ionic strength. Osmolytes such as sugars or amino acids can modulate the entropic stability of the folded protein state by increasing the difference between the free energies of the folded state and the unfolded state.^{53,54} The conformational stability can be directly linked to the colloidal stability because the partially unfolded intermediates are more aggregation-prone,^{55,56} and the Lumry-Eyring-models were developed to describe non-native protein aggregation based on reversible conformational changes.⁵⁷⁻⁵⁹

The conformational stability of a protein in a defined formulation can be studied by thermal or chemical denaturation to induce protein unfolding at a certain temperature or concentration of denaturant and monitor changes in the protein conformation. For example, calorimetric methods such as differential scanning calorimetry (DSC) and spectroscopic

methods such as fluorescence spectroscopy and circular dichroism (CD) are well established tools to characterize the structure and conformational stability of a protein.⁶⁰⁻⁶² However, the analysis of the conformational stabilities of multiple proteins in a mixture can become challenging due to the broad signals of the individual unfolding transitions. Moreover, single-domain proteins may show only one sharp single unfolding transition, while multi-domain proteins could show multiple unfolding events that might easily overlap and complicate the qualitative and quantitative analysis of the unfolding events depending on the mixing ratio of the proteins. For example, a high-intensity unfolding transition of a first protein can overlap with a low-intensity unfolding transition of the second protein, which impedes the conformational analysis of the second protein in the mixture. Nevertheless, several studies are available that applied these methods to study the conformational stability of proteins in mixtures, in general by a comparison of the co-formulation signals to the calculated sum of the single protein signals.

First, DSC has been established as one of the most important methods to study conformational stability of proteins.⁶³ The sample is heated against a reference and the difference in heat capacity is plotted against the steadily increasing temperature. Endothermic events in the sample such as unfolding will increase the difference in heat capacity compared to the reference and cause a peak signal, which can be used to derive thermodynamic parameters such as the unfolding enthalpy.⁶⁴ DSC has already been applied to study the unfolding and aggregation of proteins in mixtures based on these endothermic unfolding events and subsequent exothermic aggregation events in protein mixtures compared to the respective single protein solutions.^{65,66} It has been stated that the detected unfolding enthalpy of the protein mixture equals the sum of the unfolding enthalpies of the individual proteins.⁶⁶ Therefore, the comparison of the DSC spectrum of the protein mixture with the sum of the single protein DSC spectra revealed either stabilizing or destabilizing protein interactions for different protein mixtures.⁶⁵ A similar approach was also applied to a co-formulation of nine mAbs, where the DSC spectrum of the mixture was compared to the sum of the DSC spectra of the single mAbs. The absence of significant changes in the co-formulation spectrum indicated independent unfolding of the mAbs in the mixture.⁶⁷

Second, both the intrinsic and extrinsic fluorescence can be applied to study changes in the protein conformation. The intrinsic fluorescence spectra of proteins are composed from the fluorescence signals of tryptophan, tyrosine and phenylalanine residues. The fluorescence of tryptophan depends on the polarity of its local environment, which is very useful to collect information about structural changes of the proteins such as unfolding. However, structural

changes in regions where no tryptophan residues are located can be missed by intrinsic fluorescence spectroscopy. Although the wavelength of maximum tryptophan fluorescence and the respective quantum yield are highly sensitive to structural changes,⁶⁸ it appears challenging to assign the changes in the total fluorescence signal to structural changes in the individual proteins in protein mixtures. The fluorescence peaks are broad and different proteins show in general only little differences in the respective peak positions or peak shapes. Further, fluorescence emission spectra are in principle additive,⁶⁹ but possible inner filter effects due to the increased protein concentration in the binary mixture can disturb the comparison of the single protein spectra to the spectrum of the mixture to detect structural changes of the individual proteins in the mixture. If only one of the proteins in the mixture contains tryptophan residues, it is possible to selectively measure the fluorescence signal of the respective protein and investigate the effect of the second protein on this signal, but this is rather the exception than the rule.

The extrinsic fluorescence, which is based on covalently or non-covalently attached dyes, is an alternative approach to study changes in the conformation. For example, the non-covalent adsorption of chemical reporter dyes such as 8-anilinonaphthalene-1-sulfonic acid (ANS) or SYPRO Orange to hydrophobic patches on protein-surfaces can monitor the unfolding of proteins.^{70,71} The unfolding shifts hydrophobic amino acids from the core of the native protein to the surface, which increases the number of binding spots for the chemical dye and subsequently the respective fluorescence intensity and lifetime. The described chemical reporter dyes can be selectively excited and cause a specific fluorescence signal that depends on the accessible hydrophobic surfaces in the solution. Thus, these reporter dyes can be applied to study changes in accessible hydrophobic surfaces in the mixture. However, the reporter dye signals are usually not protein-specific and a comparative analysis of the single protein formulations should be performed to assign the position and intensity of a given unfolding transition to the respective protein in the mixture.

Circular dichroism (CD) describes the differences in the absorption of left- and right-circularly polarized light by chiral molecules. The respective absorption of light by intrinsic asymmetric peptide-bonds and amino acid residues is modified by the local chemical environment. Thus, CD spectroscopy detects changes in the proteins secondary structure by Far-UV CD at wavelengths of 180 to 240 nm and changes in the proteins tertiary structure by Near-UV CD at wavelengths of 260 – 320 nm.⁷² Both Far- and Near-UV CD can be applied to study the conformational stability of the individual proteins in protein mixtures. In Chapter II, CD spectroscopy will be applied to study the conformational stability of the protein

mixture in different formulation conditions compared to the single protein formulations,⁵⁰ and the Near-UV CD spectrum of the co-formulation will be predicted based on the single protein spectra. Therefore, CD spectroscopy can detect changes in the protein conformation in protein mixtures and even assign these changes to the respective protein, if the Near-UV CD spectra of the individual proteins differ sufficiently from each other.

Finally, nuclear magnetic resonance (NMR) spectroscopy has been successfully applied to study the protein structure in solution,^{73,74} and the high resolution of multidimensional approaches like 2D-NMR provide information on the high order structure of proteins, their structural flexibility and dynamics.⁷⁵⁻⁷⁸ Recently published studies successfully applied NMR spectroscopy to study the individual protein conformations in protein co-formulations by ¹⁹F NMR.^{79,80} The covalent labeling of the selected protein allowed the specific structural characterization of this protein in a protein mixture without interference of the non-labeled proteins. Moreover, the application of different ¹⁹F-labels on two mAbs allowed the investigation of protein interaction and aggregation for both mAbs in the mixture.⁸¹ However, the technical requirements and the elaborative data interpretation impedes the application of NMR spectroscopy to screen the conformational stability of protein mixtures in a wide range of promising formulation conditions.

I.3.3 Analysis of chemical stability in protein co-formulations

The chemical stability of protein drugs is limited by chemical changes of the composing amino acids such as oxidation, deamidation, hydrolysis, and isomerization.⁸² The chemical degradation pathways have been well described in literature and the resulting chemical changes can also impact the conformational and colloidal stability of the given protein drug.⁸²⁻⁸⁴ The selected analytical methods to assess the chemical stability in protein co-formulations have to reliably identify and quantify chemical changes of the individual proteins in the mixtures.

The most common analytical method to detect chemical changes such as oxidation of methionine residues in proteins is RP-HPLC, which separates the components of a given mixture based on the differences in hydrophobicity. The fast mass transfer in RP-HPLC systems results in sharp peaks (in contrast to HP-SEC),⁸⁵ which is beneficial to achieve a feasible selectivity in protein co-formulations. Thus, RP-HPLC is a valuable method for the quantification of individual compounds of a protein mixture such as EPO plus HSA,⁸⁶ or mixtures of mAbs.⁴⁹ For example, Perez-Robles *et al.* presented a simultaneous identification and quantification of up to four different co-formulated mAbs by RP-HPLC-MS.⁸⁷ The coupling of RP-HPLC to MS is a well-established analytical technique to detect chemical

changes in proteins and identify specific amino acids that are susceptible to oxidation. It is also possible to compare protein oxidation in single and co-formulations by RP-HPLC-MS to test for qualitative or quantitative changes in the oxidation of oxidation-prone residues like methionine.⁸⁸ Further, RP-HPLC-MS is an alternative option for the characterization of charge variants in mAb mixtures if ion exchange chromatography (IEX) is not applicable. For example, Cao *et al.* developed a peptide mapping method to identify and quantify CDR deamidation of one specific mAb in a given protein co-formulation.⁸⁹ The sensitivity was sufficient to allow the quantification of site-specific deamidation of a first low concentrated mAb in presence of a second high concentrated mAb.

Although RP-HPLC is a well-established analytical tool to separate components of a mixture based on their hydrophobicity, the combination of acidic pH values, high concentrations of organic solvents and elevated temperatures usually causes protein denaturation. In contrast, hydrophobic interaction chromatography (HIC) is able to separate proteins based on their hydrophobicity under non-denaturing conditions at neutral pH values and ambient temperature.⁹⁰ Hydrophobic interactions of the proteins to the column are triggered by high salt concentrations in the elution buffer and the applied gradient reduces the salt concentration until the proteins elute from the column. HIC methods were already successfully applied for protein co-formulations to either quantify the individual mAbs,⁴⁸ or to assess the individual stability profile of each mAb in forced degradation studies.⁸⁸

In addition, ion exchange chromatography (IEX) is also a valuable chromatographic method for the analysis of chemical degradation in protein co-formulations, especially deamidation. Proteins are separated by IEX based on differences in the respective charge-distribution on the protein surface and subsequent differences in interaction with the charged stationary phase. Several studies successfully separated mixtures of mAbs by both strong cation exchange (SCX) or weak cation exchange (WCX) chromatography.^{88,91,92} The pH gradient ion exchange chromatography allows the separation of mAb mixtures based on the different IEP values of the individual mAbs,⁹³ and the good selectivity for the separation of mAbs can be sufficient to enable charge variant characterization for the single compounds.^{88,89} However, these IEX methods rely on sufficiently different IEPs of the mAbs to achieve a feasible selectivity.

Further, capillary isoelectric focusing (cIEF) is an alternative method to IEX to separate protein mixtures based on their IEPs and has been applied to detect chemical changes in the individual proteins in co-formulations.⁸⁸ cIEF is commonly applied in proteomics research due to the very high resolution power and has been reported to baseline separate components

with a difference in their respective IEP of only 0.01.⁹⁴ Although it has been technically challenging to connect cIEF to MS based on the applied gel agents and voltages that interfere with electro-spray ionisation,⁹⁵ cIEF-MS is nowadays a powerful method for the high resolution analysis of charge variants in proteins.

I.3.4 Analysis of protein interactions and colloidal stability in protein co-formulations

Protein interactions have a significant impact on the colloidal stability of proteins in drug products. Different mechanisms have been described to explain protein aggregation,⁸² but the aggregation pathways include in general excessive attractive interactions between the native or altered protein monomers that cause protein association.^{96,97} The DLVO (Derjaguin-Landau-Verwey-Overbeek) theory is often applied to describe the balance between attractive interactions due to van der Waals forces and electrostatic repulsive forces due to surface charges, although the simplified hard-sphere model with symmetrically distributed surface charges does not necessarily apply to proteins.⁹⁸ Still, the analysis of non-specific attractive and repulsive protein interactions in different formulation conditions can guide the rational development of a protein formulation to achieve a high colloidal stability of the protein drug. The strength of these interactions can range from strong long-range electrostatic interactions mediated by opposite surface charges to weak short-range hydrophobic and electrostatic dipole interactions that are mediated by van der Waals forces. While the attractive long-range interactions between native protein monomers or (partially) unfolded intermediates favor protein aggregation across a wide range of protein concentrations, the attractive short-range interactions become relevant at high protein concentrations.⁹⁹ The type and strength of the protein interactions that can arise in protein formulations can be detected by multiple analytical methods. Based on these results, formulation parameters such as pH and ionic strength can be adjusted to maximize the colloidal stability of the protein by increased repulsive protein interactions or reduced attractive protein interactions.

The presence of different protein drugs in co-formulations increases the complexity of protein interactions even further. For example, attractive cross-interactions between different protein drugs could cause the formation of heterogeneous protein aggregates that are not detected in the single drug products. It is generally challenging to predict the specificity of protein-interactions in co-formulations,¹⁰⁰ and the risk for cross-interactions has to be evaluated during drug product development. The detection of these cross-interactions can become challenging because many analytical methods to study protein interactions are optimized for strong and specific physiological or pharmacological interactions between a receptor and a ligand, where equilibrium dissociation constants (K_D) in the nano-molar range

are detected.¹⁰¹ Viable tools for the analysis of protein interactions in co-formulations have to detect the non-specific interactions that are not linked to a biological function, if possible without immobilization or labeling which may affect the protein interaction. Several reviews have been published on the analysis of protein interactions.¹⁰² A selection of interesting analytical methods for the detection of protein interactions in co-formulations is presented in the following.

First, light scattering based techniques such as static light scattering (SLS) and dynamic light scattering (DLS) have been successfully applied to quantify the attractive or repulsive protein interactions in protein formulations.¹⁰³ The osmotic second virial coefficient B_{22} is an important parameter to quantify attractive and repulsive interactions in protein formulations and can be calculated based on SLS measurements according to the Debye equation:¹⁰⁴

$$\frac{K_c}{R_\theta} = \frac{1}{M_w} + 2B_{22}c$$

K_c is the optical constant derived from the applied laser wavelength and the differential refractive index increment dn/dc , R_θ is the excess Rayleigh ratio derived from the measured differences in both light scattering intensities and refractive indices of the protein solution and the pure solvent, M_w is the weight average molecular weight and c is the protein concentration. The interaction parameter B_{22} has been originally applied to optimize conditions for protein crystallization,¹⁰⁵ but the selection of formulation parameters to achieve highly positive B_{22} values, which are indicative for repulsive protein interactions, is also a viable formulation strategy to improve the colloidal stability of protein drugs.⁵⁵ In addition to SLS, several orthogonal methods have been described to determine the interaction parameter B_{22} , such as self-interaction chromatography, membrane osmometry, or sedimentation velocity.^{106–108} Based on the studies on self-interaction chromatography, several studies also applied cross-interaction-chromatography to characterize cross-interactions between different proteins by determination of the cross-interaction coefficient B_{23} for several mixtures, such as BSA and lysozyme,^{109,110} α -chymotrypsinogen and lysozyme,¹¹⁰ binary mixtures of lysozyme, ovalbumin, and α -amylase,¹¹¹ and binary mixtures of lysozyme, catalase, lactoferrin and concanavalin.¹¹²

The affinities, stoichiometries and kinetics of protein cross-interactions in co-formulations can be further elucidated by static light scattering methods such as composition gradient multiple angle laser light scattering (CG-MALS). CG-MALS has been used to study hetero-associations between different proteins and to identify the respective complex-

stoichiometries.^{103,113} In CG-MALS, the single protein solutions are injected into a mixing chamber at opposite gradients. A wide range of different compositions can be screened in the mixing chamber for specific ratios of both proteins. Based on the measured light scattering at a given mixing ratio, the affinity and stoichiometry of the formed protein complexes can be calculated. It is even possible to simultaneously study self- and hetero-associations between different proteins by CG-MALS,¹¹³ without labeling or immobilization. However, CG-MALS is usually applied to study high affinity interactions with affinity constants in the nanomolar range.¹⁰³ Future studies have to show that appropriate interaction models can be derived from the light scattering signals to elucidate non-specific low-affinity cross-interactions in protein co-formulations.

The described methods to determine B_{22} can become quite elaborative, which limits their use to screen multiple protein formulation conditions in short time.¹⁰⁸ Further, the high amounts of protein that are necessary for column immobilization or light scattering experiments impede the application of these methods for the analysis of protein cross-interactions in early drug product development. In contrast, DLS can be applied to determine the diffusion interaction parameter k_D , which is linked to the second virial coefficient B_{22} and has been established as an interaction parameter to detect and quantify non-specific protein interactions caused by hydrophobic or electrostatic forces in protein formulations.¹⁰⁸ DLS measurements can be performed in multiwell plates in very short time and with low protein consumption to determine k_D .¹¹⁴ k_D can be derived from the DLS measurements of the translational diffusion coefficient D_t at different protein concentrations c with D_0 being the mutual diffusion coefficient at infinite dilution:^{115,116}

$$D_t = D_0(1 + k_D c)$$

The comparison of k_D values of the single protein formulations and the binary mixture of both proteins can reveal additionally arising attractive or repulsive cross-interactions in the co-formulations.^{100,117}

In addition to k_D measurements, DLS in multiwell plates can identify formulation conditions that reduce attractive protein interactions and improve the colloidal stability of the proteins based on changes of their hydrodynamic radius (R_h). A large number of different formulation conditions can be rapidly screened with minimal sample size and protein consumption to identify the most promising formulation conditions for a given protein.¹¹⁸ For example, a thermal ramp can be applied to heat the samples and perform DLS measurements in short time intervals to identify the aggregation onset temperatures (T_{on}) in the tested

formulations. Higher T_{on} values are indicative for an increased thermal and colloidal stability of the protein in the respective formulation. The value of these methods for the development of protein co-formulations and the analysis of protein cross-interactions will be discussed in the following chapters of this thesis.

Like CG-MALS, composition gradient dynamic light scattering (CG-DLS) can also be applied to study cross-interactions without labeling or immobilization of the proteins directly in solution. For example, interactions between α -chymotrypsin and bovine pancreatic trypsin inhibitor were detected by a shift in the z-average due to formation of a complex with higher hydrodynamic radius compared to the single proteins.¹¹⁹ The shift in z-average increased with the amount of complex that is formed due to the cross-interaction. The titration of one protein against the other and the correlation of the resulting z-average against the relative concentration of one protein led to a maximum value of the z-average, determining the highest degree of complexation. However, the described interactions between α -chymotrypsin and bovine pancreatic trypsin inhibitor are interactions of high specificity and affinity. It is questionable if unspecific protein cross-interactions with low affinity that can arise in co-formulations can be reliably detected by CG-DLS.

Small angle X-ray light scattering (SAXS) detects the scattering patterns of focused X-rays by proteins in solution. These scattering patterns can be interpreted as a combination of the scattering by the protein monomers and the scattering of a complex that is formed due to protein interactions. Given the scattering pattern of the single components, the formation of complexes and the respective dissociation constant K_D can be calculated.¹²⁰ The potential use of SAXS measurements for the analysis of protein interactions was also presented in a study by Ryberg *et al.*: A combination of SAXS measurements, molecular dynamics (MD) simulations and DLS measurements was successfully applied to identify the binding sites and amino acid residues that constitute the protein cross-interaction between albumin and insulin detemir.¹²¹

In addition to the presented light scattering based methods, spectroscopic and spectrometric methods such as fluorescence spectroscopy, CD spectroscopy, mass spectrometry or surface plasmon resonance (SPR) spectroscopy can also be applied to study protein cross-interactions in co-formulations.

The fluorescence spectrum of a protein can change upon interaction with another protein, if the local environment of a tryptophan residue is involved. One potential approach to screen interactions in solution without labeling is the comparison of the measured fluorescence spectrum of the protein mixture with the calculated sum of the individual protein spectra.

Protein interactions in co-formulations can be indicated by differences between the measured fluorescence spectrum of the mixture and the calculated sum of the single protein spectra. For example, one protein can be titrated with a second protein and the arising differences between the measured fluorescence signal of the binary mixtures and the calculated sum of the single protein signals can be plotted against the concentration of the titrant to determine the dissociation constant K_D .¹²² However, the fluorescence spectra become more complex with increasing numbers of tryptophan residues in the protein and the presented approach is only feasible for proteins that contain only one single tryptophan residue that is quenched by changes in the local environment due to the protein-interaction. As the fluorescence emission of a protein is a result of the combined fluorescent amino acid residues, the sensitivity of intrinsic fluorescence to detect protein interactions decreases significantly if only a small fraction of these residues is involved in the interaction. This effect becomes even more pronounced for weak protein interactions with high K_D values in the mM range, where a high amount of protein monomers is detected in comparison to the protein complex. Further, the high sensitivity of fluorescence measurements towards changes in temperature, pH and salt concentration can easily cause changes in the fluorescence spectra that could exceed changes caused by the protein interactions. Thus, it is important to carefully control the experimental conditions and protein concentrations in order to compare the spectrum of the mixture to the theoretical sum of the single protein spectra.

Although these are very restrictive requirements for the application of intrinsic fluorescence to detect protein interactions, the presented approach can also be performed with extrinsic fluorescence experiments. For example, extrinsic fluorescent dyes that are sensitive to changes in the accessible hydrophobic surface can be applied to detect protein interactions based on the dissociation of the formed protein complexes.¹²³ Moreover, it is possible to attach different fluorophores to the proteins to study protein cross-interactions by Förster resonance energy transfer (FRET). The energy transfer between a donor fluorophore and an acceptor fluorophore causes an increased fluorescence emission of the acceptor which can be detected by fluorescence lifetime imaging microscopy (FLIM).^{124,125} Although the chemical changes caused by the attachment of a fluorescent label could alter the binding affinity of the proteins,¹²⁴ FRET experiments have been successfully applied to elucidate intracellular protein interactions,¹²⁵ and could in principle be also applied for protein cross-interactions in co-formulations.

Furthermore, fluorescence anisotropy titration, which measures the partially polarized emission of a fluorophore after excitation with polarized light,¹²⁶ can be applied to titrate a

labeled protein with increasing amounts of a second protein to study protein interactions and determine the dissociation constant K_D .¹²⁷ Fluorescence anisotropy increases when the rotational speed of the fluorophore decreases. Thus, protein interactions can be detected during the titration experiment by the increased apparent molecular size of the fluorophore, which decreases the rotational speed in solution and increases fluorescence anisotropy.

Additionally, microscale thermophoresis (MST) is another fluorescence-based method to detect protein interactions and tracks the fluorescence signal of a protein during heating with an infrared laser.¹²⁸ The fluorescence signal decreases over time due to the thermophoresis of the protein out of the detection area. Protein interactions can change the drop in the fluorescence signal during thermophoresis because the increased hydrodynamic radius of the protein complex results in a reduced diffusion speed along the thermal gradient. Thus, the titration of the labeled protein with a protein ligand can be used to correlate the changes in fluorescence to the respective ligand concentration and calculate the dissociation constant K_D .¹²⁹

Alternatively, CD spectroscopy can detect protein interactions by changes in the respective secondary or tertiary structures of the proteins. Protein interactions can cause changes in the measured ellipticity that are directly proportional to the amount of complexation.¹³⁰ Therefore, it is possible to determine the dissociation constant K_D , if one protein is titrated against the other. Protein interactions have also been detected by differences of the measured CD spectrum of the protein mixture compared to the sum of the single protein spectra.¹³¹ The deconvolution of the protein signal can be performed for mixtures with a mixing ratio of 1:1,⁵⁰ but excessive ratios inherit the risk that the low concentrated protein signal becomes negligible and structural changes of this protein cannot be reliably detected. Thus, it is necessary to compare the single protein spectra to the spectrum of the mixture and evaluate the applicable range of mixing ratios.

Moreover, the changes of the solvent-accessible surface due to protein interactions can be studied by hydrogen deuterium exchange mass spectrometry (HDX-MS).^{132,133} After incubation of the co-formulation in the targeted formulation buffer to reach the equilibrium of the complex formation, the solution is diluted into a D₂O solution where solvent accessible amides become deuterated.^{133,134} The deuteration is stopped after a defined time period, and the subsequent pepsin digestion and analysis by LC-MS allows the localization of binding sites based on the reduced solvent-accessible surface area.¹³⁵ However, weak interactions that are only mediated by the side chains of the protein with no impact on the amide backbone are likely to be missed.¹³⁵ Further, the interpretation of the obtained results can become both

elaborative and challenging for mAb mixtures due to the required additional comparison of the mixture to the single protein formulations and the high degree of primary sequence similarity between different mAbs.

Another established orthogonal analytical method to study protein interactions is SPR spectroscopy. In SPR spectroscopy, one protein is immobilized on a chip surface, the second protein is rinsed across this functionalized chip and binding events are detected by changes of the refractive index of the chip surface.^{136,137} A common procedure to immobilize proteins is the use of gold microchips that are coated with carboxymethylated dextran.¹³⁷ The carboxymethyl groups are activated by addition of N-hydroxysuccinimide to form reactive succinimide esters that react with amine groups of the protein. Excessive succinimide esters are subsequently quenched with ethanolamine, which results in a hydrophilic chip surface with the immobilized protein. Alternative protein immobilization techniques include streptavidin-biotin or S-Au binding chemistry.¹³⁸ SPR spectroscopy can be applied to determine dissociation constants and kinetic parameters of the interaction. Advantages of SPR spectroscopy include the analysis in the targeted formulation buffer, low protein consumption and high throughput. However, the immobilization can mask interactions due to the anisotropic distribution of surface charge and hydrophobicity of mAbs. Still, SPR spectroscopy has already been frequently applied to screen protein interactions between different proteins and was also already applied to analyze cross-interactions in co-formulated mAbs.^{88,138}

Similar to SPR spectroscopy, biolayer interferometry (BLI) can also be applied to study protein cross-interactions, such as antigen-antibody binding in epitope mapping experiments.¹³⁹ The analytical setup is quite similar to SPR measurements and includes the immobilization of one protein on a sensor surface. The interaction with a second protein is triggered by incubation of the functionalized chip surface in a solution of the second protein.¹⁴⁰ The label-free rapid BLI measurements enable a fast screening of protein interactions in different conditions at minimal protein consumption compared to self-interaction chromatography, k_D measurements or viscosity measurements.^{141,142}

In addition to the already presented methods, the thermal analysis offers further valuable approaches to study protein interactions in co-formulations.

Isothermal titration calorimetry (ITC) can characterize protein interactions in mixtures qualitatively and quantitatively,¹⁴³ because any binding event between proteins is associated with a more or less pronounced change of enthalpy (ΔH) and change of entropy (ΔS). In order to study cross-interactions between different proteins, one protein solution is placed in the

calorimetric cell while aliquots of the second protein solution are injected at different time points. The generated heat due to the binding event is detected for each time point and the resulting titration curve is evaluated to determine the dissociation constant K_D , ΔH and the stoichiometry of the protein interaction. K_D and ΔH can then be used to calculate ΔG and ΔS using the following equation, where R is the gas constant and T is the absolute temperature.¹⁴³

$$\Delta G = \Delta H - T\Delta S = -RT \ln K_D$$

ITC is able to detect a wide range of strong and weak interactions with K_D values from the nM to the mM range.¹⁴⁴ The label-free detection of interactions directly in the formulation without immobilization is very useful for the analysis of protein mixtures and ITC has been already applied to show the absence of cross-interactions between co-formulated mAbs.⁸⁸ However, ITC measurements are also sensitive to structural changes of the proteins, and complementary techniques such as CD spectroscopy should be applied to detect structural changes that cause heat effects by changed binding of water molecules.¹⁴⁵ Moreover, the self-interaction of the single proteins can disturb the measurements of cross-interactions, for example if the concentrated titrator protein solution contains homo-protein complexes that dissociate upon dilution in the measurement cell.¹⁴³ However, these analytical artefacts can be detected by appropriate control experiments.

Furthermore, DSC has been frequently applied to study protein ligand interactions such as protein-lipid interactions based on the effect of the ligand on transition temperatures, peak shapes or derived thermodynamic parameters.^{146,147} These approaches cannot be directly used for protein co-formulations because both proteins will show thermal transitions that may overlap each other and impede a quantitative detection of the individual transitions. Nevertheless, DSC methods were also applied to study protein interactions in mixtures by comparison of the enthalpy changes of the mixture to the sum of the enthalpy changes in the respective single protein formulations,⁶⁵ as already described in I.3.2. It appears that the DSC spectrum of a binary mixture of non-interacting proteins can be predicted by the sum of the individual DSC spectra,⁶⁶ and protein interactions can conversely be detected by deviations of this mathematical correlation.⁶⁵ The DSC analysis of multiple co-formulations that contained up to nine mAbs indicated that the mAbs unfolded independently and no stability compromising cross-interactions were observed compared to the single protein formulations.⁶⁷

Next, analytical ultracentrifugation (AUC) is an orthogonal method to study protein interactions in mixtures,¹⁴⁸ and has already been applied to study protein self- and cross-

interactions of a fluorescent labeled mAb. The labeled tracer mAb-1 was combined with non-labeled mAb-1 or mAb-2 in concentrations of up to 20 mg/mL to study differences in the sedimentation velocity of mAb-1 caused by either self- or cross-interactions.¹⁴⁹ AUC was also applied to study cross-interactions between unlabeled mAbs,⁸⁸ but only at low concentrations of up to 2 mg/mL, and the positive control that consisted of mAb-1 and an anti-mAb1 antibody showed only a small shift for the highly specific antibody-antigen interaction. Thus, it is possible that unspecific cross-interactions between the co-formulated mAbs were missed in this analytical setup.

Finally, the risk for protein interactions in co-formulations also depends on the applied concentrations. If the equilibrium constant K_D for a defined protein interaction is very high, the clinically required drug concentrations in the co-formulation may not be sufficiently high to cause a cross-interaction between the protein drugs. However, many mAbs are formulated at high protein concentrations > 100 g/L.¹⁵⁰ At such high protein concentrations, short-ranged hydrophobic interactions become relevant and can even outweigh long-ranged electrostatic interactions.⁹⁹ It has been proposed that cross-interactions in protein mixtures at high concentrations can be detected by deviations of the measured viscosity of the protein mixture from the calculated viscosity that is predicted by the extended Mooney equation:^{151,152}

$$\ln \eta_{rel} = \frac{\sum[\eta_i]w_i}{1 - \sum w_i/w_i^*}$$

In this equation, η_{rel} represents the ratio of the viscosity of the solution to that of the solvent. η_{rel} is given by the intrinsic viscosity η_i of each protein i and the respective protein mass concentration w_i . w_i^* represents the respective protein concentration at which the solution does not longer flow.¹⁵³ For binary mixtures of structurally similar proteins such as mAbs, the Arrhenius mixture model can be applied as well to predict the viscosity of the mixtures based on the viscosities of the single protein solutions.^{117,151} Deviations from this mathematical relationship can indicate additionally arising cross-interactions in the binary mixture compared to the individual protein self-interactions. For example, Woldeyes *et al.* detected attractive cross-interactions in a binary mixture of different mAbs by viscosity measurements,¹¹⁷ where the measured viscosity of the binary mixture exceeded the prediction of the Arrhenius mixture model.

In summary, a wide range of different methods is available to study protein interactions in co-formulations. The selection of the appropriate analytical methods is based on the physicochemical properties of the proteins, the targeted protein concentration in the co-formulation, the expected dissociation constant K_D and the availability of the proteins of

interest both in quantity and purity. The differentiation between protein self-interactions and cross-interactions requires the analysis of control samples, where the single protein formulations have the same precise concentration as in the co-formulation. However, for binary mixtures of similar proteins such as mAbs it is challenging to differentiate between specific cross-interactions between different mAb entities and altered self-interactions of the respective mAb entities in presence of a second protein. Analytical methods such as cross-interaction chromatography can identify specific cross-interactions in an artificial environment,¹¹⁰ but not directly in the targeted formulation conditions. ITC can be applied to compare self-interactions to specific cross-interactions by titration of a given mAb with itself and can also provide information on structural changes caused by the cross-interaction, when additional CD-measurements are performed. Overall, it is important to apply multiple methods for an in-depth characterization of protein cross-interactions in co-formulations and their impact on protein stability. In some cases, specific cross-interactions can also be detected indirectly by their effect on the colloidal stability or functionality of both co-formulated proteins compared to the single formulations.

I.3.5 Analysis of protein aggregates in co-formulations

Protein aggregation is one of the risk factors that limit the stability of therapeutic proteins,¹⁵⁴ and is caused by excessive attractive interactions of the native protein monomers or (partially) unfolded intermediates. It is important to limit protein aggregation in the formulation. Aggregation can reduce both efficacy and safety of the drug product by reduced concentrations of active protein monomers and protein aggregates can cause immunogenic reactions.¹⁵⁵ Thus, appropriate analytical methods are required to quantify soluble protein aggregates and subvisible protein particles.

First, HP-SEC is frequently applied for the analysis of protein drugs to investigate soluble aggregate formation.¹⁵⁶ Although it can be possible to separate protein mixtures, the low differences in diffusion speed of proteins limit the separation efficacy.¹⁵⁷ Especially mAbs show very similar molecular weights and hydrodynamic radii and usually it is not possible to achieve a sufficient selectivity for the different mAb monomers by HP-SEC alone based on the similar diffusion speed and mass transfer, which causes broad peak signals.¹⁵⁷ Nevertheless, HP-SEC represents a valuable stability-indicating method for protein co-formulations which was applied in several stress studies for co-formulated mAbs to analyze aggregate formation or protein fragmentation.^{49,88,91} An interesting approach to study the protein aggregation in mixtures was presented by Weisbjerg *et al.*¹⁵⁸ The serial-coupling of ion exchange chromatography (IEX) to HP-SEC allowed the separation of BSA and different

mAbs based on their respective isoelectric point (IEP): The IEX column captured BSA, while the mAbs and their aggregates were not captured and moved directly to the SEC column. After elution of the mAb and the respective aggregates, increasing salt concentrations caused the elution of BSA. Although this is a very interesting analytical setup, this approach is limited by the required differences in the respective IEPs of the proteins and the respective aggregates. Co-aggregation of proteins could potentially form mixed aggregates with a different surface charge pattern compared to the single proteins or pure aggregates.

HP-SEC is a gold standard for the analysis of soluble aggregates in protein formulations, but it is not applicable to screen multiple formulation conditions in early formulation development because of the low sample throughput. Light scattering based techniques such as dynamic light scattering (DLS) are orthogonal analytical methods to assess the colloidal stability of proteins in solution directly in the respective formulations.¹⁵⁹ In DLS measurements the Stokes-Einstein-Equation is applied to calculate the hydrodynamic radius of particles based on the intensity fluctuation rate of laser light scattered by particles or macromolecules. The smaller the particles are, the faster the amount of scattered light will change because smaller molecules have a higher diffusion speed compared to larger particles. In most cases, the resolution of DLS may not be sufficient to differentiate the monomers of two different proteins and only limited quantitative information can be derived from the obtained size distributions,¹⁶⁰ but the high sensitivity towards larger particles is useful to detect even trace amounts of protein aggregates.¹⁶¹

Further, the characterization of aggregates in protein mixtures remains challenging because it is often unclear if and to which extent co-aggregation of the individual proteins can occur in a given co-formulation. Cross-interactions between the different protein monomers may cause formation of co-aggregates with different properties compared to pure aggregates of the single proteins in terms of size, shape, charge, or immunogenicity. Thus, it is important to detect protein co-aggregation by an extensive analytical characterization of the formed aggregates in the mixture. Several studies have been published on the co-aggregation of proteins, for example for mixtures of ovalbumin and lysozyme,¹⁶³ or ovotransferrin and lysozyme,¹⁶⁴ where HP-SEC was applied to identify co-aggregation in forced-degradation studies. Gadgil *et al.* presented a coupled size exclusion chromatography and mass spectrometry (SEC-MS) method for the identification of aggregates in protein mixtures,¹⁶⁵ which indicated the absence of protein co-aggregation in the given mixture of BSA, cytochrome c and β -lactoglobulin. Another approach is the collection of HP-SEC fractions and the detection of the proteins in these fractions by an enzyme-linked immunosorbent assay (ELISA).¹⁶⁶ Using this approach,

soluble aggregates that are detected by HP-SEC could be fractionated and the collected fractions could be analyzed by a protein specific and highly sensitive ELISA to prove the presence or absence of a protein in a certain aggregate fraction. Similarly, aggregates obtained from forced degradation studies on a mixture of two mAbs were collected by HP-SEC and analyzed by SPR spectroscopy.⁸⁸ In this study, an anti-mAb-1 antibody was immobilized on a sensor chip that subsequently allowed the binding of aggregates that contained mAb-1. In a second step, the chip was flushed with anti-mAb-2 to detect the additional binding of anti-mAb-2 to the already bound aggregates. Further, a recently published patent application presents an approach for the quantification of hetero-dimers in mAb co-formulations by immunoprecipitation and subsequent liquid chromatography-assisted mass spectrometry.¹⁶⁷ In some cases, the co-aggregation may cause the formation of morphologically distinct structures compared to the pure protein aggregates,¹⁶⁸ that can be detected by transmission electron microscopy. Emerging techniques for the characterization of subvisible particles such as flow imaging microscopy could also be valuable tools to identify cross-aggregation by alterations of the particle morphology in the co-formulation compared to the single protein formulations.

I.3.6 Functional analysis of proteins in co-formulations

The development of a protein drug product has to ensure that the protein activity is maintained throughout the targeted shelf-life. A feasible formulation has to stabilize the protein against different stresses that can be encountered during manufacturing and storage, which can reduce protein activity.¹⁶⁹ While several specific activity assays are established for therapeutic enzymes,^{170,171} the activity assays for mAbs and cytokines are often performed as *in vitro* binding assays to the targeted antigen based on analytical techniques such as ELISA, BLI or SPR spectroscopy. However, besides these *in vitro* binding assays, the specific pharmacological effects of these proteins can also be monitored by elaborative cell-based assays, such as complement-dependent cytotoxicity (CDC) assays and antibody-dependent cytotoxicity (ADCC) assays for mAbs, or cell proliferation assays for cytokines.^{169,172–175}

Specific activity assays are also important tools to detect synergistic pharmacological effects of the combination. Therapeutic proteins can be rationally combined in co-formulations based on their complementary binding to different epitopes of the same antigen. For example, pathogenic viruses offer various epitopes that can be targeted in parallel by co-formulated mAbs, and the complementary binding to different epitopes reduces the risk for the generation of escaping-mutants.^{15,67,176} This complementary binding of two mAbs to a specific antigen can be detected by ELISA methods, where the binding is compared between

single and co-formulations: After immobilization of the antigen of interest, the ELISA plate can be incubated in a first step with the unlabeled mAb-1 and in a second step with the biotinylated mAb-2, and the additional binding of mAb-2 to the antigen can be subsequently quantified by streptavidin-coupled horse radish peroxidase.¹⁷⁶ Further, *in silico* approaches have been applied to screen and predict the synergistic or cooperative interaction of different protein drugs with the same receptor molecule to increase the clinical efficacy. MD simulations presented by Fuentes *et al.* indicated a co-localization and cooperative binding of trastuzumab and pertuzumab to the HER2 receptor.¹⁷⁷ However, the *in silico* models must be confirmed by experimental data. While the co-localization of pertuzumab and trastuzumab and the formation of a ternary complex was confirmed by BLI, cryo-EM and HP-SEC measurements,^{178,179} no synergistic binding was detected by any of the applied experimental methods.

The high specificity of the ELISA based techniques can in principle be used to perform identity testing and quantification of a specific mAb in a co-formulation,⁴⁹ where a specific protein quantification cannot be easily performed by UV spectrometry due to the unspecific UV absorption of all protein entities in the mixture. However, comparative studies on the co-formulations and the respective single formulations are required to prove that the applied activity assays provide sufficient selectivity for the respective proteins in the mixture to avoid any interference between the proteins in co-formulations.

Moreover, it has been reported that the antigen-binding activity of a mAb can be reduced in the presence of HSA due to electrostatic cross-interactions between the mAb and HSA that were detected by BLI and CG-MALS measurements.¹⁸⁰ Thus, the impact of unspecific protein interactions in protein co-formulations on the respective protein activity has been evaluated to optimize the formulation conditions accordingly, for example by adjusting the ionic strength of the solution to screen unspecific electrostatic cross-interactions.

I.4 Formulation challenges

Combinations of different proteins such as mAbs, cytokines, hormones, or enzymes have been tested in clinical studies, but the pharmaceutical development of protein co-formulations remains still challenging because it has to consider the individual stability profiles of the respective proteins. The specific formulation requirements of the proteins can excessively differ from each other and impede the development of a stable co-formulation product. Protein drugs require specific conditions to maintain stability such as an appropriate pH value, ionic strength and excipient composition, where the drug degradation is limited as much as

possible. Instabilities such as unfolding, aggregation or oxidation can occur if the optimal formulation conditions are not met. Healthcare professionals often hesitate to perform an intravenous co-administration of drugs through a combined dilution in normal saline because of effects on drug stability that can already be caused by dilution of the stabilizing excipients,^{181,182} and elaborative studies are performed to ensure that a co-administration of protein drugs does not negatively impact the individual in-use-stability.¹⁸³ This underlines the need for stable co-formulation products with proven stability over the targeted shelf life.

In some cases, the optimal formulation conditions that offer appropriate stability for both proteins over an acceptable shelf life would contradict each other.^{50,184} For example, well known excipients such as sucrose and arginine can stabilize mAb-1 but destabilize mAb-2 by different drug-excipient interactions.¹⁸⁵ Several pharmaceutical concepts have been developed to overcome incompatibilities of small molecule drugs by physical separation of the drugs, for example bilayered tablets or co-extrudates.^{186,187} In principle, dual chamber cartridges can be applied to physically separate biologics, and they have been already used for a fixed-dose combination of vaccines.¹⁸⁸ However, dual chamber cartridges are an expensive dosage form because two independent drug formulations have to be developed and manufactured in parallel. Thus, this approach is only reasonable as a back-up if no feasible stability can be obtained for the co-formulated proteins in a real mixture. Moreover, short-time stability of both proteins in the mixture has still to be confirmed to allow a combined administration when the cartridge has been activated. An alternative approach to combine incompatible biological drugs in a single drug product is spray freeze-drying, where a solution is sprayed through a nozzle into a drying chamber,¹⁸⁹ where the droplets are dried to obtain a powder. Each protein could be dried by spray freeze-drying at the individual formulation and process conditions and the produced powders could be mixed and filled into vials to prepare different dosing ratios of a co-formulated drug product. Like dual chamber cartridges, this approach represents a back-up solution for incompatible drugs, because the drying process has to be optimized for each protein solution, and aseptic filling of powders is both elaborative and expensive. Further, the combined reconstitution and application still requires data on the in-use stability of the protein mixture in solution.

Thus, it is desirable to develop protein co-formulations as real protein mixtures. As discussed in I.3, appropriate methods are required to analyze the protein drugs and to assign impurities to the individual proteins in the respective quantity to meet the requirements for identification and qualification of impurities according to the ICH guidelines Q6B and Q5C. Related substances in impurity testing are usually detected and quantified by chromatographic

methods and the required stability indicating methods have to provide feasible retention times, selectivity and sensitivity for the proteins and the degradation products. This can become challenging due to high similarities in size, solubility, charge, hydrophobicity and detectability of the individual entities.

Based on the available stability data of the individual proteins, an extensive formulation screen can be conducted to identify the available working space, where both proteins would show feasible stability profiles. In some cases, the proteins cannot be stabilized in the same formulation conditions because of their excessively different stability profiles. Pharmaceutical strategies to overcome this divergence depend on the individual drug properties. For example, an amphiphilic polymer was used to solubilize insulin glargine at neutral pH to enable a co-formulation with insulin lispro.¹⁸⁴ Further, insulin aspart and insulin degludec were successfully co-formulated by addition of high zinc concentrations to avoid the formation of mixed hexamers and thereby preserve the individual pharmacokinetic profile of both proteins.³²

In the course of the described formulation screen, it is important to analyze reference formulations of the individual proteins in the same formulation conditions and protein concentrations as the co-formulation. Cross-interactions between the proteins in the mixture can then be detected based on changes in stability-indicating parameters such as the aggregation onset temperature (T_{agg}), turbidity, or monomer recovery as detected by HP-SEC.^{50,163} As discussed in I.3.4 the arising non-specific interactions in a given formulation depend on the surface charge, hydrophobicity and concentration of the individual proteins. The impact of these anticipated possible cross-interactions on the development of protein co-formulations will be discussed in the following.

Excessive attractive cross-interactions can promote more protein aggregation in mixtures compared to the single protein formulations and can lead to the formation of heterogeneous cross-aggregates.^{164,168} These heterogeneous aggregates can show a different morphology compared to the individual homogenous protein aggregates and the possible formation of additional epitopes could change the immunogenicity compared to the individual drug products.¹⁹⁰ To the best of the author's knowledge, no published data is available on the possible impact of heterogeneous protein aggregates on the immunogenicity of co-formulations. Nevertheless, these heterogeneous aggregates have to be considered as impurities according to the ICH guidelines Q6B and Q5C and have to be limited to ensure patient safety. Therefore, it is important to screen the relevant pH range at low and high ionic

strength conditions to select a pH where stability-compromising long-range electrostatic cross-interactions between the co-formulated proteins can be identified and avoided.⁷

While long-range electrostatic forces can affect protein stability already at low protein concentrations, the short-range interactions become relevant at high protein concentrations. The co-formulation of multiple mAbs in a single subcutaneous injection device can improve the ambulant pharmacotherapy and patient compliance, but the limited volume that can be administered subcutaneously requires high protein concentrations to achieve the necessary drug load in a single injection.¹⁹¹ Thus, most mAb co-formulations will likely have elevated viscosities compared to the single mAb formulations based on the higher total protein concentrations. Moreover, the viscosity can further increase due to possible direct cross-interactions,¹¹⁷ or due to promoted self-interactions by molecular crowding effects caused by the second protein.¹⁹² The protein interactions that can lead to a high viscosity of a given formulation can only be partially predicted by measurements at low concentrations,^{149,193–195} and these predictions become even more complex for protein mixtures. Thus, the viscosities of the co-formulation and the respective single protein formulations should be measured to ensure an acceptable viscosity of about 15–20 cP.¹⁹⁶ It is interesting to note that the total volume that can be administered subcutaneously with a single injection can be increased to > 3 mL by co-formulation with hyaluronidase,^{197–199} which allows the formulation of proteins at lower protein concentrations to avoid excessive viscosities.

Moreover, cross-interactions in protein co-formulations can also change with the folding states of the individual proteins, because cross-interactions and cross-aggregations may occur between (a) the native monomers of both proteins, (b) native protein 1 and (partially) unfolded intermediates of protein 2, or (c) (partially) unfolded intermediates of both proteins.^{163,164} The aggregation pathway for a given protein mixture has to be characterized to identify the rate-limiting step for protein cross-aggregation and optimize the formulation conditions accordingly.

Despite the theoretical risk, several publications reported the absence of stability-compromising cross-interactions in protein co-formulations,^{67,88,200} and several patents on the stabilization of mAb co-formulations were filed.^{91,201,202} Furthermore, it is also possible that protective protein cross-interactions would arise in protein co-formulations. It has been shown in several studies that sensitive proteins such as cytokines or enzymes can be stabilized by protein excipients, such as albumin.^{203–205} Several stabilizing mechanisms such as preferential exclusion, preferential hydration and reduction of dehydration-induced denaturation during lyophilization, and saturation of interfaces have been discussed in these studies. HSA is the

most common protein excipient that can be used to stabilize a protein drug.²⁰³ HSA can reduce the interfacial stress and act as a scavenger for reactive oxygen species,²⁰⁶ but has also been used in concentrations of at least 10 g/L for the stabilization of highly concentrated mAb formulations higher than 140 g/L, which resulted in reduction of both viscosity and particle formation compared to the single mAb formulations.²⁰⁷ It has also been reported that HSA can decrease the liquid-liquid phase separation (LLPS) temperatures of mAbs by attractive cross-interactions that reduce the self-interactions and subsequently the required temperature for LLPS of the mAbs.²⁰⁸ These stabilizing effects are not limited to protein excipients, but can be also provided by active pharmaceutical ingredients (APIs). It has been reported that the degradation kinetics for a given mAb were reduced upon co-formulation with an excess of the respective Fab. Several possible mechanisms were postulated to explain this stabilization,⁵¹ such as the molecular crowding induced by the excess of Fab, the molecular screening of aggregation-prone regions of the mAb by the Fab and the direct cross-interactions between mAb and Fab that limited mAb self-interactions. The presented approach to study the impact of macromolecular crowding effects on the individual protein degradation by addition of model crowding agents such as Ficoll70 can be useful to differentiate between electrostatic or hydrophobic cross-interaction between the proteins and promoted self-interactions of one protein in presence of the second protein due to molecular crowding effects.¹⁹²

Finally, multiple dosage strengths or different dosing ratios can be required to achieve the best clinical effect with a protein co-formulation. The stability testing should include all relevant mixing ratios because different mixing ratios can also affect cross-interactions and thus the stability profiles of the proteins. It has been shown that proteins can be stabilized by addition of an excess of a second protein.^{51,205} A first protein could stabilize a second protein at a mixing ratio of 10:1 due to screening of aggregation-prone monomers of the second protein. At a mixing ratio of 1:10, the stabilizing effect can be lower due to the increased concentration of the more aggregation-prone second protein. Thus, it is important to carefully evaluate the effects of protein cross-interactions at different ratios. On the other hand, high differences in the mixing ratio can complicate the purity testing for a given co-formulation. Low concentrations of impurities of the high concentrated protein that are detected during stability testing and that cannot be reliably identified as impurities of this high concentrated protein have to be assigned to the low concentrated protein in the mixture based on the worst case scenario.³⁹ Moreover, it has been reported for fixed-dose combinations of small molecules that the presence of a second drug can accelerate impurity formation of another

drug by chemical interactions.²⁰⁹ This applies as well to protein co-formulations and it is possible that a given protein accelerates degradation of a second protein in the mixture.

I.5 Aim of the thesis

Based on the presented challenges that can arise in drug product development of protein co-formulations, multiple clinically established protein drugs will be co-formulated to study the arising protein interactions, their impact on the individual protein stability and the effect of important formulation parameters such as pH and ionic strength on these interactions. The aim of this thesis is to identify feasible analytical approaches and formulation strategies to characterize and stabilize co-formulations of different therapeutic proteins.

In Chapter II, two cytokines (EPO and G-CSF) will be co-formulated in a feasibility study to identify formulation conditions that provide sufficient protein stability for two model protein drugs with considerably different physicochemical properties. Stability-indicating methods will be developed to study the individual protein stability alone and in co-formulations and accelerated stability studies will be conducted to assess the possibility to stabilize proteins with contradicting stability profiles within a real mixture.

In Chapter III, biophysical methods will be applied to understand how the formulation conditions affect the stability and cross-interactions between EPO and G-CSF. High-throughput methods such as DLS will be applied to test their ability to detect changes of the individual protein aggregation in the co-formulations depending on the respective formulation conditions. These methods could represent powerful tools to screen a wide range of different co-formulation conditions and their impact on protein cross-interactions in a short timescale and with low protein consumption. The feasibility of these methods for the detection of protein cross-interactions in co-formulations will be investigated.

In Chapter IV, multiple clinically established mAbs will be analyzed by several computational tools to identify six mAbs that differ in net charge, charge distribution and CDR composition. A biophysical characterization of all possible binary mixtures of these mAbs will be conducted to compare the colloidal and conformational stability of the proteins alone and in combination in a wide range of formulation conditions. This experimental data will be used to identify mAb properties and formulation parameters that promote protein cross-interactions in mAb co-formulations.

In Chapter V, trastuzumab and rituximab will be used as model proteins for a more detailed analysis of the protein stability of mAbs in co-formulations. Different ratios of both proteins will be analyzed to differentiate between self- and cross-interactions. Stability-

indicating methods for co-formulations of both mAbs will be developed and forced degradation studies will be conducted to show how the stability of trastuzumab and rituximab is affected in the presence of different amounts of the second mAb.

In Chapter VI, the in-use stabilities of DNase and r-tPa will be studied after dilution in standard saline solution. The subsequent application of both enzymes is an established clinical procedure for the treatment of pleural infections. A concurrent administration of both drugs would facilitate the clinical treatment, but the compatibility and in-use-stabilities of both enzymes upon concurrent administration remains unclear. Therefore, the individual drug products will be mixed in standard saline solution according to the targeted concurrent administration and the *in vitro* stabilities of both drugs will be compared to the single drug products. Analytical techniques will be developed to investigate if the degradation of DNase or r-tPa is affected in the presence of the second protein.

Finally, Chapter VII provides a summary of the presented results on the development, characterization and stability of protein co-formulations in the context of the current state of the art and an outlook on the future work on protein co-formulations.

I.6 References

- (1) Lu, R. M. *et al.* Development of therapeutic antibodies for the treatment of diseases. *J. Biomed. Sci.* **2020**, 27 (1), 1–30. <https://doi.org/10.1186/s12929-019-0592-z>.
- (2) Middaugh, C. R. & Pearlman, R. Proteins as Drugs: Analysis, Formulation and Delivery. In: *Oxender D.L., Post L.E (eds.). Novel Therapeutics from Modern Biotechnology: Handbook of Experimental Pharmacology*, Springer, Berlin, Heidelberg, **1999**, 137, 33–58. https://doi.org/10.1007/978-3-642-59990-3_3.
- (3) Burnam, D. K. Insulin and insulin mixtures - NPH insulin. *Calif. Med.* **1951**, 75 (6), 412–415.
- (4) Roach, P. & Woodworth, J. R. Clinical Pharmacokinetics and pharmacodynamics of insulin lispro mixtures. *Clin. Pharmacokinet.* **2002**, 41 (13), 1043–1057. <https://doi.org/10.2165/00003088-200241130-00003>.
- (5) Turner, H. E. & Matthews, D. R. The use of fixed-mixture insulins in clinical practice. *Eur. J. Clin. Pharmacol.* **2000**, 56 (1), 19–25. <https://doi.org/10.1007/s002280050715>.
- (6) Logtenberg, T. Antibody cocktails: Next-generation biopharmaceuticals with improved potency. *Trends Biotechnol.* **2007**, 25 (9), 390–394. <https://doi.org/https://doi.org/10.1016/j.tibtech.2007.07.005>.
- (7) Mueller, C.; Altenburger, U.; Mohl, S. Challenges for the pharmaceutical technical development of protein coformulations. *J. Pharm. Pharmacol.* **2018**, 70 (5), 666–674. <https://doi.org/10.1111/jphp.12731>.
- (8) Chauhan, V. M. *et al.* Advancements in the co-formulation of biologic therapeutics. *J. Control. Release* **2020**, 327 (June), 397–405. <https://doi.org/10.1016/j.jconrel.2020.08.013>.
- (9) Henricks, L. M. *et al.* The use of combinations of monoclonal antibodies in clinical oncology. *Cancer Treat. Rev.* **2015**, 41 (10), 859–867. <https://doi.org/10.1016/j.ctrv.2015.10.008>.

- (10) Gottesman, M. M. *et al.* Toward a better understanding of the complexity of cancer drug resistance. *Annu. Rev. Pharmacol. Toxicol.* **2016**, *56*, 85–102. <https://doi.org/10.1146/annurev-pharmtox-010715-103111>.
- (11) Swain, S. M. *et al.* Pertuzumab, trastuzumab, and docetaxel for HER2-positive metastatic breast cancer (CLEOPATRA): End-of-study results from a double-blind, randomised, placebo-controlled, Phase 3 study. *Lancet Oncol.* **2020**, *21* (4), 519–530. [https://doi.org/10.1016/S1470-2045\(19\)30863-0](https://doi.org/10.1016/S1470-2045(19)30863-0).
- (12) Motzer, R. J. *et al.* Nivolumab plus ipilimumab versus sunitinib in first-line treatment for advanced renal cell carcinoma: Extended follow-up of efficacy and safety results from a randomised, controlled, Phase 3 trial. *Lancet Oncol.* **2019**, *20* (10), 1370–1385. [https://doi.org/10.1016/S1470-2045\(19\)30413-9](https://doi.org/10.1016/S1470-2045(19)30413-9).
- (13) Finn, R. S. *et al.* Atezolizumab plus bevacizumab in unresectable hepatocellular carcinoma. *N. Engl. J. Med.* **2020**, *382* (20), 1894–1905. <https://doi.org/10.1056/nejmoa1915745>.
- (14) Sivapalasingam, S. *et al.* Safety, pharmacokinetics, and immunogenicity of a co-formulated cocktail of three human monoclonal antibodies targeting ebola virus glycoprotein in healthy adults: A randomised, first-in-human phase 1 study. *Lancet Infect. Dis.* **2018**, *18* (8), 884–893. [https://doi.org/10.1016/S1473-3099\(18\)30397-9](https://doi.org/10.1016/S1473-3099(18)30397-9).
- (15) Baum, A. *et al.* Antibody cocktail to SARS-CoV-2 spike protein prevents rapid mutational escape seen with individual antibodies. *Science* **2020**, *369* (6506), 1014–1018. <https://doi.org/10.1126/science.abd0831>.
- (16) Zost, S. J. *et al.* Potently neutralizing and protective human antibodies against SARS-CoV-2. *Nature* **2020**, *584*, 443–449. <https://doi.org/10.1038/s41586-020-2548-6>.
- (17) FDA News Release. Coronavirus (COVID-19) Update: FDA authorizes monoclonal antibodies for treatment of COVID-19. <https://www.fda.gov/news-events/press-announcements/coronavirus-covid-19-update-fda-authorizes-monoclonal-antibodies-treatment-covid-19>. Accessed on 29.01.2021.
- (18) Escudier, B. *et al.* Phase III Trial of bevacizumab plus interferon alpha-2a in patients with metastatic renal cell carcinoma (AVOREN): Final analysis of overall survival. *J. Clin. Oncol.* **2010**, *28* (13), 2144–2150. <https://doi.org/10.1200/JCO.2009.26.7849>.
- (19) Melichar, B. *et al.* Multinational Phase II trial of bevacizumab with low-dose interferon- α 2a as first-line treatment of metastatic renal cell carcinoma: BEVLiN. *Ann. Oncol.* **2013**, *24* (9), 2396–2402. <https://doi.org/10.1093/annonc/mdt228>.
- (20) Rudick, R. A. *et al.* Natalizumab plus interferon beta-1a for relapsing multiple sclerosis. *N. Engl. J. Med.* **2006**, *354* (9), 911–923. <https://doi.org/10.1056/NEJMoa044396>.
- (21) Bello, C. *et al.* Regulation by IFN- α /IFN- γ co-formulation (HerberPAG[®]) of genes involved in interferon-STAT-pathways and apoptosis in U87MG. *Curr. Top. Med. Chem.* **2014**, *14* (3), 351–358. <https://doi.org/10.2174/1568026613666131204125725>.
- (22) Vázquez-Blomquist, D. *et al.* A co-formulation of interferons Type I and II enhances temozolomide response in glioblastoma with unmethylated MGMT promoter status. *Mol. Biol. Rep.* **2020**, *47* (7), 5263–5271. <https://doi.org/10.1007/s11033-020-05604-2>.
- (23) Anasagasti-Angulo, L. *et al.* HeberFERON, formulation based on IFNs Alpha2b and Gamma for the treatment of non-melanoma skin cancer. *Australas. Med. J.* **2017**, *10* (6), 509–515. <https://doi.org/10.21767/AMJ.2017.3013>.
- (24) Jädersten, M. *et al.* Erythropoietin and granulocyte-colony stimulating factor treatment associated with improved survival in myelodysplastic syndrome. *J. Clin. Oncol.* **2008**, *26* (21), 3607–3613. <https://doi.org/10.1200/JCO.2007.15.4906>.
- (25) Rahman, N. M. *et al.* Intrapleural use of tissue plasminogen activator and DNase in pleural infection. *N. Engl. J. Med.* **2011**, *365* (6), 518–526. <https://doi.org/10.1056/NEJMoa1012740>.

- (26) Gough, S. C. L. *et al.* One-year efficacy and safety of a fixed combination of insulin degludec and liraglutide in patients with type 2 diabetes: Results of a 26-week extension to a 26-week main trial. *Diabetes, Obes. Metab.* **2015**, *17*, 965–973.
- (27) Tol, J. *et al.* Chemotherapy, bevacizumab, and cetuximab in metastatic colorectal cancer. *N. Engl. J. Med.* **2009**, *360* (6), 563–572. <https://doi.org/10.1056/NEJMoa0808268>.
- (28) Heier, J. S. *et al.* Intravitreal combined aflibercept + anti-platelet-derived growth factor receptor β for neovascular age-related macular degeneration: Results of the phase 2 CAPELLA trial. *Ophthalmology* **2020**, *127* (2), 211–220. <https://doi.org/10.1016/j.ophtha.2019.09.021>.
- (29) Hendriks, J. J. M. A. *et al.* Fixed dosing of monoclonal antibodies in oncology. *Oncologist* **2017**, *22* (10), 1212–1221. <https://doi.org/10.1634/theoncologist.2017-0167>.
- (30) Cengiz, E. *et al.* The alteration of aspart insulin pharmacodynamics when mixed with detemir insulin. *Diabetes Care* **2012**, *35* (4), 690–692. <https://doi.org/10.2337/dc11-0732>.
- (31) Cengiz, E. *et al.* Early pharmacokinetic and pharmacodynamic effects of mixing lispro with glargine insulin: results of glucose clamp studies in youth with type 1 diabetes. *Diabetes Care* **2010**, *33* (5), 1009–1012. <https://doi.org/10.2337/dc09-2118>.
- (32) Havelund, S. *et al.* Investigation of the physico-chemical properties that enable co-formulation of basal insulin degludec with fast-acting insulin aspart. *Pharm. Res.* **2015**, *32* (7), 2250–2258. <https://doi.org/10.1007/s11095-014-1614-x>.
- (33) Haahr, H.; Fita, E. G. & Heise, T. A review of insulin degludec/insulin aspart: Pharmacokinetic and pharmacodynamic properties and their implications in clinical use. *Clin. Pharmacokinet.* **2017**, *56* (4), 339–354. <https://doi.org/10.1007/s40262-016-0455-7>.
- (34) Kapitza, C. *et al.* Preserved pharmacokinetic exposure and distinct glycemic effects of insulin degludec and liraglutide in IDegLira, a fixed-ratio combination therapy. *J. Clin. Pharmacol.* **2015**, *55* (12), 1369–1377. <https://doi.org/10.1002/jcph.549>.
- (35) Godman, B. *et al.* Fixed dose drug combinations—Are they pharmacoeconomically sound? Findings and implications especially for lower- and middle-income countries. *Expert Rev. Pharmacoeconomics Outcomes Res.* **2020**, *20* (1), 1–26. <https://doi.org/10.1080/14737167.2020.1734456>.
- (36) Bell, D. Combine and conquer: Advantages and disadvantages of fixed-dose combination therapy. *Diabetes, Obes. Metab.* **2013**, *15*, 291–300.
- (37) Rini, B. I. *et al.* Atezolizumab plus bevacizumab versus sunitinib in patients with previously untreated metastatic renal cell carcinoma (IMmotion151): A multicentre, open-label, phase 3, randomised controlled trial. *Lancet* **2019**, *393* (10189), 2404–2415. [https://doi.org/10.1016/S0140-6736\(19\)30723-8](https://doi.org/10.1016/S0140-6736(19)30723-8).
- (38) Liang, F. Optimising first-line treatment for metastatic renal cell carcinoma. *Lancet* **2020**, *395* (10219), e8. [https://doi.org/10.1016/S0140-6736\(19\)32594-2](https://doi.org/10.1016/S0140-6736(19)32594-2).
- (39) World Health Organization. Annex 5 Guidelines for registration of fixed-dose combination medicinal products. *WHO Technical Report Series* **2005**, *929*, 94–142.
- (40) FDA News Release. FDA approves breast cancer treatment that can be administered at home by health care professional <https://www.fda.gov/news-events/press-announcements/fda-approves-breast-cancer-treatment-can-be-administered-home-health-care-professional>. Accessed on 29.01.2021.
- (41) Chen, B. K.; Yang, Y. T. & Bennett, C. L. Why biologics and biosimilars remain so expensive: Despite two wins for biosimilars, the Supreme Court’s recent rulings do not solve fundamental barriers to competition. *Drugs* **2018**, *78* (17), 1777–1781. <https://doi.org/10.1007/s40265-018-1009-0>.
- (42) Sarzi-Puttini, P. *et al.* Biosimilars vs Originators: Are They the Same? *Autoimmun. Rev.* **2019**, *18* (12), 102404. <https://doi.org/https://doi.org/10.1016/j.autrev.2019.102404>.

- (43) Kwon, K. C. & Lee, C. Analysis of Fixed-Dose Combination Products Approved by the US Food and Drug Administration, 2010-2015: Implications for Designing a Regulatory Shortcut to New Drug Application. *Ther. Innov. Regul. Sci.* **2017**, *51* (1), 111–117. <https://doi.org/10.1177/2168479016663263>.
- (44) EMA-CHMP. Guideline on Clinical Development of Fixed Combination Medicinal Products. EMA/CHMP/158268/2017. **2017**.
- (45) FDA. Guidance for Industry: Codevelopment of Two or More New Investigational Drugs for Use in Combination. FDA-2010-D-0616. **2013**.
- (46) Drew, A. Fixed-combination drug products: Are phase 2 and 3 studies really necessary? <https://camargopharma.com/resources/blog/fixed-combination-drug-products-phase-2-3-studies-really-necessary/>. Camargo Pharmaceutical Services. **2016**. Accessed on 29.01.2021.
- (47) European Pharmacopoeia. Ph.Eur. 9.0/2031 Monoklonale Antikörper für Menschen.
- (48) Luo, L. *et al.* A hydrophobic interaction chromatography method suitable for quantitating individual monoclonal antibodies contained in co-formulated drug products. *J. Pharm. Biomed. Anal.* **2020**. <https://doi.org/10.1016/j.jpba.2020.113703>.
- (49) Sharma, V. K. *et al.* Characterization of co-formulated high-concentration broadly neutralizing anti-HIV-1 monoclonal antibodies for subcutaneous administration. *Antibodies* **2020**, *9* (36), 1–16.
- (50) Krieg, D. *et al.* Overcoming challenges in co-formulation of proteins with contradicting stability profiles - EPO plus G-CSF. *Eur. J. Pharm. Sci.* **2020**, *141*, 105073. <https://doi.org/10.1016/j.ejps.2019.105073>.
- (51) Zhang, H. & Dalby, P. A. Stability enhancement in a mAb and Fab coformulation. *Sci. Rep.* **2020**, *10* (1), 21129. <https://doi.org/10.1038/s41598-020-77989-w>.
- (52) Huyghues-Despointes, B. M. *et al.* Measuring the conformational stability of a protein by hydrogen exchange. *Methods Mol. Biol.* **2001**, *168*, 69–92. <https://doi.org/10.1385/1-59259-193-0:069>.
- (53) Arakawa, T. & Timasheff, S. N. Stabilization of protein structure by sugars. *Biochemistry* **1982**, *21* (25), 6536–6544. <https://doi.org/10.1021/bi00268a033>.
- (54) Arakawa, T. & Timasheff, S. N. The stabilization of proteins by osmolytes. *Biophys. J.* **1985**, *47* (3), 411–414. [https://doi.org/10.1016/S0006-3495\(85\)83932-1](https://doi.org/10.1016/S0006-3495(85)83932-1).
- (55) Chi, E. Y. *et al.* Roles of conformational stability and colloidal stability in the aggregation of recombinant human granulocyte colony-stimulating factor. *Protein Sci.* **2003**, *12* (5), 903–913. <https://doi.org/10.1110/ps.0235703>.
- (56) Chi, E. Y. *et al.* Physical stability of proteins in aqueous solution: Mechanism and driving forces in nonnative protein aggregation. *Pharm. Res.* **2003**, *20* (9), 1325–1336. <https://doi.org/10.1023/A:1025771421906>.
- (57) Lumry, R. & Eyring, H. Conformation changes of proteins. *J. Phys. Chem.* **1954**, *58* (2), 110–120. <https://doi.org/10.1021/j150512a005>.
- (58) Sanchez-Ruiz, J. M. Theoretical analysis of Lumry-Eyring models in differential scanning calorimetry. *Biophys. J.* **1992**, *61* (4), 921–935. [https://doi.org/10.1016/S0006-3495\(92\)81899-4](https://doi.org/10.1016/S0006-3495(92)81899-4).
- (59) Roberts, C. J. Kinetics of irreversible protein aggregation: Analysis of extended Lumry-Eyring models and implications for predicting protein shelf life. *J. Phys. Chem. B* **2003**, *107* (5), 1194–1207. <https://doi.org/10.1021/jp026827s>.
- (60) Menzen, T. & Friess, W. Temperature-ramped studies on the aggregation, unfolding, and interaction of a therapeutic monoclonal antibody. *J. Pharm. Sci.* **2014**, *103* (2), 445–455. <https://doi.org/10.1002/jps.23827>.
- (61) Greenfield, N. J. Using circular dichroism collected as a function of temperature to determine the thermodynamics of protein unfolding and binding interactions. *Nat. Protoc.* **2006**, *1* (6), 2527–2535. <https://doi.org/10.1038/nprot.2006.204>.

- (62) Svilenov, H.; Markoja, U. & Winter, G. Isothermal chemical denaturation as a complementary tool to overcome limitations of thermal differential scanning fluorimetry in predicting physical stability of protein formulations. *Eur. J. Pharm. Biopharm.* **2018**, *125*, 106–113. <https://doi.org/10.1016/j.ejpb.2018.01.004>.
- (63) Johnson, C. M. Differential scanning calorimetry as a tool for protein folding and stability. *Arch. Biochem. Biophys.* **2013**, *531* (1), 100–109. <https://doi.org/https://doi.org/10.1016/j.abb.2012.09.008>.
- (64) Bruylants, G.; Wouters, J. & Michaux, C. Differential scanning calorimetry in life science: Thermodynamics, stability, molecular Recognition and application in drug design. *Curr. Med. Chem.* **2005**, *12* (17), 2011–2020. <https://doi.org/10.2174/0929867054546564>.
- (65) Michnik, A. & Drzazga, Z. Thermal denaturation of mixtures of human serum proteins: DSC study. *J. Therm. Anal. Calorim.* **2010**, *101* (2), 513–518. <https://doi.org/10.1007/s10973-010-0826-5>.
- (66) Paulsson, M. & Dejmek, P. Thermal denaturation of whey proteins in mixtures with caseins studied by differential scanning calorimetry. *J. Dairy Sci.* **1990**, *73* (3), 590–600. [https://doi.org/https://doi.org/10.3168/jds.S0022-0302\(90\)78707-3](https://doi.org/https://doi.org/10.3168/jds.S0022-0302(90)78707-3).
- (67) Li, M. *et al.* An ambient temperature-stable antitoxin of nine co-formulated antibodies for botulism caused by serotypes A, B and E. *PLoS One* **2018**, *13* (5), 1–16. <https://doi.org/10.1371/journal.pone.0197011>.
- (68) Jazaj, D. *et al.* Probing conformational changes of monomeric transthyretin with second derivative fluorescence. *Sci. Rep.* **2019**, *9* (1), 10988. <https://doi.org/10.1038/s41598-019-47230-4>.
- (69) Ramamurthy, K.; Ponnusamy, K. & Chellappan, S. Excitation-resolved area-normalized emission spectroscopy: A rapid and simple steady-state technique for the analysis of heterogeneous fluorescence. *RSC Adv.* **2019**, *10* (2), 998–1006. <https://doi.org/10.1039/c9ra10154c>.
- (70) Hawe, A.; Sutter, M. & Jiskoot, W. Extrinsic fluorescent dyes as tools for protein characterization. *Pharm. Res.* **2008**, *25* (7), 1487–1499. <https://doi.org/10.1007/s11095-007-9516-9>.
- (71) Biggar, K. K.; Dawson, N. J. & Storey, K. B. Real-time protein unfolding: A method for determining the kinetics of native protein denaturation using a quantitative real-time thermocycler. *Biotechniques* **2012**, *53* (4), 231–238. <https://doi.org/10.2144/0000113922>.
- (72) Kelly, S. & Price, N. The use of circular dichroism in the investigation of protein structure and function. *Curr. Protein Pept. Sci.* **2000**, *1* (4), 349–384. <https://doi.org/10.2174/1389203003381315>.
- (73) Poppe, L. *et al.* Profiling formulated monoclonal antibodies by ¹H NMR spectroscopy. *Anal. Chem.* **2013**, *85* (20), 9623–9629. <https://doi.org/10.1021/ac401867f>.
- (74) Cavalli, A. *et al.* Protein structure determination from NMR chemical shifts. *Proc. Natl. Acad. Sci. U. S. A.* **2007**, *104* (23), 9615–9620. <https://doi.org/10.1073/pnas.0610313104>.
- (75) Wüthrich, K. NMR with proteins and nucleic Acids. *Eur. News* **1986**, *17* (1), 11–13.
- (76) Kanelis, V.; Forman-Kay, J. D. & Kay, L. E. Multidimensional NMR methods for protein structure determination. *IUBMB Life* **2001**, *52* (6), 291–302. <https://doi.org/10.1080/152165401317291147>.
- (77) Brinson, R. G. *et al.* Enabling adoption of 2D-NMR for the higher order structure assessment of monoclonal antibody therapeutics. *mAbs* **2019**, *11* (1), 94–105. <https://doi.org/10.1080/19420862.2018.1544454>.
- (78) Markwick, P. R. L.; Malliavin, T. & Nilges, M. Structural biology by NMR: Structure, dynamics, and interactions. *PLoS Comput. Biol.* **2008**, *4* (9). <https://doi.org/10.1371/journal.pcbi.1000168>.
- (79) Edwards, J. M. *et al.* ¹⁹F NMR as a tool for monitoring individual differentially labeled proteins in complex mixtures. *Mol. Pharm.* **2018**, *15* (7), 2785–2796. <https://doi.org/10.1021/acs.molpharmaceut.8b00282>.

- (80) Edwards, J. M. *et al.* Use of ¹⁹F differential labelling for the simultaneous detection and monitoring of three individual proteins in a serum environment. *Chempluschem* **2019**, *84* (5), 443–446. <https://doi.org/10.1002/cplu.201900110>.
- (81) Edwards, J. M. *et al.* ¹⁹F Dark-state exchange saturation transfer NMR reveals reversible formation of protein-specific large clusters in high-concentration protein mixtures. *Anal. Chem.* **2019**, *91* (7), 4702–4708. <https://doi.org/10.1021/acs.analchem.9b00143>.
- (82) Manning, M. C. *et al.* Stability of protein pharmaceuticals: An update. *Pharm. Res.* **2010**, *27* (4), 544–575. <https://doi.org/10.1007/s11095-009-0045-6>.
- (83) Torosantucci, R.; Schöneich, C. & Jiskoot, W. Oxidation of therapeutic proteins and peptides: Structural and biological consequences. *Pharm. Res.* **2014**, *31* (3), 541–553. <https://doi.org/10.1007/s11095-013-1199-9>.
- (84) Zapadka, K. L. *et al.* Factors affecting the physical stability (Aggregation) of peptide therapeutics. *Interface Focus* **2017**, *7* (6), 20170030. <https://doi.org/10.1098/rsfs.2017.0030>.
- (85) Fekete, S. & Guillarme, D. Reversed-phase liquid chromatography for the analysis of therapeutic proteins and recombinant monoclonal antibodies. *LC GC Eur.* **2012**, *25*, 540–550.
- (86) Rane, S. S. *et al.* Development and validation of RP-HPLC and RP-UPLC methods for quantification of erythropoietin formulated with human serum albumin. *J. Pharm. Anal.* **2012**, *2* (2), 160–165. <https://doi.org/10.1016/j.jpha.2011.11.006>.
- (87) Pérez-Robles, R. *et al.* Development and validation of a (RP)UHPLC-UV-(HESI/Orbitrap)MS method for the identification and quantification of mixtures of intact therapeutical monoclonal antibodies using a monolithic column. *J. Pharm. Biomed. Anal.* **2018**, *159*, 437–448. <https://doi.org/10.1016/j.jpba.2018.07.013>.
- (88) Kim, J. *et al.* Analytical characterization of coformulated antibodies as combination therapy. *mAbs* **2020**, *12* (1), e1738691. <https://doi.org/10.1080/19420862.2020.1738691>.
- (89) Cao, M. *et al.* Charge variants characterization and release assay development for co-formulated antibodies as a combination therapy. *mAbs* **2019**, *11* (3). <https://doi.org/10.1080/19420862.2019.1578137>.
- (90) Fekete, S. *et al.* Hydrophobic interaction chromatography for the characterization of monoclonal antibodies and related Products. *J. Pharm. Biomed. Anal.* **2016**, *130*, 3–18. <https://doi.org/https://doi.org/10.1016/j.jpba.2016.04.004>.
- (91) Babuka, S. & Li, M. Anti-Botulism Antibody Coformulations. US 8821879 B2, **2014**.
- (92) Farsang, E. *et al.* Tuning selectivity in cation-exchange chromatography applied for monoclonal antibody separations, part 1: Alternative mobile phases and fine tuning of the separation. *J. Pharm. Biomed. Anal.* **2019**, *168*, 138–147. <https://doi.org/10.1016/j.jpba.2019.02.024>.
- (93) Farnan, D. & Moreno, G. T. Multiproduct high-resolution monoclonal antibody charge variant separations by pH gradient ion-exchange chromatography. *Anal. Chem.* **2009**, *81* (21), 8846–8857.
- (94) Righetti, P. G.; Sebastiano, R. & Citterio, A. Capillary electrophoresis and isoelectric focusing in peptide and protein analysis. *Proteomics* **2013**, *13* (2), 325–340. <https://doi.org/10.1002/pmic.201200378>.
- (95) Dai, J. *et al.* Capillary isoelectric focusing-mass spectrometry method for the separation and online characterization of intact monoclonal antibody charge variants. *Anal. Chem.* **2018**, *90* (3), 2246–2254. <https://doi.org/10.1021/acs.analchem.7b04608>.
- (96) Zhang, J. & Liu, X. Y. Effect of protein-protein interactions on protein aggregation kinetics. *J. Chem. Phys.* **2003**, *119* (20), 10972–10976. <https://doi.org/10.1063/1.1622380>.
- (97) Quigley, A. & Williams, D. R. The second virial coefficient as a predictor of protein aggregation propensity: A self-interaction chromatography study. *Eur. J. Pharm. Biopharm.* **2015**, *96*, 282–290. <https://doi.org/10.1016/j.ejpb.2015.07.025>.

- (98) De Young, L. R.; Fink, A. L. & Dill, K. A. Aggregation of globular proteins. *Acc. Chem. Res.* **1993**, *26* (12), 614–620. <https://doi.org/10.1021/ar00036a002>.
- (99) Kumar, V. *et al.* Impact of short range hydrophobic interactions and long range electrostatic forces on the aggregation kinetics of a monoclonal antibody and a dual-variable domain immunoglobulin at low and high concentrations. *Int. J. Pharm.* **2011**, *421* (1), 82–93. <https://doi.org/https://doi.org/10.1016/j.ijpharm.2011.09.017>.
- (100) Singh, P. *et al.* Determination of protein-protein interactions in a mixture of two monoclonal antibodies. *Mol. Pharm.* **2019**. <https://doi.org/10.1021/acs.molpharmaceut.9b00430>.
- (101) Ma, W.; Yang, L. & He, L. Overview of the detection methods for equilibrium dissociation constant K_D of drug-receptor interaction. *J. Pharm. Anal.* **2018**, *8* (3), 147–152. <https://doi.org/10.1016/j.jpha.2018.05.001>.
- (102) Phizicky, E. M. & Fields, S. Protein-protein interactions: Methods for detection and analysis. *Microbiol. Rev.* **1995**, *59* (1), 94–123.
- (103) Some, D. Light-scattering-based analysis of biomolecular interactions. *Biophys. Rev.* **2013**, *5* (2), 147–158. <https://doi.org/10.1007/s12551-013-0107-1>.
- (104) Bajaj, H.; Sharma, V. K. & Kalonia, D. S. Determination of second virial coefficient of proteins using a dual-detector cell for simultaneous measurement of scattered light intensity and concentration in SEC-HPLC. *Biophys. J.* **2004**, *87* (6), 4048–4055. <https://doi.org/10.1529/biophysj.104.048686>.
- (105) George, A. *et al.* Second virial coefficient as predictor in protein crystal growth. In *Macromolecular Crystallography Part A; Methods in Enzymology*, **1997**, *276*, 100–110. [https://doi.org/https://doi.org/10.1016/S0076-6879\(97\)76052-X](https://doi.org/https://doi.org/10.1016/S0076-6879(97)76052-X).
- (106) Tessier, P. M.; Lenhoff, A. M. & Sandler, S. I. Rapid measurement of protein osmotic second virial coefficients by self-interaction chromatography. *Biophys. J.* **2002**, *82* (3), 1620–1631. [https://doi.org/10.1016/S0006-3495\(02\)75513-6](https://doi.org/10.1016/S0006-3495(02)75513-6).
- (107) Moon, Y. U. *et al.* Protein—protein interactions in aqueous ammonium sulfate solutions. Lysozyme and bovine serum albumin (BSA). *J. Solution Chem.* **2000**, *29* (8), 699–718. <https://doi.org/10.1023/A:1005112927213>.
- (108) Saluja, A. *et al.* Diffusion and sedimentation interaction parameters for measuring the second virial coefficient and their utility as predictors of protein aggregation. *Biophys. J.* **2010**, *99* (8), 2657–2665. <https://doi.org/10.1016/j.bpj.2010.08.020>.
- (109) Choi, S. H. & Bae, Y. C. Osmotic cross second virial coefficient (B₂₃) of unfavorable proteins: Modified Lennard-Jones potential. *Macromol. Res.* **2009**, *17* (10), 763–769. <https://doi.org/10.1007/BF03218612>.
- (110) Tessier, P. M.; Sandler, S. I. & Lenhoff, A. M. Direct measurement of protein osmotic second virial cross coefficients by cross-interaction chromatography. *Protein Sci.* **2004**, *13*, 1379–1390. <https://doi.org/10.1110/ps.03419204>.
- (111) Mehta, C. M.; White, E. T. & Litster, J. D. Osmotic second virial cross-coefficient measurements for binary combination of lysozyme, ovalbumin, and α -amylase in salt solutions. *Biotechnol. Prog.* **2013**, *29* (5), 1203–1211. <https://doi.org/10.1002/btpr.1760>.
- (112) Quigley, A. & Williams, D. R. similar interaction chromatography of proteins: A cross interaction chromatographic approach to estimate the osmotic second virial coefficient. *J. Chromatogr. A* **2016**, *1459*, 47–56. <https://doi.org/10.1016/j.chroma.2016.06.048>.
- (113) Kameyama, K. & Minton, A. P. Rapid quantitative characterization of protein interactions by composition gradient static light scattering. *Biophys. J.* **2006**, *90* (6), 2164–2169. <https://doi.org/10.1529/biophysj.105.074310>.
- (114) Roberts, D. *et al.* The role of electrostatics in protein-protein interactions of a monoclonal antibody. *Mol. Pharm.* **2014**, *11* (7), 2475–2489. <https://doi.org/10.1021/mp5002334>.

- (115) Harding, S. E. & Johnson, P. The concentration-dependence of macromolecular parameters. *Biochem. J.* **1985**, *231*, 543–547. <https://doi.org/10.1042/bj2310543>.
- (116) Connolly, B. D. *et al.* Weak interactions govern the viscosity of concentrated antibody solutions: High-throughput analysis using the diffusion interaction parameter. *Biophys. J.* **2012**, *103*, 69–78. <https://doi.org/10.1016/j.bpj.2012.04.047>.
- (117) Woldeyes, M. A. *et al.* Viscosities and protein Interactions of bispecific antibodies and their monospecific mixtures. *Mol. Pharm.* **2018**, *15* (10), 4745–4755. <https://doi.org/10.1021/acs.molpharmaceut.8b00706>.
- (118) Gentiluomo, L. *et al.* Advancing therapeutic protein discovery and development through comprehensive computational and biophysical characterization. *Mol. Pharm.* **2020**, *17* (2), 426–440. <https://doi.org/10.1021/acs.molpharmaceut.9b00852>.
- (119) Hanlon, A. D.; Larkin, M. I. & Reddick, R. M. Free-solution, label-free protein-protein interactions characterized by dynamic light scattering. *Biophys. J.* **2010**, *98* (2), 297–304. <https://doi.org/10.1016/j.bpj.2009.09.061>.
- (120) Tuukkanen, A. T. & Svergun, D. I. Weak protein-ligand interactions studied by Small-angle X-ray scattering. *FEBS J.* **2014**, *281* (8), 1974–1987. <https://doi.org/10.1111/febs.12772>.
- (121) Ryberg, L. A. *et al.* Investigations of albumin-insulin detemir complexes using molecular dynamics simulations and free energy calculations. *Mol. Pharm.* **2020**, *17* (1), 132–144. <https://doi.org/10.1021/acs.molpharmaceut.9b00839>.
- (122) Walker, K. N. *et al.* Equilibrium and pre-equilibrium fluorescence spectroscopic studies of the binding of a single-immunoglobulin-binding domain derived from protein G to the Fc fragment from human IgG1. *Biochem. J.* **1995**, *310* (1), 177–184. <https://doi.org/10.1042/bj3100177>.
- (123) Deshayes S & Divita G. Fluorescence technologies for monitoring interactions between biological molecules in vitro. *Prog Mol Biol Transl Sci.* **2013**, *113*, 109–43. doi: 10.1016/B978-0-12-386932-6.00004-1.
- (124) Elder, A. D. *et al.* Quantitative protocol for dynamic measurements of protein interactions by Förster resonance energy transfer-sensitized fluorescence emission. *J. R. Soc. Interface* **2009**, *6*. <https://doi.org/10.1098/rsif.2008.0381.focus>.
- (125) Margineanu, A. *et al.* Screening for protein-protein interactions using Förster resonance energy transfer (FRET) and fluorescence lifetime imaging microscopy (FLIM). *Sci. Rep.* **2016**, *6* (1), 28186. <https://doi.org/10.1038/srep28186>.
- (126) Gijsbers, A.; Nishigaki, T. & Sánchez-Puig, N. Fluorescence anisotropy as a tool to study protein-protein interactions. *J. Vis. Exp.* **2016**, *2016* (116), 1–9. <https://doi.org/10.3791/54640>.
- (127) Van Dieck, J. *et al.* Molecular basis of S100 proteins interacting with the P53 homologs P63 and P73. *Oncogene* **2010**, *29* (14), 2024–2035. <https://doi.org/10.1038/onc.2009.490>.
- (128) Wanner, R. *et al.* Thermo-optical protein characterization for straightforward preformulation development. *J. Pharm. Sci.* **2017**, *106* (10), 2955–2958. <https://doi.org/10.1016/j.xphs.2017.06.002>.
- (129) Magnez, R. *et al.* PD-1/PD-L1 binding studies using microscale thermophoresis. *Sci. Rep.* **2017**, *7* (1), 1–8. <https://doi.org/10.1038/s41598-017-17963-1>.
- (130) Greenfield, N. J. Circular dichroism (CD) analyses of protein-protein interactions. In: *Meyerkord C., Fu H. (eds.) Protein-Protein Interactions: Methods in Molecular Biology. Humana Press, New York, NY, USA, 2015, 1278, 239–265.* https://doi.org/10.1007/978-1-4939-2425-7_15.
- (131) Cowieson, N. P. *et al.* Evaluating protein:protein complex formation using synchrotron radiation circular dichroism spectroscopy. *Proteins* **2008**, *70* (4), 1142–1146. <https://doi.org/10.1002/prot.21631>.

- (132) Orban, J.; Alexander, P. & Bryan, P. Hydrogen-deuterium exchange in the free and immunoglobulin G-bound protein G B-domain. *Biochemistry* **1994**, *33* (19), 5702–5710. <https://doi.org/10.1021/bi00185a006>.
- (133) Dailing, A.; Luchini, A. & Liotta, L. Unlocking the secrets to protein-protein interface drug targets using structural mass spectrometry techniques. *Expert Rev. Proteomics* **2015**, *12* (5), 457–467. <https://doi.org/10.1586/14789450.2015.1079487>.
- (134) Mandell, J. G.; Falick, A. M. & Komives, E. A. Identification of protein-protein interfaces by decreased amide proton solvent accessibility. *Proc. Natl. Acad. Sci. U. S. A.* **1998**, *95* (25), 14705–14710. <https://doi.org/10.1073/pnas.95.25.14705>.
- (135) Ahn, J. & Engen, J. The use of hydrogen/deuterium exchange mass spectrometry in epitope mapping. *Chim. Oggi/Chemistry Today* **2013**, *31*, 25–28.
- (136) Kretschmann, E.; Raether & H. Notizen: Radiative decay of non radiative surface plasmons excited by light. *Zeitschrift für Naturforsch. A* **1968**, *23* (12), 2135–2136. <https://doi.org/https://doi.org/10.1515/zna-1968-1247>.
- (137) Drescher, D. G.; Selvakumar, D. & Drescher, M. J. Analysis of protein interactions by surface plasmon resonance. *Adv Protein Chem Struct Biol* **2018**, *110*, 1–30. doi: 10.1016/bs.apcsb.2017.07.003.
- (138) Nguyen, H. H. *et al.* Surface Plasmon Resonance: A Versatile Technique for Biosensor Applications. *Sensors* **2015**, *15* (5), 10481–10510. <https://doi.org/10.3390/s150510481>.
- (139) Guo, Z. *et al.* Biosensor-based epitope mapping of antibodies targeting the hemagglutinin and neuraminidase of influenza A virus. *J. Immunol. Methods* **2018**, *461*, 23–29. <https://doi.org/10.1016/j.jim.2018.07.007>.
- (140) Kumaraswamy S & Tobias R. Label-free kinetic analysis of an antibody-antigen interaction using biolayer interferometry. *Methods Mol Biol* **2015**, *1278*, 165–82. doi: 10.1007/978-1-4939-2425-7_10.
- (141) Sun, T. *et al.* High throughput detection of antibody self-interaction by bio-layer interferometry. *mAbs* **2013**, *5* (6), 838–841. <https://doi.org/10.4161/mabs.26186>.
- (142) Domnowski, M. *et al.* Analysis of antibody self-interaction by bio-layer interferometry as tool to support lead candidate selection during preformulation and developability assessments. *Int. J. Pharm.* **2020**, *589*, 119854. <https://doi.org/https://doi.org/10.1016/j.ijpharm.2020.119854>.
- (143) Velazquez-Campoy, A.; Leavitt, S. A. & Freire, E. Characterization of protein-protein interactions by Isothermal Titration Calorimetry. In: *Fu H. (eds). Protein-Protein Interactions: Methods in Molecular Biology. Humana Press, New York, NY, USA, 2004*, *261*, 35–54. <https://doi.org/10.1385/1-59259-762-9:035>.
- (144) Callies, O. & Hernández Daranas, A. Application of isothermal titration calorimetry as a tool to study natural product interactions. *Nat. Prod. Rep.* **2016**, *33* (7), 881–904. <https://doi.org/10.1039/c5np00094g>.
- (145) Duff, M. R. & Howell, E. E. Thermodynamics and solvent linkage of macromolecule–ligand interactions. *Methods (San Diego, Calif.)* **2015**, *76*, 51–60. <https://doi.org/https://doi.org/10.1016/j.ymeth.2014.11.009>.
- (146) Weber, P. C. & Salemme, F. R. Applications of calorimetric methods to drug discovery and the study of protein interactions. *Curr. Opin. Struct. Biol.* **2003**, *13* (1), 115–121. [https://doi.org/https://doi.org/10.1016/S0959-440X\(03\)00003-4](https://doi.org/https://doi.org/10.1016/S0959-440X(03)00003-4).
- (147) Cañadas, O. & Casals, C. Differential scanning calorimetry of protein-lipid interactions. In *Lipid-Protein Interactions: Methods and Protocols* **2019**, 91–106. https://doi.org/10.1007/978-1-4939-9512-7_5.
- (148) Brown, P. H.; Balbo, A. & Schuck, P. Characterizing protein-protein interactions by sedimentation velocity analytical ultracentrifugation. *Curr. Protoc. Immunol.* **2008**, *Chapter 18*, Unit 18.15. <https://doi.org/10.1002/0471142735.im1815s81>.

- (149) Yang, D. *et al.* Weak IgG self- and hetero-Association characterized by fluorescence analytical ultracentrifugation. *Protein Sci.* **2018**, *27* (7), 1334–1348. <https://doi.org/https://doi.org/10.1002/pro.3422>.
- (150) Garidel, P. *et al.* High-concentration protein formulations: how high is high? *Eur. J. Pharm. Biopharm.* **2017**, *119*, 353–360. <https://doi.org/10.1016/j.ejpb.2017.06.029>.
- (151) Galush, W. J.; Le, L. N. & Moore, J. M. R. Viscosity behavior of high-concentration protein mixtures. *J. Pharm. Sci.* **2012**, *101* (3), 1012–1020. <https://doi.org/10.1002/jps.23002>.
- (152) Grupi, A. & Minton, A. P. Concentration-dependent viscosity of binary and ternary mixtures of nonassociating proteins: Measurement and analysis. *J. Phys. Chem. B* **2013**, *117* (44), 13861–13865. <https://doi.org/10.1021/jp406530r>.
- (153) Minton, A. P. Hard quasispherical particle models for the viscosity of solutions of protein mixtures. *J. Phys. Chem. B* **2012**, *116* (31), 9310–9315. <https://doi.org/10.1021/jp302748k>.
- (154) Roberts, C. J. Therapeutic protein aggregation: Mechanisms, design, and control. *Trends Biotechnol.* **2014**, *32* (7), 372–380. <https://doi.org/10.1016/j.tibtech.2014.05.005>.
- (155) Wang, W. *et al.* Immunogenicity of protein aggregates—Concerns and realities. *Int. J. Pharm.* **2012**, *431* (1), 1–11. <https://doi.org/https://doi.org/10.1016/j.ijpharm.2012.04.040>.
- (156) Hong, P.; Koza, S. & Bouvier, E. S. P. Size-exclusion chromatography for the analysis of protein biotherapeutics and their aggregates. *J. Liq. Chromatogr. Relat. Technol.* **2012**, *35* (20), 2923–2950. <https://doi.org/10.1080/10826076.2012.743724>.
- (157) Ricker, R. D. & Sandoval, L. A. Fast, reproducible size-exclusion chromatography of biological macromolecules. *J. Chromatogr. A* **1996**, *743* (1), 43–50. [https://doi.org/10.1016/0021-9673\(96\)00283-X](https://doi.org/10.1016/0021-9673(96)00283-X).
- (158) Weisbjerg, P. L. G. *et al.* Serial coupling of ion-exchange and size-exclusion chromatography to determine aggregation levels in mAbs in the presence of a proteinaceous excipient, recombinant human serum albumin. *J. Pharm. Sci.* **2015**, *104* (2), 548–556. <https://doi.org/10.1002/jps.24275>.
- (159) Jachimska, B.; Wasilewska, M. & Adamczyk, Z. Characterization of globular protein solutions by dynamic light scattering, electrophoretic mobility, and viscosity measurements. *Langmuir* **2008**, *24* (13), 6867–6872. <https://doi.org/10.1021/la800548p>.
- (160) Karow, A. R.; Götzl, J. & Garidel, P. Resolving power of dynamic light scattering for protein and polystyrene nanoparticles. *Pharm. Dev. Technol.* **2015**, *20* (1), 84–89. <https://doi.org/10.3109/10837450.2014.910808>.
- (161) Stetefeld, J.; McKenna, S. A. & Patel, T. R. Dynamic light scattering: A practical guide and applications in biomedical sciences. *Biophys. Rev.* **2016**, *8* (4), 409–427. <https://doi.org/10.1007/s12551-016-0218-6>.
- (162) Svilenov, H. & Winter, G. Rapid sample-saving biophysical characterisation and long-term storage stability of liquid interferon alpha2a formulations: Is there a correlation? *Int. J. Pharm.* **2019**, *562*, 42–50. <https://doi.org/10.1016/j.ijpharm.2019.03.025>.
- (163) Iwashita, K.; Handa, A. & Shiraki, K. Co-aggregation of ovalbumin and lysozyme. *Food Hydrocoll.* **2017**, *67*, 206–215. <https://doi.org/10.1016/j.foodhyd.2017.01.014>.
- (164) Iwashita, K.; Handa, A. & Shiraki, K. Co-aggregation of ovotransferrin and lysozyme. *Food Hydrocoll.* **2019**, *89*, 416–424.
- (165) Gadgil, H. *et al.* SEC-MS analysis of aggregates in protein mixtures. *LC GC North Am.* **2003**, 23–24.
- (166) Hermeling, S. *et al.* Micelle-associated protein in epoetin formulations: A risk factor for immunogenicity? *Pharm. Res.* **2003**, *20* (12), 1903–1907. <https://doi.org/10.1023/B:PHAM.0000008034.61317.02>.

- (167) Yan, Y. & Wang, S. Quantification and identification of dimers in co-formulations. *US* 2020/0240998 A1, **2020**.
- (168) Raynes, J. K. *et al.* Coaggregation of κ -casein and β -lactoglobulin produces morphologically distinct amyloid fibrils. *Small* **2017**, *13* (14), 1–11. <https://doi.org/10.1002/sml.201603591>.
- (169) Bansal, R.; Dash, R. & Rathore, A. S. Impact of mAb aggregation on its biological activity: Rituximab as a case study. *J. Pharm. Sci.* **2020**, *109* (9), 2684–2698. <https://doi.org/10.1016/j.xphs.2020.05.015>.
- (170) Sinicropi, D. *et al.* Colorimetric determination of DNase I activity with a DNA-methyl green substrate. *Analytical Biochemistry*, **1994**, 351–358. <https://doi.org/10.1006/abio.1994.1502>.
- (171) Semba, C. P.; Weck, S. & Patapoff, T. Alteplase: Stability and bioactivity after dilution in normal saline solution. *J. Vasc. Interv. Radiol.* **2003**, *14* (1), 99–102. <https://doi.org/10.1097/01.RVI.0000052297.26939.05>.
- (172) Hammerling, U. *et al.* In vitro bioassay for human erythropoietin based on proliferative stimulation of an erythroid cell line and analysis of carbohydrate-dependent microheterogeneity. *J. Pharm. Biomed. Anal.* **1996**, *14* (11), 1455–1469. [https://doi.org/10.1016/0731-7085\(96\)01799-2](https://doi.org/10.1016/0731-7085(96)01799-2).
- (173) Levy, M. J. *et al.* Analytical techniques and bioactivity assays to compare the structure and function of filgrastim (granulocyte-colony stimulating factor) therapeutics from different manufacturers. *Anal. Bioanal. Chem.* **2014**, *406* (26), 6559–6567. <https://doi.org/10.1007/s00216-013-7469-x>.
- (174) Gazzano-Santoro, H. *et al.* A non-radioactive complement-dependent cytotoxicity assay for anti-CD20 monoclonal antibody. *J. Immunol. Methods* **1997**, *202* (2), 163–171. [https://doi.org/10.1016/S0022-1759\(97\)00002-1](https://doi.org/10.1016/S0022-1759(97)00002-1).
- (175) Chand, S. *et al.* Quality assurance of rituximab (anti-CD 20) antibodies by potency testing: Determining the system suitability criteria and sample acceptance criteria. *Curr. Sci.* **2018**, *114* (12), 2513–2518. <https://doi.org/10.18520/cs/v114/i12/2513-2518>.
- (176) Chao, T. *et al.* SYN023, a novel humanized monoclonal antibody cocktail, for post-exposure prophylaxis of rabies. *PLoS Negl. Trop. Dis.* **2017**, *11* (12), 1–20.
- (177) Fuentes, G. *et al.* Synergy between trastuzumab and pertuzumab for human epidermal growth factor 2 (HER2) from colocalization: An in silico based mechanism. *Breast Cancer Res.* **2011**, *13* (3). <https://doi.org/10.1186/bcr2888>.
- (178) Lua, W. H. *et al.* A search for synergy in the binding kinetics of trastuzumab and pertuzumab whole and F(Ab) to HER2. *NPJ Breast Cancer* **2015**, *1*. 2014–2016. <https://doi.org/10.1038/npjbcancer.2015.12>.
- (179) Hao, Y. *et al.* Cryo-EM structure of HER2-trastuzumab-pertuzumab complex. *PLoS One* **2019**, *14* (5), 1–10. <https://doi.org/10.1371/journal.pone.0216095>.
- (180) Kim, D. M. *et al.* Measuring the effects of macromolecular crowding on antibody function with biolayer interferometry. *mAbs* **2019**, *11* (7), 1319–1330. <https://doi.org/10.1080/19420862.2019.1647744>.
- (181) Kumru, O. S. *et al.* Compatibility, physical stability, and characterization of an IgG4 monoclonal antibody after dilution into different intravenous administration bags. *J. Pharm. Sci.* **2012**, *101* (10), 3636–3650. <https://doi.org/10.1002/jps.23224>.
- (182) Zheng, S.; Adams, M. & Mantri, R. V. An approach to mitigate particle formation on the dilution of a monoclonal antibody drug product in an iv administration fluid. *J. Pharm. Sci.* **2016**, *105* (3), 1349–1350. <https://doi.org/10.1016/j.xphs.2015.12.013>.
- (183) Glover, Z. W. *et al.* Compatibility and stability of pertuzumab and trastuzumab admixtures in i.v. infusion bags for coadministration. *J. Pharm. Sci.* **2013**, *102* (3), 794–812. <https://doi.org/10.1002/jps.23403>.

- (184) Meiffren, G. *et al.* Better glycaemic control with biochaperone glargine lispro co-formulation than with insulin lispro Mix25 or separate glargine and lispro administrations after a test meal in people with type 2 diabetes. *Diabetes, Obes. Metab.* **2019**, *21* (7), 1570–1575. <https://doi.org/10.1111/dom.13685>.
- (185) Thakkar, S. V. *et al.* Excipients differentially influence the conformational stability and pretransition dynamics of two IgG1 monoclonal antibodies. *J. Pharm. Sci.* **2012**, *101* (9), 3062–3077. <https://doi.org/10.1002/jps.23187>.
- (186) Hwang, I.; Kang, C.-Y. & Park, J.-B. Advances in hot-melt extrusion technology toward pharmaceutical objectives. *J. Pharm. Investig.* **2017**, *47* (2), 123–132. <https://doi.org/10.1007/s40005-017-0309-9>.
- (187) Dhiman, N. *et al.* Development of bilayer tablets with modified release of selected incompatible drugs. *Polim. Med.* **2016**, *46* (1), 5–15. <https://doi.org/10.17219/pim/62511>.
- (188) Werk, T. *et al.* Technology, applications, and process challenges of dual chamber systems. *J. Pharm. Sci.* **2016**, *105* (1), 4–9. <https://doi.org/https://doi.org/10.1016/j.xphs.2015.11.025>.
- (189) Emami, F. *et al.* Drying technologies for the stability and bioavailability of biopharmaceuticals. *Pharmaceutics* **2018**, *10* (3), 1–22. <https://doi.org/10.3390/pharmaceutics10030131>.
- (190) Svitel, G. *et al.* Analytical strategies for fixed-dose coformulated protein therapeutics. *Bioprocess Int.* **2019**, *17* (3), 5–9.
- (191) Shire, S. J.; Shahrokh, Z. & Liu, J. Challenges in the development of high protein concentration formulations. *J. Pharm. Sci.* **2004**, *93* (6), 1390–1402. <https://doi.org/https://doi.org/10.1002/jps.20079>.
- (192) Ellis, R. J. & Minton, A. P. Protein aggregation in crowded environments. *Biol. Chem.* **2006**, *387* (5), 485–497. <https://doi.org/10.1515/BC.2006.064>.
- (193) Calero-Rubio, C. *et al.* Predicting high-concentration interactions of monoclonal antibody solutions: comparison of theoretical approaches for strongly attractive versus repulsive conditions. *J. Phys. Chem. B* **2019**, *123* (27), 5709–5720. <https://doi.org/10.1021/acs.jpcc.9b03779>.
- (194) Calero-Rubio, C. *et al.* Predicting protein-protein interactions of concentrated antibody solutions using dilute solution data and coarse-grained molecular models. *J. Pharm. Sci.* **2018**, *107* (5), 1269–1281. <https://doi.org/10.1016/j.xphs.2017.12.015>.
- (195) Woldeyes, M. A. *et al.* How well do low- and high-concentration protein interactions predict solution viscosities of monoclonal antibodies? *J. Pharm. Sci.* **2019**, *108* (1), 142–154. <https://doi.org/10.1016/j.xphs.2018.07.007>.
- (196) Berteau, C. *et al.* Evaluation of the impact of viscosity, injection volume, and injection flow rate on subcutaneous injection tolerance. *Med. Devices Evid. Res.* **2015**, *8*, 473–484. <https://doi.org/10.2147/MDER.S91019>.
- (197) Shpilberg, O. & Jackisch, C. Subcutaneous administration of rituximab (MabThera) and trastuzumab (Herceptin) using hyaluronidase. *Br. J. Cancer* **2013**, *109* (6), 1556–1561. <https://doi.org/10.1038/bjc.2013.371>.
- (198) Adler, M. *et al.* Subcutaneous anti-HER2 Antibody formulations and uses thereof. US009345661B2, **2016**.
- (199) Teschner, W. *et al.* Stable co-formulation of hyaluronidase and immunoglobulin, and methods of use thereof. US9084743B2, **2015**. <https://doi.org/10.1021/n10602701>.
- (200) Krieg, D. *et al.* Biophysical characterization of binary therapeutic monoclonal antibody mixtures. *Mol. Pharm.* **2020**, *17* (8), 2971–2986. <https://doi.org/10.1021/acs.molpharmaceut.0c00370>.
- (201) Babuka, S. J.; Huang, C.-Y. & Li, M. Antibody coformulations. US 2011/0059079 A1, **2011**.
- (202) Sadineni, V.; Quan, Y. & Kaserer, W. Compositions comprising a combination of nivolumab and ipilimumab US10512689B2, **2019**.

- (203) Hawe, A. & Friess, W. Stabilization of a hydrophobic recombinant cytokine by human serum albumin. *J. Pharm. Sci.* **2007**, *96* (11), 2987–2999. <https://doi.org/10.1002/jps.20909>.
- (204) Shimizu, T. *et al.* Characteristics of proteinaceous additives in stabilizing enzymes during freeze-thawing and - drying. *Biosci. Biotechnol. Biochem.* **2017**, *81* (4), 687–697. <https://doi.org/10.1080/09168451.2016.1274637>.
- (205) Alam, J.; Rogge, M. & Goelz, S. Recombinant human interferon beta-1a formulation. WO 99/62542, **1999**.
- (206) Christie, M. *et al.* The role of protein excipient in driving antibody responses to erythropoietin. *J. Pharm. Sci.* **2015**, *104* (12), 4041–4055. <https://doi.org/10.1002/jps.24639>.
- (207) Bukrinski, J. T. *et al.* Antibody composition. WO 2015/063180 A1, **2015**.
- (208) Wang, Y. *et al.* Phase separation in solutions of monoclonal antibodies and the effect of human serum albumin. *Proc. Natl. Acad. Sci. U. S. A.* **2011**, *108* (40), 16606–16611. <https://doi.org/10.1073/pnas.1112241108>.
- (209) Xu, Q. Advancing USP compendial methods for fixed dose combinations: A case study of metoprolol tartrate and hydrochlorothiazide tablets. *J. Pharm. Anal.* **2019**, *9* (2), 77–82. <https://doi.org/10.1016/j.jpha.2018.12.003>.

Chapter II **Rational development of a stable co-formulation for EPO and G-CSF**

Parts of this chapter are published as:

Krieg, D.; Svilenov, H.; Gitter, J. H.; Winter, G. Overcoming challenges in co-formulation of proteins with contradicting stability profiles - EPO plus G-CSF. *Eur. J. Pharm. Sci.* **2020**, *141*, 105073. <https://doi.org/10.1016/j.ejps.2019.105073>

II.1 Introduction

There is a steadily increasing interest in the development of stable co-formulations of two or more therapeutic proteins that can be combined in one primary package and simultaneously administered to patients.¹ Such co-formulations can offer various benefits related to increased therapeutic efficacy, fewer side effects, lower number of injections, reduced costs and potential for intellectual property protection.¹ Currently, most approved protein co-formulations consist of one therapeutic protein, like a monoclonal antibody or a cytokine, and a second proteinaceous excipient, which aids the drug administration or acts as an excipient stabilizing the therapeutic protein. For example, some formulations of the monoclonal antibody trastuzumab include hyaluronidase to increase the maximum amount of drug solution that can be applied subcutaneously.² Another example is the addition of human serum albumin (HSA) to stabilize cytokines like EPO (Erythropoietin), interferon alpha-2a and interferon beta-1b.^{3,4} Using a second protein as an excipient is a formulation approach that has been used for decades. However, the combination of two therapeutic proteins in one dosage form has only recently gained more popularity in the industry with several prominent examples of co-formulations being tested or approved for market use. This includes fixed-dose-combinations of trastuzumab and pertuzumab,⁵ co-formulations of anti-PD-L1- and CTLA4-antibodies,⁶ and several marketed co-formulations of basal insulins with GLP-1 receptor agonists.⁷ The approach to combine therapeutic proteins in one primary container is interesting but it raises several questions about the compatibility and stability of the combined proteins. Moreover, the comprehensive characterization of protein co-formulations/mixtures is usually related to significant analytical challenges.⁸ The analytical setup has to take different degradation pathways of each therapeutic protein into account. Understanding the origin of different degradation products can be complicated due to an insufficient separation between the two proteins with many chromatographic or spectroscopic methods. Here, we investigate a pair of two therapeutic model proteins, EPO and G-CSF (Granulocyte-Colony Stimulating Factor), which are interesting for co-formulation development from both clinical

and physicochemical perspective. Several clinical trials already investigated the clinical benefit of a combined EPO and G-CSF therapy of the myelodysplastic syndrome.⁹⁻¹¹ Further clinical tests used this combination to improve stem cell mobilization,¹² treatment of chronic stroke,¹³ or prevention of necrotizing enterocolitis in preterm neonates.¹⁴

However, these two cytokines differ a lot in their structure and stability: EPO consists of 165 amino acids and is a glycoprotein with approximately 40% of the molecular weight (30.4 kDa) being carbohydrate.¹⁵ Several studies indicate the highest stability for this glycoprotein at physiological pH around 7.0 and reduced conformational stability at acidic pH.¹⁶⁻¹⁸ G-CSF is licensed as a drug in multiple subtypes: Filgrastim is the non-glycosylated form of G-CSF with an additional N-terminal methionine group, which is expressed in *E.coli*, lenograstim is the glycosylated form and expressed in CHO-cells, and pegfilgrastim is the PEGylated filgrastim.¹⁹ For our studies, filgrastim was used, a hydrophobic cytokine with maximum stability at pH 4.0 and low stability and fast aggregation at physiological pH.²⁰⁻²² Due to these properties, obtaining a stable co-formulation of both proteins in one solution appears challenging, if not impossible.

In this work, we share our experience and present a comprehensive study on the co-formulation of two therapeutic proteins. We first applied thermal unfolding experiments to understand the effect of pH on the stability of both proteins alone or in co-formulation. We thereby identified promising starting solution conditions and applied short-term stress studies to investigate the stability of selected liquid co-formulations. Poor stability of the proteins in the liquid state led to the development of lyophilized co-formulations. Eventually, we achieved a stable reconstituted co-formulation by applying an elegant approach in which we dissolve the freeze-dried proteins with a buffer having pH different from the one used for the initial formulations before lyophilization. We studied the colloidal, chemical and conformational stability of the most promising protein co-formulation for up 12 months in comparison to the respective single protein formulations. Alongside the formulation development, we developed and applied feasible analytical methods for the characterization of EPO and G-CSF in co-formulations.

II.2 Materials and Methods

II.2.1 Materials

The bulk solution of EPO contained 2.0 g/L protein, the bulk solution of G-CSF (filgrastim) 4.0 g/L protein. Both bulk solutions were provided in this concentration from the manufacturer. The protein concentration was measured spectrophotometrically using an Agilent 8453 UV spectrophotometer (Agilent Technologies Deutschland GmbH, Böblingen, Germany) and an extinction coefficient at 280 nm of $1.24 \text{ (mg/mL)}^{-1}\text{cm}^{-1}$ for EPO and $0.86 \text{ (mg/mL)}^{-1}\text{cm}^{-1}$ for G-CSF respectively. HEPES was obtained from VWR International GmbH (Darmstadt, Germany) and HP- β -CD from Wacker Chemie AG (Burghausen, Germany). All other chemicals were obtained from Sigma-Aldrich Chemie GmbH (Steinheim, Germany). All solutions were prepared with ultrapure water from a Sartorius arium[®] pro system (Sartorius Corporate Administration GmbH, Göttingen, Germany).

II.2.2 Preparation of co-formulations

For formulations #1-26, the single proteins were dialysed from the bulk solutions into 100x excess of the respective buffer at the given pH (see Tables 2, 3 & 4) for 24 hours at 2-8 °C using a Spectra/Por[®] dialysis membrane (cutoff 6-8 kDa, Spectrum Laboratories, Rancho Dominguez, CA, USA). The dialysis buffer was exchanged once after 8 hours. After dialysis, stock solutions of each excipient were prepared in the same buffer and mixed with dialysed protein solutions and dialysis buffer to obtain co-formulations with a concentration 0.5 g/L for each protein. pH was adjusted using a MP 220 pH meter (Mettler-Toledo GmbH, Gießen, Germany) to the targeted pH and formulations were filtered using a 0.2 μm cellulose acetate membrane filter (Whatman, FP 30/0.2 CA-S, GE Healthcare, Buckinghamshire, UK) into 2R Type I glass vials, closed with rubber stoppers and crimped.

For formulations #27-30, all excipients except the surfactant were added already to the dialysis buffer, and surfactant was added after dialysis as a stock solution in the respective buffer system.

II.2.3 Lyophilization

Three lyophilization cycles were used: Cycle 1, Cycle 2 (optimized) and Cycle 3 (final cycle). References to the respective cycle are given in the text. The freeze-drying runs were performed either on a FTS Lyostar 3 (SP Scientific, Stone Ridge, USA) or on a Martin Christ Epsilon 2-6D (Martin Christ, Osterode am Harz, Germany). Both pilot-scale freeze-dryers are equipped with a comparative pressure measurement system containing of a Pirani pressure gauge and a capacitive manometer.

Cycle 1 was performed as follows: Shelf temperature was decreased from 20°C to -50 °C with a ramp rate of 1 °C/min and equilibration for 150 minutes. Then a vacuum of 0.05 mbar was used and shelf temperature was increased to -20 °C using a ramp rate of 1 °C/min. This temperature was held for 32 hours and then increased to 25 °C using a ramp rate of 1 °C/min. This temperature was held for 6 hours.

Cycle 2 was performed as follows: Shelf temperature was decreased from 20°C to -50 °C with a ramp rate of 1 °C/min and equilibration for 240 minutes. A vacuum of 0.08 mbar was used and shelf temperature was increased to -23 °C using a ramp rate of 1 °C/min. This temperature was held for 23 hours and then increased to 25 °C using a ramp rate of 1 °C/min. This temperature was held for 6 hours.

Cycle 3 was performed as follows: Shelf temperature was decreased from 20°C to -50 °C with a ramp rate of 1 °C/min and equilibration for 150 minutes. An annealing step was included by heating to -20 °C with a ramp rate of 1 °C/min and equilibration for 240 minutes. The shelf was cooled again to a temperature of -50 °C with a ramp rate of 1 °C/min and equilibration for 180 minutes. A vacuum of 0.08 mbar was used and shelf temperature was increased to 25 °C using a ramp rate of 1 °C/min. This temperature was held for 14 hours to allow for primary and secondary drying.

For all cycles, venting was performed with nitrogen at 800 mbar with subsequent vial closing.

II.2.4 High-throughput Fluorimetric Analysis of Thermal Protein Unfolding with nanoDSF

nanoDSF was used to study the thermal unfolding and aggregation of the single proteins and the co-formulations as a function of pH. Eight different pH-values were tested after preparing single and co-formulations of EPO and G-CSF in 10 mM sodium citrate phosphate buffer pH 3.0, 4.0, 5.0, 6.0, 7.0, 7.5 and 8.0 with a concentration of 0.5 g/L per protein. The formulations were filled into standard glass capillaries (NanoTemper Technologies, Munich, Germany) and placed in the Prometheus[®] NT.48 (NanoTemper Technologies, Munich, Germany). A temperature ramp of 1 °C/min was applied from 20 to 95 °C. All measurements were performed in triplicates. The fluorescence intensity ratio (F_{350}/F_{330}) was plotted against the temperature and the apparent protein melting temperature (T_{mapp}) was derived from the maximum of the first derivative of each measurement using the PR.ThermControl V2.1 software (NanoTemper Technologies, Munich, Germany). In addition, the aggregation onset temperature (T_{agg}) from the increase in the signal from the aggregation detection optics was determined using the same software.

II.2.5 Circular dichroism (CD)

Near-UV circular dichroic spectra were collected at 25 °C with a Jasco J-810 spectropolarimeter (JASCO Deutschland GmbH, Pfungstadt, Germany). 10 accumulations of each sample were taken at a speed of 20 nm/min, and measurements were performed in triplicates. The spectrum of the respective buffer was subtracted for each sample and smoothing of the single spectra was performed using the Savitzky-Golay algorithm with 7 smoothing points.²³ The specific ellipticity was calculated and used for comparison of the spectra. Quartz cuvettes with 10 mm wavelength path were used.

To further elucidate the thermal unfolding of EPO and G-CSF at pH 4.0 and pH 7.0, a thermal ramp of 1 °C/min was applied from 20 °C – 85 °C and Far-UV absorption at 220 nm was plotted against temperature for single and co-formulations. Single and co-formulations contained 50 µg/mL per protein in 10 mM sodium citrate phosphate buffer. The raw data points are shown in Figs II.1C and II.1D and the data was fitted to a two-state unfolding model using the CDpal software.²⁴ The respective fits are visualized as lines in Figs II.1C and II.1D.

II.2.6 Flow Imaging Microscopy

Flow Imaging Microscopy was used to study the formation of insoluble aggregates (subvisible particles) in the single and co-formulations with a FlowCam 8100 (Fluid Imaging Technologies, Inc., Scarborough, ME, USA). A 10x magnification cell was used. 160 µL were injected with a flow rate of 0.15 mL/min. Images were taken with an auto image frame rate of 28 frames/second, a sampling time of 60 seconds and particle identification was performed with distance to the nearest neighbor set to 3 µm, and particle segmentation thresholds set to 13 and 10 for the dark and light pixels respectively. The particle size was measured as the equivalent spherical diameter (*ESD*). For measurements and evaluation, the VisualSpreadsheet® 4.7.6 software was used.

II.2.7 High-Performance Size Exclusion Chromatography (HP-SEC)

High-Performance Size Exclusion Chromatography was performed on either an Agilent 1100 (Agilent Technologies, Palo Alto, USA) equipped with a Dawn Heleos II detector (Wyatt Technologies Europe GmbH, Dernbach, Germany) for the HP-SEC-MALS measurements (Multiangle Light Scattering) or a Waters 2695 separation module (Waters GmbH, Eschborn, Germany) for the stability studies. 15 µg of EPO & G-CSF were injected on a Superose 12 10/300 GL column (GE Healthcare Life Sciences, Tokyo, Japan) after centrifugation at 10 000 x g for 10 min and the elution of the protein was detected by UV

spectrometry at 280 nm. 100 mM sodium phosphate pH 7.0 with 0.05 % NaN_3 was used as mobile phase. Monomer recovery was calculated by integration of the peak area and relative comparison of this peak area before and after lyophilization/storage. A sample chromatogram is provided in Figure II.6.

II.2.8 Reversed-Phase High-Performance Liquid Chromatography (RP-HPLC)

A Dionex Ultimate 3000 system (Thermo Fisher, Dreieich, Germany) was used for the reversed-phase high-performance liquid chromatography. 20 μL were injected on a BioBasic C18, 250 x 2.1, 5 μm column (Thermo Fisher, Dreieich, Germany) after centrifugation at 10 000 x g for 10 min. Detection was performed by UV spectrometry at 280 nm and fluorescence spectrometry with emission at 330 nm after excitation at 280 nm. To achieve feasible separation of both proteins and chemical altered entities, the given gradient scheme in Fig. II.6B was applied. Equilibration of the system at 20 % B was necessary to prevent elution of EPO with the void volume. Eluent A consisted of 10 % (w/v) acetonitrile and 0.1 % (w/v) trifluoroacetic acid in ultrapure water. Eluent B consisted of 0.1 % (w/v) trifluoroacetic acid in acetonitrile. The flow rate was 0.2 mL/min. The column oven temperature was set to 37 °C.

II.2.9 Differential Scanning Calorimetry (DSC)

Differential Scanning Calorimetric Analysis was performed on a DSC 214 Polyma (Netzsch-Gerätebau GmbH, Selb, Germany). 5 to 10 mg of each sample was weighted into aluminum crucibles in a nitrogen-purged glove box. A temperature ramp of 10 °C/min was applied from 10 to 200 °C. The Proteus[®] Analysis 7.10 software was used for data analysis. The measurements were performed in triplicates.

II.2.10 Gas adsorption (BET)

Gas adsorption according to the BET theory (Brunauer Emmet Teller) was applied to measure the specific surface area (SSA) of lyophilized single and co-formulations. The measurements were performed on a Quantachrome Autosorb 1 (3P Instruments, Odelzhausen, Germany). 50 mg of each lyophilization cake were crushed, put into a sample tube and degassed for at least 2 h at ambient temperature using the degassing function of the Autosorb-1. The Krypton sorption at 77 K was measured at 11 data points over a relative pressure p/p_0 ranging from 0.05 to 0.3. The Multipoint BET data evaluation function of the Autosorb 1 software v1.55 was used for data analysis. The measurements were performed in triplicates.

II.2.11 Karl Fischer Titration

The residual moisture of the lyophilization cakes was determined by Karl Fischer titration using an Aqua 40.00 titrator equipped with a headspace module (Analytik Jena AG, Jena, Germany). The lyophilization cakes were pulverized in a glove box (< 10 % relative humidity) and 15 – 30 mg of each sample were used for analysis. The oven temperature was set to 100 °C. The measurements were performed in triplicates.

II.2.12 X-ray Powder Diffraction (XRD)

Crystallinity of sucrose and mannitol was measured using a XRD 3000 TT diffractometer (GE Sensing & Inspection Technologies GmbH, Ahrensburg, Germany). A copper anode at 40 kV and 30 mA was used to generate CuK α radiation ($\lambda = 0.15417$ nm). The lyophilization cakes were pulverized and the powder was placed on a copper sample holder. Powder diffraction was measured ranging from 5° to 45° 2- θ in 0.05° measurement intervals at a hold time of 2 seconds for each measurement angle.

II.3 Results and Discussion

II.3.1 Screen for optimal pH

EPO and G-CSF differ greatly in the pH of their marketed formulations. EPO is usually formulated at physiological pH, while G-CSF is formulated at pH 4.0. A first step to obtain a stable co-formulation of both proteins in one solution is to determine an optimal pH for this combination. We used nanoDSF to study the behavior of both proteins in single and co-formulations of pH-values ranging from pH 3.0 to 8.0 (See Fig. S.II.1 in the supplementary data). A low concentration of 10 mM sodium citrate/phosphate buffer was used because G-CSF is known to aggregate in solutions with high ionic strength.²⁵ No clear fluorescence transition of EPO was detected with nanoDSF, therefore we focused on the transition of G-CSF in single and co-formulations. As shown in Fig. II.1A, the apparent melting temperature (T_{mapp}) of G-CSF is highest at pH 3.0, decreases with increasing pH up to pH 6.0 and rises again at pH 7.0 to 8.0. Since the T_{agg} values of G-CSF decrease with increasing concentration in DSF,²⁶ heat-induced protein aggregation at concentrations of 0.5 g/L may affect the melting transitions.²⁷ Therefore, the measurements characterize the behavior of G-CSF for the targeted formulation concentration, but deviate from already published melting transitions, which were measured in lower concentrations and different composition.²⁸ If aggregation occurs around the melting temperature of the protein in the intended concentration, this will shift the apparent melting temperature to lower values which will indicate lower stability and thus the

interpretation that a lower T_{mapp} is related to lower stability will still be correct.²⁹ The T_{agg} values of G-CSF are significantly decreased in co-formulation with EPO at pH-values below 6.0 and above pH 7.0 compared to the single protein formulation (See Fig. II.1B). Based on preliminary measurements, we assume that the decreased T_{agg} values for the co-formulation may be caused by attractive electrostatic interactions, since EPO and G-CSF show opposite zeta potentials at pH 4.0 (-6.8 ± 1.5 mV for EPO and 22.4 ± 0.3 mV for G-CSF, see Chapter III). The electrostatic attraction may accelerate aggregation. This may also explain why the co-formulation exhibits aggregation at pH 3.0 while the G-CSF single formulation does not and moreover, why the aggregation is facilitated at pH-values < 6.0 .

We also compared the thermal unfolding of both proteins in single and co-formulations at pH 4.0 and pH 7.0 using CD-spectroscopy (See Figs. II.1C and II.1D). It has already been shown for G-CSF alone, that the transition determined by ellipticity change at 220 nm is higher at pH 4.0 compared to pH 7.0.^{30,31} We show here that the presence of EPO has a slightly destabilizing effect on the thermal stability of G-CSF at pH 4.0, as indicated by a decreased apparent melting temperature. EPO does not show any transition at pH 4.0 in contrast to pH 7.0, which indicates a loss of structure already at room temperature at pH 4.0 for EPO, which was already shown in the literature.¹⁶ At pH 7.0, CD-spectroscopy is not able to resolve the transitions of the two proteins as observed in the respective single formulations but gives only one transition for the co-formulation. Still, the measured melting transition of the co-formulation fit resembles the calculated mean of the single formulation fits (data not shown), which does not indicate any destabilizing effect on the melting events by the presence of the second protein at pH 7.0. The transitions in secondary structure confirm the nanoDSF results with the higher melting temperature for G-CSF at pH 4.0 compared to pH 7.0 (70.6 °C for pH 4.0 and 63.0 °C for pH 7.0) and the lower melting temperatures in co-formulations (66.3 °C for pH 4.0 and 59.2 °C for pH 7.0). The used concentrations for CD-measurements (0.05 mg/mL per protein) are lower than the ones in targeted formulations (0.5 mg/mL per protein). Therefore, it is not possible to directly compare the melting transitions given by nanoDSF and CD measurements, as the melting transitions by nanoDSF may be affected by concentration-dependent protein aggregation. In fact, nanoDSF provides the apparent melting of the proteins in the targeted co-formulation concentration which is still indicative for the protein stability.²⁹ In total, there is no indication for severe destabilization of G-CSF in the co-formulation at physiological pH. In fact, the co-formulation tends to reduce the aggregation of G-CSF at physiological pH compared to the single formulation as no light scattering was

observed in the co-formulations at pH > 7.0 in the nanoDSF measurements (See Fig. II.1B). Hence, we performed a first formulation screen at physiological pH.

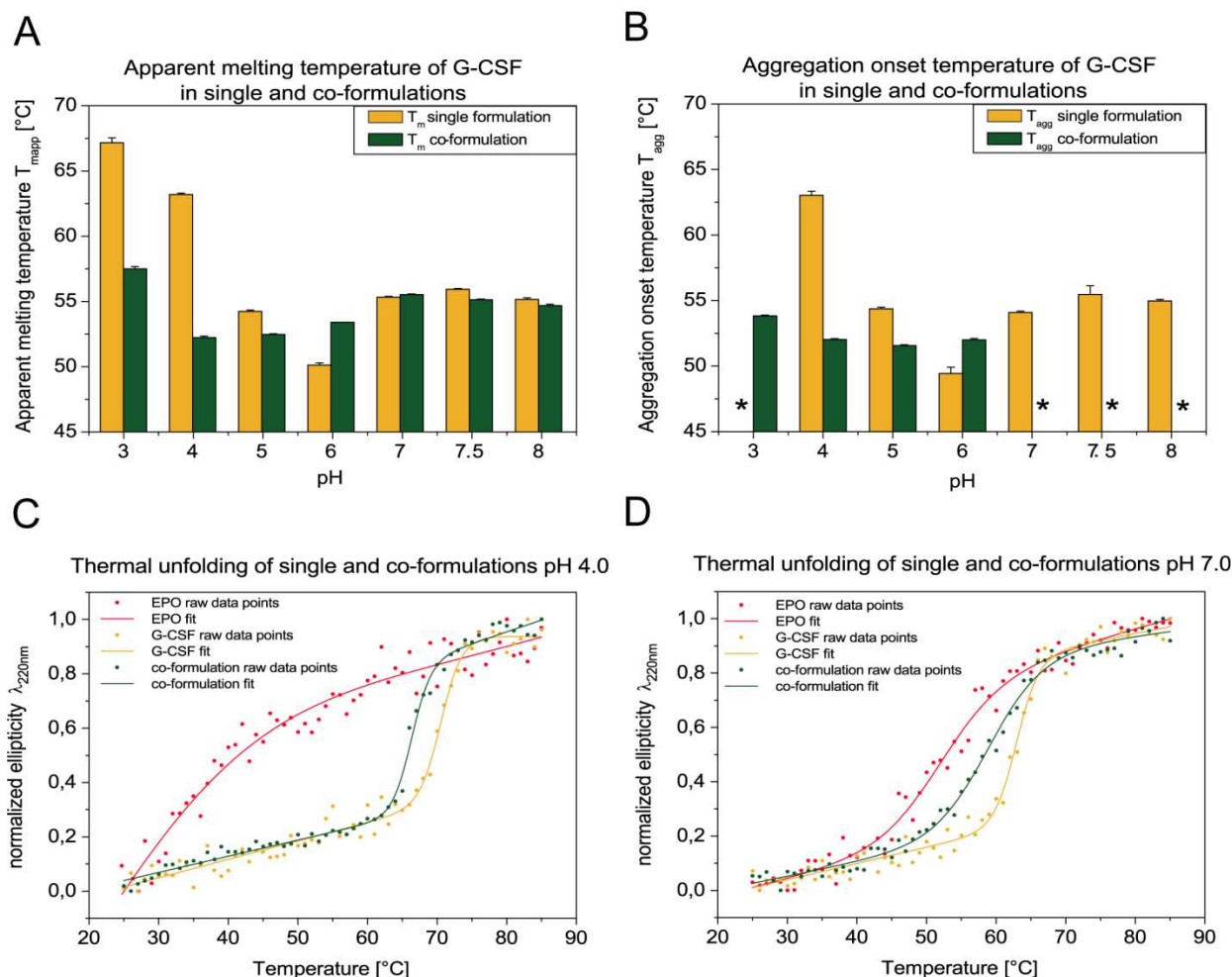


Figure II.1. Results of thermal unfolding for single and co-formulations. (A) T_{mapp} values and (B) T_{agg} values for G-CSF in single and co-formulations determined with nanoDSF. For EPO, no T_{mapp} values could be determined and no aggregation occurred in single formulations of EPO. Asterisks indicate that no aggregation was detected. (C) Transition in ellipticity at 220 nm against temperature for (C) pH 4.0 and (D) pH 7.0, measured by CD-spectroscopy.

II.3.2 Liquid co-formulations pH 7.5

Based on the results of the pH-screen, we identified a pH-range from 7.0-7.5 to be the most feasible starting point for liquid co-formulations, as no aggregation was detected in thermal unfolding experiments in co-formulations (See Fig. II.1B). In a first excipient screen, 12 formulations were prepared and stored at 40 °C for 1 week (See Table II.1A). It was anticipated that the formulation of G-CSF at this pH requires low ionic strength because it has been shown previously that elevated salt concentrations destabilize protein structure and facilitate aggregation of G-CSF.^{21,25} Sugars, sugar alcohols, surfactants, cyclodextrins and

amino acids were tested for potential stabilization of both proteins. Polysorbate 20 was selected as a surfactant because of its common use in protein formulation and reduced risk for autoxidation compared to polysorbate 80, which may be beneficial for the formulation of G-CSF at pH 7.5.^{22,32}

A 1st excipient screen for liquid co-formulations pH 7.5

| formulation # | dialysis buffer | excipients | | |
|---------------|---------------------|---------------------------|---------------------|-----------------------|
| 1 | 10 mM histidine-HCl | - | - | - |
| 2 | 10 mM Tris-HCl | - | - | - |
| 3 | 10 mM histidine-HCl | 280 mM trehalose | - | - |
| 4 | 10 mM histidine-HCl | 0.05 % polysorbate 20 | - | - |
| 5 | 10 mM histidine-HCl | 280 mM trehalose | - | 0.05 % polysorbate 20 |
| 6 | 10 mM histidine-HCl | 280 mM sorbitol | - | 0.05 % polysorbate 20 |
| 7 | 10 mM histidine-HCl | 1 % HP- β -CD | - | 0.05 % polysorbate 20 |
| 8 | 10 mM histidine-HCl | 140 mM arginine-HCl | - | 0.05 % polysorbate 20 |
| 9 | 10 mM histidine-HCl | 140 mM arginine-glutamate | - | 0.05 % polysorbate 20 |
| 10 | 10 mM histidine-HCl | 280 mM proline | - | 0.05 % polysorbate 20 |
| 11 | 10 mM histidine-HCl | 20 mM methionine | - | 0.05 % polysorbate 20 |
| 12 | 10 mM histidine-HCl | 280 mM trehalose | 140 mM arginine-HCl | 0.05 % polysorbate 20 |

B 2nd excipient screen for liquid co-formulations pH 7.5

| formulation # | dialysis buffer | excipients | | |
|---------------|---------------------|------------------|-----------------------|------------------|
| 13 | 10 mM histidine-HCl | 20 mM methionine | 0.01 % polysorbate 20 | - |
| 14 | 10 mM Tris-HCl | 20 mM methionine | 0.01 % polysorbate 20 | - |
| 15 | 10 mM HEPES | 20 mM methionine | 0.01 % polysorbate 20 | - |
| 16 | 10 mM HEPES | 20 mM methionine | 0.01 % polysorbate 20 | 280 mM trehalose |
| 17 | 10 mM HEPES | 20 mM methionine | 0.01 % polysorbate 20 | 280 mM proline |

C excipient screen for lyophilized co-formulations pH 7.5

| formulation # | dialysis buffer | excipients | | |
|---------------|-----------------|------------------|------------------------|------------------|
| 18 | 10 mM HEPES | 20 mM methionine | 0.01 % polysorbate 20 | 280 mM sucrose |
| 19 | 10 mM HEPES | 20 mM methionine | 0.01 % polysorbate 20 | 280 mM sorbitol |
| 20 | 10 mM HEPES | 20 mM methionine | 0.01 % polysorbate 20 | 280 mM trehalose |
| 21 | 10 mM HEPES | 20 mM methionine | 0.005 % polysorbate 20 | 280 mM trehalose |

D excipient screen for lyophilized co-formulations pH 4.0

| formulation # | dialysis buffer | excipients | | |
|---------------|----------------------|------------------------|------------------|-------------|
| 22 | 10 mM sodium citrate | 0.005 % polysorbate 20 | 280 mM sucrose | - |
| 23 | 10 mM sodium citrate | 0.005 % polysorbate 20 | 280 mM trehalose | - |
| 24 | 10 mM sodium citrate | 0.005 % polysorbate 20 | 280 mM mannitol | - |
| 25 | 10 mM sodium citrate | 0.005 % polysorbate 20 | 4 % mannitol | 1 % sucrose |
| 26 | 10 mM sodium citrate | 0.01 % polysorbate 20 | 4 % mannitol | 1 % sucrose |

Table II.1. Co-formulation compositions (A) liquid co-formulations pH 7.5, stored at 40°C for 1 week. (B) liquid co-formulations pH 7.5 stored at 25 °C for 8 weeks. (C) lyophilized co-formulations pH 7.5 stored at 40 °C for 6 weeks. (D) lyophilized co-formulations pH 4.0 after lyophilization. Formulation #26 was stored at 25 °C for 4 weeks.

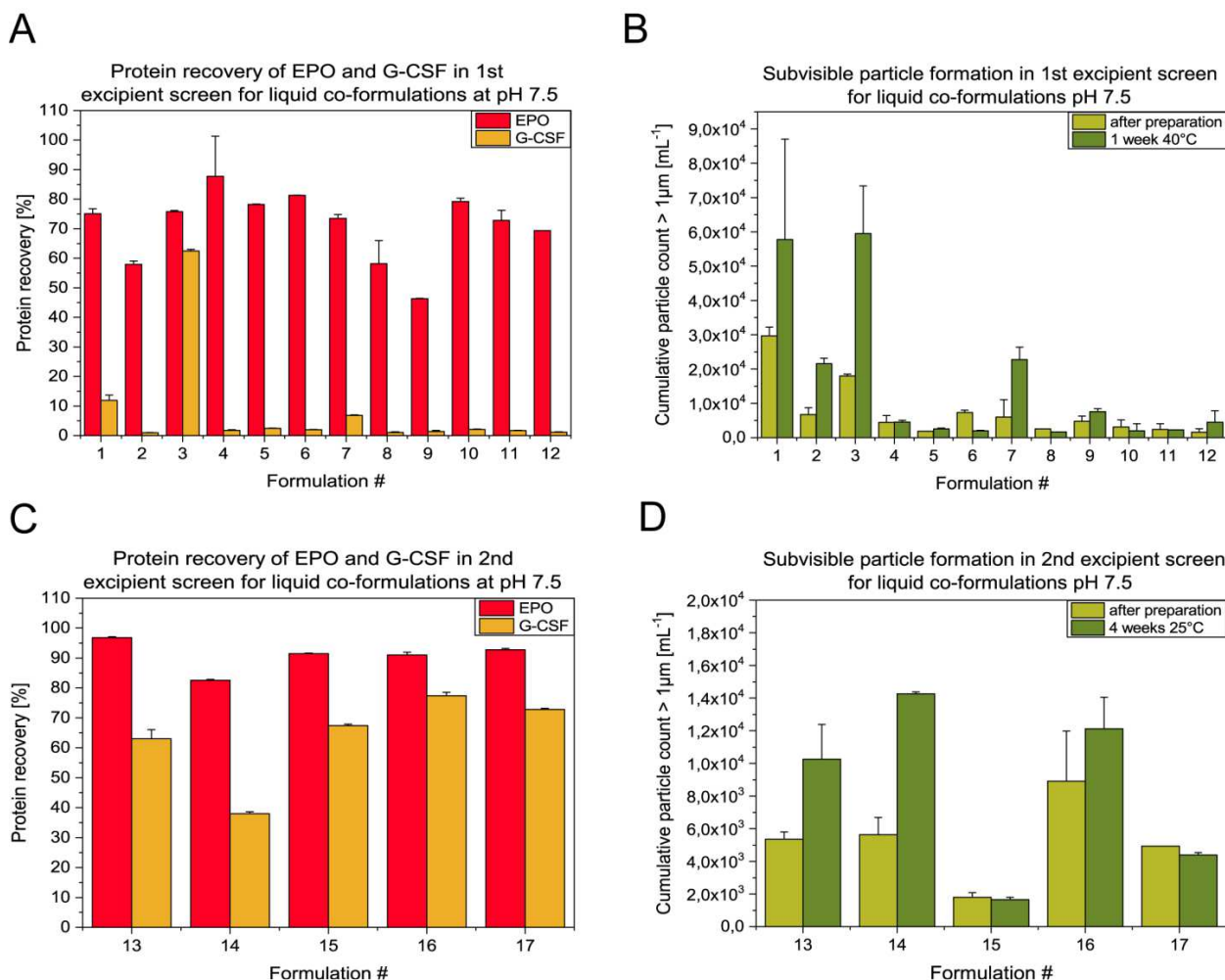


Figure II.2. Results of RP-HPLC and Flow Imaging Microscopy for prepared liquid co-formulations at pH 7.5. (A, B) formulations stored at 40 °C for 1 week. (C, D) formulations stored at 25 °C for 8 weeks. See Table II.1 for formulation compositions.

The results of this first excipient screen are shown in Fig. II.2. In general, no formulation was able to stabilize both proteins in the given conditions. However, first information about potential stabilizing effects was collected. Trehalose significantly increased monomer recovery of G-CSF, while no difference in monomer recovery of EPO and subvisible particle count could be observed. This effect was leveled by the addition of polysorbate 20. It has already been shown that elevated concentrations of polysorbate 20 can accelerate the oxidation of methionine residues in G-CSF, although less than polysorbate 80.²² However, the results also indicate that addition of a surfactant is necessary to prevent protein aggregation because the number of subvisible particles increased significantly in absence of polysorbate 20. The addition of methionine did not prevent oxidation, which indicates the severe sensitivity of G-CSF towards chemical degradation at pH 7.5 (data not shown). The nanoDSF only detects heat-induced conformational changes and aggregation but does not take into

account chemical degradation. Still, the surfactant-free formulation #3 indicated that a co-formulation may be possible at this pH if the concentration of polysorbate 20 is set high enough to prevent particle formation but low enough to prevent G-CSF degradation. Therefore, a second formulation screen was performed at pH 7.5, where the concentration of polysorbate 20 was reduced to 0.01 % (w/v), which is still above the CMC (Critical Micelle Concentration, ~0.007 % w/v).³³ The formulations are shown in Table II.1B and the respective results in Figs. II.2C and II.2D. The storage temperature was reduced to 25 °C to allow better differentiation between the different excipients and to prevent overstressing. Methionine was added to each formulation to reduce oxidation as far as possible, and HEPES was selected because it improved the stability of G-CSF at physiological pH in previous studies.^{34,35} Trehalose was selected because of its performance in the first excipient screen and proline was selected because previous studies indicate unspecific mechanisms for protein refolding, which may reduce the formation of unstable conformational intermediates of G-CSF at pH 7.5.^{36,37}

No formulation was able to sufficiently stabilize both proteins upon storage at 25 °C for 8 weeks. However, HEPES increased monomer recovery and decreased counts of subvisible particles compared to histidine and Tris. Both trehalose and proline slightly increased the monomer recovery of G-CSF, but concurrently increased particle formation. Flow-Imaging analysis also revealed the formation of large protein fibers > 25 µm in each formulation, probably caused by an insufficient amount of surfactant. Based on these results, we concluded that the surfactant concentration cannot be reduced further without causing the formation of protein fibers and that the chemical stability of G-CSF at pH 7.5 is insufficient to obtain stable liquid co-formulations. Hence, lyophilization was tested as a tool to enable co-formulation of both proteins at pH 7.5 in the solid state.

II.3.3 Lyophilized co-formulations pH 7.5

The compositions of the lyophilized co-formulations are shown in Table II.1C. Cycle I (See II.2.3.) was used for this formulation screen. Four combinations of HEPES, methionine, sugar/sugar alcohol and polysorbate 20 were tested. The formulations were stored at 40 °C for 6 weeks.

The results are shown in Figs. II.3A and II.3B. Protein recovery was significantly improved for G-CSF, but no formulation was able to stabilize both proteins to achieve > 95 % monomer recovery after reconstitution. No significant difference in subvisible particle formation was observed between the co-formulations. Further excipients (arginine hydrochloride, proline, phenylalanine and combinations) were tested, but had no positive

effect on monomer recovery (data not shown). Still, fiber formation of G-CSF was not inhibited by any formulation. Therefore, we concluded that it is not possible to stabilize both proteins at pH 7.5 because of the high sensitivity of G-CSF during freezing and lyophilization in this condition. Although the EPO structure is perturbed at pH 4.0,^{16,17,38} we hypothesized that a co-formulation of both proteins at pH 4.0 might be possible, assuming that the unfolding of EPO is reversible and aggregation can be suppressed. The short-time exposure of EPO to pH 4.0 in the liquid state during dialysis and processing may not necessarily induce significant aggregation. Upon reconstitution with a reconstitution medium with sufficient buffering capacity, a pH-shift from pH 4.0 to pH 7.0 may refold EPO without affecting the stability of G-CSF negatively. Using this approach, it would only be necessary to stabilize G-CSF at pH 7.0 for a short time after reconstitution. So, the next step was the development of a lyophilized co-formulation at pH 4.0.

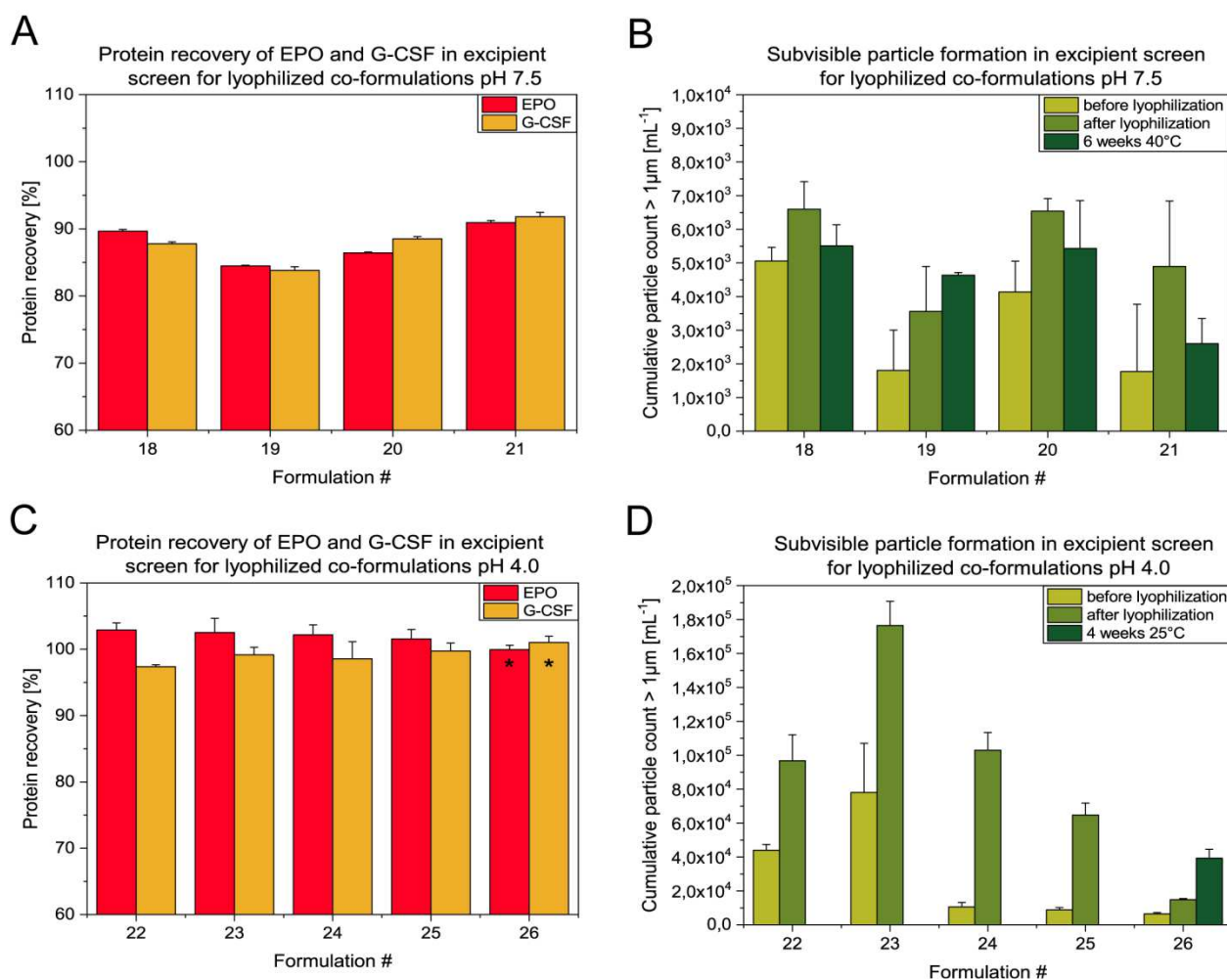


Figure II.3. Results of RP-HPLC and Flow Imaging Microscopy for prepared lyophilized co-formulations. (A, B) formulations pH 7.5 stored at 40 °C for 6 weeks using Cycle I. (C, D) formulations pH 4.0 after lyophilization using Cycle II. Asterisks indicate that recovery for formulation #26 is given after storage at 25 °C for 4 weeks. See Table II.1 for formulation compositions.

II.3.4 Lyophilized co-formulations pH 4.0

Based on previous results, five formulations were prepared with lyophilization cycle II (See Table II.1D).

The results are presented in Figs. II.3C and II.3D. The monomer recovery in RP-HPLC was > 95 % for both proteins in all formulations. Hence, we concluded that independent of further excipients and surfactant concentration, G-CSF can be stabilized in lyophilized co-formulations at pH 4.0. Subvisible particle analysis showed increased particle formation, which may be related to electrostatic attraction between the differently charged proteins at pH 4.0. Formulation #26 with 0.01 % polysorbate 20 showed the lowest subvisible particle numbers and was therefore stored at 25 °C for 4 weeks. The monomer recover was still high after storage, but elevated subvisible particle numbers indicated that higher surfactant concentrations may be necessary for sufficient stabilization of both proteins at pH 4.0. Therefore, further optimization of formulation, composition, lyophilization cycle and reconstitution medium was performed.

II.3.5 Lyophilized co-formulations pH 4.0 with optimized reconstitution medium

In the next step, four co-formulations were prepared using a rather aggressive lyophilization cycle with an additional annealing step to ensure complete crystallization of the bulking agent mannitol (Cycle III, see Table II.2). As mentioned in II.2.2, all excipients except the surfactant were already added to the dialysis buffer, and a surfactant was added after dialysis from a stock solution in the respective buffer system. WFI (water for injection) was used as a reference reconstitution medium and compared to 3 reconstitution media: 20 mM sodium phosphate pH 7.0, 100 mM HEPES pH 7.0 and 100 mM arginine phosphate pH 7.0. After reconstitution, the samples for CD spectroscopy were directly analyzed, while the vials for analysis by RP-HPLC, HP-SEC and Flow Imaging Microscopy were stored at 25 °C for 1 hour before analysis.

As shown in Fig. II.4, the monomer recovery in RP-HPLC and HP-SEC was > 95 % for all formulations after lyophilization. Hence, we concluded that it is possible to stabilize EPO in a lyophilized co-formulation at pH 4.0 without inducing protein aggregation. The reconstitution medium had no significant impact on the monomer recovery. Subvisible particle formation was low after reconstitution with WFI or 20 mM sodium phosphate pH 7.0, while reconstitution with HEPES and particularly arginine buffers promoted particle formation. No fiber formation of G-CSF was detected for any formulation. Based on these results, it can be shown that G-CSF is stable in reconstituted solutions at pH 7.0 for at least one hour and the pH-shift does not trigger degradation. Also, the unfolding of EPO is reversible by an

appropriate reconstitution medium, because the almost complete loss of tertiary structure as monitored by Near-UV CD spectroscopy can be reversed by the pH shift upon reconstitution with any reconstitution buffer, but not with WFI (data not shown for these formulations, see II.3.6. for refolding in final co-formulation). The secondary structure of G-CSF is not negatively affected and the regained structure of EPO upon reconstitution with 20 mM sodium phosphate pH 7.0 can also be observed in co-formulations.

Excipient screen for buffered reconstitution medium

| formulation # | excipients | | | | | reconstitution medium |
|---------------|---------------------|------------------|----------------------|--------------|-------------|----------------------------------|
| 27 | 2 mM sodium citrate | 20 mM methionine | 0.1 % polysorbate 20 | 4 % mannitol | 1 % sucrose | WFI |
| 28 | 2 mM sodium citrate | 20 mM methionine | 0.1 % polysorbate 20 | 4 % mannitol | 1 % sucrose | 20 mM sodium phosphate pH 7.0 |
| 29 | 2 mM sodium citrate | 20 mM methionine | 0.1 % polysorbate 20 | 4 % mannitol | 1 % sucrose | 100 mM HEPES pH 7.0 |
| 30 | 2 mM sodium citrate | 20 mM methionine | 0.1 % polysorbate 20 | 4 % mannitol | 1 % sucrose | 100 mM arginine phosphate pH 7.0 |

Table II.2. Lyophilized co-formulations at pH 4.0 with optimized reconstitution volume.

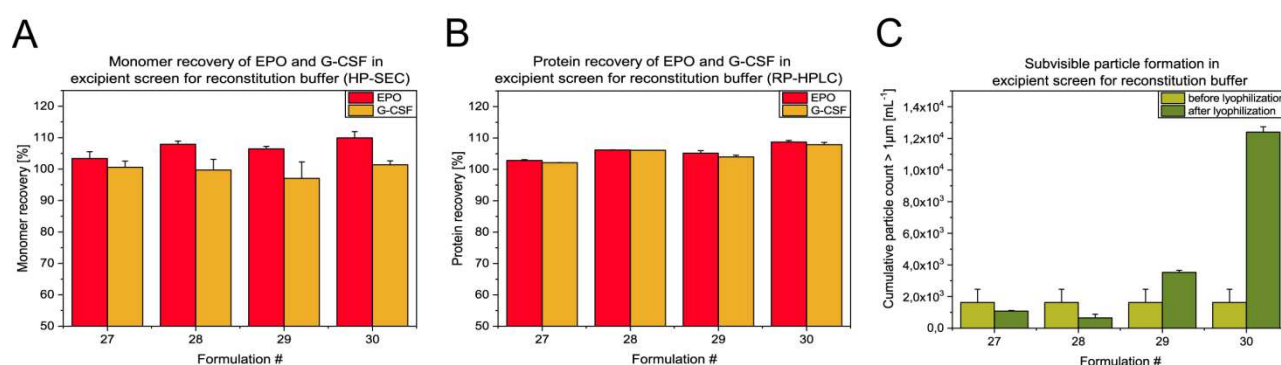


Figure II.4. Results of HP-SEC (A), RP-HPLC (B) and Flow Imaging Microscopy (C) for prepared lyophilized co-formulations pH 4.0 with optimized reconstitution volume. See Table II.2 for formulation

II.3.6 Final co-formulation of EPO and G-CSF

Based on these results a stability study was set up to investigate the stability of the prepared co-formulations at different temperatures up to 12 months. The final co-formulation consisted of 2 mM sodium citrate, 4 % mannitol, 1 % sucrose, 20 mM methionine and 0.1 % polysorbate 20, pH 4.0. 50 mM sodium phosphate pH 7.0 was selected as a reconstitution buffer. Single formulations of both proteins were prepared as a comparison.

As shown in Fig. II.5, Near-UV CD spectroscopy confirmed the refolding of EPO in single and co-formulations upon reconstitution with 50 mM sodium phosphate pH 7.0. The buffer capacity was still not high enough to reach pH 7.0 but a comparison to the reference indicated refolding of the formerly unfolded EPO. In addition, we were able to show that the co-formulation spectrum could be calculated from the respective single protein spectra. The

predicted co-formulation spectrum was in line with the calculation and indicated refolding of EPO in the co-formulation.

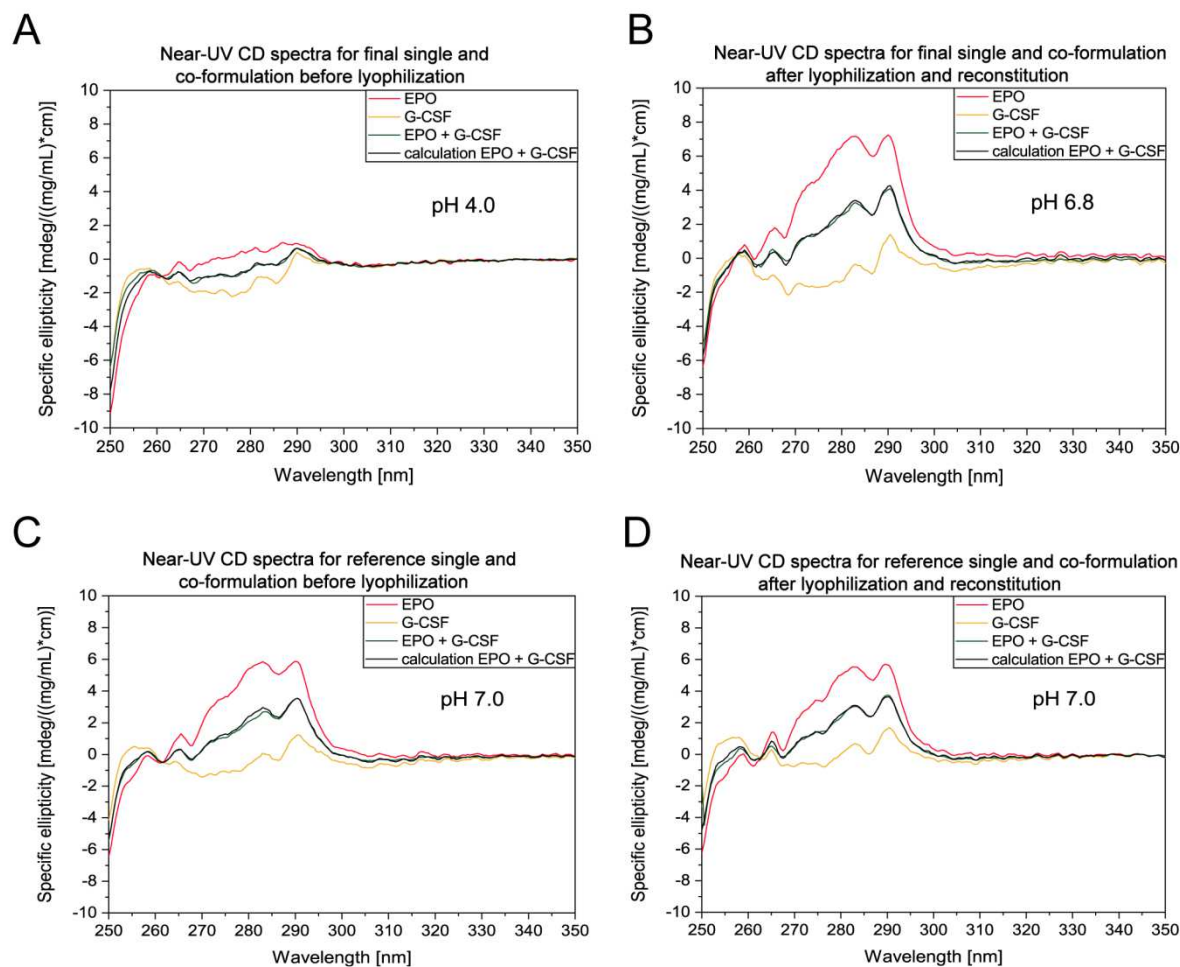


Figure II.5. Results of Near-UV CD spectroscopy for the final co-formulation before (A) and after lyophilization (B). The reference formulation (C, D) consisted of 10 mM HEPES, 4 % mannitol, 1 % sucrose, 20 mM methionine, 0.1 % polysorbate 20, pH 7.0.

The results for the stability study of the final co-formulation are presented in Figs. II.7 and II.8. No differences between the single and co-formulations were observed in HP-SEC, RP-HPLC, Flow Imaging Microscopy and Near-UV CD spectroscopy before and after lyophilization, and after storage at 4 °C for 12 months (See Figs. II.5 and II.7). For both proteins, monomer recovery was > 95 % in HP-SEC and RP-HPLC in the single and co-formulations. After storage at 25 °C for up to 6 months, the co-formulation showed comparable monomer and protein recovery compared to the single formulation of EPO and significantly higher monomer recovery in HP-SEC and protein recovery in RP-HPLC compared to the single formulation of G-CSF. After storage at 25 °C or 40 °C for 3 months, no difference was detected for EPO in single and co-formulations, while G-CSF showed significantly higher monomer and protein recovery as well as significantly reduced particle

counts in the co-formulation (See Figs. II.6 and II.7). Figs. II.6C and II.6D illustrate the stabilizing effect of EPO on G-CSF monomer recovery in HP-SEC and protein recovery in RP-HPLC in the co-formulation compared to the single formulation. It is further interesting to note that after storage at 25 °C or 40 °C, the reconstituted single formulation of G-CSF appeared cloudy, while the reconstituted co-formulation remained clear (See Fig. II.8B).

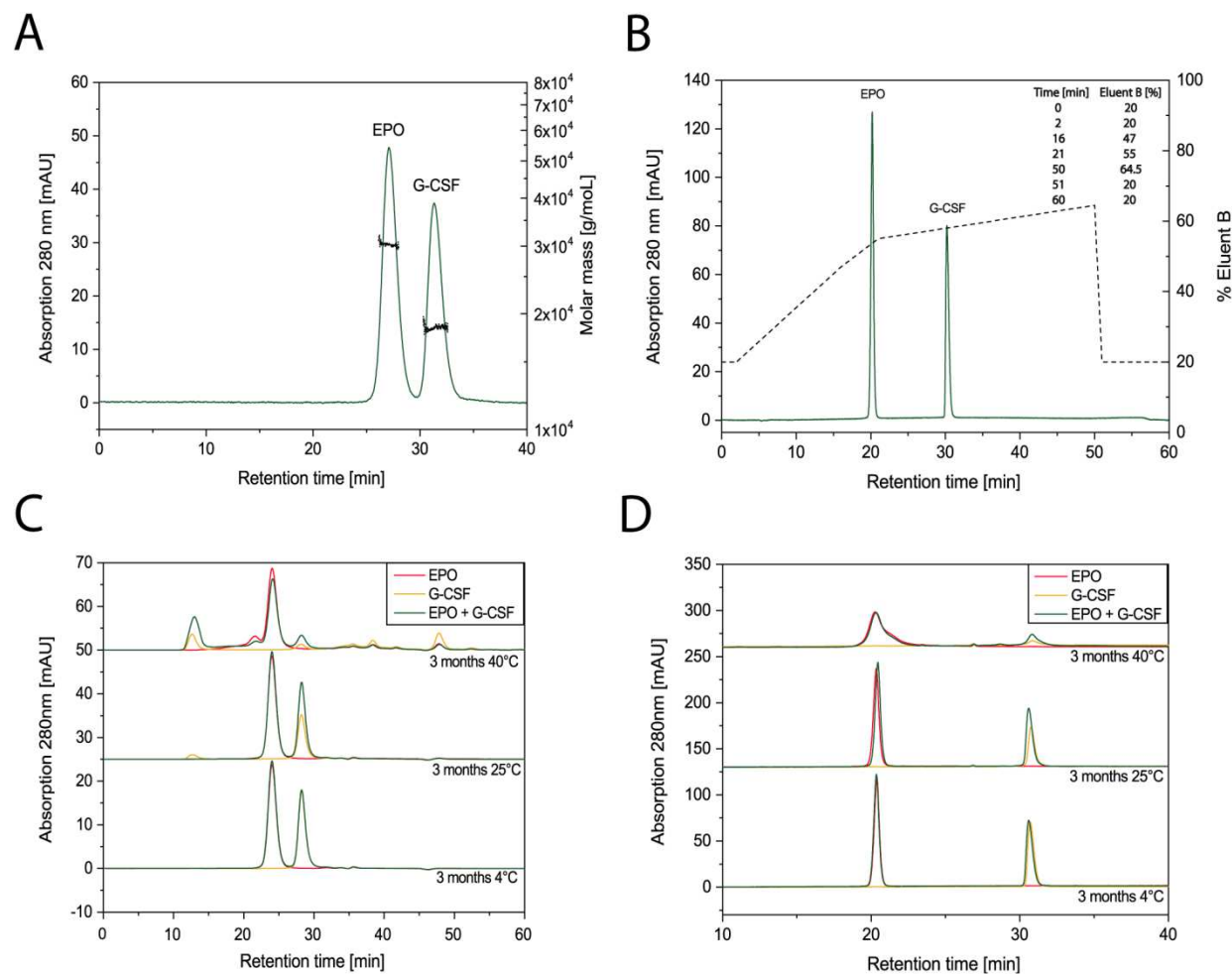


Figure II.6. (A) Example HP-SEC-MALS chromatogram for the separation of the single proteins in co-formulations. The identities of the protein peaks were confirmed by molar mass measurements via MALS. For SEC-MALS measurements, 50 μg of each protein were injected to achieve an acceptable signal-to-noise ratio for molecular weight determination. (B) Example RP-HPLC chromatogram for a co-formulation of EPO and G-CSF. The applied gradient for RP-HPLC is plotted on the second axis and also given in numbers. (C) Example HP-SEC chromatograms from the stability study of the final co-formulation (green) in comparison to the single formulations (red and yellow). (D) Example RP-HPLC chromatograms from the stability study of the final co-formulation (green) in comparison to the single formulations (red and yellow).

Although it was already reported that proteins can act as excipients for hydrophobic protein drugs,³⁹ it was surprising that G-CSF was stabilized by the presence of low concentrations of EPO. It is further interesting to note that directly after lyophilization, no difference in protein stability was detected between single and co-formulations of G-CSF by

any of the applied methods (See Fig. II.7). The differences in the stability of G-CSF in single and co-formulations arose during storage of the lyophilization cake. It is tempting to discuss several possible mechanisms for the stabilization of G-CSF:

First, the presence of EPO could cause a steric hindrance for the aggregation-prone residues of G-CSF and statistically reduce contact events of these residues. However, this explanation is only reasonable if G-CSF does not co-aggregate with EPO in the co-formulation. Until now, it is unclear, if the subvisible particles of the co-formulation consist of pure G-CSF or both proteins. The recovery rates of G-CSF in HP-SEC and RP-HPLC were increased by the presence of EPO, while the presence of G-CSF only had little effect on the recovery rates of EPO. This is a slight indication that the presence of EPO reduces particle formation of G-CSF rather than causing co-aggregation and formation of mixed protein particles. However, additional experiments are required to demonstrate the presence or absence of mixed aggregates in the co-formulation.

Second, an electrostatic attraction of both proteins towards each other can be expected based on the different zeta potentials and the low ionic strength of the formulation, as discussed in section II.3.1. As the colloidal stability of native G-CSF is high at low pH and low ionic strength,²¹ it is likely that the protein aggregation rate in the given formulation is limited by the conformational stability of G-CSF. G-CSF easily aggregates at interfaces,⁴⁰ most likely due to surface-induced unfolding and subsequent aggregation of partially unfolded intermediates.⁴¹ The electrostatic attraction towards EPO could reduce detrimental interactions of G-CSF with interfaces. Subsequently this would reduce the number of partially unfolded, aggregation-prone species of G-CSF, without triggering the co-aggregation together with EPO based on the specificity of the aggregation-prone regions of the single proteins. The reduced interface-mediated unfolding could also explain the improved chemical stability of G-CSF in co-formulation, although the impact of protein conformation on oxidation of methionine residues in proteins remains poorly understood.⁴²⁻⁴⁵ A characterization of the protein conformations in the solid state by solid state HDX-MS could be a valuable approach to study conformational changes of G-CSF in single and co-formulation in the lyophilized cake during storage.⁴⁶

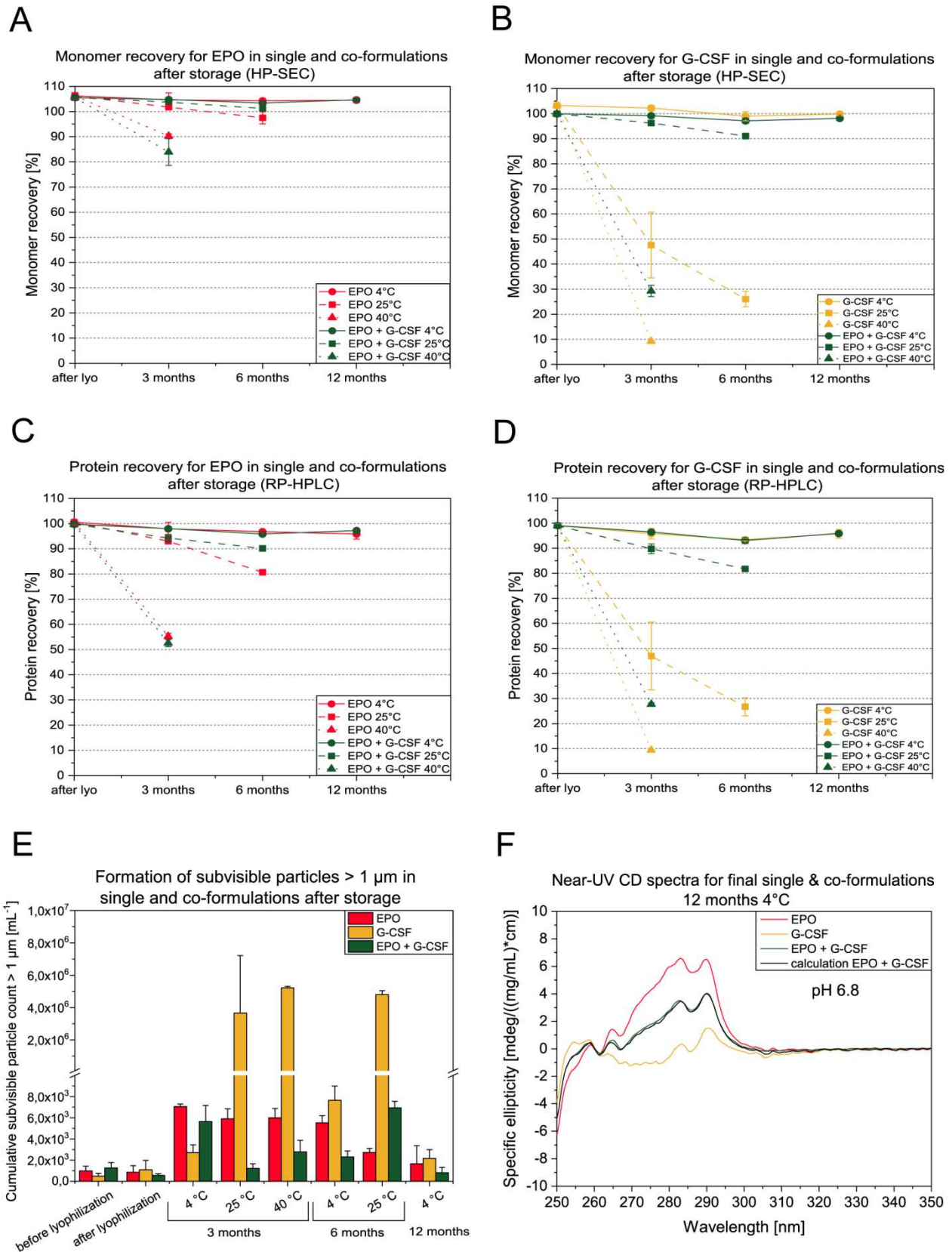


Figure II.7. Results of HP-SEC (A, B), RP-HPLC (C, D), Flow Imaging Microscopy (E) and Near-UV CD spectroscopy (F) for the conducted stability study of the final co-formulation.

Finally, the heavily glycosylated EPO could also provide an additional amorphous matrix in the lyophilization cake and provide hydrophilic groups (e.g. the sialic acids), that form additional hydrogen bonds and subsequently stabilize the native folding state of G-CSF. This explanation is supported by the results of the solid state analysis. The additional endothermic event at about 150 °C in DSC as well as the additional peaks in XRD that arose after storage at 25 °C for 12 months indicate the presence of crystalline sucrose (See Fig. II.9).⁴⁷ The lyophilization cakes exhibited macroscopic cake shrinkage at elevated storage temperature, but not upon storage at 2-8 °C (See Fig. II.8), and these cake contractions can indicate cake

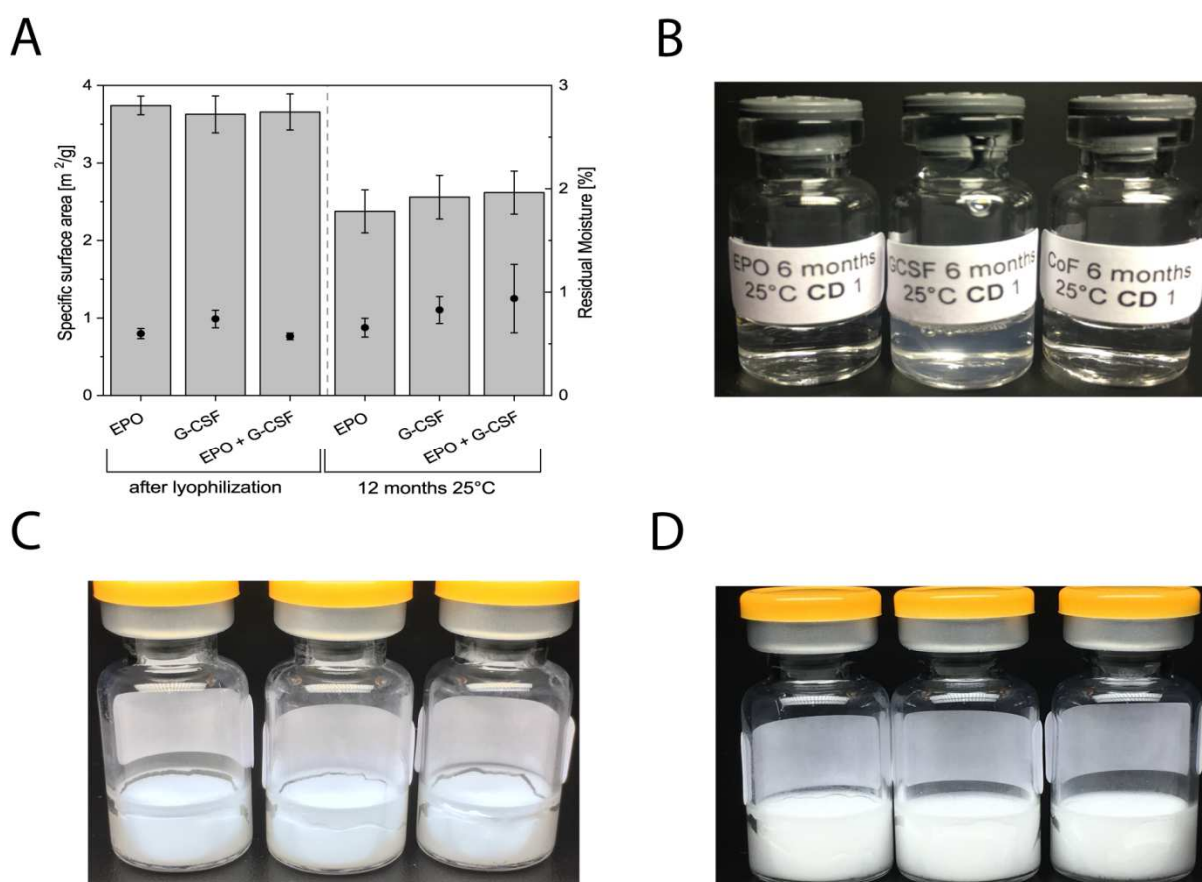


Figure II.8. Results of Gas adsorption and Karl Fischer titration for single and co-formulations after lyophilization and after storage at 25 °C for 12 months (A). Freshly reconstituted solutions of EPO (left), G-CSF (middle) and the co-formulation (right) after storage at 25 °C for 6 months (B). Lyophilization cakes for EPO (left), G-CSF (middle) and the co-formulation (right) after storage at 25 °C for 12 months (C). Lyophilization cakes for EPO (left), G-CSF (middle) and the co-formulation (right) after storage at 4 °C for 12 months (D).

collapse,⁴⁸ which is further indicated by the reduced specific surface areas (SSA) measured by gas adsorption (See Fig. II.8). Both cake shrinkage and reduced SSA could be directly caused by sucrose crystallization. If sucrose crystallizes at elevated temperatures during storage, the stabilization of G-CSF by water replacement is compromised.⁴⁹ It has already been discussed

that several proteins can stabilize enzymes by water replacement during freeze-drying,⁵⁰ although not as effective as disaccharides due to steric hindrance. Thus, the heavily glycosylated EPO could stabilize G-CSF by water replacement in this specific formulation, where sucrose crystallizes during storage at elevated temperatures due to increased monomer mobility. Besides crystallization, also hydrolysis of sucrose into its components glucose and fructose during storage at elevated temperatures can be anticipated. Before lyophilization, the used formulation has a pH value of 4.0, and the water content of the lyophilization cakes is about 0.5 – 1 % (See Fig. II.8). It has previously been studied that amorphous sucrose gets easily hydrolyzed in the solid state by citric acid at elevated temperatures even in low levels of residual moisture.⁵¹ Thus, it can be anticipated that G-CSF remains stable in single formulations upon storage at 2-8 °C because sucrose does not crystallize or degrade into glucose and fructose. However, no data for the solid state analysis at 2-8 °C is available.

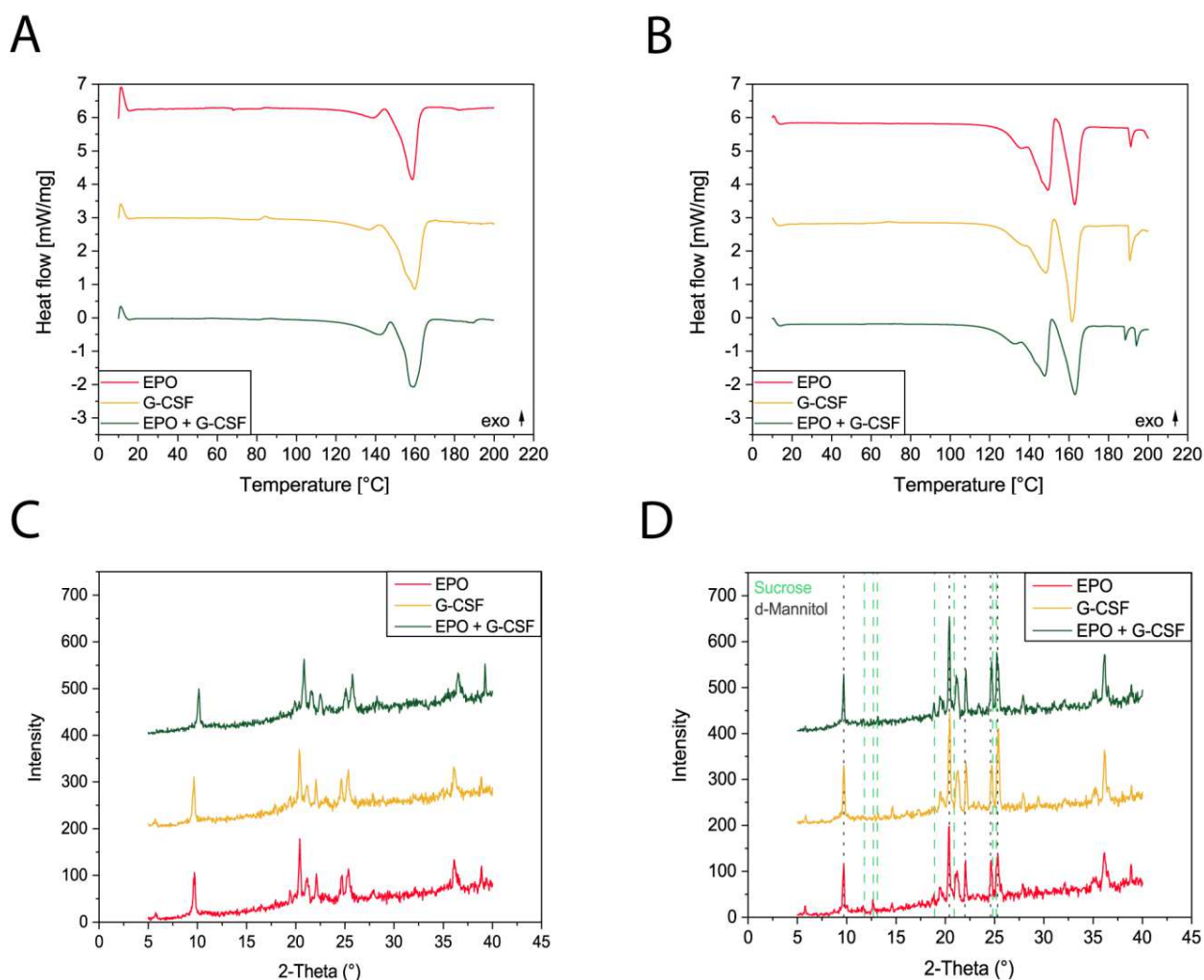


Figure II.9. Results of DSC analysis for the single and co-formulations after lyophilization (A) and after storage at 25 °C for 12 months (B). Results of XRD analysis for the single and co-formulation after lyophilization (C) and after storage at 25 °C for 12 months (D). The dashed green lines reflect characteristic diffraction peaks for sucrose (D), and the dotted grey lines reflect the peaks for δ -Mannitol (D), both taken from Horn et al.⁵²

II.4 Conclusion

In this study, we present a systematic approach to stabilize two physicochemically very different protein drugs in one formulation. It is shown that the most stable formulation conditions of the single proteins would exclude each other due to the high sensitivity of the single proteins towards certain solution conditions. However, the knowledge and exploitation of the individual stability profiles still allows the co-formulation of such different proteins as EPO and G-CSF. The screen for an optimal pH-value via nanoDSF and CD-spectroscopy led to the liquid formulation at pH 7.5, where oxidation and aggregation of G-CSF could not be inhibited. Lyophilization at pH 7.5 improved monomer recovery of both proteins but was not able to maintain > 95 % monomer and protein recovery for both proteins after reconstitution. Lyophilization of formulations with pH 4.0 increased the stability of both proteins but led to unfolding of EPO. Although EPO is unfolded at pH 4.0, the co-formulation provides sufficient stabilization of the respective proteins at pH 4.0 in the solid state during storage, while the subsequent pH-shift upon reconstitution with medium having pH 7.0 allows refolding of EPO without inducing aggregation or oxidation at pH 7.0 in the liquid state. Although only little work has been published about the impact of the reconstitution medium on protein stability,^{53,54} it turned out that selection of the reconstitution medium is the key to enable a stable co-formulation of EPO and G-CSF. We further demonstrate that a protein drug can be stabilized in the solid state through co-formulation with a second protein drug. However, the impact of this co-formulation approach on biological activity and toxicity of both proteins has not yet been studied. Future work should focus on the development of *in vivo* assays which will allow the testing for toxicity and biological activity of proteins in co-formulations.

II.5 References

- (1) Mueller, C.; Altenburger, U. & Mohl, S. Challenges for the pharmaceutical technical development of protein coformulations. *J. Pharm. Pharmacol.* **2018**, *70* (5), 666–674. <https://doi.org/10.1111/jphp.12731>.
- (2) Hamizi, S. *et al.* Subcutaneous trastuzumab: Development of a new formulation for treatment of HER2-positive early breast cancer. *Onco. Targets. Ther.* **2013**, *6*, 89–94. <https://doi.org/10.2147/OTT.S27733>.
- (3) Fernandes, P. M. & Taforo, T. Formulations for lipophilic IL-2 proteins, U.S. Patent, No. 4992271, **1991**.
- (4) Lipiäinen, T. *et al.* Formulation and stability of cytokine therapeutics. *J. Pharm. Sci.* **2015**, *104* (2), 307–326. <https://doi.org/10.1002/jps.24243>.
- (5) Kirschbrown, W. P. *et al.* Development of a subcutaneous fixed-dose combination of pertuzumab and trastuzumab: Results from the phase Ib dose-finding study. *J. Clin. Pharmacol.* **2018**, No. October, 1–15. <https://doi.org/10.1002/jcph.1362>.

- (6) Du, J. & Shah, A. Compositions comprising coformulations of Anti-PD-L1 and Anti-CTLA-4 antibodies, U.S. Patent Application, No. 15/495388, **2017**.
- (7) Perreault, L. *et al.* Optimizing fixed-ratio combination therapy in type 2 diabetes. *Adv. Ther.* **2019**, *36* (2), 265–277. <https://doi.org/10.1007/s12325-018-0868-9>.
- (8) Li, M. *et al.* An ambient temperature-stable antitoxin of nine co-formulated antibodies for botulism caused by serotypes A, B and E. *PLoS One* **2018**, *13* (5), 1–16. <https://doi.org/10.1371/journal.pone.0197011>.
- (9) Jädersten, M. *et al.* Erythropoietin and granulocyte-colony stimulating factor treatment associated with improved survival in myelodysplastic syndrome. *J. Clin. Oncol.* **2008**, *26* (21), 3607–3613. <https://doi.org/10.1200/JCO.2007.15.4906>.
- (10) Hellstrom-Lindberg, E. *et al.* Treatment of anemia in myelodysplastic syndromes with granulocyte colony-stimulating factor plus erythropoietin: Results from a randomized phase II study and long-term follow-up of 71 Patients. *Blood* **1998**, *92* (1), 68–75. <https://doi.org/10.1021/es803023a>.
- (11) Balleari, E. *et al.* Erythropoietin plus granulocyte colony-stimulating factor is better than erythropoietin alone to treat anemia in low-risk myelodysplastic syndromes: Results from a randomized single-centre study. *Ann. Hematol.* **2006**, *85* (3), 174–180. <https://doi.org/10.1007/s00277-005-0044-6>.
- (12) Hart, C. *et al.* EPO in combination with G-CSF improves mobilization effectiveness after chemotherapy with ifosfamide, epirubicin and etoposide and reduces costs during mobilization and transplantation of autologous hematopoietic progenitor cells. *Bone Marrow Transplant.* **2009**, *43* (3), 197–206. <https://doi.org/10.1038/bmt.2008.315>.
- (13) Shin, Y. K. & Cho, S. R. Exploring erythropoietin and G-CSF combination therapy in chronic stroke patients. *Int. J. Mol. Sci.* **2016**, *17* (4), 463. <https://doi.org/10.3390/ijms17040463>.
- (14) El-Ganzoury, M. M. *et al.* Enteral granulocyte-colony stimulating factor and erythropoietin early in life improves feeding tolerance in preterm infants: A randomized controlled trial. *J. Pediatr.* **2014**, *165* (6), 1140–1145.e1. <https://doi.org/10.1016/j.jpeds.2014.07.034>.
- (15) Jelkmann, W. Erythropoietin: Structure, control of production, and function. *Physiol. Rev.* **1992**, *72* (2), 449–489.
- (16) Davis, J. M. *et al.* Characterization of recombinant human erythropoietin produced in chinese hamster ovary cells. *Biochemistry* **1987**, *26* (9), 2633–2638. <https://doi.org/10.1021/bi00383a034>.
- (17) Endo, Y. *et al.* Heat-induced aggregation of recombinant erythropoietin in the intact and deglycosylated states as monitored by gel permeation chromatography combined with a low-angle laser light scattering technique. *J. Biochem.* **1992**, *112* (5), 700–706. <https://doi.org/10.1093/oxfordjournals.jbchem.a123961>.
- (18) Lah, J. *et al.* Erythropoietin unfolding: Thermodynamics and its correlation with structural features. *Biochemistry* **2005**, *44* (42), 13883–13892. <https://doi.org/10.1021/bi0512952>.
- (19) Ria, R. *et al.* Filgrastim, lenograstim and pegfilgrastim in the mobilization of peripheral blood progenitor cells in patients with lymphoproliferative malignancies. *Clin. Exp. Med.* **2015**, *15* (2), 145–150. <https://doi.org/10.1007/s10238-014-0282-9>.
- (20) Krishnan, S *et al.* Aggregation of granulocyte colony stimulating factor under physiological conditions: Characterization and thermodynamic inhibition. *Biochemistry* **2002**, *41* (20), 6422–6431. <https://doi.org/10.1021/bi012006m>.
- (21) Chi, E. Y. *et al.* Roles of conformational stability and colloidal stability in the aggregation of recombinant human granulocyte colony-stimulating factor. *Protein Sci.* **2003**, *12* (5), 903–913. <https://doi.org/10.1110/ps.0235703>.

- (22) Herman, A. C.; Boone, T. C. & Lu, H. S. Characterization, formulation, and stability of Neupogen® (Filgrastim), a recombinant human granulocyte-colony stimulating factor. In: *Pearlman R. & Wang Y.J. (eds). Formulation, Characterization, and Stability of Protein Drugs: Case Histories. Pharmaceutical Biotechnology vol 9; Springer, Boston, MA, USA, 2002*, 303–328. https://doi.org/10.1007/0-306-47452-2_7.
- (23) Savitzky, A. & Golay, M. J. E. Smoothing and differentiation of data by simplified least squares procedures. *Anal. Chem.* **1964**, *36* (8), 1627–1639. <https://doi.org/10.1021/ac60214a047>.
- (24) Niklasson, M. *et al.* Robust and convenient analysis of protein thermal and chemical stability. *Protein Sci.* **2015**, *24*, 2055–2062. <https://doi.org/10.1002/pro.2809>.
- (25) Yamazaki, K. *et al.* Effects of ionic strength on the thermal unfolding process of granulocyte-colony stimulating factor. *J. Biochem.* **2006**, *139* (1), 41–49. <https://doi.org/10.1093/jb/mvj001>.
- (26) Ablinger, E.; Leitgeb, S. & Zimmer, A. Differential scanning fluorescence approach using a fluorescent molecular rotor to detect thermostability of proteins in surfactant-containing formulations. *Int. J. Pharm.* **2013**, *441* (1–2), 255–260. <https://doi.org/10.1016/j.ijpharm.2012.11.035>.
- (27) Sanchez-Ruiz, J. M. Theoretical analysis of Lumry-Eyring models in differential scanning calorimetry. *Biophys. J.* **1992**, *61* (4), 921–935. [https://doi.org/10.1016/S0006-3495\(92\)81899-4](https://doi.org/10.1016/S0006-3495(92)81899-4).
- (28) Robinson, M. J. *et al.* T_m-values and unfolded fraction can predict aggregation rates for granulocyte colony stimulating factor variant formulations but not under predominantly native conditions. *Mol. Pharm.* **2018**, *15* (1), 256–267. <https://doi.org/10.1021/acs.molpharmaceut.7b00876>.
- (29) Roberts, C. J.; Das, T. K. & Sahin, E. Predicting solution aggregation rates for therapeutic proteins: Approaches and challenges. *Int. J. Pharm.* **2011**, *418* (2), 318–333. <https://doi.org/10.1016/j.ijpharm.2011.03.064>.
- (30) Ricci, M. S. *et al.* pH dependence of structural stability of interleukin-2 and granulocyte colony-stimulating factor. *Protein Sci.* **2003**, *12* (5), 1030–1038. <https://doi.org/10.1110/ps.0230103.1993>.
- (31) Kolvenbach, C. *et al.* Granulocyte-colony stimulating factor maintains a thermally stable, compact, partially folded structure at pH 2. *J. Pept. Res.* **2009**, *50* (4), 310–318. <https://doi.org/10.1111/j.1399-3011.1997.tb01472.x>.
- (32) Kerwin, B. A. Polysorbates 20 and 80 used in the formulation of protein biotherapeutics: Structure and degradation pathways. **2008**, *97* (8), 12–17. <https://doi.org/10.1002/jps>.
- (33) Wan, L. S. C. & Lee, P. F. S. CMC of polysorbates. *J. Pharm. Sci.* **1974**, *63* (1), 136–137.
- (34) Canning, P. C.; Kamicker, B. J. & Kasraian, K. Stabilized protein compositions. US Patent 6,979,442 B1, **2005**.
- (35) Kasraian, K. *et al.* Sustained in vivo activity of recombinant bovine granulocyte colony stimulating factor (rbG-CSF) using HEPES buffer. *Pharm. Dev. Technol.* **2001**, *6* (3), 441–447. <https://doi.org/10.1081/PDT-100002252>.
- (36) Samuel, D. *et al.* Proline inhibits aggregation during protein refolding. *Protein Sci.* **2000**, *9* (2), 344–352. <https://doi.org/10.1110/ps.9.2.344>.
- (37) Ignatova, Z. & Gierasch, L. M. Inhibition of protein aggregation in vitro and in vivo by a natural osmoprotectant. *Proc. Natl. Acad. Sci. U. S. A.* **2006**, *103* (36), 13357–13361. <https://doi.org/10.1073/pnas.0603772103>.
- (38) Narhi, L. O. *et al.* The effect of carbohydrate on the structure and stability of erythropoietin. *J. Biol. Chem.* **1991**, *266* (34), 23022–23026.
- (39) Hawe, A. & Friess, W. Stabilization of a hydrophobic recombinant cytokine by human serum albumin. *J. Pharm. Sci.* **2007**, *96* (11), 2987–2999. <https://doi.org/10.1002/jps.20909>.

- (40) Duerkop, M. *et al.* Impact of cavitation, high shear stress and air/liquid interfaces on protein aggregation. *Biotechnol. J.* **2018**, *13* (7), 1–9. <https://doi.org/10.1002/biot.201800062>.
- (41) Lee, H. J. *et al.* Molecular origins of surfactant-mediated stabilization of protein drugs. *Adv. Drug Deliv. Rev.* **2011**, *63* (13), 1160–1171. <https://doi.org/10.1016/j.addr.2011.06.015>.
- (42) Chu, J. W.; Brooks, B. R. & Trout, B. L. Oxidation of methionine residues in aqueous solutions: Free methionine and methionine in granulocyte colony-stimulating factor. *J. Am. Chem. Soc.* **2004**, *126* (50), 16601–16607. <https://doi.org/10.1021/ja0467059>.
- (43) Chu, J. W. *et al.* Molecular dynamics simulations and oxidation rates of methionine residues of granulocyte colony-stimulating factor at different pH values. *Biochemistry* **2004**, *43* (4), 1019–1029. <https://doi.org/10.1021/bi0356000>.
- (44) Pan, B. *et al.* Comparative oxidation studies of methionine residues reflect a structural effect on chemical kinetics in rhG-CSF. *Biochemistry* **2006**, *45* (51), 15430–15443. <https://doi.org/10.1021/bi061855c>.
- (45) Chennamsetty, N. *et al.* Modeling the oxidation of methionine residues by peroxides in proteins. *J. Pharm. Sci.* **2015**, *104* (4), 1246–1255. <https://doi.org/10.1002/jps.24340>.
- (46) Moorthy, B.; Iyer, L. & Topp, E. Characterizing protein structure, dynamics and conformation in lyophilized solids. *Curr. Pharm. Des.* **2015**, *21* (40), 5845–5853. <https://doi.org/10.2174/1381612821666151008150735>.
- (47) Lee, J. W.; Thomas, L. C. & Schmidt, S. J. Can the thermodynamic melting temperature of sucrose, glucose, and fructose be measured using rapid-scanning differential scanning calorimetry (DSC)? *J. Agric. Food Chem.* **2011**, *59* (7), 3306–3310. <https://doi.org/10.1021/jf104852u>.
- (48) Patel, S. M. *et al.* Lyophilized drug product cake appearance: What is acceptable? *J. Pharm. Sci.* **2017**, *106* (7), 1706–1721. <https://doi.org/10.1016/j.xphs.2017.03.014>.
- (49) Hawe, A. & Frieß, W. Formulation development for hydrophobic therapeutic proteins. *Pharm. Dev. Technol.* **2007**, *12* (3), 223–237. <https://doi.org/10.1080/10837450701247350>.
- (50) Shimizu, T. *et al.* Characteristics of proteinaceous additives in stabilizing enzymes during freeze-thawing and -drying. *Biosci. Biotechnol. Biochem.* **2017**, *81* (4), 687–697. <https://doi.org/10.1080/09168451.2016.1274637>.
- (51) Shalaev, E. Y. *et al.* Acid-catalyzed inversion of sucrose in the amorphous state at very low levels of residual water. *Pharm. Res.* **2000**, *17* (3), 366–370. <https://doi.org/10.1023/A:1007517526245>.
- (52) Horn, J. *et al.* Crystallizing amino acids as bulking agents in freeze-drying. *Eur. J. Pharm. Biopharm.* **2018**, *132*, 70–82. <https://doi.org/10.1016/j.ejpb.2018.09.004>.
- (53) Zhang, M. Z.; Wen, J. & Arakawa, T. A new strategy for enhancing the stability of lyophilized protein: the effect of the reconstitution medium on keratinocyte growth factor. *Pharm. Res.* **1995**, *12* (10), 1447–1452.
- (54) Zhang, M. Z. *et al.* The effect of the reconstitution medium on aggregation of lyophilized recombinant interleukin-2. *Pharm. Res.* **1996**, *13* (4), 643–646.

II.6 Supplementary data to Chapter II

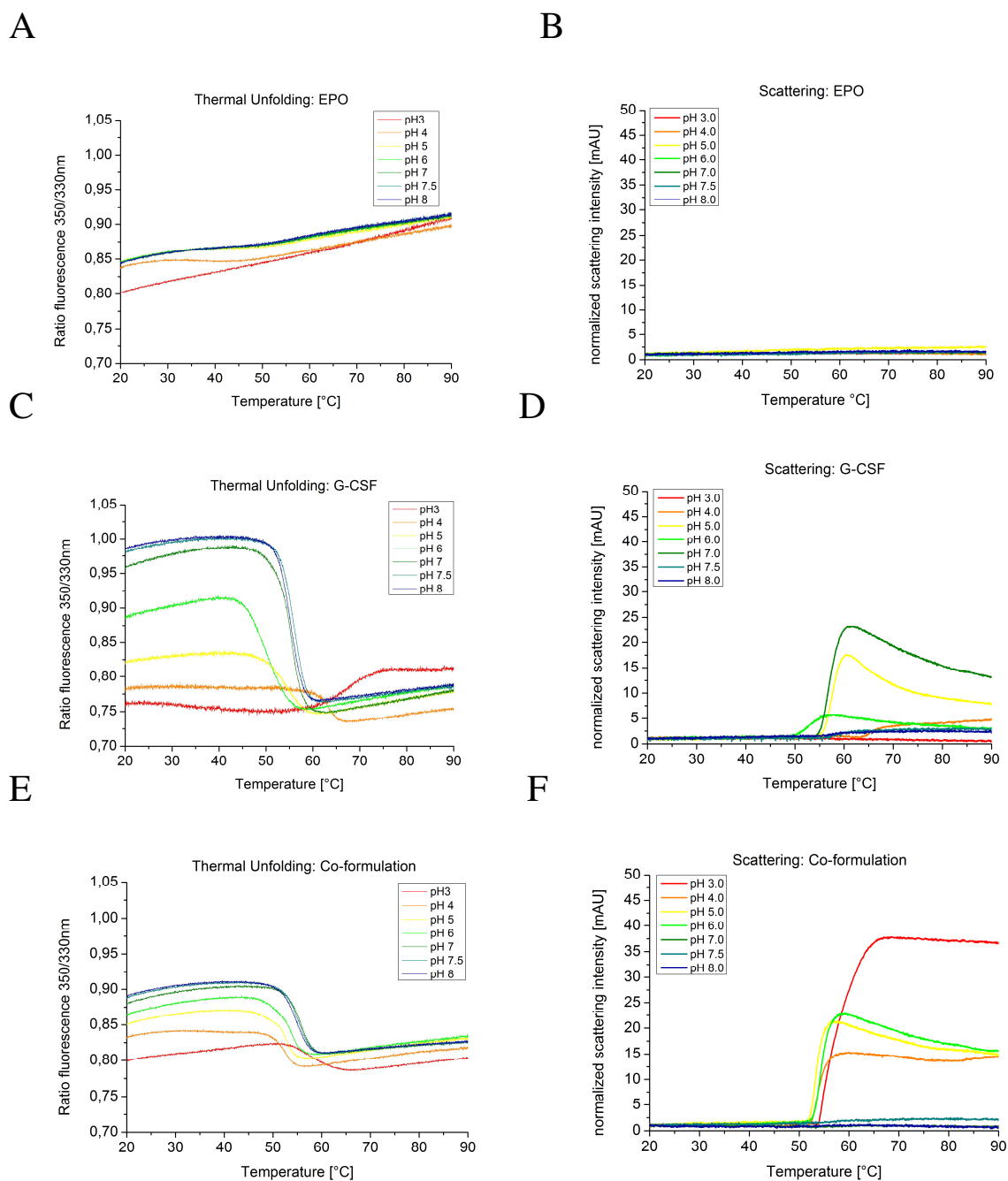


Figure S.II.1. Thermal unfolding by nanoDSF (A, C, E) and nanoDSF backscattering (B, D, F) for EPO (A, B), G-CSF (C, D) and the co-formulations (E, F). The measurements were performed in triplicates and the respective mean values are shown.

Chapter III Studies on pH- and salt-dependent protein aggregation of EPO and G-CSF in binary mixtures

III.1 Introduction

As already described in Chapter I, protein co-formulations gain increasing interest for the treatment of various diseases. However, the stabilization of multiple proteins in one solution can become challenging, because the optimal formulation conditions for the individual protein drugs can be very different.¹ A co-formulation might often require conditions that are suboptimal for the individual proteins, but satisfactory to achieve sufficient stability of both drugs simultaneously. That is why the degradation in co-formulations might be more pronounced compared to the individual most stable formulations of each protein. In co-formulations, protein aggregation can be caused by self-association or hetero-association of the inherited proteins. Thus, the development of stable protein co-formulation drug products has to evaluate the risk for arising stability-compromising cross-interactions between the different proteins.

Many analytical techniques that are established to study protein interactions are optimized for highly specific protein interactions with high affinities, such as interactions between mAbs and antigens or between receptors and specific ligands. These protein interactions provide information about physiological or pathological protein functions and signaling pathways based on the formation of biologically active protein complexes, but they are very different compared to the unspecific protein interactions that may arise in protein co-formulations. The therapeutic proteins that are to be combined in one dosage form are in general not expected to form specific dimeric complexes with defined complex structure and lifetime.²

However, the unspecific protein interactions based on long-range or short-range electrostatic forces can impact protein stability *in vitro* both in low and high concentrated protein solutions.³

Based on the results of Chapter II, EPO and G-CSF were selected as model proteins to characterize protein interactions that may arise in co-formulations. High-throughput screening tools that are applied in early formulation development were used to characterize these interactions without labeling or immobilization directly in solution at low volume and with low protein consumption. Single and co-formulations of EPO and G-CSF in either 5 mM sodium acetate or 5 mM sodium phosphate were prepared and the thermal aggregation patterns of these formulations were studied by nanoDSF backscattering and DLS. Increasing amounts of NaCl were added to further characterize the effect of the electrostatic interactions

on protein aggregation in single and co-formulations. The presented data indicates that stability-compromising heterogeneous interactions between different proteins can be indicated by decreased aggregation onset temperatures. The applied high-throughput methods are able to detect these interactions in early formulation development and can identify beneficial formulation conditions that either reduce attractive protein interactions or increase repulsive protein cross-interactions. We further confirmed the predicted detrimental cross-interactions by accelerated degradation studies.

III.2 Materials and Methods

III.2.1 Materials

As stated in Chapter II, the bulk solution of EPO contained 2.0 g/L protein, the bulk solution of G-CSF (filgrastim) 4.0 g/L protein. Both bulk solutions were provided in this concentration from the manufacturer. The protein concentration was measured spectrophotometrically using an Agilent 8453 UV spectrophotometer (Agilent Technologies Deutschland GmbH, Böblingen, Germany) and extinction coefficients at 280 nm of 1.24 (mg/mL)⁻¹cm⁻¹ for EPO and 0.86 (mg/mL)⁻¹cm⁻¹ for G-CSF. Human serum albumin (HSA), lysozyme and all chemicals were obtained from Sigma-Aldrich Chemie GmbH (Steinheim, Germany). All solutions were prepared with ultrapure water from a Sartorius arium[®] pro system (Sartorius Corporate Administration GmbH, Göttingen, Germany).

III.2.2 Preparation of protein formulations

EPO and G-CSF were dialyzed from the bulk solutions into 100x excess of the either 5 mM sodium acetate pH 4.0 or 5 mM sodium phosphate pH 7.0 for 24 hours at 2-8 °C using a Spectra/Por[®] dialysis membrane (cutoff 6-8 kDa, Spectrum Laboratories, Rancho Dominguez, CA, USA). The dialysis buffer was exchanged once after 8 hours. The dialyzed protein solutions were either diluted with buffer to obtain single protein formulations at concentration of 0.5 to 1.0 g/L or mixed to obtain co-formulations with a concentration 0.5 g/L for each protein. HSA and lysozyme were directly dissolved in either 5 mM sodium acetate pH 4.0 or 5 mM sodium phosphate pH 7.0 and diluted to the targeted concentration of 0.5 g/L to 1 g/L in the single formulations and 0.5 g/L per protein in the co-formulations. 1 M NaCl stock solutions in the respective buffer were spiked into the formulations to achieve concentrations of 0, 20, 50, 100 and 200 mM NaCl in single and co-formulations. The pH was subsequently adjusted with a MP 220 pH meter (Mettler-Toledo GmbH, Gießen, Germany) to the targeted pH and formulations were filtered using a 0.2 µm cellulose acetate membrane filter (Whatman, FP 30/0.2 CA-S, GE Healthcare, Buckinghamshire, UK).

III.2.3 Analysis of thermal Protein aggregation with nanoDSF backscattering

nanoDSF was used to study the aggregation of the single proteins and the co-formulations as a function of NaCl concentration at both pH 4.0 and pH 7.0. The protein concentration was set to 0.5 g/L or 1 g/L per protein. The formulations were filled into standard glass capillaries (NanoTemper Technologies, Munich, Germany) and placed in the Prometheus® NT.48 (NanoTemper Technologies, Munich, Germany). A temperature ramp of 1 °C/min was applied from 20 to 95 °C. All measurements were performed in triplicates. The aggregation onset temperature (T_{agg}) from the increase in the signal from the aggregation detection optics was determined using the PR.ThermControl V2.1 software (NanoTemper Technologies, Munich, Germany).

III.2.4 Dynamic Light Scattering

The measurements were performed as follows:⁴ The protein solutions were filled in a 1536 well plate (Aurora Microplates, Whitefish, USA). The plate was centrifuged at 2000 rpm for 2 min using a Heraeus Megafuge 40 centrifuge equipped with an M-20 well plate rotor (Thermo Fisher Scientific, Wilmington, USA). Silicon oil was added to seal each well. The plate was centrifuged again at 2200 rpm for 2 min and placed in a DynaPro DLS plate reader III (Wyatt Technology, Santa Barbara, USA). The aggregation of the proteins during heating was studied using a temperature ramp of 0.1 °C/min from 25 to 80 °C. Each measurement contained 3 acquisitions with an acquisition time of 3 s. The autocorrelation function of each measurement was analysed using cumulant analysis with the Dynamics V7.8 software (Wyatt Technology, Santa Barbara, USA). The apparent protein hydrodynamic radius from DLS (R_h) was calculated using the translational diffusion coefficient D_t and the Stokes-Einstein equation. The aggregation onset temperature (T_{on}) from the increase in the R_h from DLS was determined using the onset fit in the Dynamics V7.8 software.

To determinate the interaction parameter k_D , ten different protein concentrations from 0.5 to 5 g/L were prepared for EPO and G-CSF and the binary mixture in 5 mM sodium acetate pH 4.0 and NaCl concentrations of 0, 20 or 100 mM NaCl. The ratio of the proteins in the mixtures was set to 1:1 (m/m). The DLS measurements were performed at 25 °C and each measurement contained 10 acquisitions with an acquisition time of 5 s. All DLS measurements were performed in triplicates. The obtained data was analyzed with the Dynamics V7.8 software (Wyatt Technology, Santa Barbara, USA). The translational diffusion coefficient D_t was calculated from the autocorrelation functions using cumulant analysis and k_D was determined by linear regression of D_t against the respective concentration based on the following equation:^{5,6}

$$D_t = D_0 (1 + k_{DC})$$

where D_0 is the mutual diffusion coefficient at infinite dilution and c is the protein concentration.

III.2.5 Zeta potential measurements

The zeta potential was measured by electrophoretic light scattering on a Zetasizer Nano ZS (Malvern Panalytical Ltd, Malvern, UK). The Zetasizer Software V7.03 was used for data analysis. The protein concentration was set to 0.5 g/L per protein and the measurements were performed in 5 mM sodium acetate or 5 mM sodium phosphate.

III.2.6 High-Performance Size Exclusion Chromatography (HP-SEC)

HP-SEC was performed on either a Dionex Ultimate 3000 system (Thermo Fisher, Dreieich, Germany) or Waters 2695 separation module (Waters GmbH, Eschborn, Germany). 15 μ g of EPO and G-CSF were injected on a Superose 12 10/300 GL column (GE Healthcare Life Sciences, Tokyo, Japan) after centrifugation at 10 000 x g for 10 min and the elution of the protein was detected by UV spectrometry at 280 nm. 100 mM sodium phosphate pH 7.0 and 0.05% NaN₃ were used as mobile phase. The monomer recovery was calculated by integration of the peak area and relative comparison of this peak area before and after degradation.

III.3 Results & Discussion

III.3.1 Comparative analysis of protein aggregation of G-CSF in single and co-formulations by nanoDSF backscattering

Based on the results presented in Chapter II, the pH screen by nanoDSF indicated a pH dependent effect of EPO on the T_{agg} of G-CSF.¹ The zeta potential of both proteins indicated opposite charges for EPO and G-CSF at pH 4.0 (-6.8 ± 1.5 mV for EPO and 22.4 ± 0.3 mV for G-CSF) and similar charges at pH 7.0 (-25.7 ± 2.9 mV for EPO and -23.7 ± 1.4 mV for G-CSF). Apparently, the electrostatic attraction due to the opposite charges of both proteins at pH 4.0 accelerated protein aggregation, which as indicated by the decreased T_{agg} . The impact of these electrostatic protein interactions on the thermally induced protein aggregation was further characterized in single and co-formulations at 5 mM sodium acetate pH 4.0 and 5 mM sodium phosphate pH 7.0 and increasing concentrations of NaCl by nanoDSF backscattering (See Fig. III.1).

No protein aggregation was detected by nanoDSF for EPO at pH 4.0. This was likely caused by the limited sensitivity of the nanoDSF backscattering technique towards small

aggregates, because the aggregation of EPO was well detected by DLS (See Fig. III.4). The T_{agg} of the co-formulation was decreased compared to the single formulation of G-CSF for all NaCl concentrations at pH 4.0. While the T_{agg} of the G-CSF single formulation at pH 4.0 steadily decreased with increasing NaCl concentrations, the T_{agg} of the co-formulation increased up to a NaCl concentration of 50 mM and decreased at higher NaCl concentrations. The observed behavior of G-CSF is well described in literature and can be explained by the screening of electrostatic repulsive forces at pH 4.0 with increasing NaCl concentrations.⁷ In the co-formulation, it can be assumed that additionally arising electrostatic attractive forces between the negatively charged EPO and the positively charged G-CSF accelerated protein aggregation and reduced the observed T_{agg} , as well as increased the excess scattering of the co-formulation compared to G-CSF alone (See Fig. III.1D). By addition of increasing amounts of NaCl, the strength of the attractive electrostatic cross-interaction between the two proteins was reduced until the attractive forces were screened and the co-formulation reflected the aggregation behavior of G-CSF which is determined by the remaining electrostatic repulsive forces. In other words, the electrostatic repulsive self-interactions of G-CSF were observed in parallel to the electrostatic attractive cross-interactions between EPO and G-CSF. The lower zeta potential of EPO compared to G-CSF indicated that lower concentrations of NaCl were necessary to screen the electrostatic cross-interactions between EPO and G-CSF compared to the stronger electrostatic self-interactions of G-CSF. Thus, it can be assumed that NaCl stabilizes the co-formulation in concentrations up to 50 mM by the screening of electrostatic attractive cross-interactions and in higher concentrations destabilizes the co-formulation by the screening of remaining electrostatic repulsive self-interactions.

At pH 7.0, a different aggregation behavior was observed for the proteins in single and co-formulation. For EPO alone, no excess scattering was detected by nanoDSF backscattering (See Fig. III.1F). G-CSF aggregated at all NaCl concentrations and the T_{agg} decreased as the concentration of NaCl increased (See Fig. III.1E). The colloidal stability of G-CSF at pH 7.0 is determined by a combination of repulsive long-range electrostatic forces based on the proteins net charge and attractive short-range dipole-dipole-self-interactions based on asymmetric surface charge distributions.⁷ Based on the DLVO theory,⁸ the repulsive long-range electrostatic forces impede protein aggregation at low ionic strength because the repulsion of the charged surfaces increases the distance between aggregation-prone monomers. As the NaCl concentration increased, the repulsive forces were steadily screened and the distance between the protein monomers was reduced, which favored short-range dipole-dipole interactions and subsequently protein aggregation.

For the protein co-formulation, no aggregation was detected by nanoDSF backscattering at NaCl concentrations up to 20 mM NaCl (See Fig. III.1E), and the T_{agg} of the co-formulation was higher compared to G-CSF alone at NaCl concentrations ≥ 50 mM, although the total protein concentration in the co-formulation was higher (1 g/L) compared to the single formulation of G-CSF (0.5 g/L). A possible explanation for this observation is steric hindrance: The presence of EPO in the co-formulation probably reduced the possible contacts of aggregation-prone monomer residues of G-CSF per time. The surface of the heavily glycosylated EPO did not offer complementary surfaces towards G-CSF and the self-interaction of G-CSF was sterically reduced in the co-formulation, which resulted in an increased T_{agg} and a reduced excess scattering (See Fig. III.1H). Thus, we can assume that the cross-interactions between EPO and G-CSF at pH 7.0 are weaker compared to the respective self-interactions. This hypothesis is supported by the reduced aggregation in the co-formulation despite the higher total protein concentration. If the cross-interactions were stronger compared to the self-interactions, a lower T_{agg} would have been detected in the higher concentrated protein co-formulation.

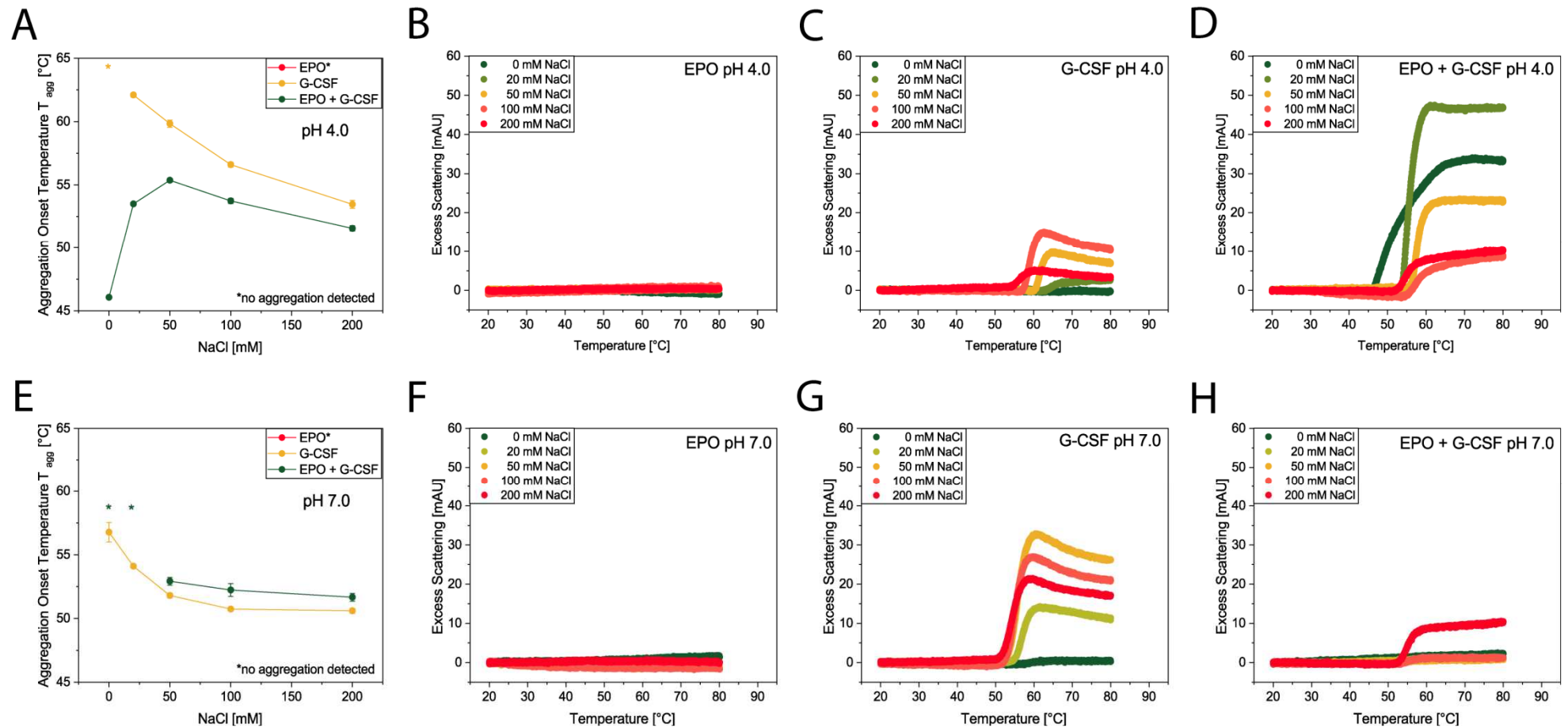


Figure III.1. nanoDSF backscattering results for single and co-formulations of EPO and G-CSF in 5 mM sodium acetate pH 4.0 (A, B, C, D) or 5 mM sodium phosphate pH 7.0 (E, F, G, H), and 0, 20, 50, 100 and 200 mM NaCl. The protein concentration was set to 0.5 g/L in the single formulations and 0.5 g/L per protein in the co-formulations. The Asterisks indicate that no aggregation was detected by the nanoDSF backscattering. The Aggregation Onset Temperatures (T_{agg}) for pH 4.0 (A) and pH 7.0 (E) are derived from the excess scattering at pH 4.0 for EPO (B), G-CSF (C), and the co-formulation (D) and at pH 7.0 for EPO (F), G-CSF (G), and the co-formulation (H).

A second pair of proteins was tested to confirm that the obtained results were indicative for electrostatic cross-interactions between oppositely charged proteins. The electrostatic interaction of HSA and lysozyme is well characterized in literature.⁹⁻¹¹ Single and co-formulations of HSA and lysozyme in 5 mM sodium acetate pH 4.0 and 5 mM sodium phosphate pH 7.0 were prepared, increasing amounts of NaCl were added and the formulations were analyzed by nanoDSF backscattering. The isoelectric points of HSA and lysozyme are 4.7 and 11.0 respectively.^{12,13} Based on these values, both proteins carry a net positive charge at pH 4.0 and no attractive electrostatic cross-interactions are expected. At pH 7.0, the net charge of HSA is negative, while lysozyme is positively charged. The nanoDSF backscattering results confirmed these assumptions. At pH 4.0, no aggregation was detected for the single and co-formulations (See Figs. III.2A-D). At pH 7.0, the co-formulation aggregated at elevated temperatures, while no aggregation was detected for the single protein formulations (See Figs. III.2E-H). Further, the T_{agg} of the co-formulation at pH 7.0 correlated with the NaCl concentration in the respective formulation, which indicated that attractive electrostatic interactions were screened by increasing NaCl concentrations. Based on these results we show that the nanoDSF backscattering detects electrostatic cross-interactions between proteins in given formulation conditions and also quantifies the impact of these electrostatic cross-interactions on the colloidal stability of the co-formulation.

For the co-formulation of EPO and G-CSF at pH 4.0 and the co-formulation of HSA and lysozyme at pH 7.0, where the proteins carried opposite net charges, the arising attractive electrostatic cross-interactions compromised the colloidal stability of a co-formulation (See Figs. III.1D and III.2H). The absence of these attractive electrostatic forces leveled the stability-compromising potential of the co-formulation of HSA and lysozyme at pH 4.0, and the co-formulation appeared non-inferior in terms of colloidal stability despite the higher protein concentration (See Fig. III.2D). Finally, the arising repulsive electrostatic cross-interaction increased the colloidal stability of the co-formulation of EPO and G-CSF at pH 7.0 compared to the single formulation of G-CSF (See Fig. III.1H).

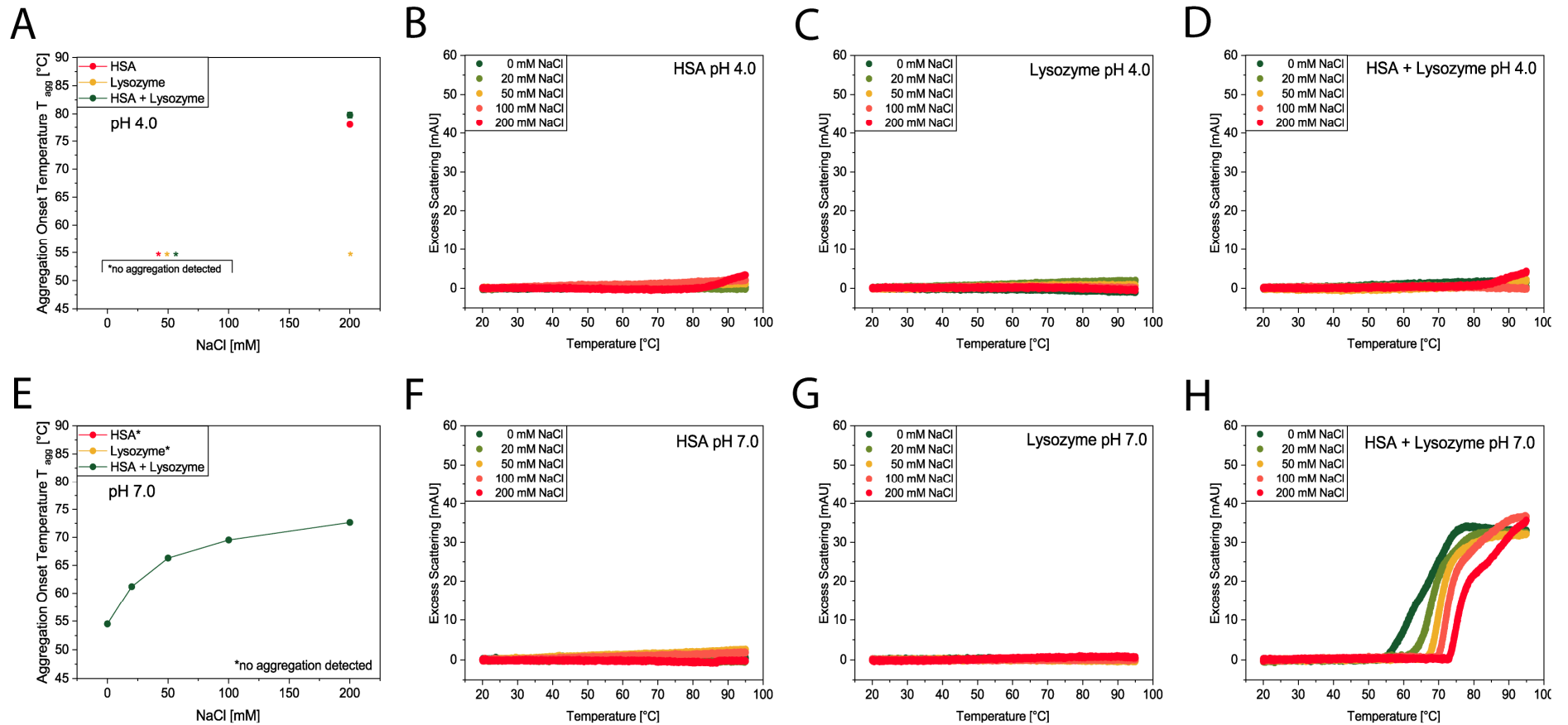


Figure III.2. nanoDSF backscattering results for single and co-formulations of HSA and lysozyme in 5 mM sodium acetate pH 4.0 (A, B, C, D) or 5 mM sodium phosphate pH 7.0 (E, F, G, H), and 0, 20, 50, 100 and 200 mM NaCl. The protein concentration was set to 0.5 g/L in the single formulations and 0.5 g/L per protein in the co-formulations. The Asterisks indicate that no aggregation was detected by the nanoDSF backscattering. The Aggregation Onset Temperatures (T_{agg}) for pH 4.0 (A) and pH 7.0 (E) are derived from the excess scattering at pH 4.0 for HSA (B), lysozyme (C), and the co-formulation (D) and at pH 7.0 for HSA (F), lysozyme (G), and the co-formulation (H).

In order to further characterize the impact of the observed cross-interactions in the co-formulation on the colloidal stability compared to the respective self-interactions, protein co-formulations of G-CSF with either EPO, HSA or lysozyme were prepared with a protein concentration of 0.5 g/L per protein. These co-formulations were compared to the single protein formulations with protein concentrations of 0.5 g/L and 1 g/L (See Fig. III.3). Using this experimental setup, it could be determined if the arising protein cross-interactions were more attractive or less attractive than the respective protein self-interactions.

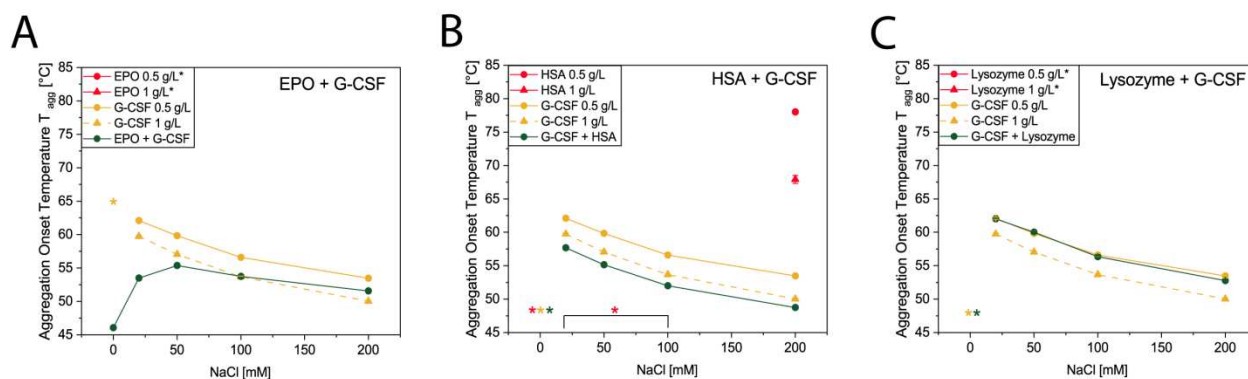


Figure III.3. nanoDSF backscattering results for single and co-formulations of EPO + G-CSF (A), HSA + G-CSF (B), and lysozyme + G-CSF (C) in 5 mM sodium acetate pH 4.0. The Asterisks indicate that no aggregation was detected by nanoDSF backscattering. The total protein concentration of the co-formulations was set to 1.0 g/L and the protein concentration of the single formulations was either set to 0.5 g/L (solid lines) or to 1.0 g/L (dashed lines).

For the co-formulations of EPO and G-CSF at pH 4.0 and NaCl concentrations up to 50 mM, the T_{agg} of the co-formulation was lower than the T_{agg} of the equally concentrated single formulation of G-CSF (See Fig. III.3A). This indicated that the attractive electrostatic cross-interactions were stronger than the self-interactions of G-CSF. At concentrations of 100 mM NaCl, the T_{agg} values of the single formulation of G-CSF and the co-formulation were comparable, and at concentrations of 200 mM NaCl, the T_{agg} of the co-formulation was higher than the T_{agg} of the single formulation of G-CSF. This indicated that the strength of the attractive electrostatic cross-interactions decreased with increasing NaCl concentrations, until the cross-interactions were less attractive compared to the self-interactions of G-CSF.

The co-formulation of HSA and G-CSF showed a different behavior compared to the co-formulation of EPO and G-CSF. The co-formulations showed decreased T_{agg} values at all NaCl concentrations compared to the equally concentrated single formulations of G-CSF (See Fig. III.3B). G-CSF has previously been formulated with HSA to prevent surface adsorption, and the reduced surface adsorption of G-CSF in presence of HSA was anticipated to be a

consequence of either a direct binding of HSA to G-CSF or a preferential binding of HSA to surfaces.¹⁴ Direct binding of HSA to a hydrophobic cytokine has previously been detected by fluorescence spectroscopy,¹⁵ and the results obtained by nanoDSF backscattering also indicated an attractive cross-interaction between HSA and G-CSF that was stronger than the self-interaction of G-CSF (See Fig. III.3B), based on the lower T_{agg} of the co-formulation. The lower T_{agg} values of the co-formulations at all NaCl concentrations and the net positive surface charge at pH 4.0 of both proteins indicated charge-independent attractive cross-interactions between HSA and G-CSF. Attractive cross-interactions between HSA and several proteins were already described and assigned to hydrophobicity, van der Waals forces or formation of hydrogen bonds.¹⁶ The reduced T_{agg} values were also likely caused by charge-independent attractive cross-interactions. Although these attractive cross-interactions apparently reduce the colloidal stability of the protein mixture, they do not necessarily compromise the overall long-term stability of the proteins in the co-formulation. More critical degradation pathways such as the surface-induced unfolding and subsequent aggregation of G-CSF can be reduced by a decreased number of free monomers of G-CSF that are susceptible to surface-induced aggregation, which results in a net stabilization of G-CSF in presence of HSA.¹⁴

The co-formulation of lysozyme and G-CSF represents a protein combination where increased T_{agg} values were detected for the co-formulations at all NaCl concentrations compared to the equally concentrated single formulations of G-CSF (See Fig. III.3C). This indicated that no stability compromising cross-interactions occurred in the co-formulation, because the protein interactions between lysozyme and G-CSF were weaker compared to the self-interactions of G-CSF. It is also possible that there were no cross-interactions at all between lysozyme and G-CSF and the increased T_{agg} values in the co-formulations were a consequence of hindered self-interactions of G-CSF by steric hindrance.

III.3.2 Comparative analysis of protein aggregation of EPO and G-CSF in single and co-formulations by DLS

As the nanoDSF backscattering technique is not sensitive enough to detect small protein aggregates,⁴ DLS has been applied as complementary technique to study the initial protein aggregation starting from the monomeric state based on the changes of the hydrodynamic radius (R_h) during heating in single and co-formulations. Single and co-formulations of EPO and G-CSF were prepared in both 5 mM sodium acetate pH 4.0 and 5 mM sodium phosphate pH 7.0 at different concentrations of NaCl. The thermally induced aggregation of the formulations was analyzed by DLS (See Fig. III.4). Although the resolution is not sufficient to

allow a separation of the respective monomer signals in co-formulation, it is possible to study changes in the thermal aggregation pattern of the proteins in co-formulations starting from the monomeric state. The results are shown in Fig. III.4.

At pH 4.0, protein aggregation was detected during heating for both EPO and G-CSF in single formulations based on the increased R_h compared to the respective protein monomers (See Figs. III.4B and III.4C). The T_{on} decreased with increasing NaCl concentration for both proteins, which confirmed the nanoDSF backscattering results. The aggregation pattern of the single formulations of EPO and G-CSF at pH 4.0 reflected the decreased colloidal stability of both proteins with increasing NaCl concentrations (See Figs. III.4B and III.4C). The co-formulation pattern differed from the single formulations and was neither an intermediate pattern nor a sum of the single protein aggregation patterns (See Fig. III.4D). The T_{on} of the co-formulation was shifted to lower temperatures and the aggregation was accelerated compared to both proteins for the 0 mM NaCl condition. While G-CSF appeared monomeric at 50 °C and EPO reached a R_h of about 5 nm, the co-formulation already reached a R_h of about 15 nm in 5 mM sodium acetate pH 4.0. Further, the addition of up to 50 mM NaCl did not decrease the T_{on} (See Fig. III.4C), in contrast to the steady shift of T_{on} towards lower temperatures for the single formulations. The T_{on} values of the co-formulation at 0 and 20 mM NaCl were likely additionally decreased by attractive electrostatic cross-interactions in the mixture at low ionic strength conditions. At 0 mM NaCl, these interactions were strong enough to reduce the T_{on} below the T_{on} of EPO alone. As the attractive electrostatic interactions were screened at 50 mM NaCl, the co-formulation followed the trend of the single proteins.

At pH 7.0, no aggregation was detected by DLS for the single formulations of EPO (See Fig. III.4A), which confirmed the nanoDSF results. The high colloidal stability of EPO at neutral pH was previously reported and assigned to limited structural changes and formation of micelle-like structures due to the bulky glycosyl residues, which limited protein association.¹⁷ The single formulation of G-CSF showed a lower colloidal stability at pH 7.0 compared to pH 4.0 based on the T_{on} values, which confirms the results of previous studies.⁷ Interestingly, the addition of NaCl had no effect on T_{on} but accelerated aggregation growth in the single formulation of G-CSF at pH 7.0 (See Fig. III.4G).

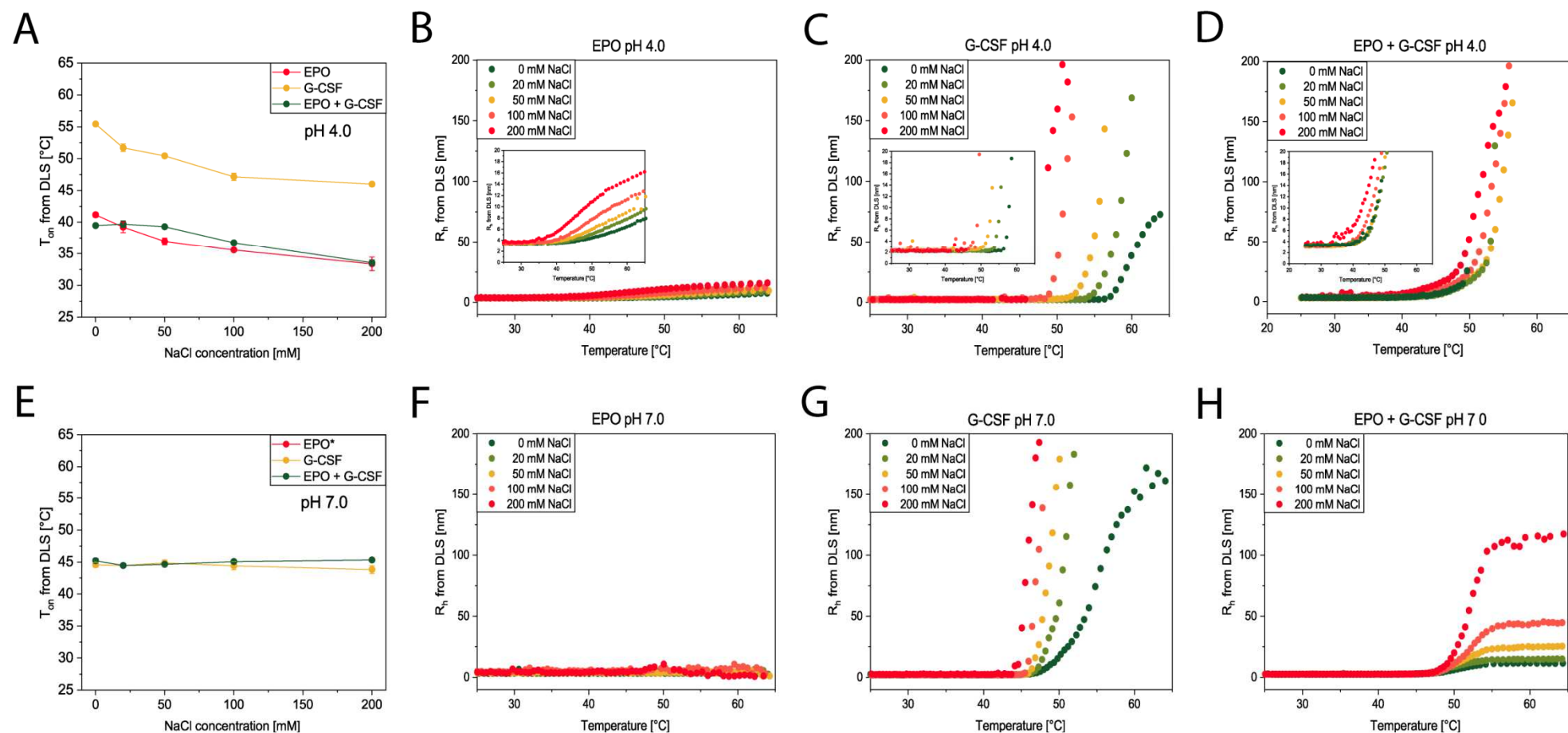


Figure III.4. DLS results for single and co-formulations of EPO and G-CSF in 5 mM sodium acetate pH 4.0 (A, B, C, D) or 5 mM sodium phosphate pH 7.0 (E, F, G, H), and 0, 20, 50, 100 and 200 mM NaCl. The graphical inserts (B, C, D) show the aggregation on a scale from 0 to 20 nm R_h (10x magnification). The Asterisks indicate that no aggregation was detected by the DLS plate reader. The protein concentration was set to 0.5 g/L in the single formulations and 0.5 g/L per protein in the co-formulations. The Aggregation Onset Temperatures (T_{on}) for pH 4.0 (A) and pH 7.0 (E) are derived from the hydrodynamic radius (R_h) at pH 4.0 for EPO (B), G-CSF (C), and the co-formulation (D) and at pH 7.0 for EPO (F), G-CSF (G), and the co-formulation (H).

The co-formulation of EPO and G-CSF at pH 7.0 exhibited a different protein aggregation compared to the single protein formulations (See Fig. III.4H). While aggregation of G-CSF alone was unlimited, the co-formulation aggregation growth stopped at a certain R_h size that increased with increasing NaCl concentration. Given a zeta potential of -25.7 ± 2.9 mV for EPO and -23.7 ± 1.4 mV for G-CSF at pH 7.0, it can be assumed that the electrostatic repulsion at pH 7.0 impeded aggregate growth. These repulsive electrostatic forces were screened with increasing concentrations of NaCl, and the size of the formed aggregates increased accordingly. However, even at high ionic strength conditions of 200 mM NaCl, the aggregation in the binary mixture stopped at a certain size compared to the single protein formulation of G-CSF. Based on the DLS data alone, we can neither prove the presence of pure homogenous aggregates of each protein next to each other, nor the formation of hetero-aggregates due to cross-interactions, and it remains unclear, why the protein aggregation growth in the co-formulation stopped at a certain size at pH 7.0. As discussed already for the nanoDSF results (See III.3.1), it can be assumed that the aggregation of G-CSF followed the same pathway as in the single formulation based on the asymmetric charge distribution of G-CSF,⁷ and the heavily glycosylated EPO did not offer complementary surfaces for protein association, which resulted in a steric hindrance of G-CSF aggregation. The increasing NaCl concentrations reduced the colloidal stability G-CSF due to the screening of repulsive protein interactions, which led to larger aggregate sizes in co-formulations with higher NaCl concentrations. Further experiments have to be conducted to investigate the protein aggregation in this co-formulation, because the presented data indicates that protein aggregation in co-formulations can differ substantially from the aggregation in the respective single protein formulations, and the underlying mechanisms have to be further studied.

III.3.3 Comparative analysis of protein interactions of EPO and G-CSF in single and co-formulations by the apparent diffusion interaction parameter (Apparent k_D)

Until now, the protein cross-interactions between EPO and G-CSF have been studied by thermally induced protein aggregation in the single and co-formulations. Based on the nanoDSF backscattering and DLS data, both pH-dependent and NaCl-dependent changes in the protein aggregation were detected in the co-formulation. At pH 4.0, additional electrostatic cross-interactions between EPO and G-CSF were indicated, and DLS measurements were applied at ambient temperature to confirm these results.

The diffusion interaction parameter k_D is an established tool to characterize protein interactions at ambient temperature. Based on attractive or repulsive protein interactions between monomers, the diffusion coefficient of the protein will increase or decrease

respectively because the interactions affect the diffusion in a given medium. k_D measurements are typically applied for a single protein, but were recently also applied for protein mixtures.^{4,18} Based on the very different nature of EPO and G-CSF compared to mixtures of mAbs, such as different R_h and D_0 values, it is important to point out that we consider this artificial, apparent k_D value of the co-formulation to deliver information on relative changes of attractive and repulsive forces compared to the single formulation, but not to represent a typical k_D value as for single proteins or mixtures of rather uniform mAbs.

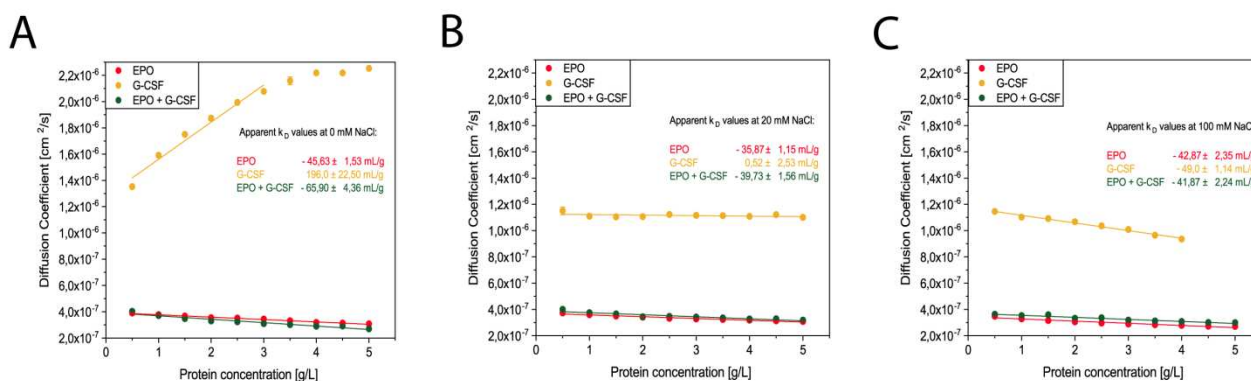


Figure III.5. Apparent k_D values for EPO (red), G-CSF (yellow) and EPO + G-CSF (green) in 5 mM sodium acetate pH 4.0 and 0 mM NaCl (A), 20 mM NaCl (B) or 100 mM NaCl (C). The Diffusion Coefficients were plotted against protein concentration and the apparent k_D value was calculated by linear regression.

The results are shown in Fig. III.5. Repulsive protein interactions were detected for G-CSF at 0 mM NaCl, which are screened at concentrations of 20 mM. At 100 mM NaCl, attractive protein interactions were detected. For G-CSF at 0 mM NaCl, the correlation of concentration and diffusion coefficient was not linear for the whole concentration range. This was most likely caused by the detection limit of the DLS PlateReader. The already very small hydrodynamic radius of G-CSF of about 1 nm and the additional reduction of the apparent hydrodynamic radius due to repulsive interactions caused the continuous detection of R_h values of about 1 nm at G-CSF concentrations higher than 3 g/L and subsequent calculation of a respective diffusion coefficient (See Fig. III.5A). Further, it has been previously reported that electrostatic migration at low ionic strength can interfere with the concentration-dependency of the hydrodynamic radius obtained by DLS and cause non-linearity,¹⁹ which also explains the observed behavior of G-CSF.

For EPO, equally attractive protein interactions were detected at all NaCl concentrations. Interestingly, the measured diffusion coefficients of the co-formulation did not represent an arithmetic mean of the single proteins, but very similar values compared to the single

formulation of EPO. This can partly be explained by the larger hydrodynamic radius of EPO (about 3 nm) compared to G-CSF (about 1 nm), which favors the EPO signal detected by DLS in the mixture. At 0 and 20 mM NaCl, the apparent k_D values of the co-formulation were more negative compared to the single formulation of EPO, while at 100 mM NaCl, no difference could be detected between the single formulation of EPO and the co-formulation. However, it is questionable if the differences between the single formulation of EPO and the co-formulation at 0 and 20 mM NaCl reliably indicate protein cross-interactions, especially as the differences in the measured diffusion coefficient only arise at higher protein concentrations. For protein co-formulations up to 1 g/L, the DLS measurements at ambient temperature did not indicate a significantly reduced diffusion coefficient and thus no additionally arising cross-interactions in the co-formulation. Based on the presented DLS and nanoDSF measurements at steadily increasing temperatures, the protein cross-interactions seemed to arise at elevated temperatures, which could indicate that (partially) unfolded intermediates of at least one protein are involved. With increasing flexibility of the protein chains at increased temperatures, cross-interactions of partially unfolded protein intermediates could arise in the co-formulation. This could be further investigated with k_D measurements at elevated temperatures,²⁰ to quantify the cross-attraction between the unfolded intermediates of different proteins.

III.3.4 Forced degradation studies by HP-SEC

Until now, the presented results have indicated a compromised colloidal stability for co-formulations of EPO and G-CSF at pH 4.0 and low ionic strength conditions (See Fig. III.1). Nevertheless, a stabilized co-formulation of EPO and G-CSF at pH 4.0 and low ionic strength prior to lyophilization was presented in Chapter II. In order to study the impact of electrostatic cross-interactions on the colloidal stability of this particular co-formulation compared to the single formulations, increasing concentrations of NaCl were added to single and co-formulation and the thermally induced protein aggregation was measured by nanoDSF backscattering. Further, the prepared single and co-formulations were stressed at 40 °C and 300 rpm for 10 h and the monomer recovery was determined by HP-SEC. The nanoDSF backscattering measurements confirmed the previously obtained results (See Fig. III.6A). For EPO alone, no aggregation was detected, while G-CSF alone and the co-formulation showed the same trends as in 5 mM sodium acetate pH 4.0 (See Fig. III.1). Interestingly, the monomer recoveries in HP-SEC of both EPO and G-CSF were significantly higher in single protein formulations compared to the co-formulations for all NaCl concentrations (See Fig. III.6B and III.6C). Further, the monomer recoveries for both proteins in co-formulation reflected the

prediction by nanoDSF backscattering and showed additionally decreased values at 0 mM NaCl, which indicated that the electrostatic cross-interactions between EPO and G-CSF accelerated protein aggregation at low ionic strength conditions. At all NaCl concentrations the monomer recovery was significantly reduced and the formation of soluble aggregates significantly increased in the co-formulation.

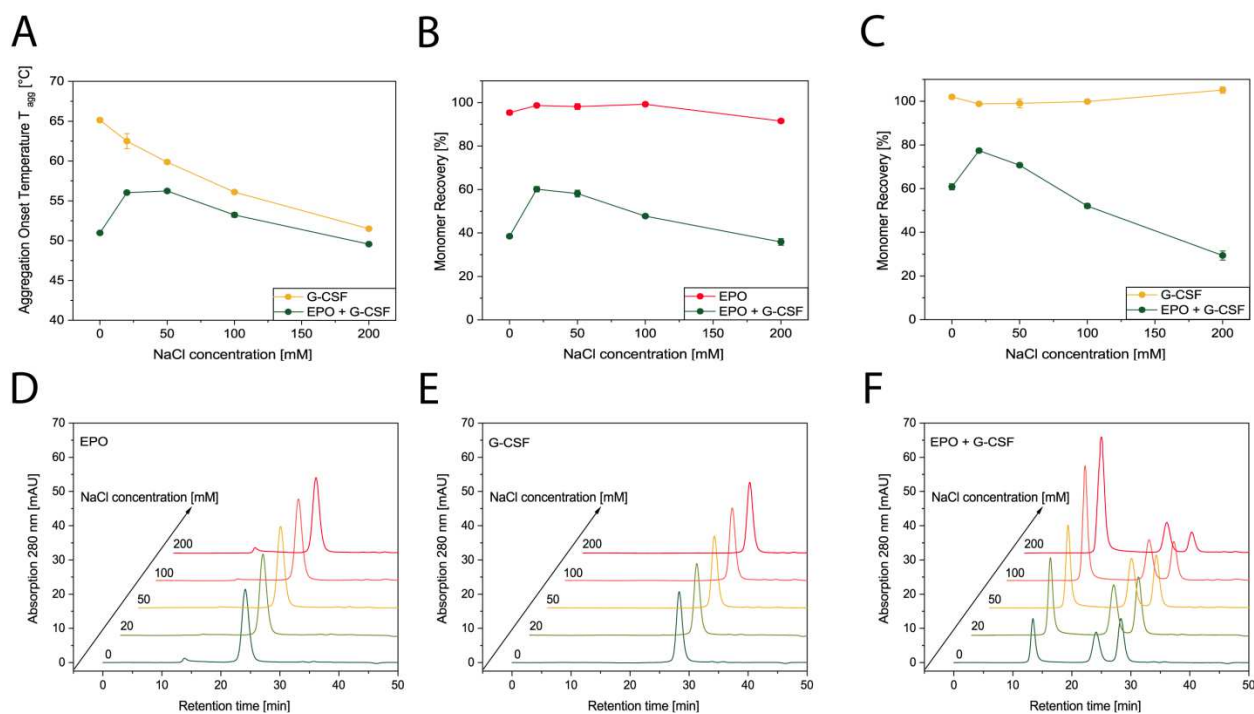


Figure III.6. Aggregation Onset Temperatures (T_{agg}) for G-CSF in single and co-formulation (2 mM sodium citrate, 5 % mannitol, 1 % sucrose, 20 mM methionine and 0.1 % polysorbate 20) and addition of 0, 20, 50, 100 and 200 mM NaCl (A, yellow line for G-CSF; green line for EPO + G-CSF). For EPO, no aggregation was detected by nanoDSF backscattering. Monomer recoveries in HP-SEC for EPO (B) and G-CSF (C) in single and co-formulations. Example HP-SEC chromatograms of the stressed formulations of EPO (D), G-CSF (E) and EPO + G-CSF (F) to illustrate the results in (B) and (C). The formulations were stressed in a thermocycler for 10 h at 40 °C and 300 rpm.

Thus, the accelerated protein aggregation in the co-formulation cannot be explained by the anticipated electrostatic cross-interactions at low ionic strength conditions alone. As discussed in the previous section, at least partly thermally induced unfolding of both proteins with subsequent exposure of hydrophobic patches may have formed and accelerated cross-interactions between the unfolded states of both proteins. These hydrophobic interactions were then favored in high ionic strength conditions, which could explain the decreased monomer recoveries of both proteins with increasing NaCl concentration in the co-formulation.

In order to characterize the cross-interactions between the two proteins further and exclude that the differences in the monomer recoveries were only caused by the higher total protein concentration in the co-formulation, the total protein concentrations were fixed to 1 g/L in the next step for single and co-formulations. Co-formulations with different ratios of EPO and G-CSF were stressed and analyzed by HP-SEC. Both proteins showed the highest monomer recoveries in the respective single formulations (See Fig. III.7). The presence of the second protein led to decreased protein recoveries for both proteins in all tested mixing ratios compared to the single protein formulations. While the monomer recovery of G-CSF continuously decreased with increasing relative EPO concentrations, the monomer recovery of EPO decreased at low relative G-CSF concentrations, reached a minimum at a mixing ratio of 1:1 and increased at higher relative G-CSF concentrations. Further, small amounts of G-CSF (EPO:G-CSF ratio of 10:1) significantly reduced the monomer recovery of EPO and increased the formation of soluble aggregates, while small amounts of EPO (EPO:G-CSF ratio of 1:10) had a less severe effect on the monomer recovery of G-CSF. Thus, the impact of the electrostatic cross-interactions between EPO and G-CSF at pH 4.0 on the protein stability depends on the mixing ratio of both proteins.

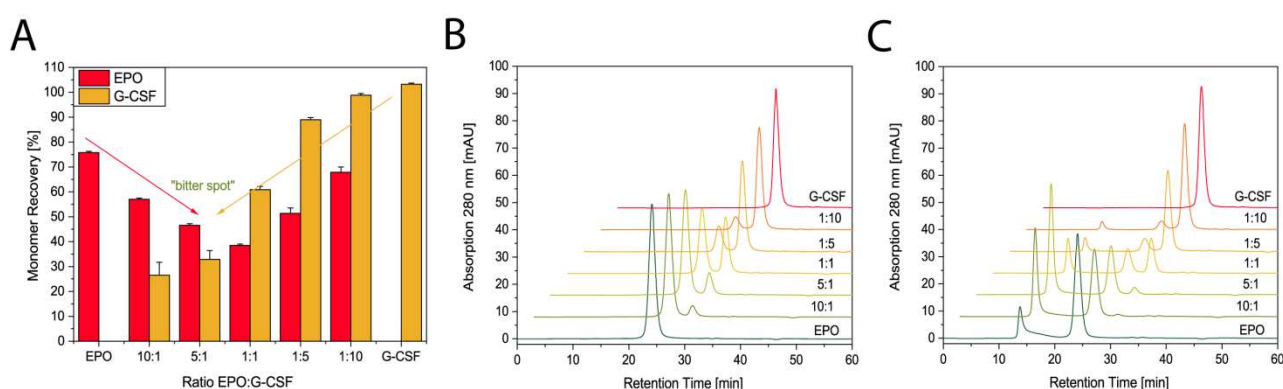


Figure III.7. Monomer recoveries in HP-SEC for EPO and G-CSF in co-formulations of different ratios (w/w) for EPO and G-CSF (A). The co-formulations consisted of 2 mM sodium citrate, 4 % mannitol, 1 % sucrose, 20 mM methionine and 0.1 % polysorbate 20. The total protein concentration was set to 1 g/L for all ratios of EPO and G-CSF. HP-SEC chromatograms of native co-formulations (B). HP-SEC chromatograms for stressed co-formulations (C). The formulations were stressed in a thermocycler for 10 h at 40 °C and 300 rpm.

Based on these results, the prediction by nanoDSF can be confirmed that EPO cross-interacts with G-CSF at pH 4.0, and these cross-interactions reduce the colloidal stability of the protein mixture compared to the single protein formulations. While G-CSF showed no monomer loss in the single formulation, increasing amounts of EPO reduced the monomer recovery of G-CSF (See Fig. III.7A). Further, the formation of soluble aggregates was increased in certain co-formulations of EPO and G-CSF compared to the single formulation of

EPO with an equal total protein concentration of 1 g/L (See Fig. III.7C). Thus, the cross-interactions between EPO and G-CSF depend on a specific protein ratio, and certain protein ratios cause stronger cross-interactions compared to the respective self-interactions.

III.4 Conclusion

In this chapter, the protein aggregation of the two model proteins EPO and G-CSF was studied by high-throughput screening methods and HP-SEC. The impact of a second protein on the thermally induced protein aggregation at different pH values and NaCl concentrations was characterized. Based on the differences in the respective colloidal and conformational stability of both proteins, conditions were identified that (a) accelerate protein aggregation based on attractive cross-interactions between the two proteins, or (b) reduce protein aggregation based on repulsive cross-interactions and steric hindrance. The impact of the co-formulation on the individual protein stability was closely linked to the respective stability profile of the individual proteins and most likely also included contributions of partially unfolded intermediates and glycosylation.

For a given co-formulation, the stability compromising heterogeneous protein interactions can be identified by high-throughput methods as DLS and nanoDSF. The methods provide insight into changes of the individual protein aggregation pathways in the co-formulations and can support the protein development scientist to identify detrimental protein interactions in co-formulations early on. Formulation conditions that may not be critical for the single proteins, but favor stability-compromising cross-aggregations in the protein mixture, can be rapidly identified at low protein consumption and in low volume without the application of elaborative immobilization or labeling techniques. Further, it is possible to characterize these cross-interactions further by the addition of increasing amounts of NaCl to identify formulation conditions that either reduce attractive long-range electrostatic interactions between different proteins or favor repulsive long-range electrostatic interactions that can reduce aggregation in protein mixtures.

Based on the obtained results in nanoDSF backscattering, DLS and HP-SEC it can be assumed that the protein cross-interactions at pH 4.0 caused the formation of mixed protein aggregates of EPO and G-CSF. In both nanoDSF backscattering and DLS measurements, the thermal aggregation pattern at pH 4.0 in low concentrations of NaCl differs compared to the single formulations, and the HP-SEC results indicate concentration- and ratio-dependent cross-interactions between the proteins. However, there is no final proof for the formation of mixed protein aggregates, and additional studies are required to elucidate the aggregation

pathways in these protein mixtures. The fractionation, up-concentration and subsequent analysis of the soluble aggregates by preparative RP-HPLC, which is able to separate both proteins as presented in Chapter II, could be helpful to distinguish between pure or mixed aggregates. The attachment of different fluorescent labels to each protein before aggregation may be also helpful, although these labels may change the aggregation behavior compared to the non-labeled proteins. Alternative approaches could also include the determination of second virial cross-coefficients,²¹ for instance by self-interaction chromatography,²² which has also been successfully applied to screen cross-interactions between bovine serum albumin (BSA) and lysozyme.²³

Although the anticipated cross-interactions reduced the colloidal stability of the protein mixture compared to the single protein formulations in liquid formulations, an increased colloidal and chemical stability was presented for the lyophilized co-formulation of EPO and G-CSF in Chapter II. These apparently opposing observations can be explained by different behaviors of both proteins in the liquid and the solid state. As discussed in Chapter II, the presence of EPO could reduce the surface-induced unfolding and aggregation of G-CSF. Therefore, the cross-interactions between EPO and G-CSF that reduce the colloidal stability in the liquid state can result in a net stabilization of G-CSF in the solid state, because more critical degradation pathways are prevented.

In summary, we evaluated nanoDSF and DLS for their ability to identify stability-compromising heterogeneous protein interactions in co-formulations and showed that these interactions can be detected by shifts of the T_{agg} or T_{on} values and changes in the respective aggregation traces of the protein mixture compared to the single protein formulations. Both nanoDSF and DLS proved to be value tools in protein co-formulation development to rapidly screen detrimental interactions of proteins in different formulation conditions and accelerate the rational development of protein co-formulations.

III.5 References

- (1) Krieg, D. *et al.* Overcoming challenges in co-formulation of proteins with contradicting stability profiles - EPO plus G-CSF. *Eur. J. Pharm. Sci.* **2020**, *141*, 105073. <https://doi.org/10.1016/j.ejps.2019.105073>.
- (2) Hoppe, T. & Minton, A. P. Non-specific interactions between macromolecular solutes in concentrated solution: Physico-chemical manifestations and biochemical consequences. *Front. Mol. Biosci.* **2019**, *6*, 1–12. <https://doi.org/10.3389/fmolb.2019.00010>.
- (3) Chari, R. *et al.* Long- and short-range electrostatic interactions affect the rheology of highly concentrated antibody solutions. *Pharm. Res.* **2009**, *26* (12), 2607–2618. <https://doi.org/10.1007/s11095-009-9975-2>.
- (4) Krieg, D. *et al.* Biophysical characterization of binary therapeutic monoclonal antibody mixtures. *Mol. Pharm.* **2020**, *17* (8), 2971–2986. <https://doi.org/10.1021/acs.molpharmaceut.0c00370>.
- (5) Harding, S. E. & Johnson, P. The concentration-dependence of macromolecular parameters. *Biochem. J.* **1985**, *231*, 543–547. <https://doi.org/10.1042/bj2310543>.
- (6) Connolly, B. D. *et al.* Weak interactions govern the viscosity of concentrated antibody solutions: High-throughput analysis using the diffusion interaction parameter. *Biophys. J.* **2012**, *103*, 69–78. <https://doi.org/10.1016/j.bpj.2012.04.047>.
- (7) Chi, E. Y. *et al.* Roles of conformational stability and colloidal stability in the aggregation of recombinant human granulocyte colony-stimulating factor. *Protein Sci.* **2003**, *12* (5), 903–913. <https://doi.org/10.1110/ps.0235703>.
- (8) Leckband, D. & Sivasankar, S. Forces controlling protein interactions: Theory and experiment. *Colloids Surfaces B Biointerfaces* **1999**, *14* (1–4), 83–97. [https://doi.org/10.1016/S0927-7765\(99\)00027-2](https://doi.org/10.1016/S0927-7765(99)00027-2).
- (9) Vieyra-Eusebio, M. T. & Costas, M. Protein-protein interactions at high concentrations. Isothermal titration calorimetry determination of human serum albumin-lysozyme interaction enthalpy at several pH values. *Thermochim. Acta* **2016**, *641*, 39–42. <https://doi.org/https://doi.org/10.1016/j.tca.2016.08.011>.
- (10) Chen, Y. M. *et al.* Colorimetric detection of lysozyme based on electrostatic interaction with human serum albumin-modified gold nanoparticles. *Langmuir* **2008**, *24* (7), 3654–3660. <https://doi.org/10.1021/la7034642>.
- (11) Vasylyeva, M. & Gromovoy, T. MALDI-TOF investigation of lysozyme-albumin interaction. *Chem. J. Mold.* **2017**, *9* (2), 107–110. [https://doi.org/10.19261/cjm.2014.09\(2\).15](https://doi.org/10.19261/cjm.2014.09(2).15).
- (12) Vlasova, I. M. & Saletsky, A. M. Study of the denaturation of human serum albumin by sodium dodecyl sulfate using the intrinsic fluorescence of albumin. *J. Appl. Spectrosc.* **2009**, *76* (4), 536–541. <https://doi.org/10.1007/s10812-009-9227-6>.
- (13) Wu, H. *et al.* Purification and characterization of recombinant human lysozyme from eggs of transgenic chickens. *PLoS One* **2015**, *10* (12), 1–17. <https://doi.org/10.1371/journal.pone.0146032>.
- (14) Wang, P. L.; Udeani, G. O. & Johnston, T. P. Inhibition of granulocyte colony stimulating factor (G-CSF) adsorption to polyvinyl chloride using a nonionic surfactant. *Int. J. Pharm.* **1995**, *114* (2), 177–184. [https://doi.org/10.1016/0378-5173\(94\)00236-X](https://doi.org/10.1016/0378-5173(94)00236-X).
- (15) Hawe, A. & Friess, W. Stabilization of a hydrophobic recombinant cytokine by human serum albumin. *J. Pharm. Sci.* **2007**, *96* (11), 2987–2999. <https://doi.org/10.1002/jps.20909>.
- (16) Chanphai, P.; Bekale, L. & Tajmir-Riahi, H. A. Effect of hydrophobicity on protein–protein Interactions. *Eur. Polym. J.* **2015**, *67*, 224–231. <https://doi.org/https://doi.org/10.1016/j.eurpolymj.2015.03.069>.
- (17) Endo, Y. *et al.* Heat-induced aggregation of recombinant erythropoietin in the intact and deglycosylated states as monitored by gel permeation chromatography combined with a low-angle laser light scattering technique. *J. Biochem.* **1992**, *112* (5), 700–706. <https://doi.org/10.1093/oxfordjournals.jbchem.a123961>.
- (18) Singh, P. *et al.* Determination of protein–protein interactions in a mixture of two monoclonal antibodies. *Mol. Pharm.* **2019**, *16* (12), 4775–4786. <https://doi.org/10.1021/acs.molpharmaceut.9b00430>.

- (19) Sorret, L. L. *et al.* Challenges in predicting protein-protein interactions from measurements of molecular diffusivity. *Biophys. J.* **2016**, *111* (9), 1831–1842. <https://doi.org/10.1016/j.bpj.2016.09.018>.
- (20) Menzen, T. & Friess, W. Temperature-ramped studies on the aggregation, unfolding, and interaction of a therapeutic monoclonal antibody. *J. Pharm. Sci.* **2014**, *103* (2), 445–455. <https://doi.org/10.1002/jps.23827>.
- (21) Ersch, C. *et al.* Interactions in protein mixtures. Part II: A virial approach to predict phase behavior. *Food Hydrocoll.* **2016**, *52*, 991–1002. <https://doi.org/https://doi.org/10.1016/j.foodhyd.2015.07.021>.
- (22) Quigley, A. & Williams, D. R. The second virial coefficient as a predictor of protein aggregation propensity: A self-interaction chromatography study. *Eur. J. Pharm. Biopharm.* **2015**, *96*, 282–290. <https://doi.org/10.1016/j.ejpb.2015.07.025>.
- (23) Tessier, P. M.; Sandler, S. I. & Lenhoff, A. M. Direct measurement of protein osmotic second virial cross coefficients by cross-interaction chromatography. *Protein Sci.* **2004**, *13*, 1379–1390. <https://doi.org/10.1110/ps.03419204>.

Chapter IV Biophysical characterization of binary therapeutic monoclonal antibody mixtures

This chapter is published as:

Krieg, D.; Berner, C.; Winter, G.; Svilenov, H. L. Biophysical characterization of binary therapeutic monoclonal antibody mixtures. *Mol. Pharm.* **2020**, *17* (8), 2971–2986. <https://doi.org/10.1021/acs.molpharmaceut.0c00370>

IV.1 Introduction

Fixed-dose combinations and co-formulations of monoclonal antibodies (mAbs) are becoming increasingly popular for the development of new medicines. Such formulations can be used to achieve better therapeutic efficacy due to synergistic pharmacological effects between the two molecules. Co-formulations of mAbs could also improve patient compliance by reducing the number of injections in the course of medication. Furthermore, combining therapeutic proteins can generate value for the pharmaceutical industry by creating new opportunities for intellectual property rights.

Despite the many advantages that co-formulations of mAbs could offer, there are only few published studies that focus on the analytical characterization and stabilization of therapeutic antibody mixtures.^{1–6} The physicochemical behavior of these proteins in co-formulations remains poorly understood. For example, it is unclear when detrimental cross-interactions between two different antibodies in a binary mixture can negatively affect the overall physical stability of the protein solution. Some published studies indicate elevated protein interactions in certain combinations,⁵ while others show the absence of cross-interactions between different mAbs.⁴

In the context of the bigger picture, it is important to know when mAbs with different physicochemical features can be combined in solution without a risk of unfavorable cross-interactions. This information will aid the rational development of drug products containing two or more therapeutic antibodies.

The different properties of mAbs typically arise from differences in the amino acid residues in the variable domains and more specifically, in the complementarity-determining regions (CDRs) that exhibit the highest variability. Therefore, it is crucial to study how mAbs with different charge, hydrophobicity and amino acid residues in the CDR loops behave in binary mixtures. Such studies can be based on computational and biophysical characterization methods that are indicative for antibody physical stability and developability potential.^{7–11}

The use of high-throughput methods that provide information about the protein conformational and colloidal stability is particularly useful at this stage.

Here, we present a study with six therapeutic monoclonal antibodies (trastuzumab, adalimumab, rituximab, bevacizumab, omalizumab and infliximab) and their binary mixtures. The model mAbs differ in key features like isoelectric points, net charge, charge distribution, and amino acid residues in the CDRs to represent different co-formulation scenarios. We applied several established biophysical methods to study the conformational and colloidal stability of the six mAbs alone or in binary mixtures. The mAbs and their binary mixtures were analyzed at pH 5.0 and 7.4, with or without 250 mM NaCl, to investigate a wide range of different solution conditions that are relevant for therapeutic protein co-formulations. The measured biophysical parameters are shared as a comprehensive dataset that can aid researchers during the development of co-formulations with therapeutic antibodies. Remarkably, we show that the six mAbs from the IgG1 class with different features can be combined in binary mixtures at different pH and NaCl concentration without detrimental effects on important biophysical parameters that are indicative for the conformational and colloidal protein stability.

IV.2 Materials and Methods

IV.2.1 Materials

Trastuzumab (Herceptin[®]), adalimumab (Humira[®]), rituximab (Mabthera[®]), bevacizumab (Avastin[®]), omalizumab (Xolair[®]) and infliximab (Remicade[®]) were used as model proteins in this study. Sodium dihydrogen phosphate was purchased from Grüssing GmbH. Disodium hydrogen phosphate was purchased from VWR Chemicals. Acetic acid and sodium acetate were purchased from Sigma Aldrich. NaCl was purchased from Bernd Kraft GmbH. All formulations were prepared with ultrapure water from a Sartorius arium[®] pro system (Sartorius Corporate Administration GmbH, Göttingen, Germany).

IV.2.2 *In silico* comparison of mAb properties and selection of model proteins

Six marketed monoclonal antibodies were selected as model proteins based on the isoelectric points of the antibodies,^{12,13} and the calculated isoelectric points of the respective heavy chain variable domain (V_H) and light chain variable domain (V_L) of each antibody (See Table 1). The primary sequences for the V_H and V_L domains were taken from Jain *et al.*,⁷ and the isoelectric points of these domains were calculated using the Protein-Sol webserver.¹⁴ The primary sequences of the six mAbs were aligned and compared with Protein BLAST.¹⁵ The used primary sequences are provided in the supplementary data. Since the homology

between the Fc fragments of the different mAbs is between 99 and 100% (Table S.IV.1), further computational work is performed only on the Fab fragments of each antibody which exhibit higher differences (See Tables S.IV.2 and S.IV.3).

The hydrophobicity and charged surface area of the respective Fab fragments at pH 5.0 and 7.4 were calculated based on the respective PDB entries for trastuzumab (4HKZ), adalimumab (4NYL), rituximab (2OSL), bevacizumab (1BJ1), omalizumab (2XA8), and infliximab (4G3Y). Missing residues in the PDB files were inserted by using the respective original structure as a template to build a comparative model with the full sequence in the SWISS-MODEL server.¹⁶ The Fab PDB files were processed using H++ to calculate the total charge at pH 5.0 and 7.4 and to adjust the protonation state of each ionizable amino acid at the respective pH at a salinity of 10 mM.¹⁷ The electrostatic surface of the Fab was displayed with UCSF Chimera v1.14 using Coulomb surface coloring with the default parameters and the hydrophobic surface was displayed with the hydrophobicity surface preset.¹⁸ The results for the Coulomb and hydrophobicity surfaces of each Fab can be found in the supplementary data (See Fig S.IV.1).

The hydrophobicity and relative positively and negatively charged areas of the solvent-accessible surface area were calculated as follows: The default atom selection macro *hydrophobic*, *acidic* and *basic* of the VMD 1.9.4 software were applied consecutively for each Fab region. The *basic* macro was adjusted to select arginine, lysine and protonated histidine residues (HIP). The built-in *measure sasa* command was used to calculate the solvent-accessible surface area (SASA) of the full protein and each selection.¹⁹ Furthermore, the H++-processed Fab PDB files were analyzed by the AggresScan3D webserver.²⁰

We also compared the CDR sequences of the mAbs, because these regions represent the main differences between the single mAbs and certain CDR compositions may correlate to increased (cross-)interaction propensity of the mAbs.^{21,22} It has been shown earlier, that net positive charges in the six CDRs may be connected to low antibody specificity and an increased risk of non-specific interactions,⁸ which could also be critical in the context of developing co-formulations. The six CDR regions of each mAb were identified using the Paratome webserver,²³ and are shown in Table IV.1. The CDR regions were then analyzed by counting the number of hydrophobic residues (A, F, I, L, M, V, W, Y), the number of positive charges for histidine (+0.1), lysine (+1) arginine (+1) and the number of negative charges for aspartate (-1) and glutamate (-1), following the approach used by Rabia *et al.*⁸

IV.2.3 Preparation of mAb formulations

The antibodies were purified from the marketed formulations by strong cation exchange chromatography using a Superose HiTrap SP column (GE Healthcare LifeScience, USA), an ÄKTA protein purification system and a linear salt gradient. Subsequently, the proteins were extensively dialyzed into 10 mM sodium acetate pH 5.0 or 10 mM sodium phosphate pH 7.4. The mAbs were then concentrated using Vivaspin 20 5 MWCO PES centrifugal concentrators (Sartorius Lab Instruments, Goettingen, Germany). Subsequently, the concentration was measured with a Nanodrop 2000 (Thermo Fisher Scientific, USA) using the respective extinction coefficients at 280 nm. These solutions were sterile filtered with 0.2 μm filters in a laminar flow hood.

Binary mixtures that include all possible combinations of the six model mAbs were prepared. The ratio between two mAbs in a binary mixture was always 1:1 (m/m). We studied the behavior of the single mAbs and the combinations in four different conditions: 10 mM sodium acetate pH 5.0 with or without 250 mM NaCl, and 10 mM sodium phosphate pH 7.4 with or without 250 mM NaCl. For the addition of NaCl, a 500 mM NaCl stock solution was spiked into the dialyzed protein solutions.

The 10 mM sodium acetate pH 5.0 was selected to display long-range electrostatic interactions of the mAbs at low ionic strength, while 10 mM sodium phosphate pH 7.4 was used to study the behavior of the mAb combinations at physiological pH. Both buffer systems are commonly applied in various marketed mAb formulations, and represent the borders of a pH-range that is relevant for the development of stable mAb formulations.²⁴ The addition of 250 mM NaCl was used to screen the long-range electrostatic interactions and investigate mostly the hydrophobic interactions between the mAbs at pH 5 and 7.4.²⁵ The binary mixtures contained 0.5 g/L of each mAb which accounts to a total protein concentration of 1 g/L. The solutions containing only one mAb had a protein concentration of 0.5 and 1 g/L.

Binary mixtures at high protein concentrations were prepared for trastuzumab, rituximab and omalizumab and contained 25 g/L per protein and compared to the single proteins formulations that contained 50 g/L. Binary mixtures of trastuzumab and rituximab that contained 50 g/L per protein were also prepared and compared to single protein formulations that contained 100 g/L.

IV.2.4 High-throughput fluorimetric analysis of thermal protein unfolding with nanoDSF

Protein solutions were filled into standard nanoDSF capillaries. The capillaries were sealed and placed in a Prometheus NT.48 (NanoTemper Technologies, Munich, Germany). A temperature ramp of 1 °C/min was applied from 20 to 100 °C. The intrinsic protein fluorescence intensity at 330 and 350 nm after excitation at 280 nm was measured for single formulations (0.5 and 1 g/L) and binary mixtures (0.5 g/L of each mAb). The inflection points of the first and second thermal unfolding transitions (IP_1 and IP_2), detected by the change in the fluorescence intensity ratio (FI_{350nm}/FI_{330nm}), were derived from the maximum of the first derivative of each measurement using the ThermControl software V2.1 (NanoTemper Technologies, Munich, Germany). Protein aggregation during heating was also monitored using the backscattering detector of the device. The aggregation onset temperature (T_{agg}) was determined from the increase in the scattering using the same software. The signal for scattered light was also normalized and the excess in scattering was plotted against the temperature for comparisons between different samples. Each measurement was performed in triplicates.

IV.2.5 Dynamic light scattering

The protein solutions were filled in a 1536 well plate (Aurora Microplates, Whitefish, USA). The plate was centrifuged at 2000 rpm for 2 min using a Heraeus Megafuge 40 centrifuge equipped with an M-20 well plate rotor (Thermo Fisher Scientific, Wilmington, USA). Silicon oil was added to seal each well. The plate was centrifuged again at 2200 rpm for 2 min and placed in a DynaPro DLS plate reader III (Wyatt Technology, Santa Barbara, USA). The aggregation of the proteins during heating was studied using a temperature ramp of 0.1 °C/min from 25 to 85 °C. Each measurement contained 3 acquisitions with an acquisition time of 3 s. The autocorrelation function of each measurement was analysed using cumulant analysis with the Dynamics V7.8 software (Wyatt Technology, Santa Barbara, USA). The apparent protein hydrodynamic radius from DLS (R_h) was calculated using the translational diffusion coefficient D_t and the Stokes-Einstein equation. The aggregation onset temperature (T_{on}) from the increase in the R_h from DLS was determined using the onset fit in the Dynamics V7.8 software.

To determinate the interaction parameter k_D , ten different protein concentrations from 0.5 to 9 g/L were prepared for each monoclonal antibody and the binary mixtures. The ratio of monoclonal antibodies in the mixtures was set to 1:1 (m/m). The DLS measurements were performed at 25 °C and each measurement contained 10 acquisitions with an acquisition time

of 5 s. All DLS measurements were performed in triplicates. The obtained data was analyzed with the Dynamics V7.8 software (Wyatt Technology, Santa Barbara, USA). The translational diffusion coefficient D_t was calculated from the autocorrelation functions using cumulant analysis and k_D was determined by linear regression of D_t against the respective concentration based on the following equation:^{26,27}

$$D_t = D_0 (1 + k_{DC})$$

where D_0 is the mutual diffusion coefficient at infinite dilution and c is the protein concentration.

IV.3 Results

IV.3.1 Results overview

The obtained results are structured in several sections and figures. First, we present the *in silico* analysis of the mAbs and show their difference in sequence composition, charge and hydrophobicity (See Fig. IV.1, Tables IV.1 and IV.2). The following sections present the experimental data: The aggregation onset temperatures from DLS (See Fig. IV.2), the temperature of the first inflection point measured with nanoDSF (See Fig. IV.3), the aggregation onset temperatures measured with the backscattering detector of the Prometheus NT.48 (See Fig. IV.4) and interaction parameters (See Fig. IV.5). The mean values and standard deviations are provided at the end in Tables IV.4 and IV.5 for measurements at pH 5.0 and 7.4 respectively. Three binary mixtures (trastuzumab + rituximab, trastuzumab + omalizumab and rituximab + omalizumab) were also tested at elevated protein concentrations in the same conditions (See Table IV.6). The full dataset is provided in the supplementary data.

IV.3.2 *In silico* comparison of the model mAbs

We compared the selected mAbs and the respective Fab regions in terms of charge and hydrophobicity to identify structural elements that may correlate with increased cross-interaction propensity. We focused mainly on the analysis of the Fab regions (See Fig. IV.1A), especially of the CDR domains, as the BLAST alignment of the primary sequences shows a very high similarity (99-100%) between the Fc regions (See Table S.IV.1). This is not surprising because all six model mAbs belong to the IgG1 subclass.²⁸

The mAbs differ in their pI and the calculated pI of the respective V_H and V_L domains (See Table IV.1). The calculated net charge (See Fig. IV.1C) of the Fab fragments at both pH 5.0 and 7.4 also differs between the mAbs. At pH 5.0, the Fabs of trastuzumab, adalimumab,

rituximab and bevacizumab exhibit higher positive net charges than the infliximab Fab and omalizumab Fab (See Fig. IV.1C). At pH 7.4, all Fab regions show decreased net charges compared to pH 5.0, but to a different extent. The calculated net charges of the bevacizumab Fab and omalizumab Fab decreased more compared to the Fab regions of trastuzumab, adalimumab and rituximab, while the infliximab Fab carries almost no net charge at pH 7.4 (See Fig. IV.1C). As all Fab regions show positive or close to neutral net charges in the H++ calculations, strong attractive long-range electrostatic Fab-Fab interactions between different mAbs are not expected at pH 5.0 or 7.4. Therefore, the binary mixtures of the mAbs in our dataset will present a different case compared to protein pairs with opposite net charges (like BSA and lysozyme in a certain pH range).

All these calculations provide first insights into the properties of the mAbs but do not reflect potential asymmetric charge distributions, which may favor electrostatic self- or cross-interaction despite the similar net charge of the molecule.²² Thus, we compared the 3D structures of the Fab regions and displayed surface charge and hydrophobicity for both pH 5.0 and 7.4, based on the respective H++ calculations (See Figs. IV.1B and S.IV.1). The Fab fragments show differences in their surface charge distributions, although the absolute values for positively and negatively charged surface areas show small differences between the six Fab fragments at both pH 5.0 and 7.4 (See Figs. IV.1D and IV.1E).

No large difference in the Fab hydrophobic surface area is predicted by the calculations and likewise displayed by the 3D structures (See Figs. IV.1F, IV.1G and S.IV.1). The maximum score from AggreScan 3D is lowest for trastuzumab and adalimumab, and highest for bevacizumab (See Fig. IV.1H). The average AggreScan 3D score also indicates small differences between the Fab regions (See Fig. IV.1I).

The CDR loops are solvent exposed and contain high levels of charged and hydrophobic residues that promote antigen-binding, but could also favor non-specific protein-protein interactions.²⁹ Hence, the CDR sequences of all studied mAbs were analyzed in terms of hydrophobicity and charge at pH 5.0 and 7.4 to identify sequences that may promote cross-interactions (See Table IV.1). While the number of hydrophobic residues in the CDRs is similar for all studied mAbs, there are differences in the net CDR charge (See Table IV.1).

In general, the selected mAbs exhibit differences in the magnitude of the net charge, charge distributions and CDR compositions. Thus, the 15 binary mixtures of these six model mAbs represent a range of possible scenarios that could lead to detrimental protein interactions in mAb co-formulations. However, all selected antibodies are approved and clinically established drugs with acceptable physicochemical properties. No early stage

development drugs with unfavorable biophysical properties were included in this study. Such problematic molecules are interesting to study, but from a practical point of view will have a lower chance to pass all criteria on the way to market approval, even when formulated without the presence of a second protein. Although all mAbs in this study are marketed products, it is interesting to note that some of them have different issues in assays used for developability assessment. The results of 12 different biophysical assays performed by Jain *et al.* for the selected monoclonal antibodies are summarized in Table IV.3 and reflect the covered range of biophysical properties.⁷ The selected drugs represent various scenarios for co-formulation of therapeutic mAbs.

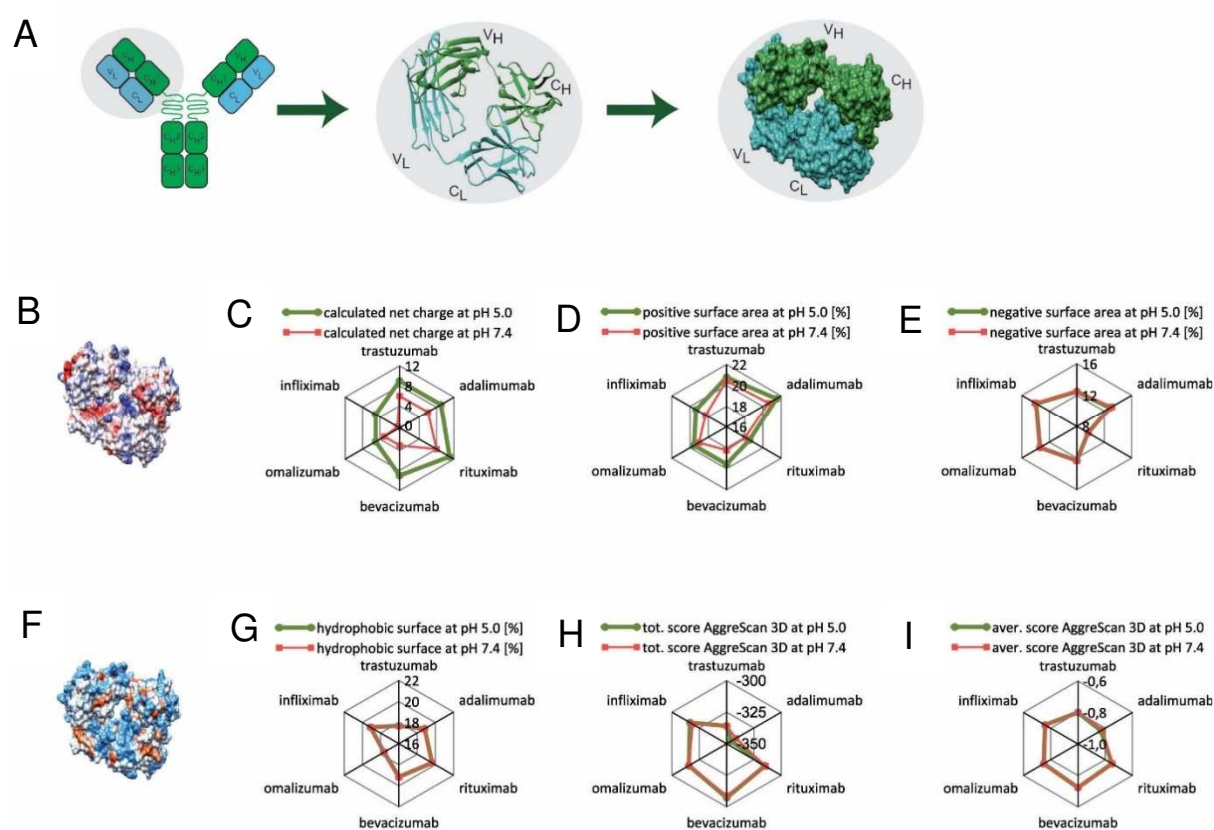


Figure IV.1. *In silico* analysis of the Fab regions. (A) exemplary orientation and surface display of trastuzumab Fab using UCSF Chimera v1.14 (B) exemplary Coulomb surface coloring of trastuzumab Fab (the other images can be found in Fig S1), (C) calculated surface net charge of the six Fab regions, (D) positive and (E) negative surface area of the respective Fabs, (F) exemplary visual presentation of the surface hydrophobicity of trastuzumab Fab (the other images can be found in Fig S.IV.1), (G) calculated hydrophobic surface area of each Fab, (H) total and (I) average score from AggreScan 3D for the Fabs of each model mAb.

Table IV.1. Key features of the selected model mAbs: pI of the entire mAb,^{12,13} calculated pIs of the respective VH and VL domains, composition of the CDR loops and calculated CDR charges.⁸

| antibody | Isoelectric points | | | CDR sequence (residues) | | | | | | | CDR charge at pH 5.0 | | | CDR charge at pH 7.4 | | |
|-------------|--------------------|-------------------|-------------------|-------------------------|------------------------|----------------------|-----------------------|-----------------------------|-----------------------------|----------------------|----------------------|----------|------------|----------------------|----------|------------|
| | pI | pI V _H | pI V _L | V _L CDR1 | V _L CDR2 | V _L CDR3 | V _H CDR1 | V _H CDR2 | V _H CDR3 | hydrophobic residues | positive | negative | net charge | positive | negative | net charge |
| trastuzumab | 9.10 | 9.06 | 9.55 | QDVNTAVA (27-34) | LLIYSASFLYS (46-56) | QQHYTTPP (89-96) | FNKIDTYIH (27-35) | WVARIYPTNGYTRY (47-60) | RWGGDGFYAMDY (98-109) | 30 | 4.2 | 4 | 0.2 | 4.2 | 4 | 0.2 |
| adalimumab | 8.90 | 5.22 | 10.66 | QGIRNYLA (27-34) | LLIYAASLQSL (46-56) | QRYNRAPY (89-96) | FTFDDYAMH (27-35) | WVSAITWNSGHIDY (47-60) | KVSYLSTASSLDY (98-110) | 32 | 4.2 | 3 | 1.2 | 4.2 | 4 | 0.2 |
| rituximab | 9.40 | 9.50 | 9.84 | SSVSYIH (27-33) | PWIYATSNLAS (45-55) | QQWTSNPP (88-95) | YTFTSYNMH (27-35) | WIGAIYPGNGDTSY (47-60) | RSTYYGGDWYFNV (98-110) | 26 | 1.2 | 2 | -0.8 | 1.2 | 2 | -0.8 |
| bevacizumab | 8.30 | 7.80 | 7.73 | QDISNYLN (27-34) | VLIYFTSSLHS (46-56) | QQYSTVPW (89-96) | YTFTNYGMN (27-35) | WVGWINTYTGEPTY (47-60) | KYPHYGSSHWFYFDV (98-112) | 29 | 1.3 | 3 | -1.7 | 1 | 3 | -2 |
| omalizumab | 6.80 | 9.12 | 4.65 | QSVDDYDGSYMN (27-38) | LLIYAASYLES (50-60) | QQSHEDPY (93-100) | YSITSGYSWN (27-36) | WVASITYDGSTNYNP (48-62) | ARGSHYFGHWHFAV (97-110) | 29 | 1.4 | 7 | -5.6 | 1.3 | 7 | -5.7 |
| infliximab | 7.30 | 6.40 | 5.65 | QFVGSSIH (27-34) | LLIKYASESMS (46-56) | QQSHSWPF (89-96) | FIFSNHWMN (27-35) | WVAEIRSKSINSATHY (47-62) | RNYYGSTYDY (100-109) | 27 | 4.4 | 3 | 1.4 | 4.2 | 3 | 1.2 |

Table IV.2. Numerical results from the *in silico* analysis of the Fab regions

| Fab region | calculated net charge | | positive surface area [%] | | negative surface area [%] | | hydrophobic surface [%] | | total score value Aggrescan3D 2.0 | | average score value Aggrescan3D 2.0 | |
|-------------|-----------------------|--------|---------------------------|--------|---------------------------|--------|-------------------------|--------|--------------------------------------|---------|--|--------|
| | pH 5.0 | pH 7.4 | pH 5.0 | pH 7.4 | pH 5.0 | pH 7.4 | pH 5.0 | pH 7.4 | pH 5.0 | pH 7.4 | pH 5.0 | pH 7.4 |
| trastuzumab | 9 | 6 | 20.78 | 20.43 | 12.49 | 12.48 | 17.69 | 17.68 | -325.79 | -325.79 | -0.775 | -0.775 |
| adalimumab | 9 | 6 | 21.49 | 20.63 | 12.84 | 13.12 | 18.83 | 18.77 | -335.34 | -326.92 | -0.806 | -0.784 |
| rituximab | 11 | 8 | 18.52 | 18.05 | 9.63 | 9.62 | 19.65 | 19.65 | -308.69 | -308.05 | -0.735 | -0.735 |
| bevacizumab | 9 | 3 | 19.56 | 18.23 | 12.33 | 12.34 | 19.15 | 19.19 | -300.23 | -301.12 | -0.706 | -0.706 |
| omalizumab | 5 | 3 | 19.57 | 19.02 | 13.36 | 13.33 | 17.62 | 17.61 | -304.57 | -304.57 | -0.723 | -0.723 |
| infliximab | 5 | 0 | 19.34 | 18.29 | 13.92 | 14.12 | 19.11 | 19.11 | -307.55 | -306.80 | -0.737 | -0.734 |

Table IV.3. Results of the selected monoclonal antibodies in the 12 biophysical assays performed by Jain *et al.*⁷ The Asteriks mark values that exceed the thresholds proposed by Jain *et al.* that indicate unfavorable biophysical properties.

| mAb | HEK Titer (mg/L) | Fab T _m by DSF (°C) | SGAC-SINS AS100 ((NH ₄) ₂ SO ₄ mM) | HIC Retention Time (Min) | SMAC Retention Time (Min) | Slope for Accelerated Stability | Poly-Specificity Reagent (PSR) SMP Score (0-1) | Affinity-Capture Self-Interaction Nanoparticle Spectroscopy (AC-SINS) $\Delta\lambda_{max}$ (nm) Average | CIC Retention Time (Min) | CSI-BLI Delta Response (nm) | ELISA | BVP ELISA |
|-------------|------------------|--------------------------------|--|--------------------------|---------------------------|---------------------------------|--|--|--------------------------|-----------------------------|-------|-----------|
| trastuzumab | 159.5 | 78.5 | 800.0 | 9.7 | 8.8 | 0.04 | 0.00 | 2.0 | 8.8 | -0.02 | 1.06 | 1.34 |
| adalimumab | 134.9 | 71.0 | 900.0 | 8.8 | 8.7 | 0.05 | 0.00 | 1.1 | 8.9 | -0.01 | 1.08 | 1.49 |
| rituximab | 164.1 | 69.0 | 700.0 | 10.8 | 9.1 | 0.03 | 0.38 * | 2.1 | 10.1 * | -0.01 | 1.19 | 2.93 |
| bevacizumab | 50.0 | 63.5 | 700.0 | 11.8 * | 11.1 | 0.22 * | 0.00 | 0.8 | 9.8 | -0.02 | 1.29 | 2.78 |
| omalizumab | 150.4 | 77.5 | 800.0 | 9.5 | 8.7 | 0.05 | 0.00 | -0.4 | 8.5 | -0.02 | 1.12 | 1.17 |
| infliximab | 6.6 | 64.5 | 0.0 * | 10.4 | 8.9 | 0.18 * | 0.00 | 29.6 * | 9.0 | 0.05 * | 1.04 | 1.37 |

IV.3.3 Aggregation during heating determined with DLS

We used DLS to measure the increase in R_h for the single mAbs and their binary mixtures (See Fig. IV.2A). The T_{on} values differed greatly between the six model mAbs (See Figs. IV.2B and IV.2C). Except for infliximab, all studied mAbs showed highest T_{on} values in 10 mM sodium acetate pH 5.0. In most cases, the T_{on} values were lower at pH 7.4 compared to pH 5.0, which could be explained by decreased electrostatic repulsion at pH 7.4, where the solution pH is closer to the isoelectric points of the proteins. The addition of 250 mM NaCl at pH 5.0 significantly reduced the T_{on} of all mAbs, while at pH 7.4, only minor effects from the NaCl could be observed. The drop of the T_{on} value upon addition of salt at pH 5.0 was caused by reduced electrostatic repulsion, and thus facilitated aggregation.²⁵ For infliximab, an increased hydrodynamic radius was detected at pH 7.4 compared to pH 5.0 (See Figs. S.IV.2 and S.IV.3), which indicated the presence of oligomers in the sample. Published data shows that infliximab exhibits weak reversible self-association in solution.³⁰ These weakly associated aggregates probably disintegrated after moderate heating (See Fig. S.IV.3).

Despite the individual behavior of the single mAbs, almost all binary mixtures exhibited an equal or slightly higher T_{on} -value compared to the least stable equally concentrated single mAb of the respective mixture (See Figs. IV.2D, IV.2E, IV.2F and IV.2G). This was true for all four tested solution conditions. Very slightly decreased T_{on} values could only be detected for the binary mixture of trastuzumab plus omalizumab in 10 mM sodium phosphate pH 7.4 with 250 mM NaCl and rituximab plus infliximab in 10 mM sodium phosphate pH 7.4 with 250 mM NaCl (See Fig. IV.2G). These were minor differences in the onset temperatures, and we should note that the DLS aggregation curves of the binary mixtures showed very similar shapes like the aggregation curves of the single proteins (See Figs. S.IV.2 and S.IV.3). In general, the T_{on} of the less stable mAb was not negatively affected by the presence of a second mAb. The traces of the binary mixtures followed the trend of the least stable antibody or gave intermediate traces, but did not show compromised stability profiles compared to the least stable antibody of the respective mixture (See Figs. S.IV.2 and S.IV.3). This was true for combinations with similar T_{on} -values of the single mAbs, e.g. trastuzumab plus omalizumab in 10 mM sodium acetate pH 5.0 with 250 mM NaCl (See Fig. S.IV.2), but also for combinations with very different T_{on} -values of the single mAbs, e.g. trastuzumab plus infliximab in 10 mM sodium acetate pH 5.0. This data indicates that there are no unfavorable effects on the colloidal stability of the proteins in this dataset, arising from the addition of a second mAb.

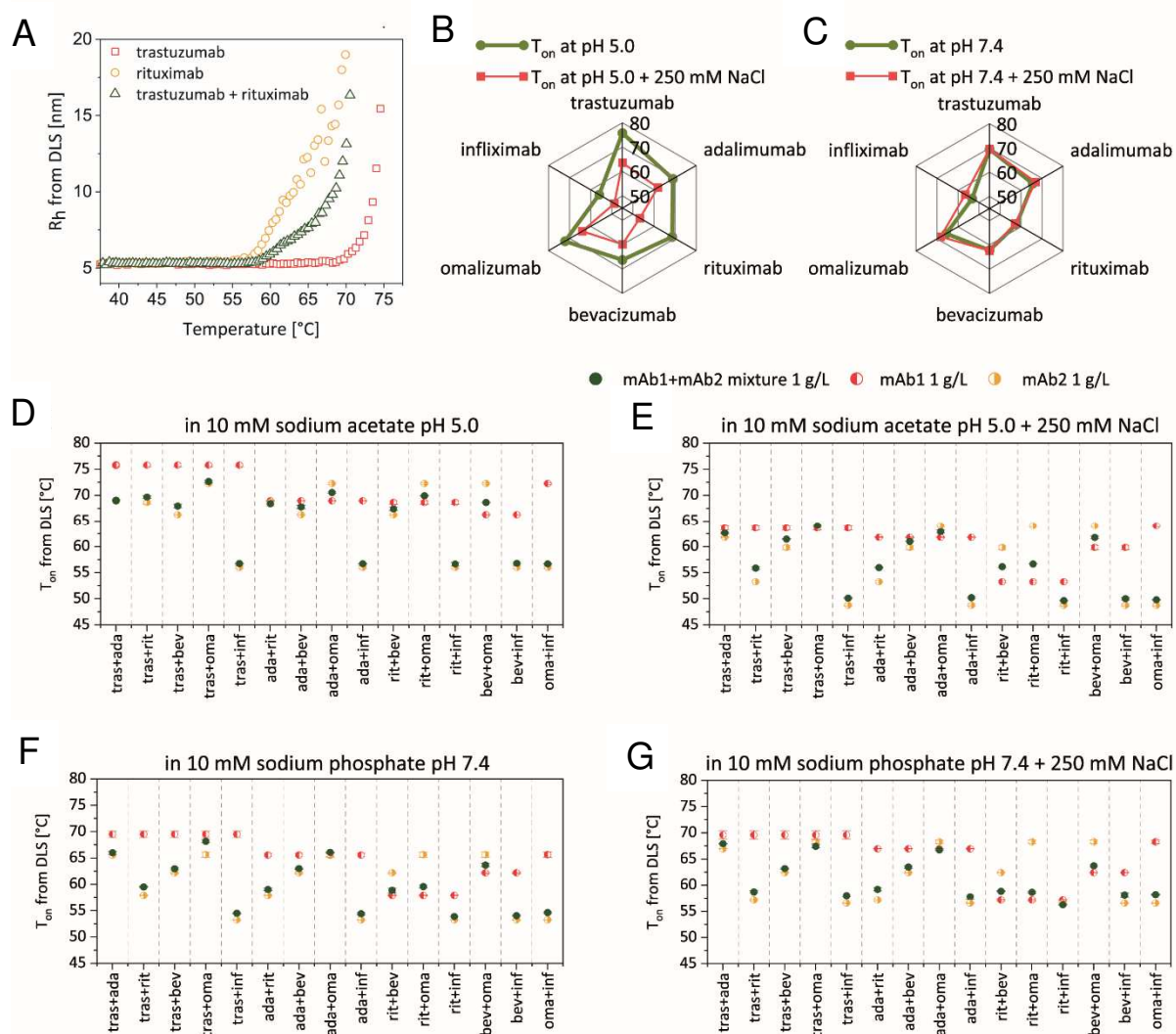


Figure IV.2. Aggregation onset temperature from DLS (T_{on}). (A) Example dataset for trastuzumab (1 g/L), rituximab (1 g/L) and the binary combination of trastuzumab and rituximab (0.5 g/L of each antibody). Radar diagrams for the T_{on} -values of the single mAbs (1 g/L) at pH 5.0 (B) and pH 7.4 (C). (D, E, F, G) T_{on} -values for all 15 binary mixtures compared to the respective single mAbs. “mAb1” refers to the first protein in the code “mAb1+mAb2”, e.g. in tra+ada mAb1 is trastuzumab and mAb2 is adalimumab.

IV.3.4 Thermal unfolding with nanoDSF

The thermal unfolding of the single proteins and the binary mixtures was studied with nanoDSF (Fig. IV.3A). The inflection points of the first thermal unfolding at lower temperature (IP1) and the second thermal unfolding at higher temperature (IP2) were derived from the curves as explained in the Methods section. The IPs from nanoDSF are surrogate parameters for the apparent protein melting temperatures. The transition at lower temperature

usually reflects the unfolding of the C_H2 domains, while the transition at higher temperature typically corresponds to the unfolding of the Fabs and the C_H3 domains, as described earlier.³¹

The IP1 values of the six mAbs differed, indicating that these proteins have different conformational stability (See Figs. IV.3B and IV.3C). In general, the IP1 values were higher at pH 7.4 compared to pH 5.0. This can be linked to a decreased energetic state of the folded state at pH 7.4.³² At pH 5.0, the additional charges can destabilize the native state compared to pH 7.4 and thus reduce the conformational stability. The addition of 250 mM NaCl reduced the IP1 values at pH 5.0, while at pH 7.4 the addition of salt had only minor effects on the transitions (See Figs. IV.3B and IV.3C). The IP2 values of the six mAbs are above 76 °C which indicates high conformational stability of the Fab/C_H3 domains in all four tested solution conditions (See Tables IV.3 and IV.4). This high intrinsic conformational stability is expected for marketed mAbs.⁷

In general, the binary mAb mixtures showed IP1 and IP2 values that were not lower compared to the less stable mAb in the mixture (See Figs. IV.3D, IV.3E, IV.3F and IV.3G, Tables IV.3 and IV.4). Noteworthy, the traces of the binary mixtures showed intermediate results compared to the single mAbs, but not always an arithmetic mean (See Figs S.IV.4 and S.IV.5). This can be a result of the different contribution of aromatic amino residues from the two mAbs to the intrinsic protein fluorescence of the binary mixture.

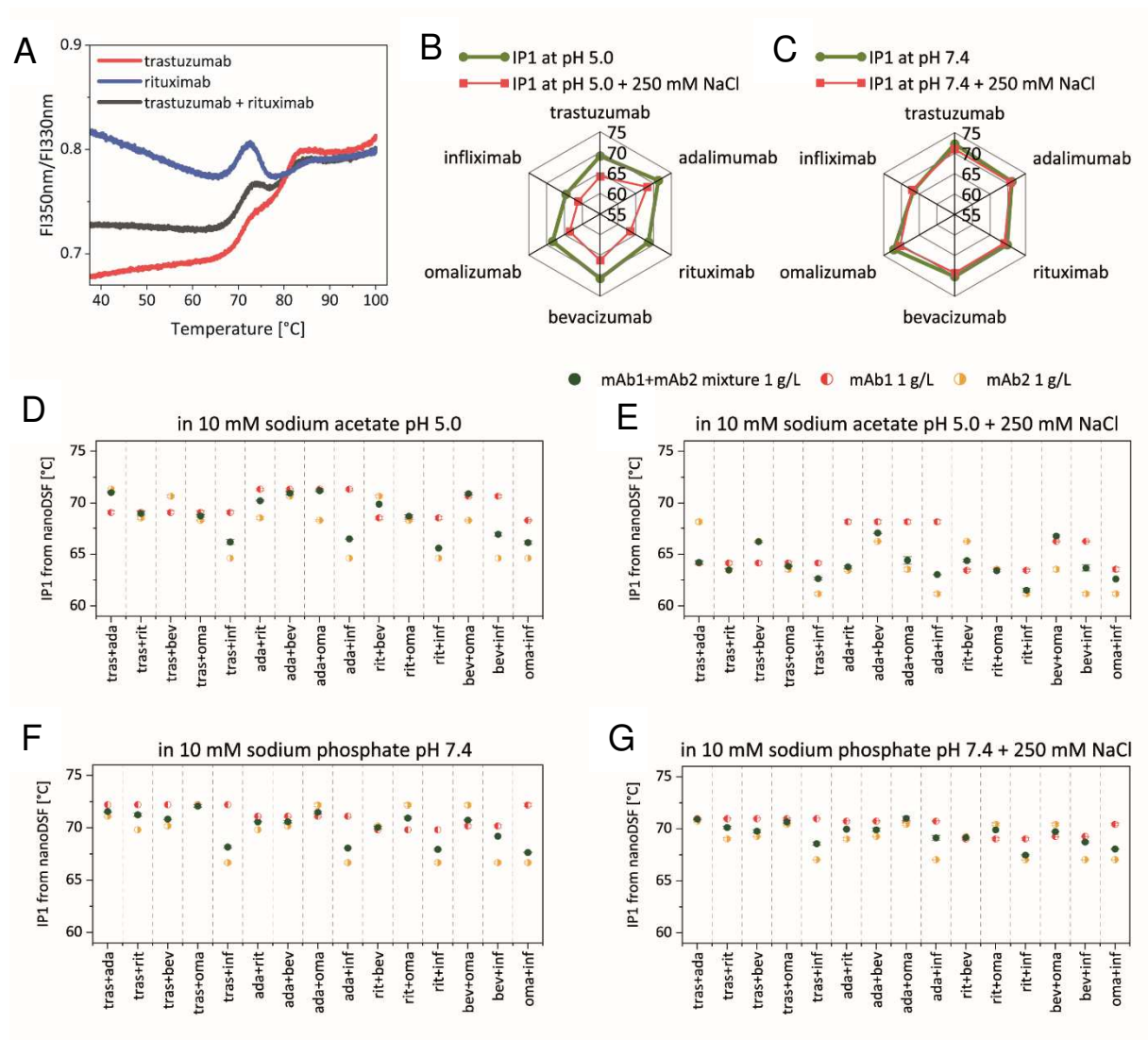


Figure IV.3. Thermal protein unfolding studied with nanoDSF. (A) Example dataset for trastuzumab (1 g/L), rituximab (1 g/L) and the binary combination of trastuzumab and rituximab (0.5 g/L of each antibody). Radar diagrams for the IP1 values of the single mAbs (1 g/L) at pH 5.0 (B) and pH 7.4 (C). (D, E, F, G) IP1 values for all 15 binary mixtures compared to the respective single mAbs. “mAb1” refers to the first protein in the code “mAb1+mAb2”, e.g. in tra+ada mAb1 is trastuzumab and mAb2 is adalimumab.

IV.3.5 Aggregation during heating determined with nanoDSF backscattering

We evaluated the aggregation during heating of the single mAbs and their binary mixtures from the change in the backscattering signal obtained from nanoDSF (Fig. IV.4A). This information is complementary to the DLS data presented in IV.3.3. However, there are some essential differences between the two approaches. Detecting aggregation onset temperature with DLS provides information about the formation of small soluble aggregates in the solution, but as the aggregates grow and the sample becomes more heterogeneous, the DLS

data becomes less meaningful. On the contrary, the backscattering detector from nanoDSF detects only aggregates above a certain size, but the data is still informative when very large aggregates form in the sample or when precipitation occurs.^{33,34}

The T_{agg} values differed between the six model mAbs (See Fig. IV.4B and IV.4C). Interestingly, no aggregation was detected by nanoDSF backscattering in 10 mM sodium acetate pH 5.0 for any sample (See Figs. IV.4B, IV.4C and S.IV.6). This can be explained by the strong electrostatic repulsion in this condition which inhibits the aggregate growth and therefore the aggregates do not reach a size that is detectable by the backscattering detector used in nanoDSF.³⁵

Remarkably, the backscattering signal from the binary mixtures allowed us to see the underlying aggregation profiles of the individual mAbs for multiple binary mixtures at pH 5.0 with 250 mM NaCl and at pH 7.4 with or without 250 mM NaCl (See Figs. IV.4A, S.IV.6 and S.IV.7). The aggregation pattern detected by nanoDSF backscattering often showed a 2-step transition, which reflected the aggregation pattern of the respective single mAbs (See Figs. IV.4A, S.IV.6 and S.IV.7). The aggregation onsets in the binary mixtures occurred at the same temperature as in the single formulations and the excess scattering of the binary mixture resembled the sum of the excess scattering signals of the individual mAbs with the same concentration (See Fig. S.IV.6 and S.IV.7). Like the previously measured biophysical parameters, the T_{agg} of the binary mixtures was not lower than the T_{agg} of the least stable mAb (See Figs. IV.4E, IV.4F and IV.4G). This was true for all 15 combinations in all tested conditions and indicates that no stability compromising interactions occurred between these antibodies.

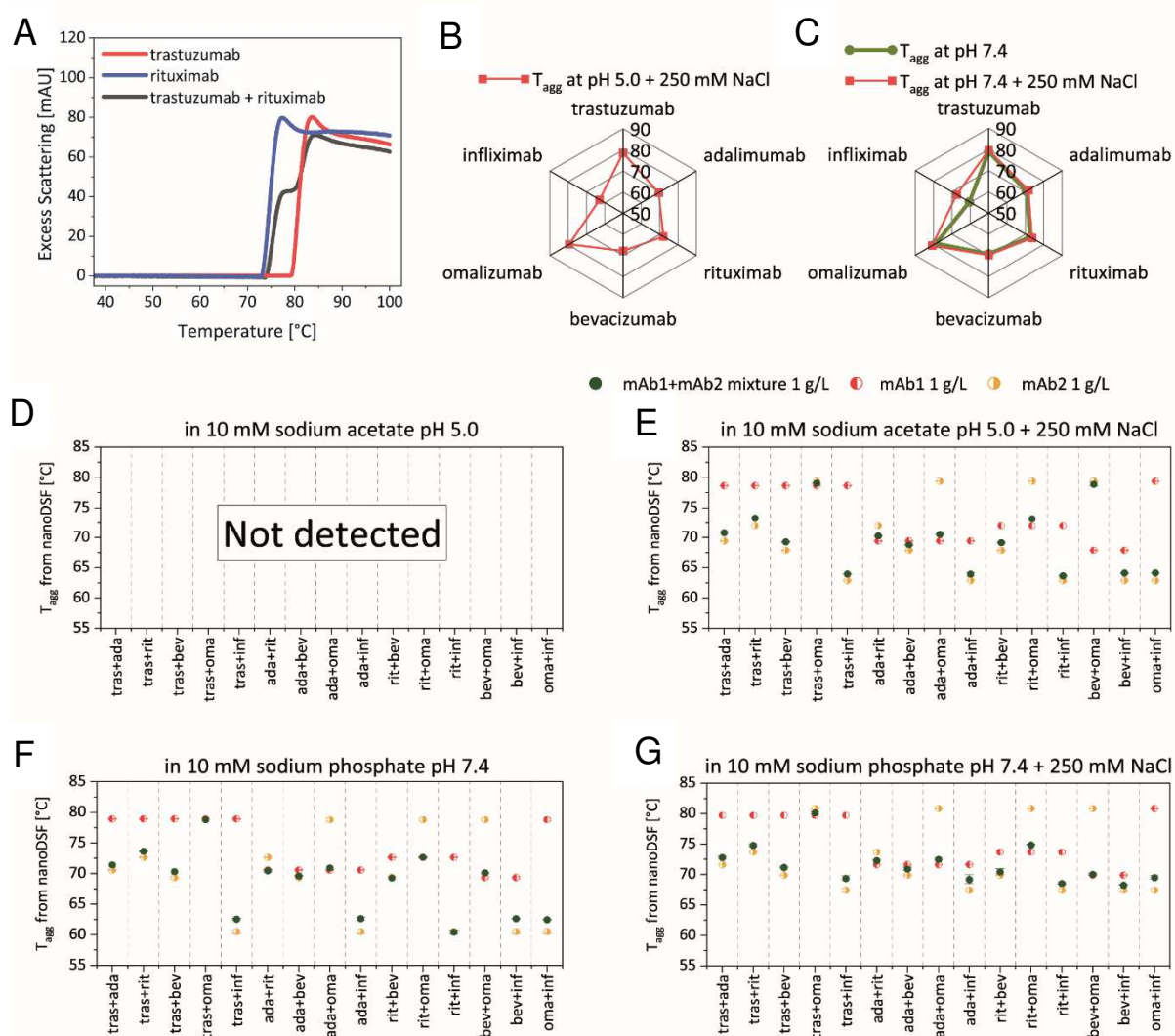


Figure IV.4. Aggregation during heating detected from the nanoDSF backscattering signal. (A) Example dataset for trastuzumab (1 g/L), rituximab (1 g/L) and the binary combination of trastuzumab and rituximab (0.5 g/L of each antibody). Radar diagrams for the T_{agg} values of the single mAbs (1 g/L) at pH 5.0 (B) and pH 7.4 (C). (D) No aggregation was detected by nanoDSF backscattering for any mAb and any binary mixture in 10 mM sodium acetate pH 5.0 (E, F, G). T_{agg} values for all 15 binary mixtures compared to the respective single mAbs. “mAb1” refers to the first protein in the code “mAb1+mAb2”, e.g. in tra+ada mAb1 is trastuzumab and mAb2 is adalimumab.

IV.3.6 Analysis of the diffusion interaction parameter (k_D)

We used DLS to measure the protein concentration dependence of D_t and to determine the k_D of the individual mAbs and their binary mixtures (See Fig. IV.5A). The individual proteins exhibited different k_D values depending on the solution conditions (See Figs. IV.5B and IV.5C). At pH 5.0 without NaCl, positive k_D values were detected for all six mAbs. The k_D values became negative upon addition of 250 mM NaCl to the 10 mM sodium acetate pH 5.0 buffer. At pH 7.4 the k_D values were also negative independent of the addition of 250 mM NaCl. The higher k_D values at pH 5.0 without NaCl indicated stronger repulsive electrostatic protein interactions compared to the other three conditions.²⁵ This concurs well with the high T_{on} , T_{agg} values and the small aggregate sizes that were observed during heating of the individual mAbs in 10 mM sodium acetate pH 5.0. No k_D values were determined for omalizumab in 10 mM sodium phosphate pH 7.4 and infliximab in 10 mM sodium phosphate (with or without NaCl) because the protein concentration dependence of D_t was not linear (See Fig. S.IV.9). This was most likely caused by protein oligomerization due to strong self-association, resulting from long-range electrostatic protein self-interactions. This is further supported by the observation that the addition of 250 mM NaCl to the 10 mM sodium phosphate pH 7.4 reduced the oligomerization of omalizumab and allowed the calculation of a negative k_D value (See Fig. S.IV.9). In the case of infliximab, we also observed non-linear decrease in D_t as protein concentration is increased (See Fig. S.IV.9). This can be explained with the almost neutral net charge of infliximab at pH 7.4, which is indicated by its isoelectric point of 7.3 and the low calculated net charge of the Fab. This indicates that hydrophobic interactions are probably the dominant factor towards oligomerization of infliximab at pH 7.4 and supports previous reports, where dimerization of infliximab was assigned to hydrogen bonding and hydrophobic interactions.³⁰

The DLS data shows that the binary mAb mixtures did not exhibit more negative k_D values compared to the least stable mAb in the mixture (See Figs. IV.5D, IV.5E, IV.5F and IV.5G). In most cases, the measured D_t in the binary mixture was an intermediate value of the D_t values of the single mAbs at the same concentration (See Figs. S.IV.8 and S.IV.9). The combinations rituximab plus omalizumab in 10 mM sodium acetate pH 5.0 with 250 mM NaCl, adalimumab plus bevacizumab in 10 mM sodium phosphate pH 7.4 and trastuzumab plus omalizumab in 10 mM sodium phosphate pH 7.4 with 250 mM NaCl showed slightly more negative values compared to the single mAbs (See Tables IV.3 and IV.4). This could be an indication for additional attractive interactions in the mixture. However, these differences

were very small and occurred only for mixtures of mAbs with very similar k_D values. Thus, these differences are not expected to have an impact on the physical stability of the proteins.

IV.3.7 Results for high protein concentrations

Until now, we performed the characterization on the model mAbs and their binary mixtures at relative low concentrations (< 10 g/L protein). Weak protein (cross-)interactions can be dependent on the protein concentration. Thus, binary mixtures of selected antibodies were also prepared at high protein concentrations up to 100 g/L and their conformational and colloidal stability was studied by nanoDSF, nanoDSF backscattering and DLS. Based on the *in silico* analysis of the Fab regions (See Fig. IV.1), trastuzumab, rituximab and omalizumab were selected. While trastuzumab and rituximab show similar isoelectric points, but opposite CDR-charges at pH 5.0 and pH 7.4, trastuzumab and omalizumab exhibit different isoelectric points and opposite CDR-charges at pH 5.0 and pH 7.4 (See Table IV.1). Rituximab and omalizumab show different isoelectric points and negative CDR charge at pH 5.0 and pH 7.4.

The results are given in Table IV.6 and the complete dataset is presented in the supplementary data (See Figs. S.IV.10, S.IV.11, S.IV.12, and S.IV.13). In general, the results for high protein concentrations confirm the results for low protein concentrations. All binary mixtures at high protein concentrations exhibited an equal or slightly higher T_{on} value compared to the least stable equally concentrated single mAb of the respective mixture in all tested conditions. Furthermore, no stability-compromising aggregation pattern was detected for the binary mixture of rituximab and omalizumab in 10 mM sodium phosphate pH 7.4 at 50 g/L (See Fig. S.IV.12K), although the binary mixture exhibits an increased apparent hydrodynamic radius at ambient temperature, which may be assigned to weak cross-interactions between mAb-1 and mAb-2. This indicates that even in the presence of weak cross-interactions, the colloidal stability of binary mAb mixtures is not compromised compared to the single mAb formulations. Further, even if there is cross-interaction between these two mAbs at higher concentration, this cross-interaction can be screened by formulation optimization, as the increased hydrodynamic radius was not observed in the remaining conditions.

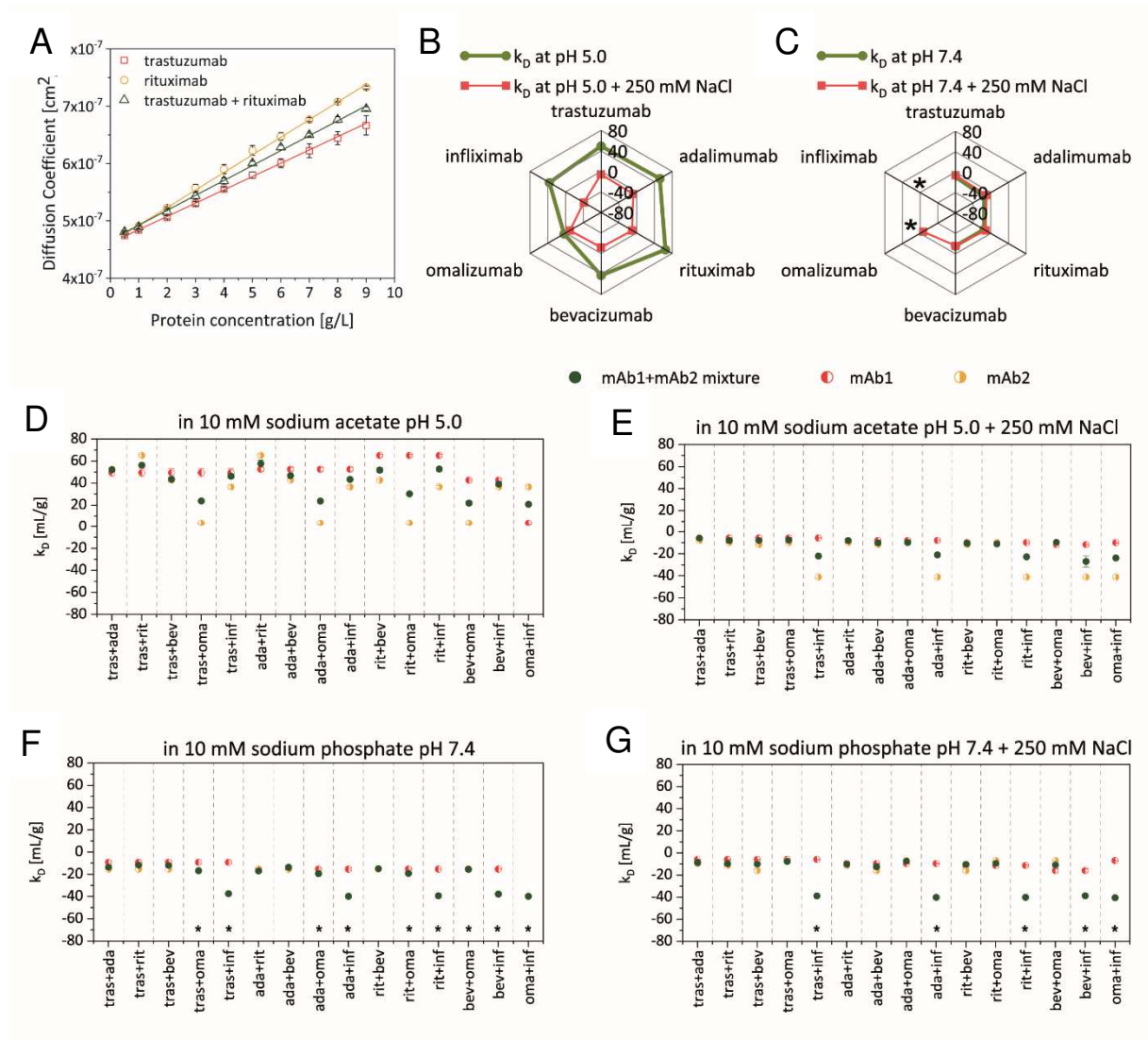


Figure IV.5. Diffusion interaction parameter k_D assessed with DLS. (A) Example dataset for trastuzumab, rituximab and the binary combination of trastuzumab and rituximab in 10 mM sodium acetate pH 5.0. Radar diagrams for the k_D values of the single mAbs at pH 5.0 (B) and pH 7.4 (C) without or with 250 mM NaCl. (D, E, F, G) k_D values for all 15 binary mixtures (green) compared to the respective single mAbs (red and yellow). “mAb1” refers to the first protein in the code “mAb1+mAb2”, e.g. in tra+ada mAb1 is trastuzumab and mAb2 is adalimumab. The asterisks indicate that no k_D -value was obtained because the protein concentration dependence of D_t was not linear in this condition.

Table IV.4. Summary for the biophysical parameters of the single mAbs and their binary mixtures (0.5 + 0.5 g/L) in 10 mM sodium acetate pH 5.0 with or without 250 mM NaCl. All measurements were performed in triplicates. The mean values with standard deviation are shown in the table.

| | 10 mM sodium acetate pH 5.0 | | | | | | | | | |
|---------------------|-----------------------------|----------------------|-----------------------|----------------------|-----------------------|----------------------|----------------------|-----------------------|----------------------|-----------------------|
| | + 0 mM NaCl | | | | | + 250 mM NaCl | | | | |
| | IP ₁ [°C] | IP ₂ [°C] | T _{agg} [°C] | T _{on} [°C] | k _D [mL/g] | IP ₁ [°C] | IP ₂ [°C] | T _{agg} [°C] | T _{on} [°C] | k _D [mL/g] |
| trastuzumab 1 g/L | 69.10 ± 0.17 | 81.33 ± 0.06 | n.a. | 75.79 ± 0.25 | 49.47 ± 3.78 | 64.13 ± 0.15 | 79.33 ± 0.15 | 78.63 ± 0.06 | 63.59 ± 0.43 | -5.77 ± 0.28 |
| trastuzumab 0.5 g/L | 68.83 ± 0.21 | 81.40 ± 0.00 | n.a. | 76.19 ± 0.61 | | 64.13 ± 0.15 | 77.43 ± 0.45 | 79.10 ± 0.10 | 64.98 ± 0.43 | |
| + adalimumab | 71.03 ± 0.06 | 81.57 ± 0.15 | n.a. | 69.01 ± 0.17 | 52.00 ± 0.61 | 64.20 ± 0.17 | 78.57 ± 0.15 | 70.80 ± 0.00 | 62.63 ± 0.14 | -5.84 ± 0.38 |
| + rituximab | 69.00 ± 0.17 | 81.87 ± 0.06 | n.a. | 69.67 ± 0.23 | 56.20 ± 0.40 | 63.47 ± 0.15 | 79.50 ± 0.10 | 73.30 ± 0.00 | 55.88 ± 0.29 | -7.96 ± 1.02 |
| + bevacizumab | 70.67 ± 0.12 | 81.37 ± 0.15 | n.a. | 67.95 ± 0.37 | 43.43 ± 1.82 | 66.20 ± 0.10 | 79.37 ± 0.06 | 69.27 ± 0.06 | 61.45 ± 0.10 | -7.98 ± 0.66 |
| + omalizumab | 68.77 ± 0.12 | 81.10 ± 0.20 | n.a. | 72.64 ± 0.27 | 23.83 ± 0.80 | 63.83 ± 0.06 | 78.83 ± 0.23 | 79.03 ± 0.06 | 64.09 ± 0.24 | -7.52 ± 0.31 |
| + infliximab | 66.17 ± 0.25 | 81.53 ± 0.15 | n.a. | 56.75 ± 0.10 | 46.27 ± 1.78 | 62.63 ± 0.12 | 79.77 ± 0.15 | 63.93 ± 0.12 | 50.14 ± 0.14 | -22.07 ± 0.12 |
| adalimumab 1 g/L | 71.33 ± 0.12 | 82.97 ± 0.38 | n.a. | 68.95 ± 0.08 | 52.50 ± 1.61 | 68.20 ± 0.17 | 80.57 ± 0.40 | 69.43 ± 0.06 | 61.77 ± 0.12 | -8.00 ± 0.61 |
| adalimumab 0.5 g/L | 71.36 ± 0.15 | 83.20 ± 0.17 | n.a. | 70.16 ± 0.09 | | 67.96 ± 0.30 | 80.26 ± 0.15 | 70.36 ± 0.12 | 62.28 ± 0.13 | |
| + rituximab | 70.23 ± 0.06 | 82.77 ± 0.12 | n.a. | 68.40 ± 0.42 | 57.57 ± 3.44 | 63.77 ± 0.12 | 80.23 ± 0.15 | 70.27 ± 0.12 | 55.99 ± 0.07 | -8.13 ± 0.98 |
| + bevacizumab | 70.97 ± 0.15 | 82.37 ± 0.21 | n.a. | 67.78 ± 0.35 | 46.73 ± 1.03 | 67.03 ± 0.06 | 80.87 ± 0.15 | 68.80 ± 0.10 | 61.02 ± 0.07 | -10.13 ± 0.67 |
| + omalizumab | 71.20 ± 0.10 | 82.07 ± 0.12 | n.a. | 70.54 ± 0.15 | 23.67 ± 0.40 | 64.40 ± 0.36 | 80.03 ± 0.29 | 70.53 ± 0.12 | 62.88 ± 0.26 | -9.78 ± 0.68 |
| + infliximab | 66.47 ± 0.06 | 83.07 ± 0.21 | n.a. | 56.71 ± 0.12 | 43.33 ± 0.51 | 63.03 ± 0.06 | 80.67 ± 0.15 | 63.90 ± 0.26 | 50.23 ± 0.13 | -20.97 ± 0.80 |
| rituximab 1 g/L | 68.57 ± 0.15 | 83.03 ± 0.29 | n.a. | 68.64 ± 0.35 | 65.10 ± 0.89 | 63.43 ± 0.12 | 80.30 ± 0.17 | 72.00 ± 0.00 | 53.27 ± 0.16 | -9.85 ± 0.55 |
| rituximab 0.5 g/L | 68.50 ± 0.15 | 83.46 ± 0.15 | n.a. | 68.14 ± 0.26 | | 63.23 ± 0.11 | 80.03 ± 0.15 | 72.8 ± 0.00 | 54.47 ± 0.08 | |
| + bevacizumab | 69.90 ± 0.00 | 82.70 ± 0.17 | n.a. | 67.40 ± 0.33 | 51.70 ± 2.21 | 64.37 ± 0.12 | 81.03 ± 0.21 | 69.13 ± 0.12 | 56.17 ± 0.21 | -10.55 ± 0.74 |
| + omalizumab | 68.73 ± 0.15 | 82.20 ± 0.17 | n.a. | 69.91 ± 0.05 | 30.23 ± 0.40 | 63.40 ± 0.00 | 79.23 ± 0.15 | 73.20 ± 0.00 | 56.67 ± 0.10 | -11.07 ± 0.65 |
| + infliximab | 65.57 ± 0.06 | 83.00 ± 0.10 | n.a. | 56.66 ± 0.28 | 52.70 ± 1.60 | 61.50 ± 0.20 | 81.17 ± 0.15 | 62.63 ± 0.15 | 49.67 ± 0.12 | -22.77 ± 0.68 |
| bevacizumab 1 g/L | 70.67 ± 0.12 | 81.87 ± 0.12 | n.a. | 66.28 ± 0.08 | 42.73 ± 0.72 | 66.23 ± 0.06 | 80.77 ± 0.06 | 67.87 ± 0.06 | 59.86 ± 0.44 | -11.77 ± 0.67 |
| bevacizumab 0.5 g/L | 70.66 ± 0.11 | 82.16 ± 0.12 | n.a. | 68.03 ± 0.07 | | 66.16 ± 0.05 | 80.06 ± 0.06 | 68.86 ± 0.05 | 60.26 ± 0.45 | |
| + omalizumab | 70.90 ± 0.10 | 81.57 ± 0.21 | n.a. | 68.63 ± 0.03 | 21.87 ± 1.56 | 66.73 ± 0.12 | 80.00 ± 0.17 | 78.87 ± 0.25 | 61.76 ± 0.26 | -9.78 ± 0.68 |
| + infliximab | 66.90 ± 0.17 | 82.60 ± 0.26 | n.a. | 56.77 ± 0.18 | 38.97 ± 0.38 | 63.67 ± 0.31 | 80.17 ± 0.15 | 64.10 ± 0.10 | 50.03 ± 0.23 | -27.03 ± 5.02 |
| omalizumab 1 g/L | 68.33 ± 0.06 | 80.50 ± 0.17 | n.a. | 72.24 ± 0.16 | 3.41 ± 0.81 | 63.53 ± 0.21 | 77.27 ± 0.15 | 79.37 ± 0.06 | 64.04 ± 0.22 | -9.94 ± 0.49 |
| omalizumab 0.5 g/L | 68.43 ± 0.15 | 80.46 ± 0.25 | n.a. | 72.84 ± 0.10 | | 63.36 ± 0.31 | 76.96 ± 0.23 | 80.96 ± 0.05 | 65.16 ± 0.04 | |
| + infliximab | 66.10 ± 0.17 | 81.33 ± 0.12 | n.a. | 56.69 ± 0.07 | 20.80 ± 0.87 | 62.60 ± 0.00 | 80.53 ± 0.25 | 64.13 ± 0.06 | 49.83 ± 0.08 | -23.83 ± 0.06 |
| infliximab 1 g/L | 64.60 ± 0.00 | 82.43 ± 0.25 | n.a. | 56.02 ± 0.26 | 36.43 ± 1.05 | 61.17 ± 0.15 | 80.07 ± 0.15 | 62.87 ± 0.12 | 48.78 ± 0.21 | -41.13 ± 0.87 |
| infliximab 0.5 g/L | 64.50 ± 0.00 | 82.46 ± 0.15 | n.a. | 56.62 ± 0.24 | | 60.5 ± 0.17 | 80.43 ± 0.31 | 63.36 ± 0.15 | 49.13 ± 0.12 | |

Table IV.5. Summary for the biophysical parameters of the single mAbs and their binary mixtures (0.5 + 0.5 g/L) in 10 mM sodium phosphate pH 7.4 with or without 250 mM NaCl. All measurements were performed in triplicates. The mean values with standard deviation are shown in the table.

| | 10 mM sodium phosphate pH 7.4 | | | | | | | | | |
|---------------------|-------------------------------|----------------------|-----------------------|----------------------|-----------------------|----------------------|----------------------|-----------------------|----------------------|-----------------------|
| | + 0 mM NaCl | | | | | + 250 mM NaCl | | | | |
| | IP ₁ [°C] | IP ₂ [°C] | T _{agg} [°C] | T _{on} [°C] | k _D [mL/g] | IP ₁ [°C] | IP ₂ [°C] | T _{agg} [°C] | T _{on} [°C] | k _D [mL/g] |
| trastuzumab 1 g/L | 72.20 ± 0.00 | 80.53 ± 0.06 | 78.93 ± 0.06 | 69.51 ± 0.58 | -9.25 ± 1.09 | 70.97 ± 0.06 | 80.17 ± 0.06 | 79.70 ± 0.00 | 69.59 ± 0.82 | -5.83 ± 0.48 |
| trastuzumab 0.5 g/L | 72.23 ± 0.06 | 80.43 ± 0.12 | 78.96 ± 0.06 | 70.50 ± 0.22 | | 70.90 ± 0.00 | 79.67 ± 0.11 | 79.90 ± 0.00 | 71.34 ± 0.38 | |
| + adalimumab | 71.53 ± 0.06 | 81.37 ± 0.06 | 71.40 ± 0.00 | 65.98 ± 0.29 | -13.57 ± 0.57 | 70.93 ± 0.06 | 80.50 ± 0.00 | 72.77 ± 0.15 | 67.92 ± 0.05 | -8.71 ± 0.99 |
| + rituximab | 71.23 ± 0.15 | 81.37 ± 0.06 | 73.63 ± 0.06 | 59.21 ± 0.12 | -11.73 ± 1.17 | 70.13 ± 0.12 | 80.73 ± 0.06 | 74.77 ± 0.23 | 58.69 ± 0.30 | -9.65 ± 0.60 |
| + bevacizumab | 70.83 ± 0.06 | 81.47 ± 0.06 | 70.30 ± 0.00 | 62.96 ± 0.19 | -12.00 ± 0.30 | 69.77 ± 0.15 | 80.43 ± 0.15 | 71.13 ± 0.15 | 63.18 ± 0.12 | -9.99 ± 1.04 |
| + omalizumab | 72.07 ± 0.12 | 80.27 ± 0.06 | 78.77 ± 0.12 | 68.18 ± 0.31 | -16.73 ± 0.76 | 70.67 ± 0.15 | 80.23 ± 0.06 | 80.07 ± 0.23 | 67.42 ± 0.31 | -7.65 ± 0.43 |
| + infliximab | 68.17 ± 0.12 | 81.17 ± 0.12 | 62.53 ± 0.15 | 54.51 ± 0.11 | n.a. | 68.57 ± 0.15 | 80.27 ± 0.12 | 69.33 ± 0.35 | 57.99 ± 0.22 | - n.a. |
| adalimumab 1 g/L | 71.10 ± 0.10 | 83.17 ± 0.21 | 70.57 ± 0.06 | 65.55 ± 0.32 | -15.40 ± 1.00 | 70.73 ± 0.06 | 82.70 ± 0.20 | 71.63 ± 0.06 | 66.95 ± 0.04 | -9.62 ± 0.36 |
| adalimumab 0.5 g/L | 71.03 ± 0.06 | 83.40 ± 0.00 | 71.16 ± 0.06 | 66.18 ± 0.28 | | 70.66 ± 0.11 | 82.33 ± 0.55 | 72.56 ± 0.12 | 67.71 ± 0.21 | |
| + rituximab | 70.57 ± 0.06 | 83.00 ± 0.20 | 70.47 ± 0.21 | 59.02 ± 0.23 | -16.87 ± 1.29 | 69.97 ± 0.06 | 82.23 ± 0.12 | 72.27 ± 0.12 | 59.19 ± 0.30 | -10.05 ± 1.44 |
| + bevacizumab | 70.57 ± 0.12 | 82.73 ± 0.15 | 69.60 ± 0.10 | 62.98 ± 0.14 | -13.67 ± 0.32 | 69.90 ± 0.17 | 82.37 ± 0.21 | 70.90 ± 0.26 | 63.47 ± 0.26 | -12.40 ± 1.73 |
| + omalizumab | 71.47 ± 0.12 | 82.47 ± 0.21 | 70.90 ± 0.00 | 66.06 ± 0.11 | -19.37 ± 0.06 | 71.00 ± 0.20 | 81.67 ± 0.12 | 72.47 ± 0.25 | 66.76 ± 0.19 | -7.37 ± 0.21 |
| + infliximab | 68.07 ± 0.06 | 82.70 ± 0.20 | 62.63 ± 0.21 | 54.42 ± 0.21 | n.a. | 69.13 ± 0.23 | 82.70 ± 0.17 | 69.17 ± 0.75 | 57.78 ± 0.42 | n.a. |
| rituximab 1 g/L | 69.80 ± 0.00 | 83.43 ± 0.06 | 72.63 ± 0.06 | 57.88 ± 0.10 | -15.40 ± 0.46 | 69.03 ± 0.12 | 82.67 ± 0.25 | 73.67 ± 0.15 | 57.19 ± 0.15 | -11.40 ± 0.61 |
| rituximab 0.5 g/L | 69.46 ± 0.15 | 83.40 ± 0.17 | 73.10 ± 0.00 | 58.69 ± 0.17 | | 68.70 ± 0.00 | 82.76 ± 0.21 | 74.60 ± 0.10 | 57.89 ± 0.45 | |
| + bevacizumab | 70.03 ± 0.12 | 82.70 ± 0.00 | 69.30 ± 0.00 | 58.85 ± 0.47 | -15.07 ± 0.35 | 69.17 ± 0.15 | 81.67 ± 0.15 | 70.40 ± 0.46 | 58.83 ± 0.10 | -10.32 ± 1.12 |
| + omalizumab | 70.93 ± 0.12 | 82.70 ± 0.20 | 72.63 ± 0.12 | 59.58 ± 0.27 | -19.13 ± 1.23 | 69.90 ± 0.00 | 81.47 ± 0.06 | 74.83 ± 0.06 | 58.65 ± 0.14 | -9.24 ± 0.28 |
| + infliximab | 67.93 ± 0.06 | 82.57 ± 0.29 | 60.43 ± 0.32 | 53.89 ± 0.02 | n.a. | 67.47 ± 0.06 | 82.17 ± 0.06 | 68.50 ± 0.17 | 56.28 ± 0.12 | n.a. |
| bevacizumab 1 g/L | 70.17 ± 0.15 | 82.93 ± 0.06 | 69.33 ± 0.15 | 62.20 ± 0.15 | -15.33 ± 0.38 | 69.27 ± 0.06 | 81.70 ± 0.17 | 69.90 ± 0.10 | 62.40 ± 0.04 | -15.93 ± 1.32 |
| bevacizumab 0.5 g/L | 70.5 ± 0.00 | 83.13 ± 0.15 | 69.96 ± 0.06 | 62.29 ± 0.45 | | 69.50 ± 0.00 | 81.66 ± 0.15 | 70.03 ± 0.15 | 62.64 ± 0.22 | |
| + omalizumab | 70.73 ± 0.06 | 82.60 ± 0.36 | 70.10 ± 0.17 | 63.66 ± 0.32 | -15.53 ± 1.19 | 69.73 ± 0.06 | 81.10 ± 0.00 | 70.00 ± 0.17 | 63.69 ± 0.13 | -10.73 ± 0.06 |
| + infliximab | 69.20 ± 0.00 | 82.40 ± 0.10 | 62.63 ± 0.12 | 54.07 ± 0.09 | n.a. | 68.73 ± 0.06 | 81.27 ± 0.15 | 68.23 ± 0.06 | 58.11 ± 0.41 | n.a. |
| omalizumab 1 g/L | 72.17 ± 0.15 | 80.17 ± 0.38 | 78.80 ± 0.17 | 65.62 ± 0.49 | n.a. | 70.43 ± 0.12 | 80.17 ± 0.15 | 80.83 ± 0.06 | 68.27 ± 0.31 | - 6.89 ± 0.18 |
| omalizumab 0.5 g/L | 72.20 ± 0.17 | 79.53 ± 0.50 | 79.93 ± 0.57 | 68.73 ± 0.50 | | 70.66 ± 0.15 | 79.13 ± 0.41 | 82.00 ± 0.10 | 67.95 ± 0.28 | |
| + infliximab | 67.63 ± 0.06 | 82.03 ± 0.06 | 62.47 ± 0.06 | 54.64 ± 0.18 | n.a. | 68.07 ± 0.06 | 81.17 ± 0.12 | 69.47 ± 0.25 | 58.19 ± 0.09 | n.a. |
| infliximab 1 g/L | 66.67 ± 0.12 | 82.10 ± 0.10 | 60.50 ± 0.30 | 53.25 ± 0.04 | n.a. | 67.03 ± 0.06 | 81.90 ± 0.26 | 67.43 ± 0.23 | 56.59 ± 0.12 | n.a. |
| infliximab 0.5 g/L | 66.40 ± 0.30 | 82.20 ± 0.10 | 62.56 ± 0.12 | 54.68 ± 0.19 | | 66.56 ± 0.06 | 81.56 ± 0.11 | 67.73 ± 0.23 | 57.78 ± 0.10 | |

Table IV.6. Summary for the biophysical parameters of the single mAbs and their binary mixtures at high protein concentrations. All measurements were performed in triplicates. The mean values with standard deviation are shown in the table.

| | 10 mM sodium acetate pH 5.0 | | | | | | | |
|--|-------------------------------|----------------------|-----------------------|----------------------|----------------------|----------------------|-----------------------|----------------------|
| | + 0 mM NaCl | | | | + 250 mM NaCl | | | |
| | IP ₁ [°C] | IP ₂ [°C] | T _{agg} [°C] | T _{on} [°C] | IP ₁ [°C] | IP ₂ [°C] | T _{agg} [°C] | T _{on} [°C] |
| trastuzumab 100 g/L | 68.17 ± 0.06 | 81.57 ± 0.06 | 77.57 ± 0.21 | 67.14 ± 0.10 | 65.83 ± 0.06 | 81.90 ± 0.00 | 64.57 ± 0.35 | 61.75 ± 0.10 |
| rituximab 100 g/L | 66.13 ± 0.06 | 82.87 ± 0.06 | 70.73 ± 0.12 | 58.24 ± 0.05 | 63.57 ± 0.06 | 82.60 ± 0.10 | 55.97 ± 0.32 | 51.59 ± 0.25 |
| trastuzumab 50 g/L + rituximab 50 g/L | 67.47 ± 0.06 | 81.93 ± 0.06 | 72.57 ± 0.21 | 62.67 ± 0.10 | 64.63 ± 0.06 | 80.77 ± 0.06 | 59.23 ± 0.25 | 53.51 ± 0.17 |
| trastuzumab 50 g/L | 68.43 ± 0.06 | 81.37 ± 0.06 | 77.87 ± 0.31 | 66.21 ± 0.12 | 65.20 ± 0.00 | 81.80 ± 0.00 | 63.60 ± 0.36 | 61.22 ± 0.12 |
| rituximab 50 g/L | 65.77 ± 0.06 | 82.67 ± 0.06 | 70.47 ± 0.42 | 61.19 ± 0.29 | 61.47 ± 0.25 | 82.37 ± 0.06 | 57.07 ± 0.42 | 50.81 ± 0.25 |
| omalizumab 50 g/L | 68.13 ± 0.06 | 81.10 ± 0.00 | 76.37 ± 0.21 | 68.53 ± 0.21 | 64.80 ± 0.00 | 82.93 ± 0.06 | 64.17 ± 0.32 | 60.66 ± 0.20 |
| trastuzumab 25 g/L + rituximab 25 g/L | 67.60 ± 0.10 | 81.80 ± 0.00 | 70.53 ± 0.15 | 64.32 ± 0.20 | 63.60 ± 0.10 | 80.70 ± 0.00 | 58.73 ± 0.45 | 52.47 ± 0.11 |
| trastuzumab 25 g/L + omalizumab 25 g/L | 68.27 ± 0.06 | 81.30 ± 0.00 | 77.00 ± 0.17 | 68.24 ± 0.37 | 65.03 ± 0.06 | 81.77 ± 0.06 | 64.67 ± 0.31 | 61.12 ± 0.17 |
| rituximab 25 g/L + omalizumab 25 g/L | 67.30 ± 0.10 | 82.27 ± 0.15 | 70.80 ± 0.17 | 63.99 ± 0.27 | 63.47 ± 0.21 | 82.00 ± 0.10 | 59.23 ± 0.32 | 52.44 ± 0.32 |
| | 10 mM sodium phosphate pH 7.4 | | | | | | | |
| | + 0 mM NaCl | | | | + 250 mM NaCl | | | |
| | IP ₁ [°C] | IP ₂ [°C] | T _{agg} [°C] | T _{on} [°C] | IP ₁ [°C] | IP ₂ [°C] | T _{agg} [°C] | T _{on} [°C] |
| trastuzumab 100 g/L | 71.30 ± 0.14 | 81.80 ± 0.00 | 68.00 ± 0.30 | 66.80 ± 0.05 | 70.77 ± 0.06 | 82.33 ± 0.12 | 70.47 ± 0.45 | 67.65 ± 0.14 |
| rituximab 100 g/L | 68.77 ± 0.06 | 83.43 ± 0.06 | 57.60 ± 0.20 | 54.28 ± 0.10 | 68.03 ± 0.06 | 83.30 ± 0.00 | 57.53 ± 0.06 | 53.59 ± 0.18 |
| trastuzumab 50 g/L + rituximab 50 g/L | 69.67 ± 0.06 | 81.43 ± 0.06 | 59.43 ± 0.12 | 55.74 ± 0.03 | 68.97 ± 0.06 | 81.03 ± 0.06 | 58.70 ± 0.30 | 54.99 ± 0.12 |
| trastuzumab 50 g/L | 71.57 ± 0.06 | 81.40 ± 0.10 | 69.00 ± 0.20 | 66.38 ± 0.15 | 70.83 ± 0.06 | 82.03 ± 0.06 | 70.70 ± 0.50 | 67.96 ± 0.25 |
| rituximab 50 g/L | 68.73 ± 0.06 | 83.10 ± 0.10 | 57.23 ± 0.21 | 53.60 ± 0.25 | 68.20 ± 0.17 | 83.13 ± 0.23 | 57.00 ± 0.10 | 53.57 ± 0.08 |
| omalizumab 50 g/L | 71.40 ± 0.10 | 82.53 ± 0.06 | 70.20 ± 0.30 | 67.62 ± 0.14 | 70.50 ± 0.00 | 82.87 ± 0.06 | 70.33 ± 0.31 | 67.67 ± 0.13 |
| trastuzumab 25 g/L + rituximab 25 g/L | 70.07 ± 0.12 | 81.47 ± 0.21 | 59.07 ± 0.35 | 54.80 ± 0.10 | 69.07 ± 0.06 | 81.07 ± 0.06 | 58.27 ± 0.15 | 55.18 ± 0.09 |
| trastuzumab 25 g/L + omalizumab 25 g/L | 71.33 ± 0.06 | 80.83 ± 0.21 | 70.40 ± 0.17 | 67.30 ± 0.24 | 70.63 ± 0.12 | 82.37 ± 0.06 | 70.60 ± 0.36 | 67.61 ± 0.14 |
| rituximab 25 g/L + omalizumab 25 g/L | 70.63 ± 0.06 | 82.93 ± 0.06 | 60.70 ± 0.17 | 55.88 ± 0.17 | 68.83 ± 0.06 | 82.17 ± 0.12 | 60.07 ± 0.15 | 55.31 ± 0.25 |

IV.4 Discussion

In this work, we performed a biophysical characterization on 15 binary mixtures of six mAbs from the IgG1 subclass with different physicochemical features. Remarkably, no detrimental mAb cross-interaction was observed in any of the 15 binary mixtures in the four tested conditions (pH 5.0 and 7.4, with or without 250 mM NaCl). The biophysical parameters for the binary combinations were not inferior in the sense of indicating compromised physical stability compared to the least stable mAb in the respective mixture. Non-specific protein cross-interactions in solution are possible and were previously reported for several model protein pairs, e.g. for ovalbumin and lysozyme,^{36,37} for lysozyme and chymotrypsinogen,³⁸ for insulin and several proteins like BSA or lysozyme,³⁹ or for some mAb mixtures.⁵ If such cross-interactions affect protein stability negatively, this creates challenges for the development of co-formulations of therapeutic proteins. However, the presented results confirm previous findings that stability-compromising cross-interactions between different monoclonal antibodies might be less prevalent in co-formulations of mAbs.^{4,40,41}

We used six mAbs from the IgG1 subclass in the presented dataset. Although having different physicochemical features, these six mAbs still share a lot of similarities (such as high homology in the Fc region, magnitude of the net charge, etc.) and are well-behaved molecules that are stable enough to become marketed drugs. These similarities could explain our findings and the lack of deleterious effects on the biophysical parameters of the proteins in binary mixtures. Thus, it is questionable if these findings reflect the behavior of biophysical unfavorable mAbs that may arise in early development, in binary mixtures. On the opposite, our study indicates that the combination of two mAbs from the IgG1 subclass in co-formulation might be more straightforward than expected, provided that both of the molecules exhibit drug-like features.

In this study, the T_{on} and T_{agg} values indicate that antibody combinations show similar or slightly better colloidal stability during heating compared to the least stable single mAb. An equal or higher T_{on} and T_{agg} value can be detected in almost all binary mixtures compared to the less stable equally concentrated single mAb, e.g. rituximab plus omalizumab in 10 mM sodium phosphate pH 7.4, while the unfolding and aggregation patterns of the single mAbs remain unchanged in the mixtures (based on nanoDSF data). For certain combinations like rituximab plus omalizumab in 10 mM sodium acetate pH 5.0 with 250 mM NaCl, the combination even shows a slightly higher T_{on} value compared to the less stable mAb at 0.5

g/L. When comparing the 95% confidence intervals of the mean values, we can confirm that this increase in T_{on} is significant (data not shown). This observation is interesting and opens the question about the reasons behind the unaffected or slightly increased T_{on} and T_{agg} of the less stable mAb in the binary mixture. A possible explanation is that the non-specific cross-interactions in the 15 binary mAb mixtures in our dataset are weaker or almost absent compared to the self-interactions. Further support of this hypothesis can be found in the k_D values of the binary mixtures, which are not more negative than the k_D values of the individual mAbs. Previously published work with combinations of three other mAbs from the IgG1 class also did not indicate cross-interactions between the molecules in solution.⁴⁰ Furthermore, a recent study on a co-formulation of one IgG1 and one IgG2 antibody did not find cross-interactions between the proteins as well.⁴

Another aspect to consider in the context of co-formulation development is what type of aggregates are formed in the binary protein mixtures. If the mAbs aggregate by forming homo-oligomers this will explain why the nanoDSF backscattering profiles of the binary mixtures (0.5 g/L of each mAb) closely resemble the sum of backscattering profiles of the individual mAbs with concentration 0.5 g/L (See Figs. S.IV.6 and S.IV.7). Although the DLS and nanoDSF measurements detect the aggregate formation, they do not give information about the composition of the aggregates. In follow up work, complementary methods must be applied to study the morphology and composition of the aggregates formed by the individual mAbs and in the binary mixtures. This information will improve our understanding of the degradation mechanisms in co-formulations of mAbs. Preliminary results in our group indicate that the mAbs follow their own degradation pathway in binary mixtures. The binary mixture of trastuzumab and rituximab in 10 mM sodium acetate pH 5.0 contains mAbs with different aggregation onset temperatures (See Figs. S.IV.2 and S.IV.6). If this specific binary mixture and the respective single formulations of trastuzumab and rituximab are incubated at temperatures above the aggregation temperature of the least stable mAb rituximab, the protein unfolding trace detected by nanoDSF changes with incubation time for rituximab, while the unfolding trace of trastuzumab remains unchanged (See Fig. S.IV.14). The binary mixture reflects the transition change of rituximab and the signal converges towards the unfolding trace of trastuzumab. This indicates that rituximab degrades in the binary mixture in the same manner as in the single formulation, while trastuzumab remains stable. Still, additional experiments have to be performed in the future to further elucidate the degradation pathways in mAb mixtures.

The slightly increased T_{on} and T_{agg} values in some binary mixtures could be explained by hindered contacts between the aggregating monomers in the presence of a second mAb. Therefore, it is tempting to speculate that some mAb co-formulations could even provide a slightly better physical stability by unspecific shielding of the aggregation-prone regions (only if there is no detrimental cross-interaction between the two mAbs). Such a scenario is not unlikely as other molecules like albumin are used as excipients that improve the physical stability of some proteins.¹³

Noteworthy, the backscattering profiles and intrinsic fluorescence of the binary mAb mixtures resemble closely the profiles of the individual mAbs. This indicates that there are also no harmful cross-interactions between the unfolded state of the less stable mAb and the native or unfolded state of the mAb that aggregates at a higher temperature. In this respect, protein self-association can be characterized as specific recognition events of complementary surfaces that cannot be easily provided in the same fashion by a second protein.⁶ These specific interactions were already described for the co-aggregation of ovalbumin and native lysozyme, where the unfolded ovalbumin offers specific binding regions for the cross-interaction with native lysozyme,³⁷ and were also assigned to a high degree of geometric complementarity for the model proteins α -chymotrypsinogen and lysozyme.³⁸ Unfortunately and to best of our knowledge, there is no straightforward and reliable computational tool to check for potential complementary surfaces between two different proteins that can lead to native or non-native hetero aggregation and thus stability problems in co-formulations. Such a tool would be very valuable in the context of the current work.

As no damaging effects on the measured biophysical parameters occur in any of the 15 binary mixtures independent of protein net charge, charge distribution, composition of the CDR regions and formulation conditions, we cannot identify critical factors that could predict unfavorable cross-interactions in mAb co-formulations. On the contrary, it appears that well-behaved marketed mAbs from the IgG1 subclass could be combined in solution in a straightforward way even when they exhibit different features in their variable domains. This picture might change if more problematic mAb molecules that exhibit asymmetric charge distributions, high hydrophobicity or low conformational stability are tested.⁵ In respect to this, defining groups of IgGs with certain structural features and biophysical properties that allow straightforward co-formulation development will be particularly interesting in the future.

IV.5 Conclusion

We present a study with six marketed mAbs from the IgG1 subclass and their 15 binary mixtures. The proteins differ in their net charge, charge distribution, CDR composition and biophysical parameters. Thus, they represent a wide range for combinations of two mAbs. We assessed several biophysical parameters (T_{on} , IP1, IP2, T_{agg} and k_D) that are indicative for conformational and colloidal protein stability. Remarkably, in this large dataset no detrimental effects on the stability of the mAbs were evident from any of the assessed biophysical parameters in four solution conditions (pH 5.0 and 7.4, with or without 250 mM NaCl). Our findings suggest that the co-formulation of well-behaved mAbs from the IgG1 subclass should be possible in a straightforward way. In future, we hope to see more studies on co-formulation of mAbs with more diverse physicochemical properties that will help us to define rules and rationalize the co-formulation development of antibodies that exhibit synergistic therapeutic effects.

IV.6 References

- (1) Mueller, C.; Altenburger, U. & Mohl, S. Challenges for the pharmaceutical technical development of protein coformulations. *J. Pharm. Pharmacol.* **2018**, *70* (5), 666–674. <https://doi.org/10.1111/jphp.12731>.
- (2) Patel, A. *et al.* Coformulation of broadly neutralizing antibodies 3BNC117 and PGT121: Analytical challenges during preformulation characterization and storage stability studies. *J. Pharm. Sci.* **2018**, *107* (12), 3032–3046. <https://doi.org/10.1016/j.xphs.2018.08.012>.
- (3) Cao, M. *et al.* Charge variants characterization and release assay development for co-formulated antibodies as a combination therapy. *mAbs* **2019**, *11* (3). <https://doi.org/10.1080/19420862.2019.1578137>.
- (4) Kim, J. *et al.* Analytical characterization of coformulated antibodies as combination therapy. *mAbs* **2020**, *12* (1), e1738691. <https://doi.org/10.1080/19420862.2020.1738691>.
- (5) Woldeyes, M. A. *et al.* Viscosities and protein interactions of bispecific antibodies and their monospecific mixtures. *Mol. Pharm.* **2018**, *15* (10), 4745–4755. <https://doi.org/10.1021/acs.molpharmaceut.8b00706>.
- (6) Singh, P. *et al.* Determination of protein–protein interactions in a mixture of two monoclonal antibodies. *Mol. Pharm.* **2019**, *16* (12), 4775–4786. <https://doi.org/10.1021/acs.molpharmaceut.9b00430>.
- (7) Jain, T. *et al.* Biophysical properties of the clinical-stage antibody landscape. *Proc. Natl. Acad. Sci. U. S. A.* **2017**, *114* (5), 944–949. <https://doi.org/10.1073/pnas.1616408114>.
- (8) Rabia, L. A. *et al.* Net charge of antibody complementarity-determining regions is a key predictor of specificity. *Protein Eng. Des. Sel.* **2018**, *31* (11), 409–418. <https://doi.org/10.1093/protein/gzz002>.
- (9) Gentiluomo, L. *et al.* Advancing therapeutic protein discovery and development through comprehensive computational and biophysical characterization. *Mol. Pharm.* **2020**, *17* (2), 426–440. <https://doi.org/10.1021/acs.molpharmaceut.9b00852>.
- (10) Starr, C. G. & Tessier, P. M. Selecting and engineering monoclonal antibodies with drug-like specificity. *Curr. Opin. Biotechnol.* **2019**, *60*, 119–127. <https://doi.org/10.1016/j.copbio.2019.01.008>.

- (11) Lecerf, M. *et al.* Sequence features of variable region determining physicochemical properties and polyreactivity of therapeutic antibodies. *Mol. Immunol.* **2019**, *112*, 338–346. <https://doi.org/10.1016/j.molimm.2019.06.012>.
- (12) Goyon, A. *et al.* Determination of isoelectric points and relative charge variants of 23 therapeutic monoclonal antibodies. *J. Chromatogr. B* **2017**, *1065–1066*, 119–128.
- (13) Weisbjerg, P. L. G. *et al.* Serial coupling of ion-exchange and size-exclusion chromatography to determine aggregation levels in mAbs in the presence of a proteinaceous excipient, recombinant human serum albumin. *J. Pharm. Sci.* **2015**, *104* (2), 548–556. <https://doi.org/10.1002/jps.24275>.
- (14) Hebditch, M. *et al.* Protein-Sol: A web tool for predicting protein solubility from sequence. *Bioinformatics* **2017**, *33* (19), 3098–3100. <https://doi.org/10.1093/bioinformatics/btx345>.
- (15) Johnson, M. *et al.* NCBI BLAST: A better web interface. *Nucleic Acids Res.* **2008**, *36* (Web Server issue), 5–9. <https://doi.org/10.1093/nar/gkn201>.
- (16) Waterhouse, A. *et al.* SWISS-MODEL: Homology modelling of protein structures and complexes. *Nucleic Acids Res.* **2018**, *46* (web server issue), W296–W303. <https://doi.org/10.1093/nar/gky427>.
- (17) Anandakrishnan, R.; Aguilar, B. & Onufriev, A. V. H++ 3.0: Automating PK prediction and the preparation of biomolecular structures for atomistic molecular modeling and simulations. *Nucleic Acids Res.* **2012**, *40* (Web Server issue), W537–W541. <https://doi.org/10.1093/nar/gks375>.
- (18) Pettersen, E. F. *et al.* UCSF Chimera - A visualization system for exploratory research and analysis. *J. Comput. Chem.* **2004**, *25* (13), 1605–1612. <https://doi.org/10.1002/jcc.20084>.
- (19) Humphrey, W.; Dalke, A. & Schulten, K. VMD: Visual molecular dynamics. *J. Mol. Graph.* **1996**, *14*, 33–38. [https://doi.org/10.1016/0263-7855\(96\)00018-5](https://doi.org/10.1016/0263-7855(96)00018-5).
- (20) Zambrano, R. *et al.* AGGRESCAN3D (A3D): Server for prediction of aggregation properties of protein structures. *Nucleic Acids Res.* **2015**, *43* (web server issue), W306–W313. <https://doi.org/10.1093/nar/gkv359>.
- (21) Fukuda, J. *et al.* Factors to govern soluble and insoluble aggregate-formation in monoclonal antibodies. *Anal. Sci.* **2015**, *31*, 1233–1240.
- (22) Yadav, S. *et al.* The influence of charge distribution on self-association and viscosity behavior of monoclonal antibody solutions. *Mol. Pharm.* **2012**, *9* (4), 791–802. <https://doi.org/10.1021/mp200566k>.
- (23) Kunik, V.; Ashkenazi, S. & Ofran, Y. Paratome: An online tool for systematic identification of antigen-binding regions in antibodies based on sequence or structure. *Nucleic Acids Res.* **2012**, *40* (W1), 521–524. <https://doi.org/10.1093/nar/gks480>.
- (24) Zbacnik, T. J. *et al.* Role of buffers in protein formulations. *J. Pharm. Sci.* **2017**, *106* (3), 713–733. <https://doi.org/10.1016/j.xphs.2016.11.014>.
- (25) Roberts, D. *et al.* The role of electrostatics in protein-protein interactions of a monoclonal antibody. *Mol. Pharm.* **2014**, *11* (7), 2475–2489. <https://doi.org/10.1021/mp5002334>.
- (26) Harding, S. E. & Johnson, P. The concentration-dependence of macromolecular parameters. *Biochem. J.* **1985**, *231*, 543–547. <https://doi.org/10.1042/bj2310543>.
- (27) Connolly, B. D. *et al.* Weak interactions govern the viscosity of concentrated antibody solutions: High-throughput analysis using the diffusion interaction parameter. *Biophys. J.* **2012**, *103*, 69–78. <https://doi.org/10.1016/j.bpj.2012.04.047>.
- (28) Vidarsson, G.; Dekkers, G. & Rispens, T. IgG subclasses and allotypes: From structure to effector functions. *Front. Immunol.* **2014**, *5*, 520. <https://doi.org/10.3389/fimmu.2014.00520>.
- (29) Tiller, K. E. & Tessier, P. M. Advances in antibody design. *Annu. Rev. Biomed. Eng.* **2015**, *17* (1), 191–216. <https://doi.org/10.1146/annurev-bioeng-071114-040733>.

- (30) Lerch, T. F. *et al.* Infliximab crystal structures reveal insights into self-association. *MAbs* **2017**, *9* (5), 874–883. <https://doi.org/10.1080/19420862.2017.1320463>.
- (31) Ionescu, R. M. *et al.* Contribution of variable domains to the stability of humanized IgG1 monoclonal antibodies. *J. Pharm. Sci.* **2008**, *97* (4), 1414–1426. <https://doi.org/10.1002/jps.21104>.
- (32) Hebditch, M.; Kean, R. & Warwicker, J. Modelling of pH-dependence to develop a strategy for stabilising mAbs at acidic steps in production. *bioRxiv* **2019**, 711416. <https://doi.org/10.1101/711416>.
- (33) Svilenov, H. & Winter, G. Rapid sample-saving biophysical characterisation and long-term storage stability of liquid interferon alpha2a formulations: is there a correlation? *Int. J. Pharm.* **2019**, *562*, 42–50. <https://doi.org/10.1016/j.ijpharm.2019.03.025>.
- (34) Svilenov, H. *et al.* Orthogonal techniques to study the effect of pH, sucrose, and arginine salts on monoclonal antibody physical stability and aggregation during long-term storage. *J. Pharm. Sci.* **2020**, *109* (1), 584–594. <https://doi.org/10.1016/j.xphs.2019.10.065>.
- (35) Roberts, C. J. Therapeutic protein aggregation: mechanisms, design, and control. *Trends Biotechnol.* **2014**, *32* (7), 372–380. <https://doi.org/10.1016/j.tibtech.2014.05.005>.
- (36) Iwashita, K.; Handa, A. & Shiraki, K. Co-aggregation of ovalbumin and lysozyme. *Food Hydrocoll.* **2017**, *67*, 206–215. <https://doi.org/10.1016/j.foodhyd.2017.01.014>.
- (37) Iwashita, K.; Handa, A. & Shiraki, K. Coacervates and coaggregates: Liquid–liquid and liquid–solid phase transitions by native and unfolded protein complexes. *Int. J. Biol. Macromol.* **2018**, *120*, 10–18. <https://doi.org/10.1016/j.ijbiomac.2018.08.063>.
- (38) Tessier, P. M.; Sandler, S. I. & Lenhoff, A. M. Direct measurement of protein osmotic second virial cross coefficients by cross-interaction chromatography. *Protein Sci.* **2004**, *13*, 1379–1390. <https://doi.org/10.1110/ps.03419204>.
- (39) Dubey, K. *et al.* Evidence of rapid coaggregation of globular proteins during amyloid formation. *Biochemistry* **2014**, *53*, 8001–8004. <https://doi.org/10.1021/bi501333q>.
- (40) Galush, W. J.; Le, L. N. & Moore, J. M. R. Viscosity behavior of high-concentration protein mixtures. *J. Pharm. Sci.* **2012**, *101* (3), 1012–1020. <https://doi.org/10.1002/jps.23002>.
- (41) Wang, Y. *et al.* Quantitative evaluation of colloidal stability of antibody solutions using PEG-induced liquid-liquid phase separation. *Mol. Pharm.* **2014**, *11* (5), 1391–1402. <https://doi.org/10.1021/mp400521b>.

IV.7 Supplementary data

Biophysical characterization of binary therapeutic monoclonal antibody mixtures

*Dennis Krieg^{*1}, Carolin Berner¹, Gerhard Winter¹, Hristo L. Svilenov^{1,2}*

**Corresponding author: dennis.krieg@cup.uni-muenchen.de*

1 Department of Pharmacy, Pharmaceutical Technology and Biopharmaceutics, Ludwig-Maximilians-Universitaet Muenchen, Butenandtstrasse 5-13, Munich D-81377, Germany

2 Current affiliation: Department of Chemistry, Technische Universitaet Muenchen, 85747 Garching, Germany

IV.7.1 Primary sequences used in this work

A.1 trastuzumab

A.1.1 mAb

>Anti-HER2 Light chain (1 and 2)

DIQMTQSPSSLSASVGDRTITCRASQDVNTAVAWYQQKPGKAPKLLIYSASFLYSGVPSRFSGSRSGTDFLTITSSLPEDFATYYC
QQHYTTPPTFGQGTKVEIKRTVAAPSVFIFPPSDEQLKSGTASVCLLNNFYPREAKVQWKVDNALQSGNSQESVTEQDSKSTYS
LSSTLTLSKADYEKHKVYACEVTHQGLSSPVTKSFNRGEC

>Anti-HER2 Heavy chain (1 and 2)

EVQLVESGGGLVQPGGSLRLSCAASGFNIKDTYIHWVRQAPGKLEWVARIYPTNGYTRYADSVKGRFTISADTSKNTAYLQMNS
LRAEDTAVYYCSRWGGDGFYAMDYWGQGLVTVSSASTKGPSVFPLAPSSKSTSGGTAALGCLVKDYFPEPVTVSWNSGALTSG
VHTFPAVLQSSGLYSLSSVTVPSSSLGTQTYICNVNHKPSNTKVDKKEPKSCDKTHTCPPCPAPPELLGGPSVFLFPPKPKDTLMIS
RTPEVTCVVDVSHEDPEVKFNWYVDGVEVHNAKTKPREEQYNSTYRVVSVLTVLHQDWLNGKEYKCKVSNKALPAPIEKTISK
AKGQPREPQVYTLPPSREEMTKNQVSLTCLVKGFYPSDIAVEWESNGQPENNYKTTTPVLDSDGSFFLYSKLTVDKSRWQQGNVFS
CSVMHEALHNHYTQKSLSLSPGK

A.1.2 Fab region

>4HKZ:AIPDBIDICHAINISEQUENCE

DIQMTQSPSSLSASVGDRTITCRASQDVNTAVAWYQQKPGKAPKLLIYSASFLYSGVPSRFSGSRSGTDFLTITSSLPEDFATYYC
QQHYTTPPTFGQGTKVEIKRTVAAPSVFIFPPSDEQLKSGTASVCLLNNFYPREAKVQWKVDNALQSGNSQESVTEQDSKSTYS
LSSTLTLSKADYEKHKVYACEVTHQGLSSPVTKSFNRGE

>4HKZ:BIPDBIDICHAINISEQUENCE

EVQLVESGGGLVQPGGSLRLSCAASGFNIKDTYIHWVRQAPGKLEWVARIYPTNGYTRYADSVKGRFTISADTSKNTAYLQMNS
LRAEDTAVYYCSRWGGDGFYAMDYWGQGLVTVSSASTKGPSVFPLAPSSKSTSGGTAALGCLVKDYFPEPVTVSWNSGALTSG
VHTFPAVLQSSGLYSLSSVTVPSSSLGTQTYICNVNHKPSNTKVDKKEPK

A.1.3 Fc region

>Anti-HER2

SCDKTHTCPPCPAPPELLGGPSVFLFPPKPKDTLMISRTPEVTCVVDVSHEDPEVKFNWYVDGVEVHNAKTKPREEQYNSTYRVVS
VLTVLHQDWLNGKEYKCKVSNKALPAPIEKTISKAKGQPREPQVYTLPPSREEMTKNQVSLTCLVKGFYPSDIAVEWESNGQPENN
YKTTTPVLDSDGSFFLYSKLTVDKSRWQQGNVFS

A.2. adalimumab

A.2.1 mAb

> Adalimumab Light chain:

DIQMTQSPSSLSASVGDRTVITCRASQGIKIRNYLAWYQQKPGKAPKLLIYAASLTQSGVPSRFSGSGSGTDFTLTISSLQPEDVATYYC
QRYNRAPYTFGGGTKVEIKRTVAAPSVFIFPPSDEQLKSGTASVCLLNNFYFREAKVQWKVDNALQSGNSQESVTEQDSKSTYS
LSSTLTLSKADYEKHKVYACEVTHQGLSSPVTKSFNRGEC

> Adalimumab Heavy chain:

EVQLVESGGGLVQPGRSLRLSCAASGFTFDDYAMHWVRQAPGKGLEWVSITWNSGHIDYADSVGRFTISRDNKNSLYLQMN
SLRAEDTAVYYCAKVSYLSTASSLDYWGQGLVTVSSASTKGPSVFPLAPSSKSTSGGTAALGCLVKDYFPEPVTVSWNSGALTSG
VHTFPAVLQSSGLYSLSSVTVPSSSLGTQTYICNVNHKPSNTKVDKKVEPKSCDKTHTCPPCPAPELLGGPSVFLFPPKPKDTLMIS
RTPEVTCVVDVSHEDPEVKFNWYVDGVEVHNAKTKPREEQYNSTYRVVSVLTVLHQDWLNGKEYKCKVSNKALPAPIEKTISK
AKGQPREPQVYTLPPSRDELTKNQVSLTCLVKGFYPSDIAVEWESNGQPENNYKTTTPVLDSDGSFFLYSKLTVDKSRWQQGNVFS
CSVMHEALHNHYTQKSLSLSPGK

A.2.2. Fab region

>4NYL:LIPDBIDICHAINISEQUENCE

DIQMTQSPSSLSASVGDRTVITCRASQGIKIRNYLAWYQQKPGKAPKLLIYAASLTQSGVPSRFSGSGSGTDFTLTISSLQPEDVATYYC
QRYNRAPYTFGGGTKVEIKRTVAAPSVFIFPPSDEQLKSGTASVCLLNNFYFREAKVQWKVDNALQSGNSQESVTEQDSKSTYS
LSSTLTLSKADYEKHKVYACEVTHQGLSSPVTKSFNRGEC

>4NYL:HIDDBIDICHAINISEQUENCE

EVQLVESGGGLVQPGRSLRLSCAASGFTFDDYAMHWVRQAPGKGLEWVSITWNSGHIDYADSVGRFTISRDNKNSLYLQMN
SLRAEDTAVYYCAKVSYLSTASSLDYWGQGLVTVSSASTKGPSVFPLAPSSKSTSGGTAALGCLVKDYFPEPVTVSWNSGALTSG
VHTFPAVLQSSGLYSLSSVTVPSSSLGTQTYICNVNHKPSNTKVDKKVEPKSCHHHHHH

A.2.3 Fc region

> Adalimumab:

DKTHTCPPCPAPELLGGPSVFLFPPKPKDTLMISRTPPEVTCVVDVSHEDPEVKFNWYVDGVEVHNAKTKPREEQYNSTYRVVSVL
TVLHQDWLNGKEYKCKVSNKALPAPIEKTISKAKGQPREPQVYTLPPSRDELTKNQVSLTCLVKGFYPSDIAVEWESNGQPENNYK
TTPVLDSDGSFFLYSKLTVDKSRWQQGNVFSVMHEALHNHYTQKSLSLSPGK

A.3. rituximab

A.3.1 mAb

>Rituximab light chain chimeric

QIVLSQSPAILSASPGEKVTMTCRASSSVSYIHWFQQKPGSSPKPWYATSNLASGVPVRFSGSGSGTSYSLTISRVEAEDAATYYCQ
QWTSNPPTFGGGTKLEIKRTVAAPSVFIFPPSDEQLKSGTASVCLLNPFYPREAKVQWKVDNALQSGNSQESVTEQDSKDYSL
STLTLSKADYEKHKVYACEVTHQGLSSPVTKSFNRGEC

>Rituximab heavy chain chimeric

QVQLQPGAEELVKPGASVKMSCKASGYFTSYNMHWVKQTPGRGLEWIGAIYPGNGDTSYNQKFKGKATLTADKSSSTAYMQLS
SLTSEDSAVYYCARSTYYGGDWFYFNVWGAGTTVTVSAASTKGPSVFPLAPSSKSTSGGTAALGCLVKDYFPEPVTVSWNSGALTS
GVHTFPAVLQSSGLYSLSSVTVPSSSLGTQTYICNVNHKPSNTKVDKKAEPKSCDKTHTCPPCPAPELGGPSVFLFPPKPKDTLMI
SRTPEVTCVVDVSHEDPEVKFNWYVDGVEVHNAKTKPREEQYNSTYRVVSVLTVLHQDWLNGKEYKCKVSNKALPAPIEKTIS
KAKGQPREPQVYTLPPSRDELTKNQVSLTCLVKGFYPSDIAVEWESNGQPENNYKTPPVLDSDGSFFLYSKLTVDKSRWQQGNV
SCSVMHEALHNHYTQKLSLSPGK

A.3.2 Fab region

>2OSL:LIPDBIDICHAINISEQUENCE

QIVLSQSPAILSASPGEKVTMTCRASSSVSYIHWFQQKPGSSPKPWYATSNLASGVPVRFSGSGSGTSYSLTISRVEAEDAATYYCQ
QWTSNPPTFGGGTKLEIKRTVAAPSVFIFPPSDEQLKSGTASVCLLNPFYPREAKVQWKVDNALQSGNSQESVTEQDSKDYSL
STLTLSKADYEKHKVYACEVTHQGLSSPVTKSFNRGEC

>2OSL:HIDDBIDICHAINISEQUENCE

QVQLQPGAEELVKPGASVKMSCKASGYFTSYNMHWVKQTPGRGLEWIGAIYPGNGDTSYNQKFKGKATLTADKSSSTAYMQLS
SLTSEDSAVYYCARSTYYGGDWFYFNVWGAGTTVTVSAASTKGPSVFPLAPSSKSTSGGTAALGCLVKDYFPEPVTVSWNSGALTS
GVHTFPAVLQSSGLYSLSSVTVPSSSLGTQTYICNVNHKPSNTKVDKKAEPKSC

A.3.3 Fc region

>Rituximab

DKTHTCPPCPAPELGGPSVFLFPPKPKDTLMISRTPEVTCVVDVSHEDPEVKFNWYVDGVEVHNAKTKPREEQYNSTYRVVSVL
TVLHQDWLNGKEYKCKVSNKALPAPIEKTISKAKGQPREPQVYTLPPSRDELTKNQVSLTCLVKGFYPSDIAVEWESNGQPENNYK
TPPVLDSDGSFFLYSKLTVDKSRWQQGNVFCFSVMHEALHNHYTQKLSLSPGK

A.4. bevacizumab

A.4.1 mAb

>"Bevacizumab light chain"

DIQMTQSPSSLSASVGDRTITCSASQDISNYLNWYQQKPGKAPKVLIIYFTSSLHSGVPSRFSGSGSGTDFLTISLQPEDFATYYCQ
QYSTVPWTFGGQTKVEIKRTVAAPSVFIFPPSDEQLKSGTASVVCLLNNFYPRKAVQWKVDNALQSGNSQESVTEQDSKDSYSL
SSTLTLSKADYEKHKVYACEVTHQGLSSPVTKSFNRGEC

>"Bevacizumab heavy chain"

EVQLVESGGGLVQPGGSLRLSCAASGYTFTNYGMNWVRQAPGKGLEWVGWINTYTGEPTYAADFKRRFTFSLDTSKSTAYLQMN
SLRAEDTAVYYCAKYPHYYGSSHWYFDVWGQGLVTVSSASTKGPSVFPLAPSSKSTSGGTAALGCLVKDYFPEPVTVSWNSGAL
TSGVHTFPAVLQSSGLYSLSSVTVPSSSLGTQTYICNVNHKPSNTKVDKKVEPKSCDKTHTCPPCPAPELGGPSVFLFPPKPKDTL
MISRTPEVTCVVDVSHEDPEVKFNWYVDGVEVHNAKTKPREEQYNSTYRVVSVLTVLHQDWLNGKEYKCKVSNKALPAPIEKT
ISKAKGQPREPQVYTLPPSREEMTKNQVSLTCLVKGFYPSDIAVEWESNGQPENNYKTTTPVLDSDGSFFLYSKLTVDKSRWQQGN
VFSCSVMEALHNHYTQKSLSLSPGK

A.4.2 Fab region

>1BJ1:LIPDBID|CHAIN|SEQUENCE

DIQMTQSPSSLSASVGDRTITCSASQDISNYLNWYQQKPGKAPKVLIIYFTSSLHSGVPSRFSGSGSGTDFLTISLQPEDFATYYCQ
QYSTVPWTFGGQTKVEIKRTVAAPSVFIFPPSDEQLKSGTASVVCLLNNFYPRKAVQWKVDNALQSGNSQESVTEQDSKDSYSL
SSTLTLSKADYEKHKVYACEVTHQGLSSPVTKSFNRGEC

>1BJ1:HIDPDBID|CHAIN|SEQUENCE

EVQLVESGGGLVQPGGSLRLSCAASGYTFTNYGMNWVRQAPGKGLEWVGWINTYTGEPTYAADFKRRFTFSLDTSKSTAYLQMN
SLRAEDTAVYYCAKYPHYYGSSHWYFDVWGQGLVTVSSASTKGPSVFPLAPSSKSTSGGTAALGCLVKDYFPEPVTVSWNSGAL
TSGVHTFPAVLQSSGLYSLSSVTVPSSSLGTQTYICNVNHKPSNTKVDKKVEPKSCDKTHT

A.4.3 Fc region

>"Bevacizumab

CPPCPAPELGGPSVFLFPPKPKDTLMISRTPEVTCVVDVSHEDPEVKFNWYVDGVEVHNAKTKPREE
QYNSTYRVVSVLTVLHQDWLNGKEYKCKVSNKALPAPIEKTISKAKGQPREPQVYTLPPSREEMTKNQVSLTCLVK
GFYPSDIAVEWESNGQPENNYKTTTPVLDSDGSFFLYSKLTVDKSRWQQGNVFSCSVMEALHNHYTQKSLSLSPG
K

A.5 omalizumab

A.5.1 mAb

>Omalizumab light chain

DIQLTQSPSSLSASVGDRTITCRASQSVDDYDGDSYMNWYQQKPGKAPKLLIYAASYLESGVPSRFSGSGSDFTLTISSLQPEDFA
TYYCQQSHEDPYTFGQGTKVEIKRTVAAPSVFIFPPSDEQLKSGTASVVCLLNNFYPREAKVQWKVDNALQSGNSQESVTEQDSKD
STYLSSTLTLSKADYEKHKVYACEVTHQGLSSPVTKSFNR

>Omalizumab heavy chain

EVQLVESGGGLVQPGGSLRLSCAVSGYSITSGYSWNWIRQAPGKGLEWVASITYDGSTNYADSVKGRFTISRDDSKNTFYLMNSL
RAEDTAVYYCARGSHYFGHWHFAVWGQGTLLVTVSSGPSVFPLAPSSKSTSGGTAALGCLVKDYFPEPVTVSWNSGALTSGVHTFP
AVLQSSGLYSLSSVVTVPSSSLGTQTYICNVNHKPSNTKVDKKAEPKSCDKTHTCPPCPAPELLGGPSVFLFPPKPKDTLMISRTPEV
TCVVVDVSHEDPEVKFNWYVDGVEVHNAKTKPREEQYNSTYRVVSVLTVLHQDWLNGKEYKCKVSNKALPAPIEKTISKAKGQP
REPQVYTLPPSRDELTKNQVSLTCLVKGFYPSDIAVEWESNGQPENNYKTTTPVLDSDGSFFLYSKLTVDKSRWQQGNVFCSSVMH
EALHNHYTQKSLSLSPGK

A.5.2 Fab region

>2XA8:LIPDBIDICHAINISEQUENCE

DIQLTQSPSSLSASVGDRTITCRASQSVDDYDGDSYMNWYQQKPGKAPKLLIYAASYLESGVPSRFSGSGSDFTLTISSLQPEDFA
TYYCQQSHEDPYTFGQGTKVEIKRTVAAPSVFIFPPSDEQLKSGTASVVCLLNNFYPREAKVQWKVDNALQSGNSQESVTEQDSKD
STYLSSTLTLSKADYEKHKVYACEVTHQGLSSPVTKSFNRGEC

>2XA8:HIPDBIDICHAINISEQUENCE

EVQLVESGGGLVQPGGSLRLSCAVSGYSITSGYSWNWIRQAPGKGLEWVASITYDGSTNYNPSVKGRITISRDDSKNTFYLMNSL
RAEDTAVYYCARGSHYFGHWHFAVWGQGTLLVTVSSASTKGPSVFPLAPSSKSTSGGTAALGCLVKDYFPEPVTVSWNSGALTSGV
HTFPAVLQSSGLYSLSSVVTVPSSSLGTQTYICNVNHKPSNTKVDKKV

A.5.3 Fc region

>Omalizumab

AEPKSCDKTHTCPPCPAPELLGGPSVFLFPPKPKDTLMISRTPEVTCVVVDVSHEDPEVKFNWYVDGVEVHNAKTKPREEQYNSTY
RVVSVLTVLHQDWLNGKEYKCKVSNKALPAPIEKTISKAKGQPREPQVYTLPPSRDELTKNQVSLTCLVKGFYPSDIAVEWESNGQ
PENNYKTTTPVLDSDGSFFLYSKLTVDKSRWQQGNVFCSSVMHEALHNHYTQKSLSLSPGK

A.6 infliximab

A.6.1 mAb

> Infliximab light chain:

DILLTQSPAILSVPGERVVSFSCRASQFVGSIIHWYQRTNGSPRLLIKYASESMSGIPSRFSGSGGTDFTLSINTVESEDIADYYCQQ
SHSWPFTFGSGTNLEVKRTVAAPSVFIFPPSDEQLKSGTASVVCLLNNFYPREAKVQWKVDNALQSGNSQESVTEQDSKDYSLSS
TLTSLKADYEKHKVYACEVTHQGLSSPVTKSFNRGEC

> Infliximab Heavy chain:

EVKLEESGGGLVQPGGSMKLSCVASGFIFSNHWMNWVRQSPEKGLEWVAEIRSKSINSATHYAESVKGRFTISRDDSKSAVYLQM
TDLRTEDTGYYCSRNYYGSTYDYWGQGTTLTVSSASTKGPSVFPLAPSSKSTSGGTAALGCLVKDYFPEPVTVSWNSGALTSGV
HTFPAVLQSSGLYSLSSVTVPSSSLGTQTYICNVNHKPSNTKVDKKVEPKSCDKTHTCPPCPAPELLGGPSVFLFPPKPKDTLMISR
TPEVTCVVVDVSHEDPEVKFNWYVDGVEVHNAKTKPREEQYNSTYRVVSVLTVLHQDWLNGKEYKCKVSNKALPAPIEKTISKA
KGQPREPQVYTLPPSRDELTKNQVSLTCLVKGFYPSDIAVEWESNGQPENNYKTTTPVLDSGDSFFLYSKLTVDKSRWQQGNVFC
SVMHEALHNHYTQKSLSLSPGK

A.6.2 Fab region

>4G3Y:LIPDBIDICHAINISEQUENCE

DILLTQSPAILSVPGERVVSFSCRASQFVGSIIHWYQRTNGSPRLLIKYASESMSGIPSRFSGSGGTDFTLSINTVESEDIADYYCQQ
SHSWPFTFGSGTNLEVKRTVAAPSVFIFPPSDEQLKSGTASVVCLLNNFYPREAKVQWKVDNALQSGNSQESVTEQDSKDYSLSS
TLTSLKADYEKHKVYACEVTHQGLSSPVTKSFNRGEC

>4G3Y:HIPDBIDICHAINISEQUENCE

EVKLEESGGGLVQPGGSMKLSCVASGFIFSNHWMNWVRQSPEKGLEWVAEIRSKSINSATHYAESVKGRFTISRDDSKSAVYLQM
TDLRTEDTGYYCSRNYYGSTYDYWGQGTTLTVSSASTKGPSVFPLAPSSKSTSGGTAALGCLVKDYFPEPVTVSWNSGALTSGV
HTFPAVLQSSGLYSLSSVTVPSSSLGTQTYICNVNHKPSNTKVDKKVEPKSCDKT

A.6.3 Fc region

> Infliximab:

HTCPPCPAPELLGGPSVFLFPPKPKDTLMISRTPPEVTCVVVDVSHEDPEVKFNWYVDGVEVHNAKTKPREEQYNSTYRVVSVLTVL
HQDWLNGKEYKCKVSNKALPAPIEKTISKAKGQPREPQVYTLPPSRDELTKNQVSLTCLVKGFYPSDIAVEWESNGQPENNYKTTTP
PVLDSGDSFFLYSKLTVDKSRWQQGNVFCFSVMHEALHNHYTQKSLSLSPGK

IV.7.2 Sequence identity in % from BLAST alignment

Table S.IV.1. Fc region Identity Primary Sequence [%]

| mAb | trastuzumab | adalimumab | rituximab | bevacizumab | omalizumab | infliximab |
|-------------|-------------|------------|-----------|-------------|------------|------------|
| trastuzumab | | | | | | |
| adalilumab | 99 | | | | | |
| rituximab | 99 | 100 | | | | |
| bevacizumab | 100 | 99 | 99 | | | |
| omalizumab | 99 | 100 | 100 | 99 | | |
| infliximab | 99 | 100 | 100 | 99 | 100 | |

Table S.IV.2. Fab Light Chain Identity Primary Sequence [%]

| mAb | trastuzumab | adalimumab | rituximab | bevacizumab | omalizumab | infliximab |
|-------------|-------------|------------|-----------|-------------|------------|------------|
| trastuzumab | | | | | | |
| adalilumab | 92 | | | | | |
| rituximab | 81 | 81 | | | | |
| bevacizumab | 92 | 93 | 81 | | | |
| omalizumab | 91 | 91 | 82 | 91 | | |
| infliximab | 88 | 78 | 80 | 77 | 79 | |

Table S.IV.3. Fd region Identity Primary Sequence [%]

| mAb | trastuzumab | adalimumab | rituximab | bevacizumab | omalizumab | infliximab |
|-------------|-------------|------------|-----------|-------------|------------|------------|
| trastuzumab | | | | | | |
| adalilumab | 85 | | | | | |
| rituximab | 73 | 71 | | | | |
| bevacizumab | 83 | 82 | 75 | | | |
| omalizumab | 84 | 82 | 73 | 85 | | |
| infliximab | 80 | 79 | 70 | 78 | 78 | |

IV.7.3 Surface charge and hydrophobicity of Fab regions

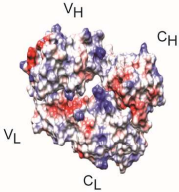
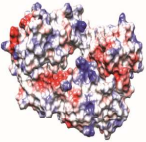
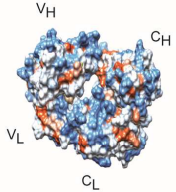
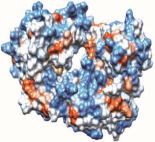
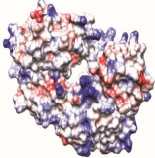
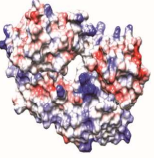
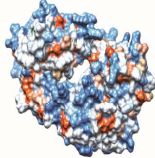
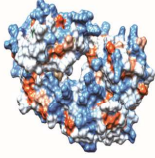
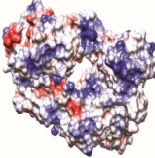
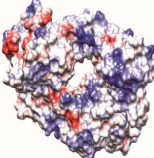
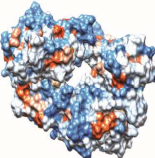
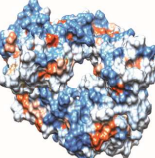
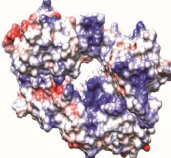
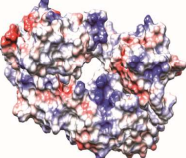
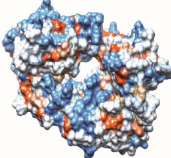
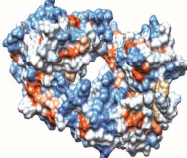
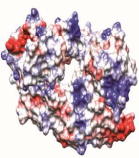
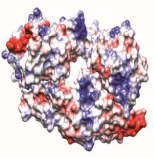
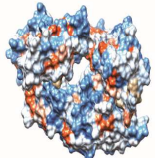
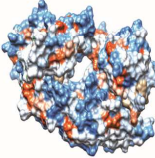
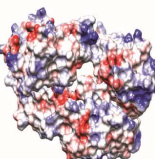
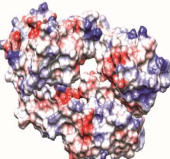
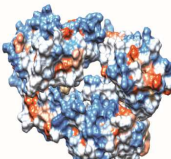
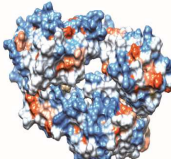
| Fab region | surface charge | | surface hydrophobicity | |
|-------------|---|---|--|---|
| | pH 5.0 | pH 7.4 | pH 5.0 | pH 7.4 |
| trastuzumab |  |  |  |  |
| adalimumab |  |  |  |  |
| rituximab |  |  |  |  |
| bevacizumab |  |  |  |  |
| omalizumab |  |  |  |  |
| infliximab |  |  |  |  |

Figure S.IV.1. Surface charge and hydrophobicity for the Fab regions at pH 5.0 and 7.4. For the surface charges, positive charges are marked in blue and negative charges are marked in red. For the surface hydrophobicity, hydrophilic surface areas are colored in blue and hydrophobic surface areas are colored in orange.

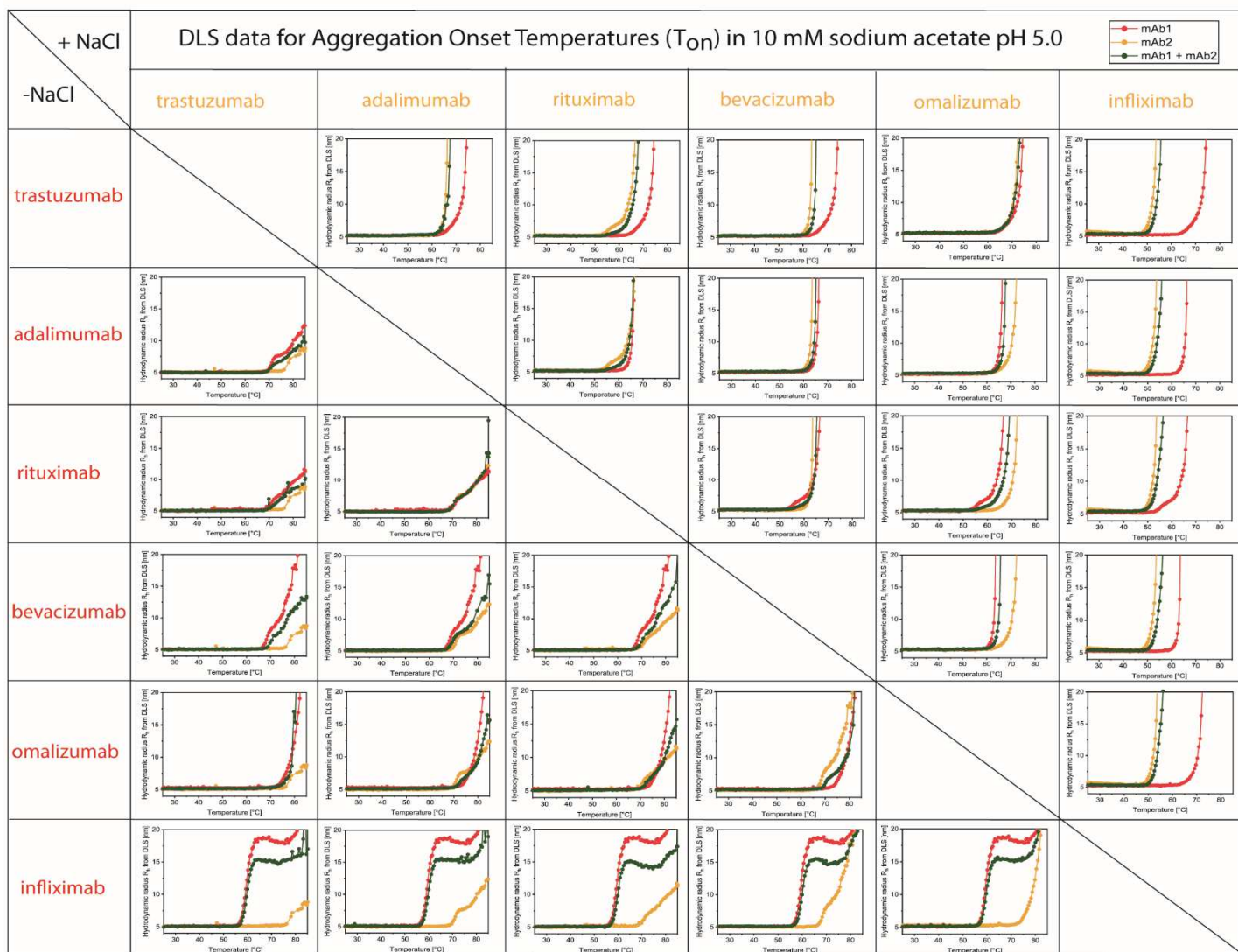
IV.7.4 DLS data for the Aggregation Onset Temperature (T_{on})

Figure S.IV.2. DLS data for Aggregation Onset Temperature (T_{on}) of all binary mixtures (0.5 g/L per antibody, green) and the respective single mAbs (1 g/L, red and yellow). In the left bottom section: in 10 mM sodium acetate pH 5.0. In the top right section: in 10 mM sodium acetate + 250 mM NaCl pH 5.0.

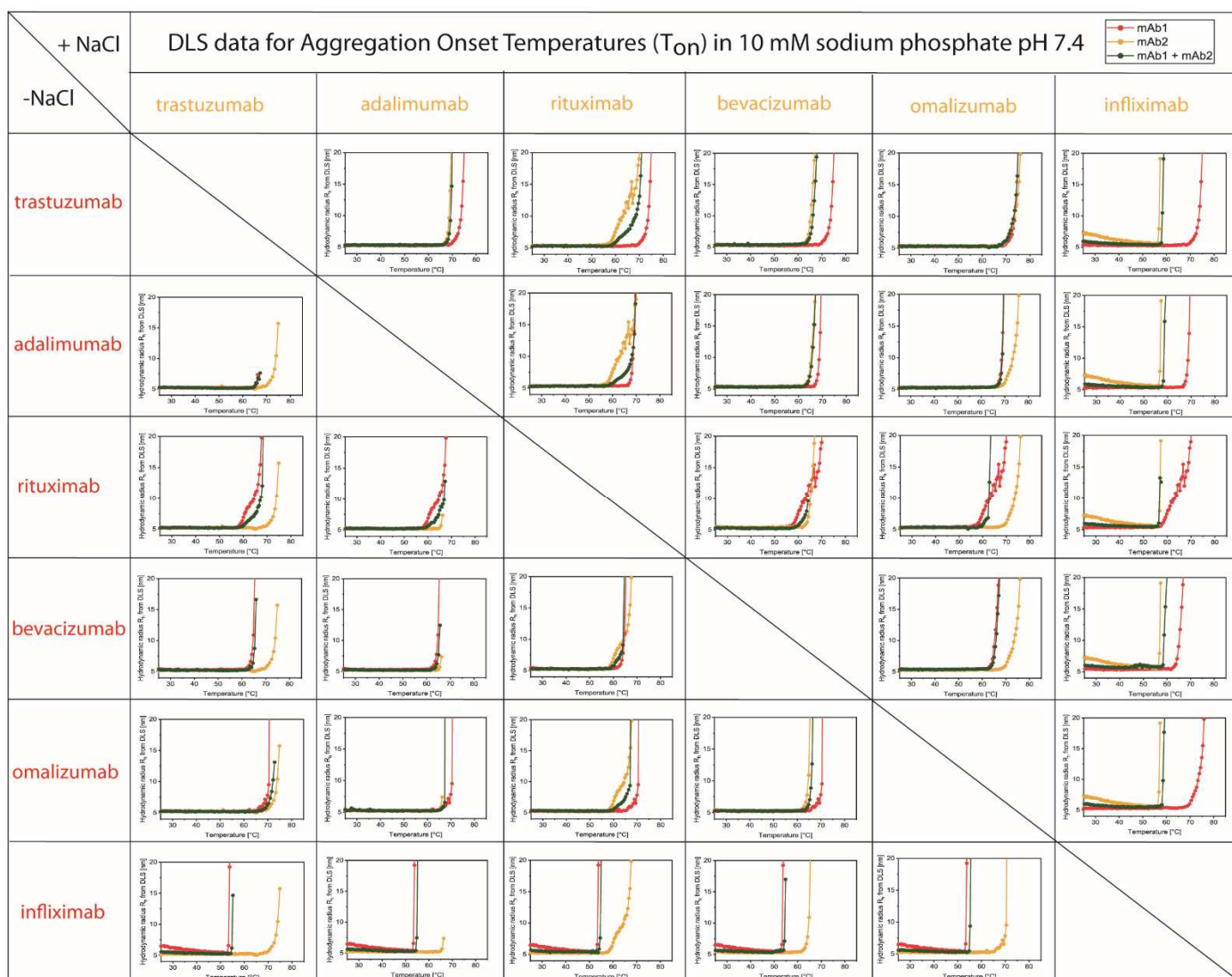


Figure S.IV.3. DLS data for Aggregation Onset Temperature (T_{on}) of all binary mixtures (0.5 g/L per antibody, green) and the respective single mAbs (1 g/L, red and yellow). In the left bottom section: in 10 mM sodium phosphate pH 7.4. In the top right section: in 10 mM sodium phosphate + 250 mM NaCl pH 7.4.

IV.7.5 Thermal Unfolding Traces for Inflection Points of Thermal Unfolding Transitions (IP1 and IP2)

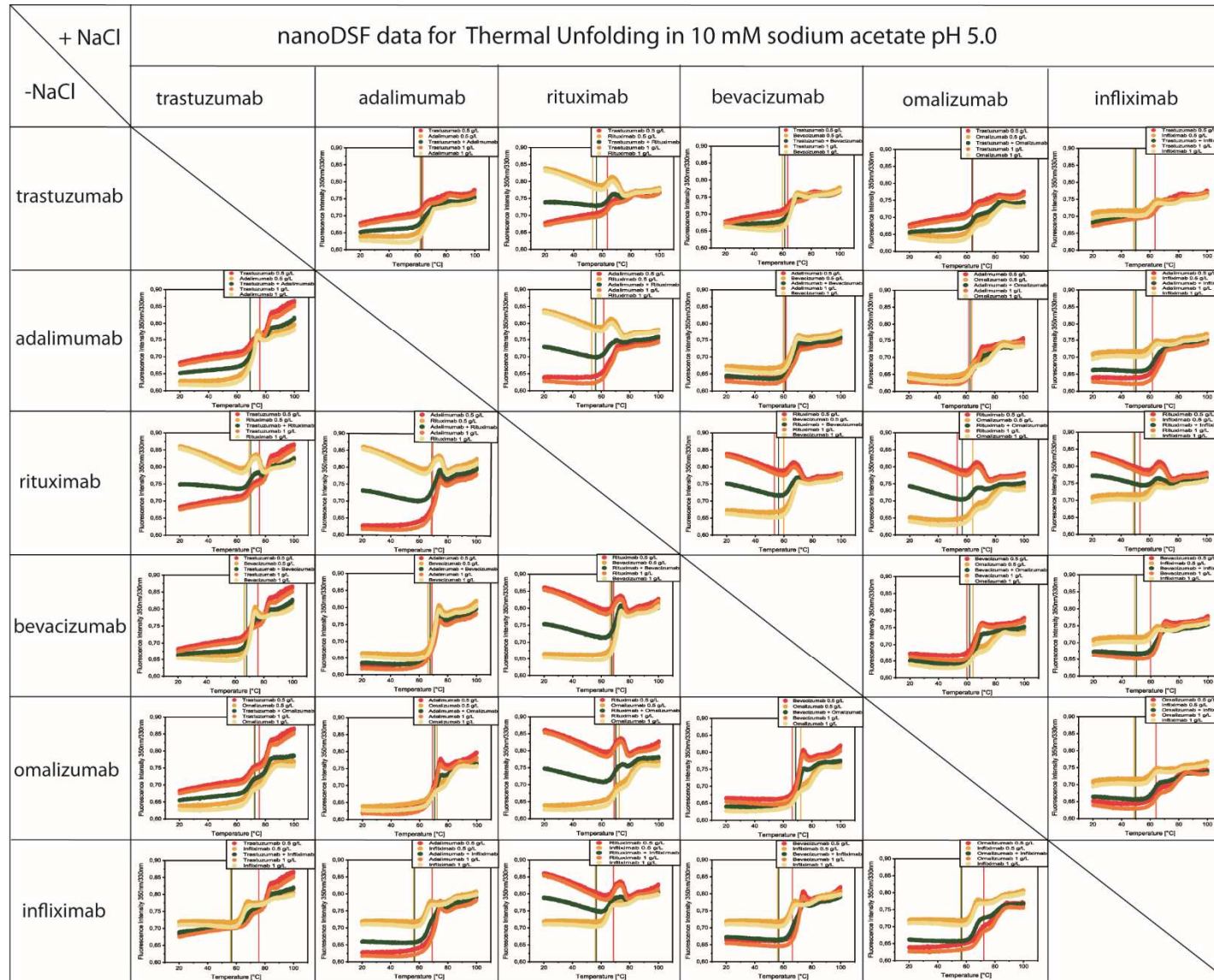


Figure S.IV.4. nanoDSF data for the Inflection Points of Thermal Unfolding (IP₁ and IP₂) of all binary mixtures (0.5 g/L per antibody, green) and the respective single mAbs (1 g/L, red and yellow). The reference lines mark the respective T_{on}-values. In the left bottom section: in 10 mM sodium acetate pH 5.0. In the top right section: in 10 mM sodium acetate + 250 mM NaCl pH 5.0.

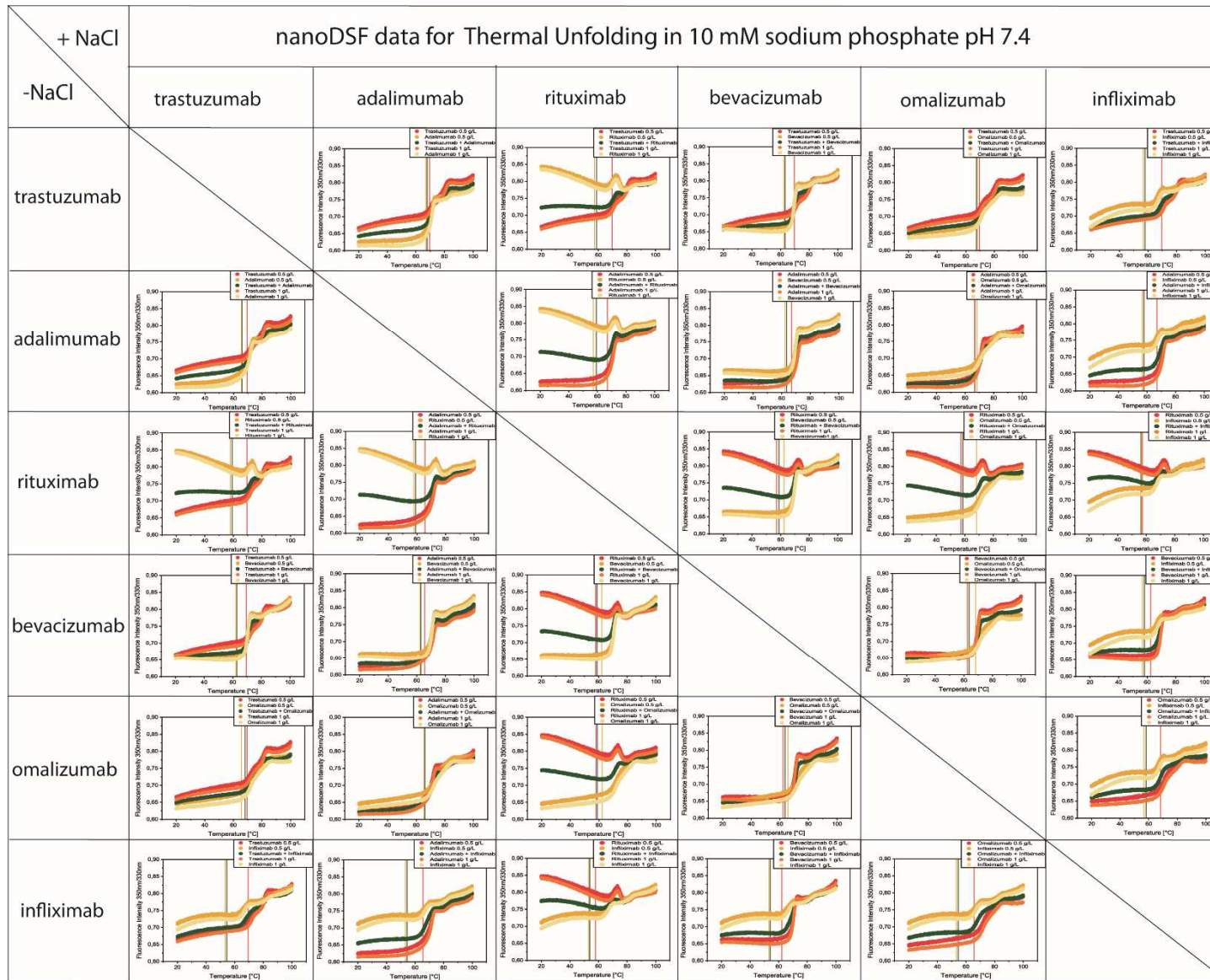


Figure S.IV.5. nanoDSF data for the Inflection Points of Thermal Unfolding (IP₁ and IP₂) of all binary mixtures (0.5 g/L per antibody, green) and the respective single mAbs (1 g/L, red and yellow). The reference lines mark the respective T_{on}-values. In the left bottom section: in 10 mM sodium phosphate pH 7.4. In the top right section: in 10 mM sodium phosphate + 250 mM NaCl pH 7.4.

IV.7.6 nanoDSF Backscattering Data for Aggregation Onset Temperature (T_{agg})

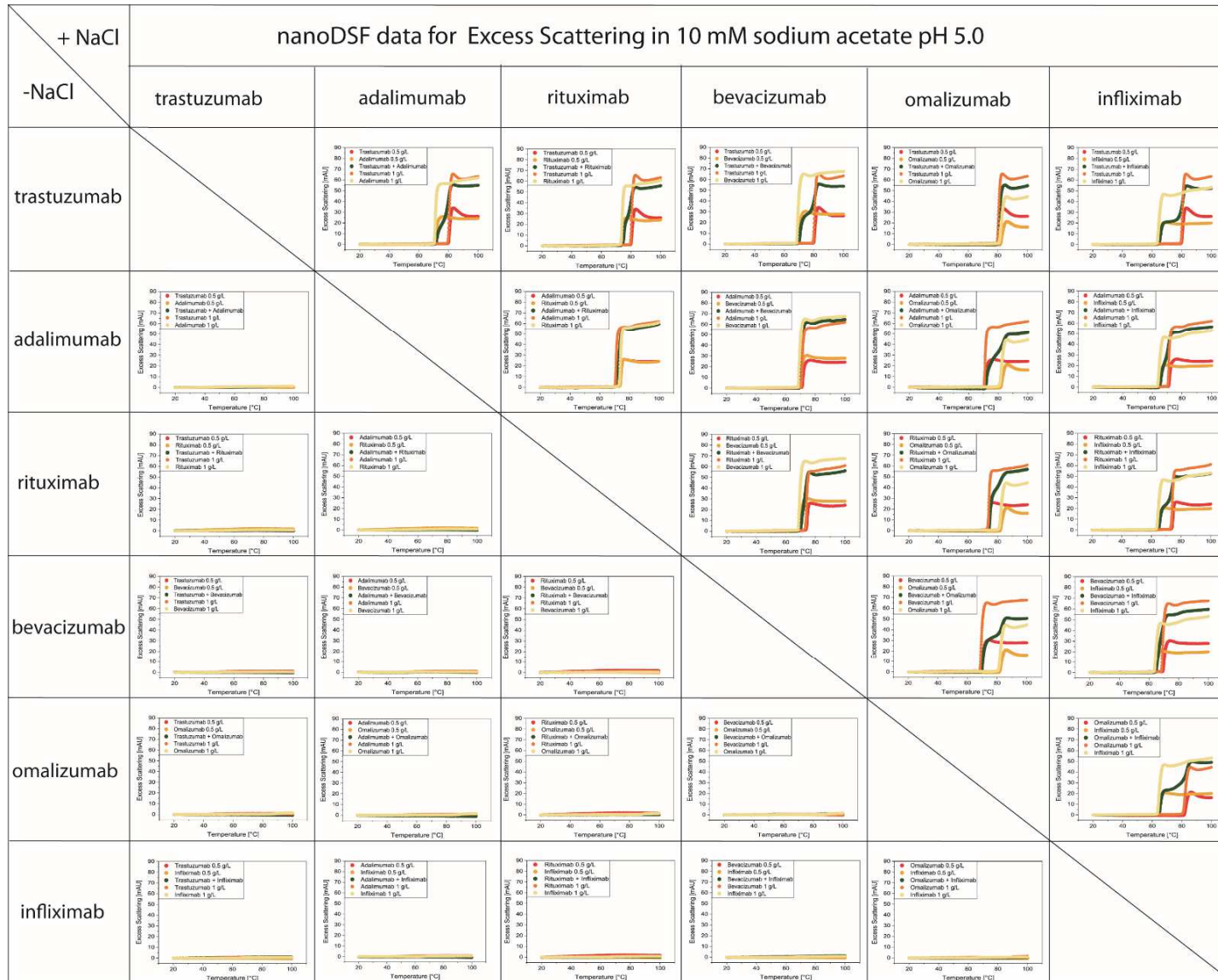


Figure S.IV.6. nanoDSF backscattering data for the Aggregation Onset Temperature (T_{agg}) of all binary mixtures (0.5 g/L per antibody, green) and the respective single mAbs (1 g/L, red and yellow). In the left bottom section: in 10 mM sodium acetate pH 5.0. In the top right section: in 10 mM sodium acetate + 250 mM NaCl pH 5.0.

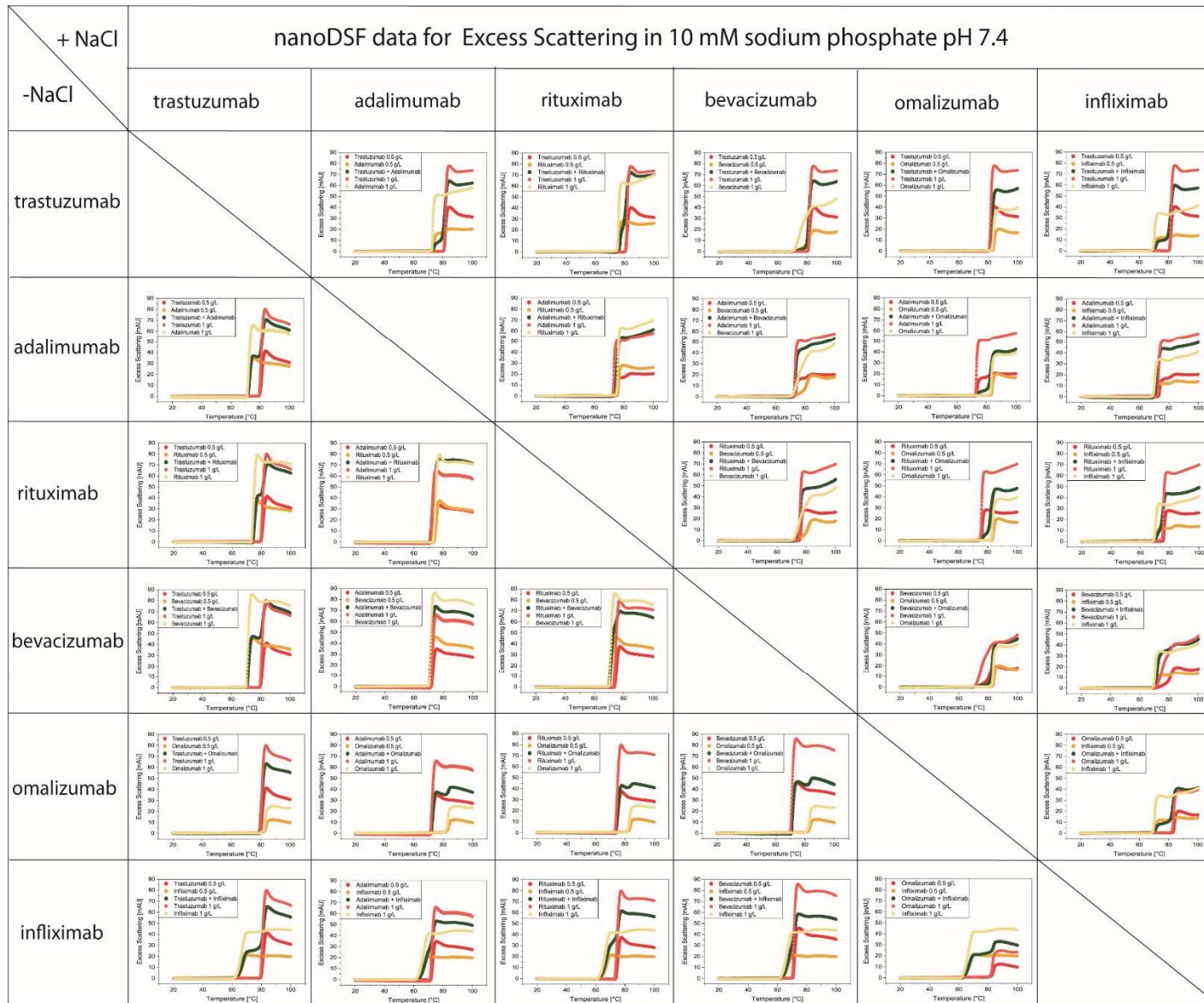


Figure S.IV.7. nanoDSF backscattering data for the Aggregation Onset Temperature (T_{agg}) of all binary mixtures (0.5 g/L per antibody, green) and the respective single mAbs (1 g/L, red and yellow). In the left bottom section: in 10 mM sodium phosphate pH 7.4. In the top right section: in 10 mM sodium phosphate + 250 mM NaCl pH 7.4.

IV.7.7 DLS data for Diffusion Interaction Parameter (k_D)

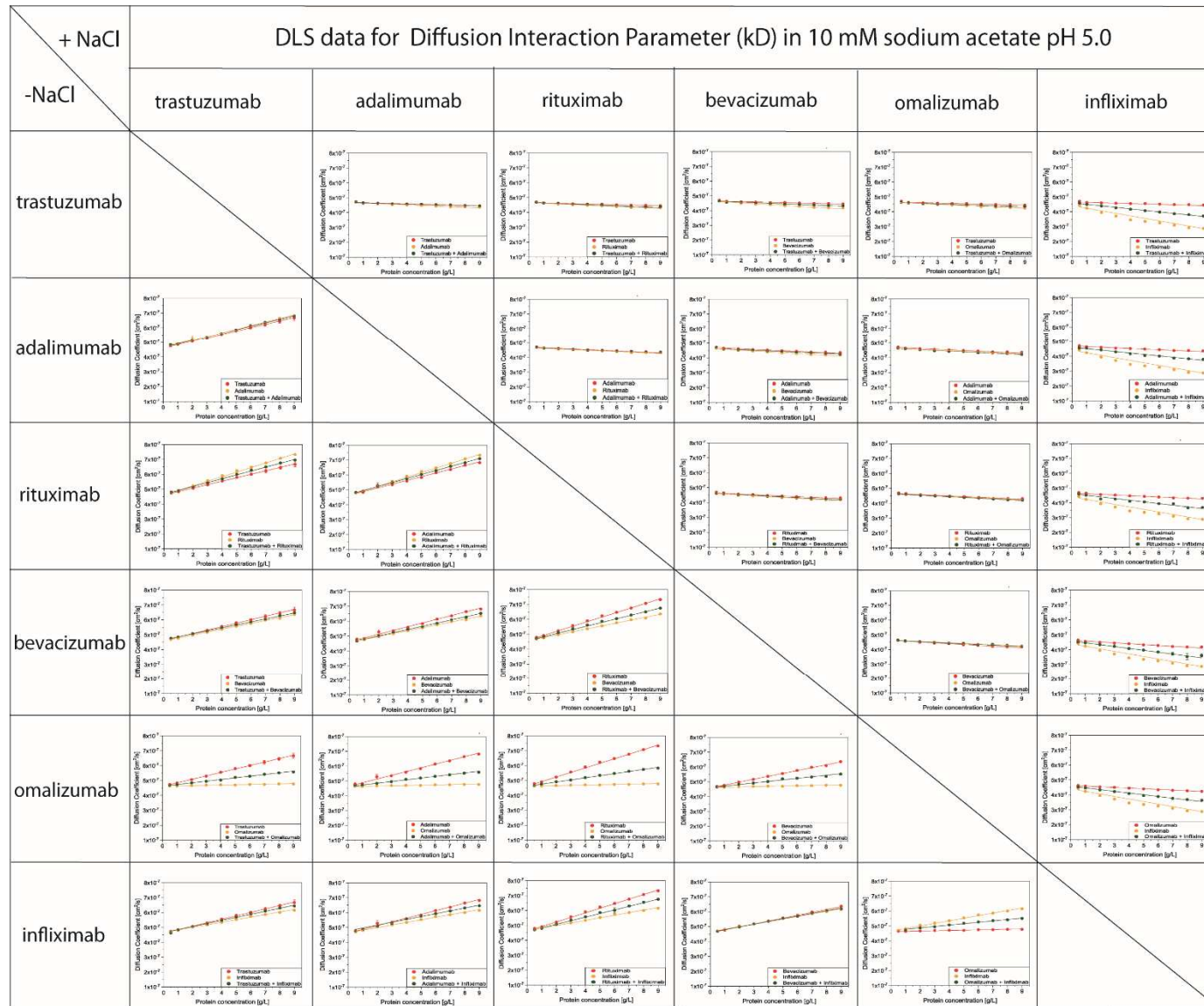


Figure S.IV.8. DLS data for Diffusion Interaction Parameter (k_D) of all binary mixtures (0.5 g/L per antibody, green) and the respective single mAbs (1 g/L, red and yellow). In the left bottom section: in 10 mM sodium acetate pH 5.0. In the top right section: in 10 mM sodium acetate + 250 mM NaCl pH 5.0.

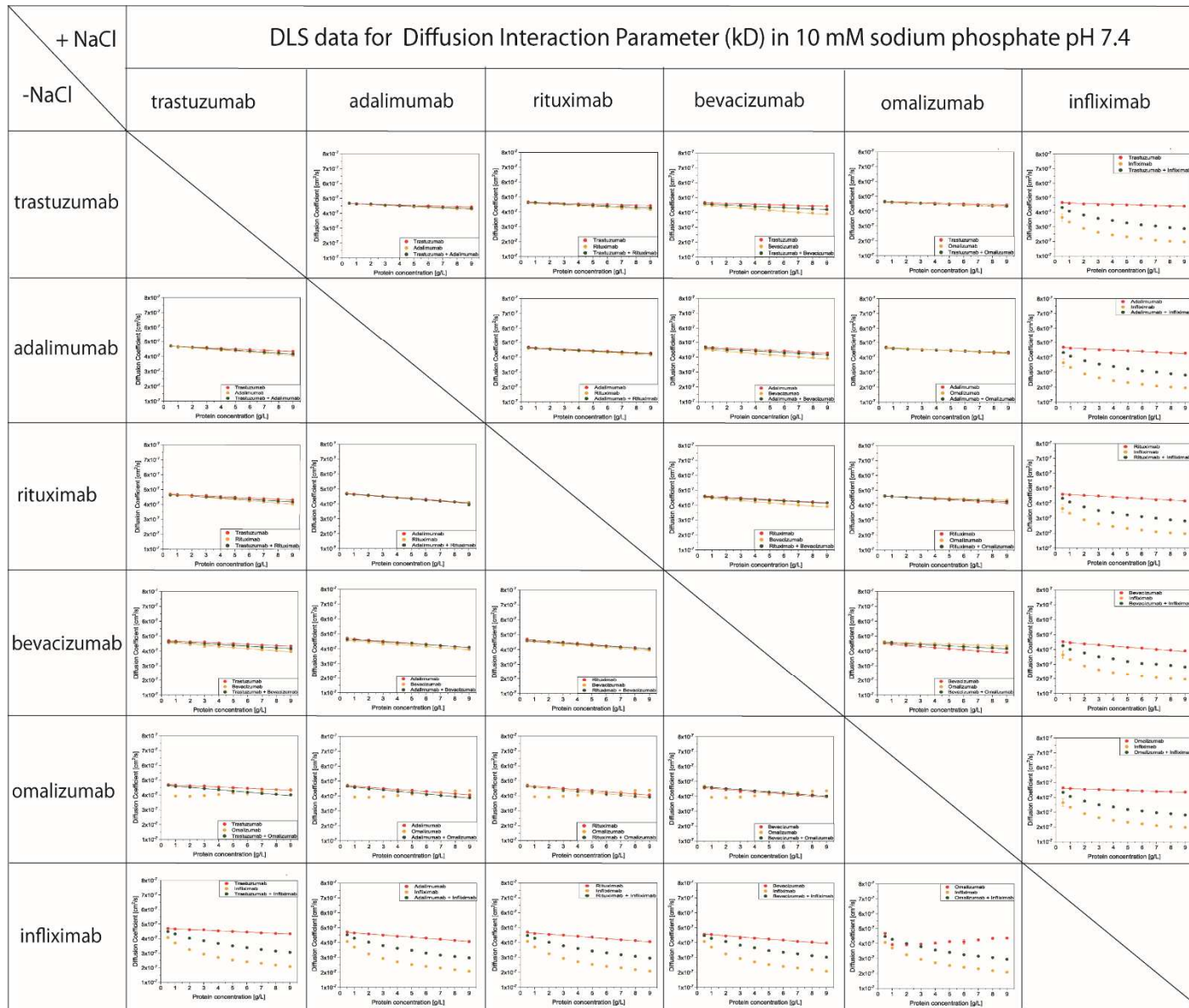


Figure S.IV.9. DLS data for Diffusion Interaction Parameter (k_D) of all binary mixtures (0.5 g/L per antibody, green) and the respective single mAbs (1 g/L, red and yellow). In the left bottom section: in 10 mM sodium phosphate pH 7.4. In the top right section: in 10 mM sodium phosphate + 250 mM NaCl pH 7.4.

IV.7.8 Results for high protein concentrations

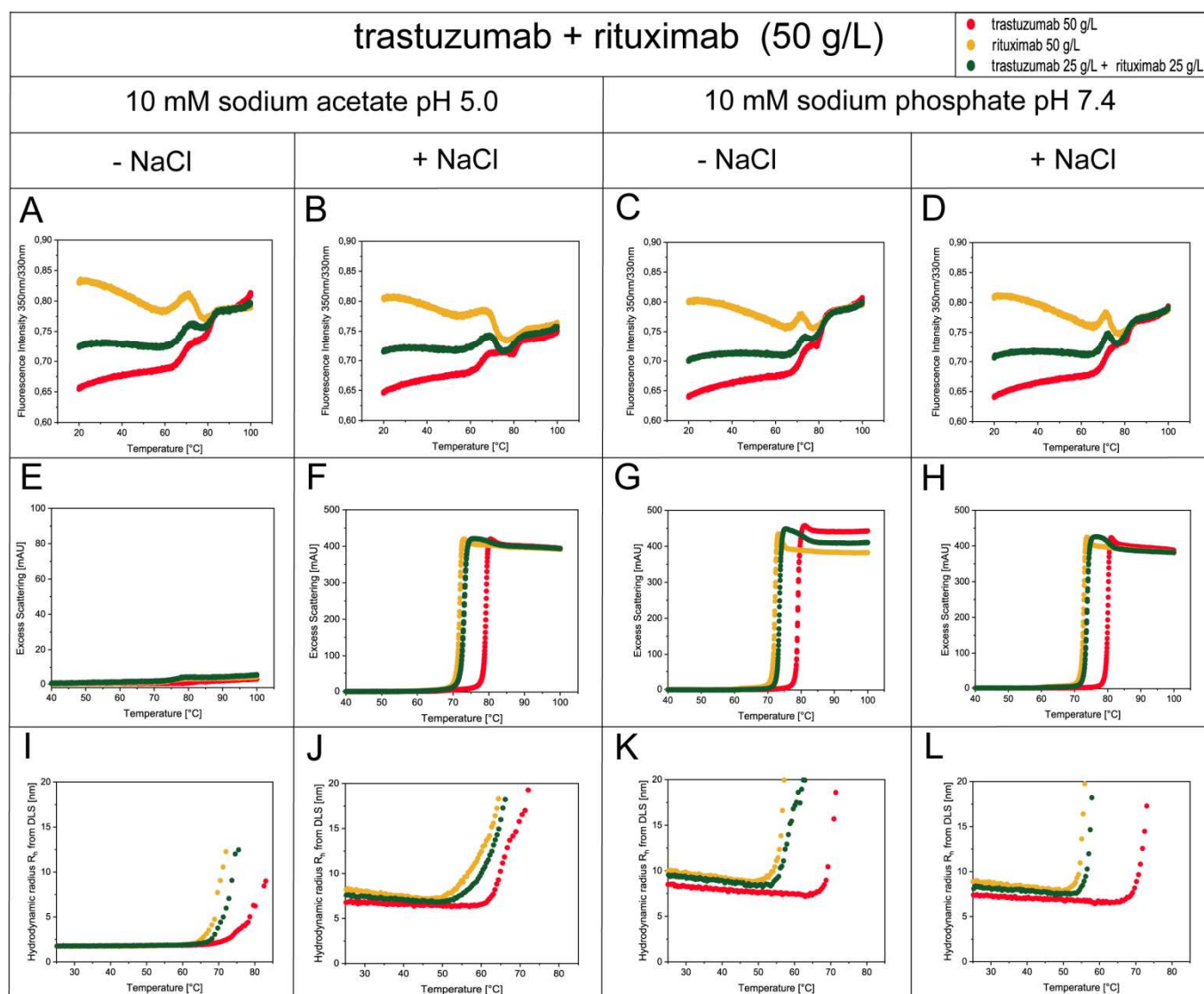


Figure S.IV.10. nanoDSF data for the Inflection Points of Thermal Unfolding (A, B, C, D), nanoDSF backscattering data for the Aggregation Onset Temperature (E, F, G, H), and the DLS data for Aggregation Onset Temperature (I, J, K, L) of trastuzumab at 50 g/L (red), rituximab at 50 g/L (yellow) and the binary mixture at 25 g/L of each mAb (green).

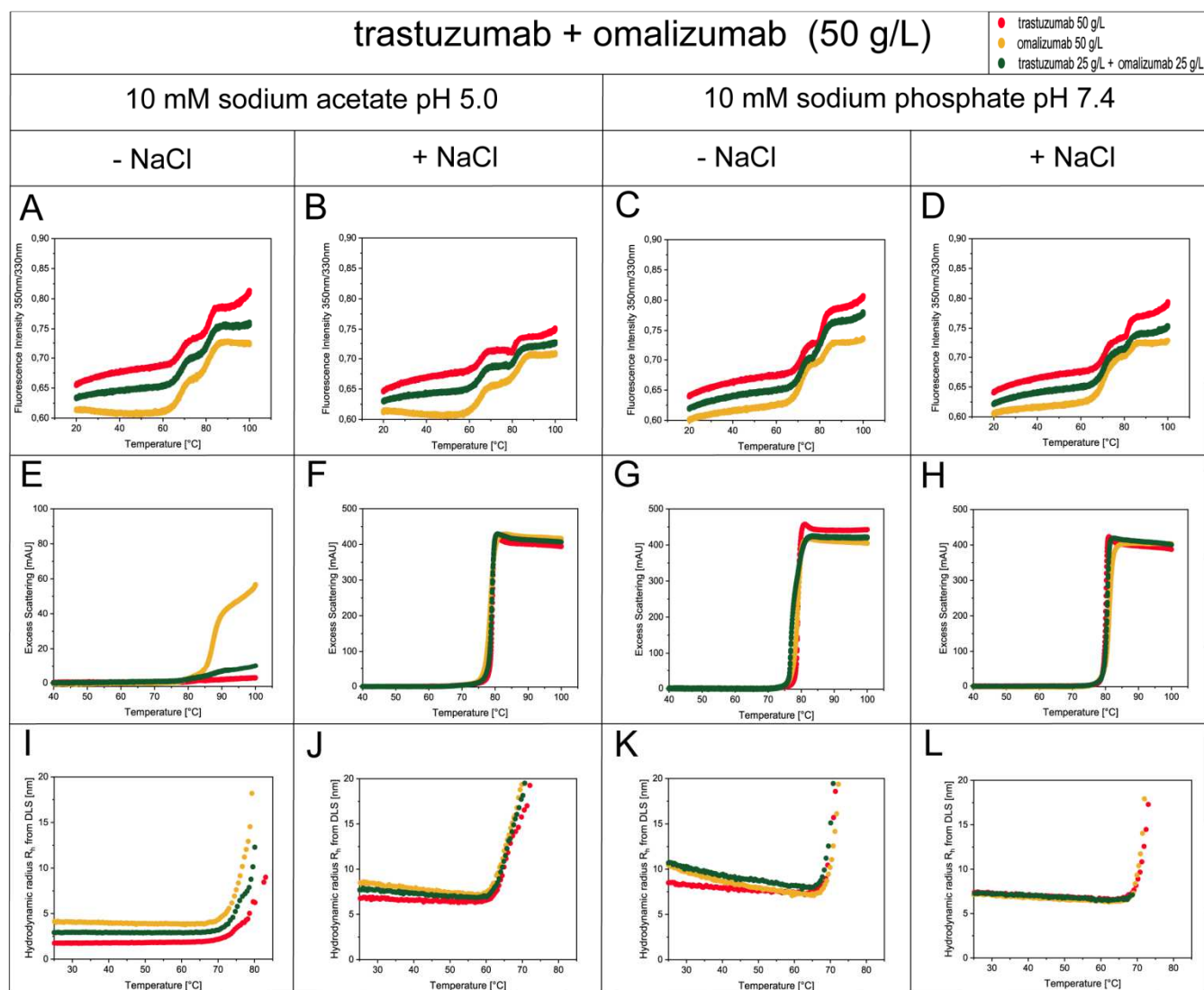


Figure S.IV.11. nanoDSF data for the Inflection Points of Thermal Unfolding (A, B, C, D), nanoDSF backscattering data for the Aggregation Onset Temperature (E, F, G, H), and the DLS data for Aggregation Onset Temperature (I, J, K, L) of trastuzumab at 50 g/L (red), omalizumab at 50 g/L (yellow) and the binary mixture at 25 g/L of each mAb (green).

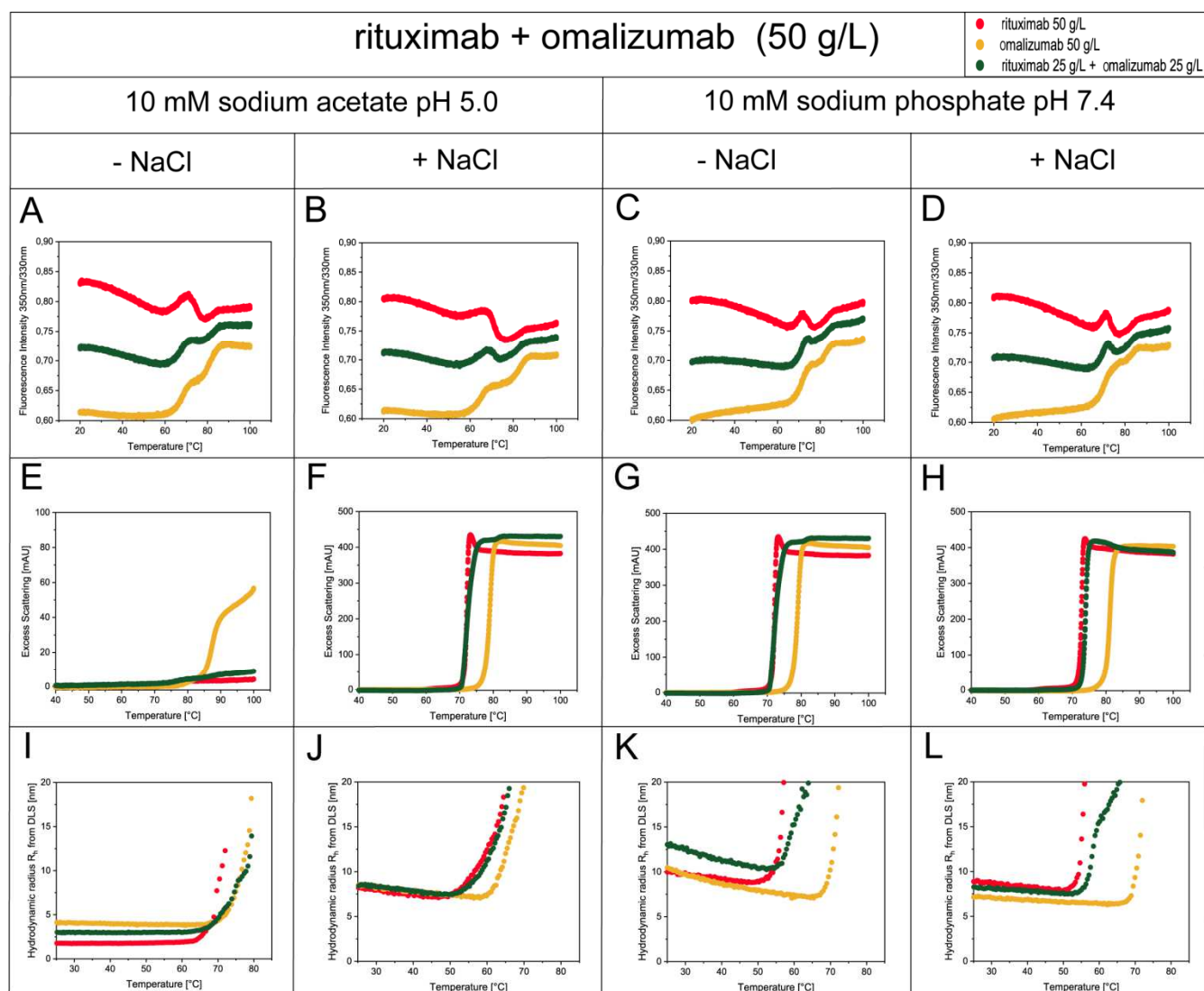


Figure S.IV.12. nanoDSF data for the Inflection Points of Thermal Unfolding (A, B, C, D), nanoDSF backscattering data for the Aggregation Onset Temperature (E, F, G, H), and the DLS data for Aggregation Onset Temperature (I, J, K, L) of rituximab at 50 g/L (red), omalizumab at 50 g/L (yellow) and the binary mixture at 25 g/L of each mAb (green).

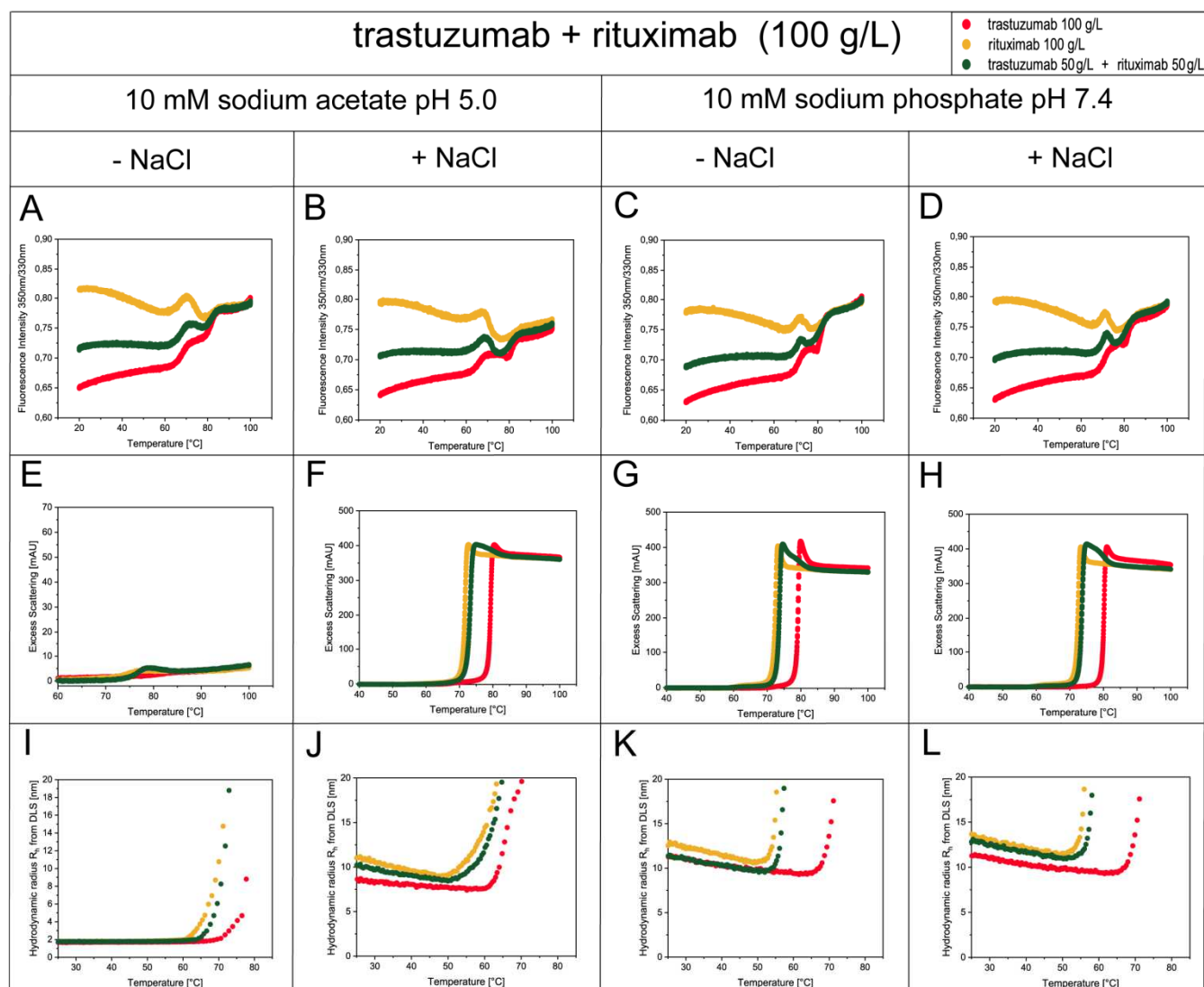


Figure S.IV.13. nanoDSF data for the Inflection Points of Thermal Unfolding (A, B, C, D), nanoDSF backscattering data for the Aggregation Onset Temperature (E, F, G, H), and the DLS data for Aggregation Onset Temperature (I, J, K, L) of trastuzumab at 100 g/L (red), rituximab at 100 g/L (yellow) and the binary mixture at 50 g/L of each mAb (green).

IV.7.9 Analysis of stressed mAb solutions

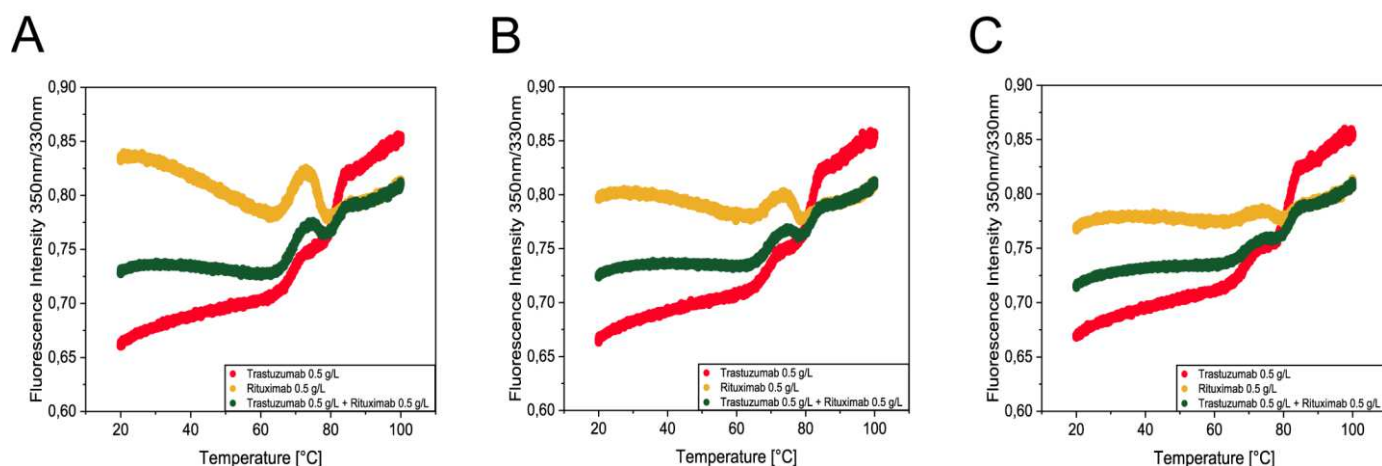


Figure S.IV.14. nanoDSF data for the Thermal Unfolding of trastuzumab at 0.5 g/L (red), rituximab at 0.5 g/L (yellow) and the binary mixture at 0.5 g/L of each mAb (green) in 10 mM sodium acetate pH 5.0. (A) unfolding of unstressed solutions, (B) unfolding of previously stressed solutions (incubation at 70 °C for 30 min), (C) unfolding of previously stressed solutions (incubation at 70 °C for 60 min).

Chapter V Further studies on binary mAb mixtures of trastuzumab and rituxumab

V.1 Introduction

The presented biophysical characterization in Chapter IV indicated that no stability-compromising protein cross-interactions arose in binary mixtures of various clinically established monoclonal antibodies.¹ Although the applied high-throughput methods such as nanoDSF and DLS provide valuable results to predict the stability of the individual proteins in binary mixtures at low protein consumption, these predictions should be confirmed for at least one pair of mAbs by additional studies. Based on their availability and the previously described differences in the respective aggregation behavior (See Chapter IV), trastuzumab and rituximab were selected as model proteins to study the aggregation behavior of co-formulated monoclonal antibodies at different protein ratios by DLS and nanoDSF. The previously indicated higher colloidal stability of trastuzumab in DLS and nanoDSF backscattering measurements allowed us to study the effect of a second mAb on the aggregation of a less stable mAb in more detail. Further, chromatographic methods were applied in forced degradation studies to assess the degradation of the individual mAbs in the binary mixtures, and viscosity measurements were performed to detect possible attractive cross-interactions between trastuzumab and rituximab in different formulation conditions at high protein concentrations. The presented results provide additional evidence for the compatibility of mAbs in binary mixtures and the non-inferior stability of such co-formulations compared to the respective single formulations.

V.2 Materials and Methods

V.2.1 Materials

Trastuzumab (Herceptin[®]) and rituximab (Mabthera[®]) were used as model proteins. Sodium dihydrogen phosphate was purchased from Grüssing GmbH. Disodium hydrogen phosphate was purchased from VWR Chemicals. Acetic acid, sodium acetate, Trizma[®] base, imidazole, piperazine and sodium azide were purchased from Sigma Aldrich. NaCl was purchased from Bernd Kraft GmbH. Protein formulations and mobile phases for HPLC analysis were prepared with ultrapure water from a Sartorius arium[®] pro system (Sartorius Corporate Administration GmbH, Göttingen, Germany).

V.2.2 Preparation of protein formulations and binary mixtures

The dialysis of the monoclonal antibodies and the preparation of the protein formulations was described in detail in Chapter IV.¹ For the forced degradation studies, 0.5 mL of each formulation were filled into microcentrifuge tubes and stressed in a heating block at 70 °C for 30 or 60 min. The microcentrifuge tubes were sealed with parafilm to avoid evaporation and were centrifuged at 10 000 x g for 10 min before analysis.

V.2.3 DLS and nanoDSF backscattering

The applied methods and parameters were already described in detail in Chapter IV. Single formulations of rituximab were prepared at 5 different protein concentrations ranging from 0.1 g/L to 0.5 g/L. In parallel, binary mixtures of trastuzumab and rituximab were prepared with the same rituximab concentration and a trastuzumab concentration that was necessary to achieve a total protein concentration of 1 g/L in the binary mixture. The 5 single formulations of rituximab (0.1 g/L – 0.5 g/L) and the 5 binary mixtures (1 g/L) with different mixing ratios of trastuzumab and rituximab were analyzed by DLS and nanoDSF backscattering as described in Chapter IV. All measurements were performed in triplicates.

V.2.4 High performance size exclusion chromatography (HP-SEC)

High performance size exclusion chromatography was performed on a Waters 2695 separation module (Waters GmbH, Eschborn, Germany). 20 µL of sample solution were injected on a Superdex 200 Increase 10/300 GL column (GE Healthcare Bio-Sciences, Uppsala, Sweden) after centrifugation at 10 000 x g for 10 min and the elution of the mAbs was detected by UV absorption at a wavelength of 280 nm. The mobile phase consisted of 100 mM sodium phosphate pH 7.0, 200 mM NaCl and 0.05 % NaN₃. The flow rate was set to 1.0 mL/min. Monomer recovery was calculated by integration of the peak area and relative comparison of this peak area before and after degradation. Baseline separation was not achieved for trastuzumab and rituximab, thus the monomeric mAbs co-eluted and the total peak area was analyzed in the binary mixture (See Fig. V.3D). All measurements were performed in triplicates.

V.2.5 Weak cation exchange high performance chromatography (WCX-HPLC)

Weak cation exchange high performance chromatography was performed on a Dionex Ultimate 3000 system (Thermo Fisher Scientific, Dreieich, Germany). 20 µL of sample solution were injected on a ProPac-WCX 10 column (Thermo Fisher Scientific, Dreieich, Germany) after centrifugation at 10 000 x g for 10 min and the elution of the mAbs was

detected by UV absorption at a wavelength of 280 nm. To achieve a feasible separation of both mAbs based on their isoelectric points (See Fig. V.4D), a pH gradient method was applied that was described by Farnan *et al.*² Eluent A consisted of 10 mM Tris, 10 mM imidazole, 10 mM piperazine and 10 mM NaCl pH 6.0, while Eluent B consisted 10 mM Tris, 10 mM imidazole, 10 mM piperazine and 10 mM NaCl pH 9.5. The flow rate was 1.0 mL/min and following five step gradient was applied: (1) from 0 to 5 min: 40 % B; (2) from 5 to 35 min: 40 to 100 % B; (3) from 35 to 44 min: 100 % B; (4) from 44 to 45 min: 100 to 40 % B; and (5) from 45 to 50 min: 40 % B. All measurements were performed in triplicates.

V.2.6 Viscosity measurements

Viscosity measurements were performed for binary mixtures of trastuzumab and rituximab with 50 g/L per mAb (which results in a total protein concentration of 100 g/L) and the obtained apparent viscosities were compared to the apparent viscosities of single formulations of trastuzumab and rituximab with a protein concentration of 100 g/L. A m-VROC viscosimeter (RheoSense Inc., San Ramon, CA, USA) equipped with an A05 chip was used for analysis. The protein formulations were filled into 500 μ L hamilton syringes and the viscosities were determined at an applied flow rate of 500 μ L/min for 10 seconds. For the protein formulations in 10 mM sodium phosphate pH 7.4, the measurement time was increased to 30 seconds due to longer equilibrium times. The measurements were performed in triplicates at a constant temperature of 25 °C.

V.3 Results and Discussion

V.3.1 DLS and nanoDSF

Fig. V.1 provides a short summary of the DLS, nanoDSF and nanoDSF backscattering data for single formulations and binary mixtures of trastuzumab and rituximab that were already presented in Chapter IV (See Table IV.4 for the numerical results):

First, the aggregation onset temperature by DLS T_{on} of the binary mixture was slightly higher compared to rituximab alone, and the aggregation trace was intermediate compared to the single formulations of trastuzumab and rituximab alone in both 10 mM sodium acetate pH 5.0 and 10 mM sodium acetate pH 5.0 with 250 mM NaCl (See Figs. V.1A and V.1D).

Second, in 10 mM sodium acetate pH 5.0, no aggregation was detected for the single formulations and the binary mixture (See Fig. V.1B). In 10 mM sodium acetate pH 5.0 with 250 mM NaCl, the aggregation onsets in the binary mixture occurred at the same temperature as in the single formulations and the excess scattering of the binary mixture resembled the

sum of the excess scattering signals of the individual mAbs with the same concentration (See Fig. V.1E).

Finally, the numerical inflection points of the binary mixtures were the same compared to rituximab alone, and the unfolding traces were intermediate compared to the single formulations of trastuzumab and rituximab in both 10 mM sodium acetate pH 5.0 without or with 250 mM NaCl (See Figs. V.1C and V.1F).

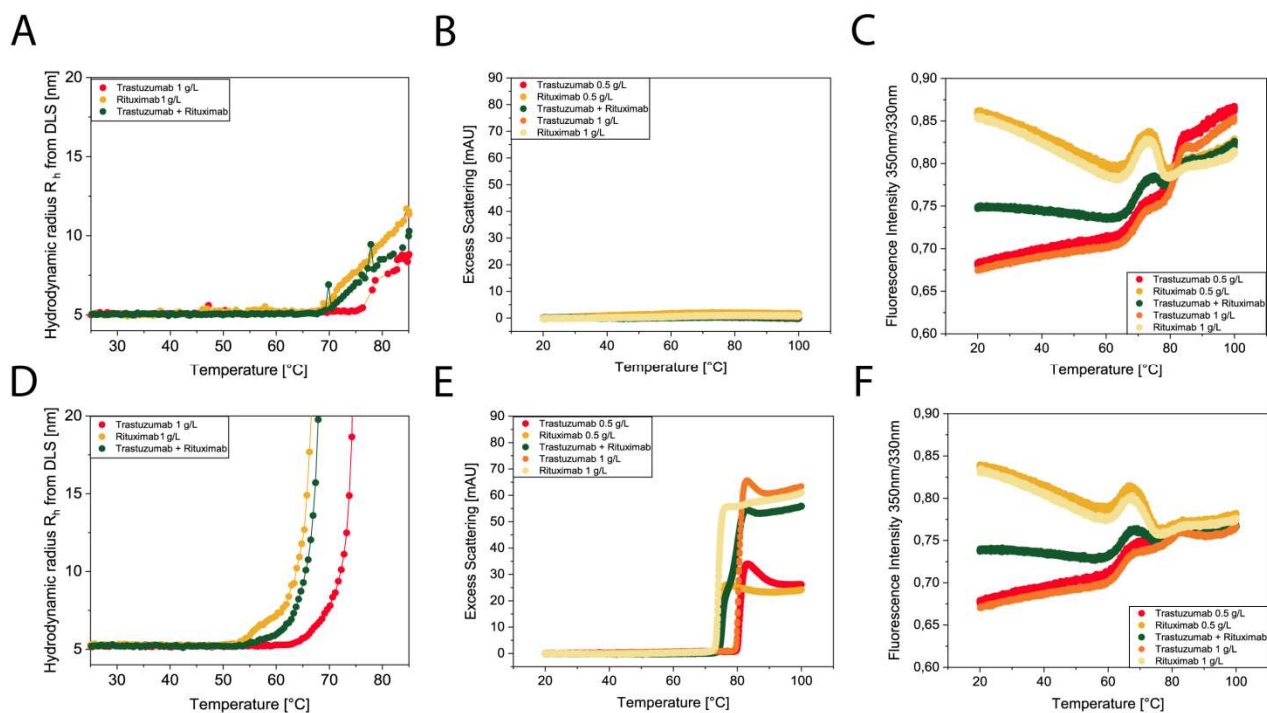


Figure V.1. DLS, nanoDSF and nanoDSF backscattering results for single formulations of trastuzumab (red) and rituximab (yellow) and also the binary mixture (green). Aggregation during heating detected by DLS in 10 mM sodium acetate pH 5.0 (A), and 10 mM sodium acetate pH 5.0 with 250 mM NaCl (D). Aggregation during heating detected by nanoDSF backscattering in 10 mM sodium acetate pH 5.0 (B), and in 10 mM sodium acetate pH 5.0 with 250 mM NaCl (E). Thermal Unfolding detected by nanoDSF in 10 mM sodium acetate pH 5.0 (C), and in 10 mM sodium acetate pH 5.0 with 250 mM NaCl (F).

Based on the different T_{on} and T_{agg} values of trastuzumab and rituximab in 10 mM sodium acetate pH 5.0 with 250 mM NaCl, single formulations of the less stable mAb rituximab were prepared in 10 mM sodium acetate pH 5.0 with 250 mM NaCl at 5 different protein concentrations ranging from 0.1 g/L to 0.5 g/L. In parallel, binary mixtures of trastuzumab and rituximab were prepared with a rituximab concentration ranging from 0.1 g/L to 0.5 g/L and a trastuzumab concentration that was necessary to achieve a total protein concentration of 1 g/L in the binary mixture. The 5 single formulations of rituximab (0.1 g/L – 0.5 g/L) and the

5 binary mixtures (total protein concentration: 1 g/L) with different mixing ratios of trastuzumab and rituximab were analyzed by DLS and nanoDSF backscattering (See Fig. V.2).

The T_{on} values detected by DLS decreased with increasing rituximab concentration for the single formulations and binary mixtures (See Figs. V.2A, V.2B and V.2C). All binary mixtures showed higher T_{on} values and lower slopes of the thermal aggregation trace compared to the single formulations of rituximab, despite the higher total protein concentration of the binary mixture. As the dynamic light scattering provides a cumulative signal of all components and not a specific signal of the individual mAbs, it can be assumed that both mAbs followed their individual aggregation pathway in the binary mixture in the same way as they did in the single formulation. The presence of the second, still monomeric protein trastuzumab shifted the apparent hydrodynamic radius in the binary mixture to lower values, until a temperature was reached where trastuzumab started to aggregate as well.

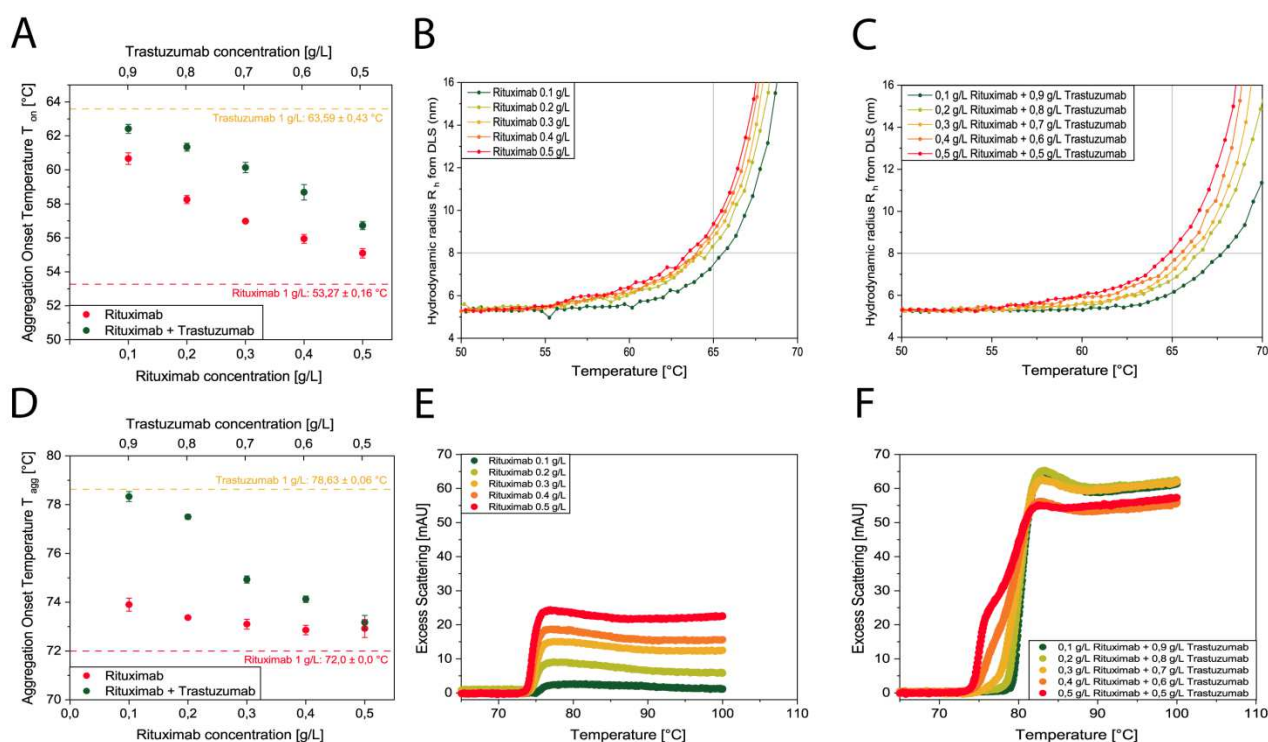


Figure V.2. DLS and nanoDSF backscattering results in 10 mM sodium acetate pH 5.0 with 250 mM NaCl. T_{on} values from DLS (A) and T_{agg} values from nanoDSF backscattering (D) for single formulations of rituximab (red) and binary mixtures of rituximab and trastuzumab (green). For the binary mixtures in (A) and (D), the respective concentration of trastuzumab is given by the top x-axis. Aggregation during heating detected by DLS for single formulations of rituximab (B), and for binary mixtures of rituximab and trastuzumab (C). The grey lines in (B) and (C) mark a threshold of 8 nm at 65 °C for easier comparison. Aggregation during heating detected by nanoDSF backscattering for single formulations of rituximab (E), and for binary mixtures of rituximab and trastuzumab (F).

Similar to the DLS measurement, the T_{agg} values decreased with increasing rituximab concentrations for the single formulations and binary mixtures (See Figs. V.2D, V.2E and V.2F). All binary mixtures showed similar or higher T_{agg} values compared to the single formulations of rituximab, despite the higher total protein concentration of the binary mixture. The excess scattering of the rituximab single formulations was limited after a single aggregation step, while the presence of trastuzumab in the binary mixture caused a second aggregation step until a plateau of excess scattering was reached (See Fig. V.2F). Interestingly, the relative intensity in excess scattering of both aggregation steps in the binary mixture corresponds to the respective individual protein ratio. At a protein ratio of trastuzumab and rituximab of 1:1 (w/w), where the protein concentration is 0.5 g/L for both mAbs, the intensity in excess scattering was the same for both aggregation steps, and the intensity of the first aggregation step in the binary mixture was the same as the intensity of the excess scattering for rituximab alone at a concentration of 0.5 g/L. Increasing amounts of trastuzumab in the binary mixture reduced the intensity of the first aggregation step and increased the intensity of the second aggregation step (See Fig. V.2F). Thus, it appeared that both mAbs aggregated in the binary mixture in the same way as they did in the respective single formulations, and the presence of the second proteins did not cause additional protein aggregation.

V.3.2 Forced degradation studies by HP-SEC and WCX-HPLC

Forced degradation studies on binary mixtures of trastuzumab and rituximab and the respective single formulations were performed based on the results obtained by nanoDSF and DLS measurements (See Fig. V.1). The use of WCX-HPLC impeded the investigation of the protein degradation in 10 mM sodium acetate pH 5.0 with 250 mM NaCl due to loss of column retention by exceeding salt concentrations in the sample and subsequent elution of the proteins in the void peak. Dilution of the samples in mobile phase A would in principle allow the analysis of these samples, but also lead to lower UV detector signals of potential degradation products. Thus, forced degradation studies were performed in 10 mM sodium acetate pH 5.0 using HP-SEC and WCX-HPLC. Based on the previous DLS results (See Fig. V.1A), rituximab started to aggregate at approximately 70 °C while trastuzumab remained monomeric until approximately 76 °C and the binary mixture of both mAbs showed an intermediate aggregation behavior. Thus, single formulations of trastuzumab and rituximab in concentrations of either 0.5 g/L or 1.0 g/L of the respective mAb and the binary mixture with a concentration of 0.5 g/L of each mAb were prepared, incubated at 70 °C for up to 60 min and subsequently analyzed by HP-SEC and WCX-HPLC. With this experimental setup, we

aimed to cause protein aggregation in rituximab and the binary mixture, but not in the single formulations of trastuzumab. Using this approach, it was possible to determine if (a) the binary mixture reflected the unchanged aggregation of rituximab or (b) mixed aggregation products of both mAbs were formed in the binary mixture.

Fig. V.3 shows the results of HP-SEC analysis. No baseline separation was achieved for trastuzumab and rituximab in the binary mixture. However, linearity for both mAbs in the respective single formulations as well as additivity of the monomer peak areas of the single mAbs in the binary mixture was shown (See Figs. V.3B and V.3D). The monomer peak area of the binary mixture that contained 0.5 g/L of each mAb equaled the sum of the single mAb formulations that contained 0.5 g/L of the respective mAb. Interestingly, this additivity of peak areas was not only shown for the native samples, but also for the stressed samples after incubation at 70 °C for up to 60 min (See Figs. V.3E and V.3F). This indicated that the monomer recovery in the binary mixture was the same for both mAbs as in the respective single formulations. While trastuzumab most likely remained monomeric and contributed equally to the total monomeric peak area in the binary mixtures, rituximab degraded in the same way in the binary mixture as in the single formulation. However, the insufficient resolution of size exclusion chromatography impedes the separation and direct quantification of the individually formed aggregates and the presented assumptions are based on the limited significance of a comparison of the single formulations and the binary mixture. Nevertheless, the total protein concentration in the binary mixture was higher (0.5 g/L trastuzumab + 0.5 g/L rituximab), but the soluble aggregate formation in the binary mixture was the same compared to the rituximab single formulation with a protein concentration of 0.5 g/L (See Fig. V.3C). Thus, the presence of trastuzumab in the binary mixture did not increase soluble aggregate formation. It can be assumed that rituximab aggregated in the same manner as in the single formulation and the fraction of soluble aggregates in the binary mixture represented aggregates of pure rituximab. Therefore, it can also be assumed that the initial aggregation observed in the DLS measurements for the binary mixture reflected the aggregation of rituximab alone (See Fig. V.1A). However, additional analytical methods such as the specific detection of one labeled mAb or multidimensional chromatography are required to quantify the individual mAbs in the monomer peak fraction and in the soluble aggregate fraction to confirm this hypothesis.

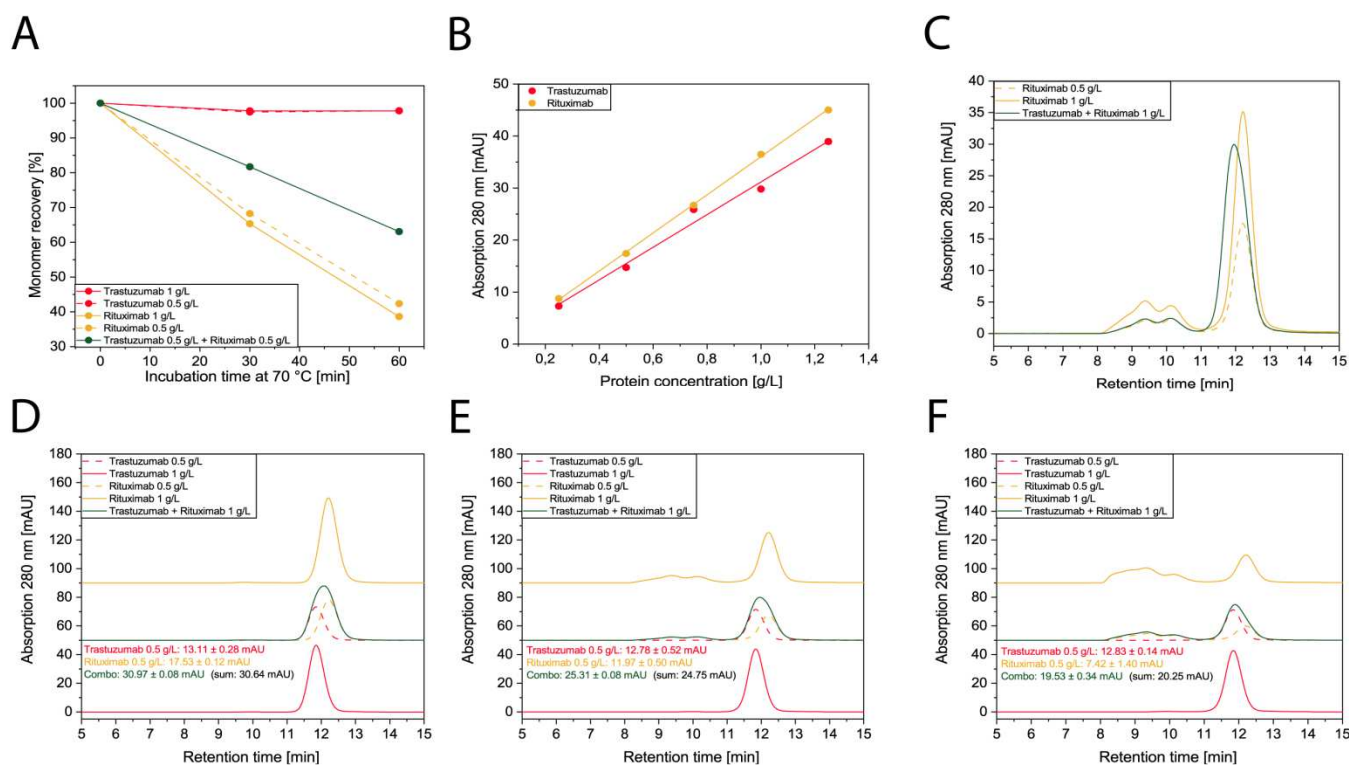


Figure V.3. Results of HP-SEC for the forced degradation of binary mixtures of trastuzumab and rituximab compared to the respective single formulations. Monomer recovery for trastuzumab (red), rituximab (yellow) and the binary mixture of trastuzumab and rituximab (green) (A). Linearity for trastuzumab (red) and rituximab (yellow) (B). Comparison of soluble aggregate formation of rituximab in single formulations (yellow) and in binary mixtures with trastuzumab (green) (C). HP-SEC-chromatograms of native trastuzumab (red), rituximab (yellow) and the binary mixture (green) (D). HP-SEC-chromatograms of trastuzumab (red), rituximab (yellow) and the binary mixture (green) after incubation at 70 °C for 30 min (E) and 60 min (F).

Fig. V.4 shows the results of WCX-HPLC analysis. Using the pH-gradient method, a baseline separation was achieved for trastuzumab and rituximab in the binary mixture (See Fig. V.4D), and linearity for the quantification of both mAbs in the binary mixture was shown (See Fig. V.4C). The protein recovery of trastuzumab in the binary mixture was the same as in the single formulation (See Fig. V.4A). Thus, no destabilization of trastuzumab in the binary mixture was observed. For rituximab, the protein recovery was higher in the binary mixture compared to the single formulation with a concentration of 0.5 g/L after incubation at 70 °C for 30 min and the same after incubation at 70 °C for 60 min (See Fig. V.4B). The presence of trastuzumab appeared to provide a limited stabilization against the chemical degradation of rituximab. The stability of both mAbs was not compromised in the binary mixture and these results further support the assumption that both mAbs followed the same degradation pathway in the binary mixture compared to the respective single formulations as no critical changes in the chromatograms were detected in the binary mixture compared to the single formulations.

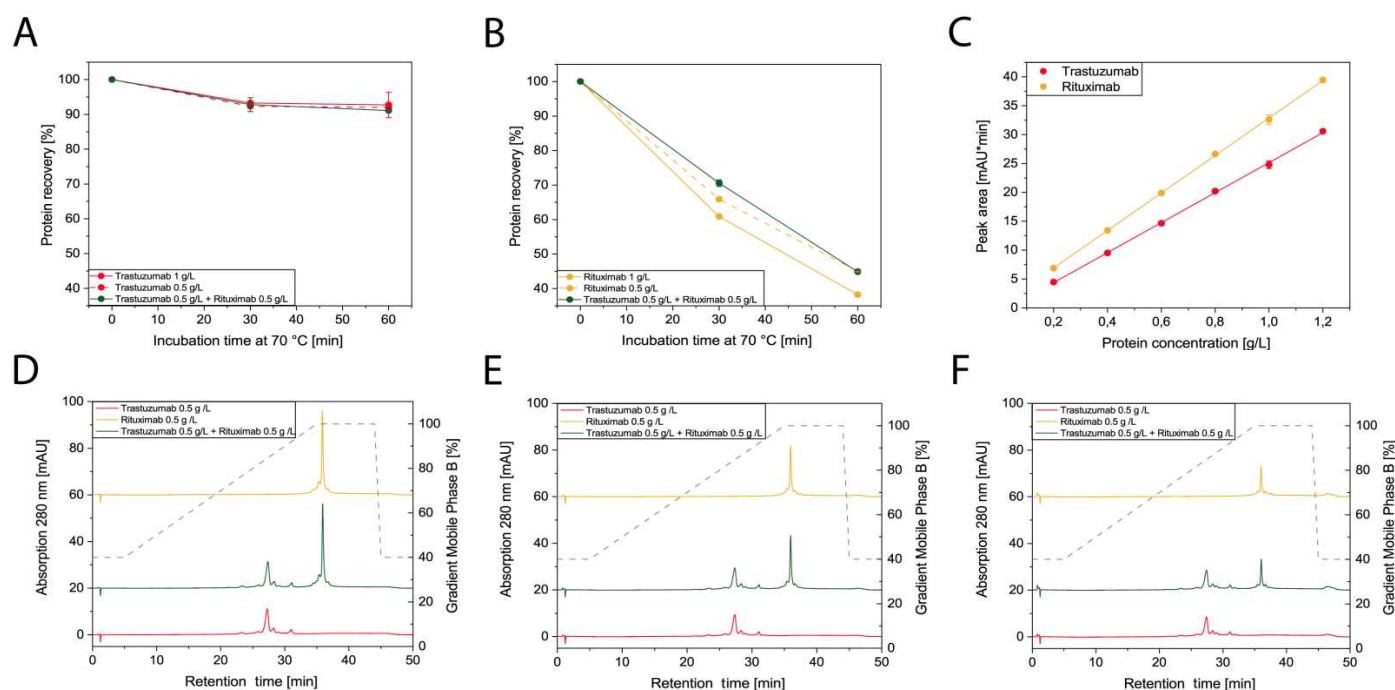


Figure V.4. Results of WCX-HPLC for the forced degradation of binary mixtures of trastuzumab and rituximab compared to the respective single formulations. Protein recovery for trastuzumab in single formulation (red) and the binary mixture (green) (A). Protein recovery for rituximab in single formulation (red) and the binary mixture (green) (B). Linearity for trastuzumab (red) and rituximab (yellow) (C). WCX-chromatograms of native trastuzumab (red), rituximab (yellow) and the binary mixture (green) (D). WCX-chromatograms of tratuzumab (red), rituximab (yellow) and the binary mixture (green) after incubation at 70 °C for 30 min (E) and 60 min (F). The dotted grey lines (D, E and F) illustrate the applied gradient method.

V.3.3 Viscosity measurements

Finally, viscosity measurements were performed to detect additional attractive protein interactions in the binary mixtures of trastuzumab and rituximab. As discussed in Chapter IV, weak protein interactions can impact the behavior of highly concentrated protein formulations. Attractive protein self-interactions can arise in high protein concentrations (e.g. 100 g/L) and cause high viscosities of these protein formulations based on higher-order network formation.³ Further, it was previously shown that binary mixtures of mAbs do not necessarily represent intermediate values of the single mAb formulations, but can exceed the single viscosities by additional arising cross-interactions in the binary mixture.⁴ Thus, we compared the viscosity of the binary mixtures of trastuzumab and rituximab to the respective single protein formulations to detect protein cross-interactions that arise in the binary mixtures in protein concentrations up to 100 g/L in 10 mM sodium acetate pH 5.0 with and without 250 mM NaCl, and in 10 mM sodium phosphate pH 7.4 with and without 250 mM NaCl (See Fig. V.5).

The binary mixtures of trastuzumab and rituximab showed intermediate apparent viscosities compared to the equally concentrated single protein formulations in all formulation conditions (See Fig. V.5). There was no evidence for additionally arising protein interactions in the binary mixtures of trastuzumab and rituximab in total protein concentrations up to 100 g/L.

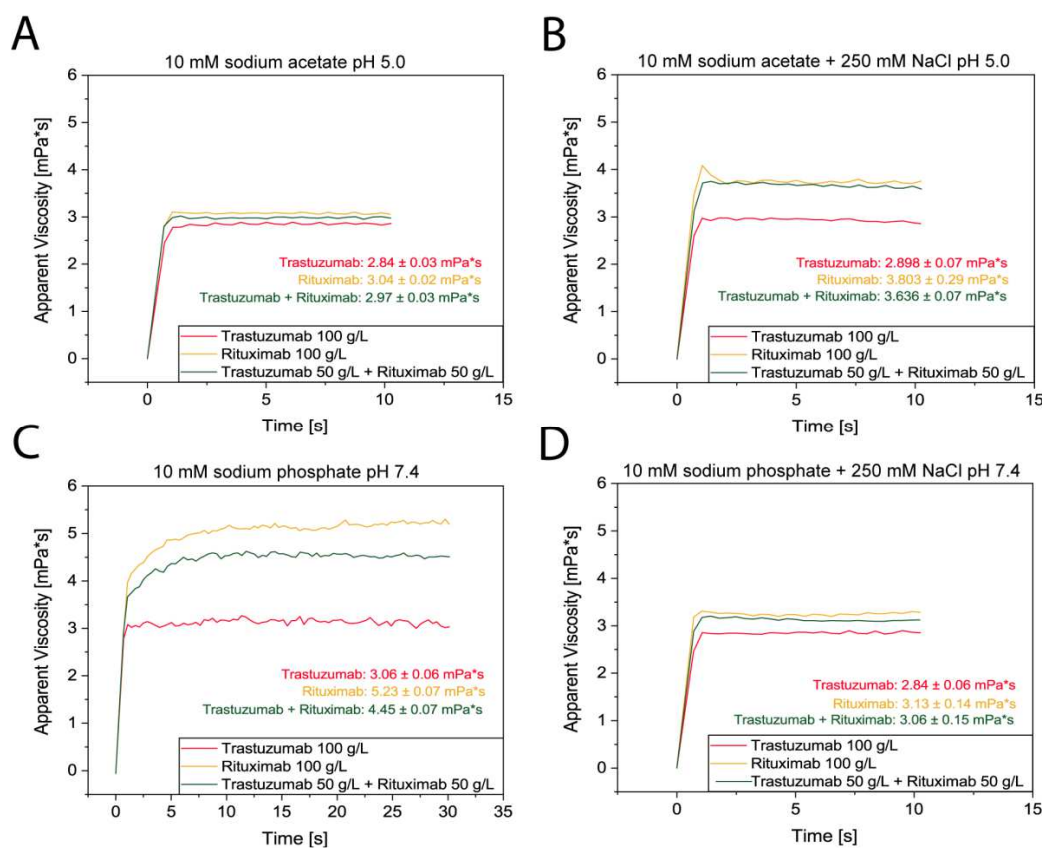


Figure V.5. Apparent viscosity of single formulations of trastuzumab (red), rituximab (yellow) and the binary mixture (green) in 10 mM sodium acetate pH 5.0 (A), 10 mM sodium acetate pH 5.0 with 250 mM NaCl (B), 10 mM sodium phosphate pH 7.4 (C) and 10 mM sodium phosphate pH 7.4 with 250 mM NaCl (D).

V.4 Conclusion

Supplementary experiments were performed on binary mixtures of trastuzumab and rituximab and the respective single formulations to confirm the predicted absence of stability-compromising cross-interactions between the individual proteins that was presented in Chapter IV. Based on the presented results by DLS, nanoDSF backscattering and forced degradation studies at high temperatures, where the loss of the monomeric mAbs was investigated by HP-SEC and WCX-HPLC, it appears that the individual mAbs behave the same in binary mixtures compared to the respective single formulations. No evidence for

stability-compromising cross-interactions, co-aggregation or accelerated degradation of the mAbs was detected in any formulation condition by any of the applied methods.

Therefore, the presented results support the previously reported results of Chapter IV and confirm that co-formulations of well-behaved mAbs can be possible in a straight-forward way.¹ However, the presented dataset is limited to one pair of clinically established, well-characterized and biophysically well behaving mAbs. The presented approach to study the behavior of the single mAbs in a given binary mixture in different formulation conditions and different ratios by a set of orthogonal analytical methods has to be applied to a higher number of mAbs with different biophysical behavior to identify drug properties and formulation parameters that are critical for the development of stable mAb co-formulations.

V.5 References

- (1) Krieg, D. *et al.* Biophysical characterization of binary therapeutic monoclonal antibody mixtures. *Mol. Pharm.* **2020**, *17* (8), 2971–2986. <https://doi.org/10.1021/acs.molpharmaceut.0c00370>.
- (2) Farnan, D. & Moreno, G. T. Multiproduct high-resolution monoclonal antibody charge variant separations by pH gradient ion-exchange chromatography. *Anal. Chem.* **2009**, *81* (21), 8846–8857.
- (3) Tomar, D. S. *et al.* Molecular basis of high viscosity in concentrated antibody solutions: Strategies for high concentration drug product development. *MAbs* **2016**, *8* (2), 216–228. <https://doi.org/10.1080/19420862.2015.1128606>.
- (4) Woldeyes, M. A. *et al.* Viscosities and protein interactions of bispecific antibodies and their monospecific mixtures. *Mol. Pharm.* **2018**, *15* (10), 4745–4755. <https://doi.org/10.1021/acs.molpharmaceut.8b00706>.

Chapter VI Short-time and in-use stability of binary mixtures of DNase and r-tPa

VI.1 Introduction

Pleural infection is a severe clinical condition with high morbidity and mortality.¹ 20 % of patients require surgery and another 20 % of patients die within the first year of diagnosis.² The concurrent intrapleural application of DNase and r-tPa has improved the non-surgical treatment,³ while the application of the single drugs has no significant effect on the clinical outcome.⁴ The mechanisms of this synergistic pharmacological effect remains poorly understood,² and both in-use stability of both drugs during co-administration and storage stability of co-formulations have not been characterized yet. Physicians hesitate to combine DNase and r-tPa in one syringe, and it is clinical practice to use two separate syringes for administration of both drugs with subsequent flushing with saline after application of each drug.⁵ A combined administration of both drugs in one syringe could simplify the complex clinical dosing procedure, reduce work-load for the clinical professionals and improve patient welfare. To evaluate the feasibility a co-administration of DNase and r-tPa, we studied the physicochemical stability and *in vitro* activity of both drugs upon dilution of the single protein formulations and the combined dilution in 0.9 % NaCl.

It has already been reported that the dilution of protein formulations in 0.9 % NaCl can compromise the protein stability in single drug products because of the excessive dilution of stabilizing excipients,^{6,7} which is also relevant for both r-tPa and DNase: First, the dilution of r-tPa in 0.9 % NaCl is clinically established for intravenous infusions, but it is critical to avoid excessive dilution based on the low solubility of the drug and sufficient concentration of the solubilizer arginine.^{8,9} Second, DNase is typically applied as a nebulizer assisted inhalation without further dilution. DNase requires calcium for structural stability and activity,¹⁰ and is thus formulated in 1 mM CaCl₂ and 154 mM NaCl in the marketed formulation (Pulmozyme®). It has been shown that the *in vitro* activity decreased upon removal of calcium after treatment with EDTA over time,^{11,12} but right after the initial treatment, the enzymatic activity still remained 90 % compared to the non-treated sample.¹¹

Besides the problems that arise due to dilution of the single proteins, the quality and safety of the drugs could be compromised upon co-administration by incompatibilities that arise either from the drugs themselves or the excipients of the respective drug product formulations.

Incompatibilities of injectable drugs are a commonly known risk for small molecule drug combinations and can for example cause precipitation based on different mechanisms like

charge-mediated interactions or pH-shifts.¹³ For the combination of DNase and r-tPa, a drug incompatibility may arise based on the serine protease function of r-tPa. Despite r-tPa being known for high substrate specificity towards plasminogen based on a specific single peptide bond (Arg⁵⁶⁰-Val⁵⁶¹),¹⁴ r-tPa cleaves several small chemical entities or synthetic peptides that mimic the Arg-Val peptide bond.¹⁵⁻¹⁷ Further it has been reported that DNase is a substrate for the non-specific serin protease trypsin,¹⁰ and based on its primary sequence, DNase presents four different Arg-Val peptide bonds,¹⁰ that could form a potential substrate of r-tPa. Further, the excipients of the marketed formulations of DNase and r-tPa appear incompatible, because DNase is formulated with calcium in the marketed drug product (Pulmozyme[®]), while all available marketed r-tPa products contain phosphate (See Table VI.1). A concurrent dilution of both drug products in 0.9 % might cause the formation of poorly soluble calcium phosphate (0.02 g/L in water at 20 °C)¹⁸, which could result in decreased DNase activity or particle formation.

Table VI.1. Excipients in marketed r-tPa drug products based on the prescribing informations for professionals.

| Drug | Drug product | Excipients |
|--------------|--|---|
| Alteplase | Actilyse [®] /Activase [®] | L-Arginine Phosphoric Acid Polysorbate 80 Sterile Water for Injection |
| Retepase | Rapilysin [®] | L-Arginine Phosphoric Acid Polysorbate 80 Sterile Water for Injection |
| | Retavase [®] | Dipotassium Hydrogen Phosphate Phosphoric Acid Polysorbate 80 Sucrose Tranexamic Acid Sterile Water for Injection |
| Tenecteplase | Metalyse [®] | L-Arginine Phosphoric Acid Polysorbat 20 Sterile Water for Injection Gentamicin (trace amounts based on the production process) |

Here, we present a short time stability study of DNase and r-tPa upon dilution in 0.9 % NaCl. We compared dilutions of the single formulations and a combined dilution of both protein formulations and applied several established analytical techniques to study the individual protein stability alone and in the binary mixture. We used *in vitro* activity assays for both enzymes to test for altered *in vitro* activity in the combined dilution, Near-UV CD spectroscopy to detect changes in the respective tertiary structures, and RP-HPLC to examine

chemical degradation. Further we applied HP-SEC to monitor soluble protein aggregate formation and Flow Imaging Microscopy to quantify particle formation.

The presented results indicate that the drugs themselves do not compromise their individual stability. However, the respective excipients impede the co-administration of both drugs together in one syringe, because the available marketed r-tPa formulations contain phosphate, which compromises the *in vitro* activity of DNase.

VI.2 Material and Methods

VI.2.1 Materials

Dornase alfa (Pulmozyme[®], DNase) was kindly provided from Genentech (San Francisco, USA), and is formulated in 154 mM NaCl + 1 mM CaCl₂. r-tPa (BM 06.022) was kindly provided from Roche Diagnostics GmbH, Mannheim, Germany), and is formulated in 500 mM arginine + 250 mM phosphoric acid + 0.1 % polysorbate 80 pH 7.2. The liquid stock formulation of BM 06.022 was stored at - 80 °C, freshly thawed and filtered before use (Whatman[®] Anotop[®] 10 syringe filters, 0.02 μm). Ultrapure water was produced with a Sartorius arium[®] pro system. All used chemicals were of analytical grade and purchased from either VWR International (Darmstadt, Germany) or Sigma Aldrich (Steinheim, Germany).

VI.2.2 Preparation of protein formulations

The applied dosing scheme for the concurrent application of DNase and r-tPa states a dilution of 5 mg DNase and 10 mg r-tPa in 50 mL saline solution each.^{5,19} We tested the *in vitro* stability of both drugs upon concurrent application in one syringe and prepared the formulations by dilution of the formulations alone or in combination in 50 mL 0.9 % NaCl. Thus, the concentration of DNase was set to 0.1 g/L, which was confirmed spectrophotometrically using a Nanodrop 2000 (Thermo Fisher Scientific, USA) and the respective extinction coefficient at 280 nm of 1.57 (mg/mL)⁻¹cm⁻¹.²⁰ The concentration of the used recombinant tPa variant BM 06.022 (r-tPa) was set to 0.2 g/L using an extinction coefficient of 1.69 (mg/mL)⁻¹cm⁻¹.²¹ The formulations were analyzed after dilution into 0.9 % NaCl and after storage at 37 °C for 2 h to evaluate the in-use stability of both proteins.

VI.2.3 DNase activity assay

DNase activity was measured using the BioVision fluorometric activity assay kit (BioVision Inc., Milpitas, USA). The enzyme activity is quantified upon cleavage of a ~ 30 bp DNA probe and subsequent formation of a fluorescent DNA product, as the probe contains a fluorescent dye attached to the 5' end and a fluorescent quencher attached to the 3' end.²²

The formation rate of this reaction product can be monitored fluorometrically using an excitation wavelength of 651 nm and an emission wavelength of 681 nm. Briefly, 50 μL of sample solution were pipetted in triplicates into a 96 well NBS flat bottom microplate (Corning Inc., Corning, USA) and mixed with 50 μL of the freshly prepared reaction mix that contained 25 μM DNA probe. Emission at 681 nm was recorded every 30 seconds for 90 minutes. The reaction rate was quantified using a standard curve that was recorded in the same measurement run. The enzymatic activity calculated from the slope of the reaction curve and is expressed in $\mu\text{U/mL}$, where 1 U is defined as the activity that cleaves 1 pmol DNA per min.

VI.2.4 r-tPa activity assay

The amidolytic activity of r-tPa was measured using the synthetic tripeptide Chromogenix S-2288 (Diapharma Group, Inc, West Chester, USA) based on the proposed microplate method.²³ Briefly, the Chromogenix substrate was reconstituted with 8.65 mL water for injection to achieve a S-2288 concentration of 5 mmol/L. Samples were diluted to obtain a r-tPa concentration of 10 $\mu\text{g/mL}$. 100 μL of reaction buffer (0.1 M Tris + 0.1 M NaCl pH 8.4) and 100 μL of sample solution were mixed in triplicates in a 96 well flat bottom microplate (Greiner Bio-One GmbH, Frickenhausen, Germany) and incubated at 37 °C for 5 min. The S-2288 solution was incubated as well and after addition of 100 μL substrate solution, UV absorption at 405 nm was measured every 30 seconds for 270 seconds. Thus, the formation rate of p-Nitroaniline upon hydrolysis of S-2288 is quantified by UV-spectrometry at 405 nm, using a molar extinction coefficient of 9600 L/mol. A tPa standard (Technoclone Herstellung von Diagnostika und Arzneimitteln GmbH, Vienna, Austria) was tested to evaluate the activity of BM 06.022. The enzymatic activity is calculated from the slope of the reaction curve and expressed in $\mu\text{kat/L}$, where 1 $\mu\text{kat/L}$ is defined as the activity that converts 1 mol of substrate per min.²⁴

VI.2.5 Near-UV CD spectroscopy

As already described in Chapter II, Near-UV CD spectra were collected at 25 °C with a Jasco J-810 spectropolarimeter (JASCO Deutschland GmbH, Pfungstadt, Germany). 5 accumulations of each sample were taken at a speed of 20 nm/min and measurements were performed in triplicates. The spectrum of the respective buffer was subtracted for each sample and smoothing of the single spectra was performed using the Savitzky-Golay algorithm with 7 smoothing points.²⁵ Quartz cuvettes with 10 mm wavelength path were used.

VI.2.6 Reversed-Phase High-Performance Liquid Chromatography (RP-HPLC)

A Dionex Ultimate 3000 system (Thermo Fisher, Dreieich, Germany) was used for the reversed-phase high-performance liquid chromatography. 1 µg of DNase and 2 µg of r-tPa were injected on a BioBasic C18, 250 x 2.1, 5 µm column (Thermo Fisher, Dreieich, Germany) after centrifugation at 10 000 x g for 10 min. Detection was performed by UV spectrometry at 280 nm. To achieve a feasible separation of both proteins and chemical altered entities, the given gradient scheme in Fig. VI.4 was applied. Eluent A consisted of 10 % (w/v) acetonitrile and 0.1 % (w/v) trifluoroacetic acid in ultrapure water. Eluent B consisted of 0.1 % (w/v) trifluoroacetic acid in acetonitrile. The flow rate was 0.2 mL/min. The column oven temperature was set to 37 °C.

VI.2.7 High-Performance Size Exclusion Chromatography (HP-SEC)

High-Performance Size Exclusion Chromatography was performed on a Waters 2695 separation module (Waters GmbH, Eschborn, Germany). 5 µg of DNase and 10 µg of r-tPa were injected on a Superdex 200 Increase 10/300 GL column (GE Healthcare Bio-Sciences, Uppsala, Sweden) after centrifugation at 10 000 x g for 10 min and the elution of the protein was detected by UV spectrometry at 280 nm. The mobile phase consisted of 50 mM sodium phosphate pH 6.8, 200 mM arginine hydrochloride and 0.05 % NaN₃. The flow rate was set to 0.5 mL/min. Monomer recovery was calculated by integration of the peak area and relative comparison of this peak area before and after storage. Baseline separation was not achieved for DNase and r-tPa, thus the peak areas were quantified by perpendicular drop integration.

VI.2.8 Flow Imaging Microscopy

As already described in Chapter II, Flow Imaging Microscopy was used to study the formation of insoluble aggregates (subvisible particles) in the single and co-formulations with a FlowCam 8100 (Fluid Imaging Technologies, Inc., Scarborough, ME, USA). A 10x magnification cell was used. 160 µL were injected with a flow rate of 0.15 mL/min. Images were taken with an auto image frame rate of 28 frames/second, a sampling time of 60 seconds and particle identification was performed with distance to the nearest neighbor set to 3 µm, and particle segmentation thresholds set to 13 and 10 for the dark and light pixels respectively. The particle size was measured as the equivalent spherical diameter (ESD). For measurements and evaluation, the VisualSpreadsheet® 4.7.6 software was used.

VI.3 Results & Discussion

VI.3.1 DNase activity assay

The combined dilution of the DNase and r-tPa formulations in 0.9 % NaCl significantly reduced the *in vitro* activity of DNase compared to the dilution of DNase alone (See Fig. VI.1A). The drop of activity was directly observed after dilution and remained the same after storage at 37 °C for 2 h (See Fig. VI.1B). Thus, the explanation for reduced activity by enzymatic cleavage of DNase seemed unlikely. It was more likely that phosphate reduced the concentration of calcium in solution directly after mixing, which explained the immediate loss of activity. Consequently, we prepared a placebo formulation of r-tPa that consisted of 500 mM arginine + 250 mM phosphoric acid pH 7.2 + 0.1 % polysorbate 80 and tested the activity of DNase after combined dilution in 0.9 % NaCl. Further, we prepared sodium phosphate and arginine hydrochloride solutions at pH 7.2 and diluted them together with DNase in 0.9 % NaCl to achieve the same molar concentrations of phosphate and arginine as in the dilutions, where the placebo formulation of r-tPa was used. The combination of DNase with the placebo formulation of r-tPa reduced the DNase activity to the same extent as the protein formulation (See Fig. VI.1C). Sodium phosphate also decreased the DNase activity, while arginine hydrochloride increased the activity. We can conclude that the activity compromising effect is caused by the incompatibility of the used excipients and further proved this by excessive dialysis of r-tPa into 0.9 % NaCl and subsequent dilution together with DNase in 0.9 % NaCl. The dialyzed r-tPa did neither compromise the DNase activity directly after dilution, nor after storage at 37 °C for 2 h (See Figs. VI.1D and VI.1E), while the enzymatic r-tPa activity was preserved after dialysis (See Fig. VI.2D).

Based on these results, the altered activity of DNase impedes the co-administration of DNase and r-tPa. However, there is residual activity of DNase in the mixture. Most likely, this is caused by the strong interaction of DNase to calcium, which has been reported earlier. At least one calcium remains strongly bound to DNase after extensive dialysis or treatment with EDTA.^{10,12} The given phosphate concentration in the combined dilution of the DNase and r-tPa formulations in 0.9 % NaCl is not sufficiently high to remove calcium completely. Still, it remains unclear if the residual activity of DNase is sufficient to achieve the targeted clinical effect.

It is further interesting to note that arginine increased the *in vitro* activity of DNase. The mechanism of this possible interaction remains unclear. However, it has been previously reported that the reaction velocity of the DNase reaction is pH-dependent and reaches a maximum in the pH range 7 - 7.5, based on the methyl green assay.²⁰ Thus, the observed

increase in activity upon addition of arginine hydrochloride is expected to be caused by the measured pH-shift from pH 6.5 in dilutions of DNase in 0.9 % NaCl to pH 7.1 in combined dilutions of DNase and arginine hydrochloride in 0.9 % NaCl. However, this has to be confirmed in further investigations.

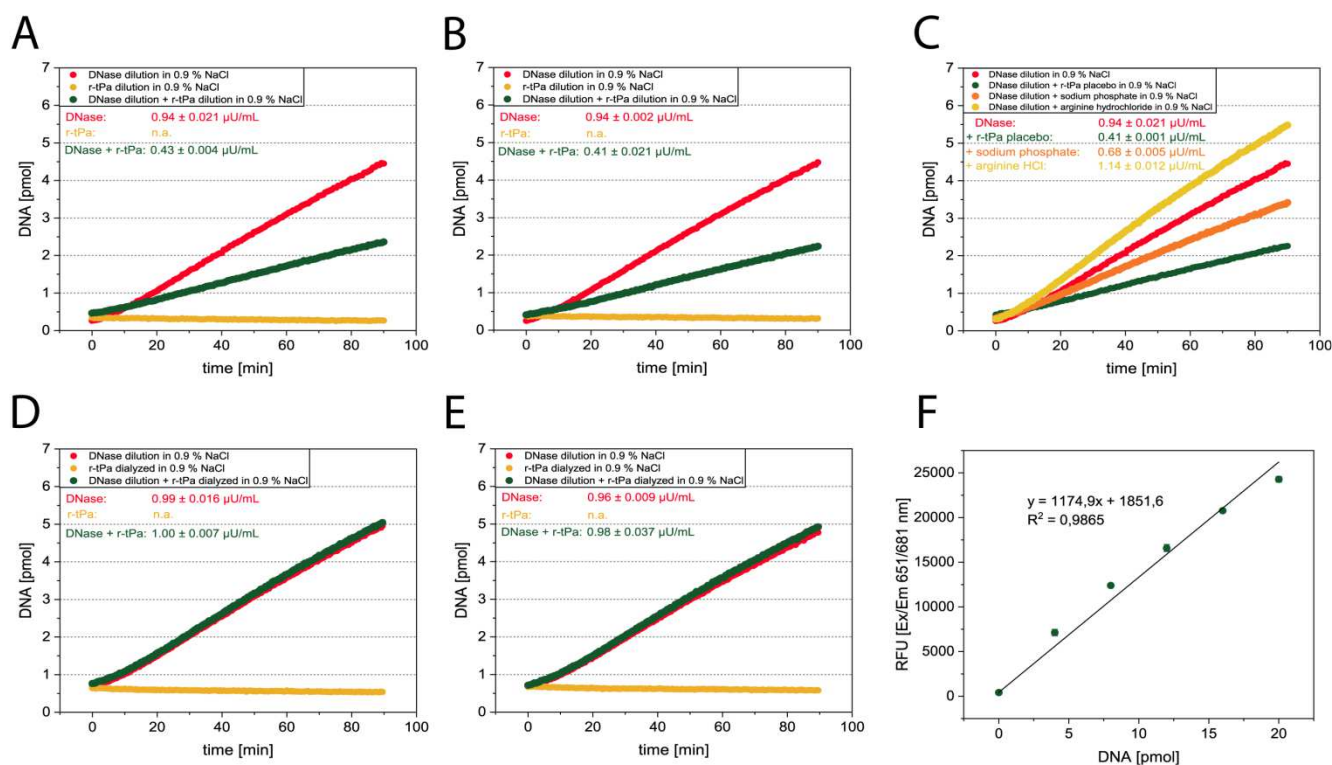


Figure VI.1. *In vitro* DNase activity of Pulmozyme® alone and in combination with r-tPa upon dilution in 0.9 % NaCl after mixing (A) and after storage at 37 °C for 2 h (B). DNase activity of Pulmozyme® alone and in combination with the placebo formulation of r-tPa, 50 mM sodium phosphate pH 7.2 or 70 mM arginine hydrochloride pH 7.2 upon dilution in 0.9% NaCl (C). DNase activity of Pulmozyme® alone and in combination with dialyzed r-tPa upon dilution in 0.9 % NaCl after mixing (D) and after storage at 37 °C for 2 h (E). Standard curve for the correlation of fluorescence signal and formation of free DNA (F).

VI.3.2 r-tPa activity assay

The amidolytic activity of r-tPa was not compromised upon dilution in 0.9 % NaCl together with DNase and was preserved after storage at 37 °C for 2 h (See Figs. VI.2A and VI.2B). Samples were also stored at 70 °C for 2 h to prove that the assay is able to monitor changes in the enzymatic activity (See Fig. VI.2C). Further, r-tPa was excessively dialyzed into 0.9 % NaCl as discussed in section VI.3.1 and tested for preserved amidolytic activity. The dialyzed r-tPa showed an elevated amidolytic activity (See Fig. VI.2D), which confirmed previous results by Hovest *et al.*, where arginine decreased the enzymatic cleavage of the

chromogenic substrate.²⁶ We further proved this by dilution of the r-tPa formulation in the formulation buffer, which exhibited an even higher drop of activity compared to the dilution in 0.9 % NaCl, based on the high concentration of arginine (See Fig. VI.2D). Finally, we also compared the activity of the used r-tPa variant BM 06.022 to a marketed tPa standard, which was also formulated in 500 mM arginine (See Fig. VI.2D). The results confirm that the used r-tPa has the same amidolytic activity as tPa.²¹

The amidolytic activity assay indicates that DNase and r-tPa are compatible drugs. However, it is important to point out that the amidolytic activity and fibrinolytic activity do not necessarily correlate,²³ and orthogonal activity assays like the assessment of clot lysis time should be applied to confirm these results.²⁷

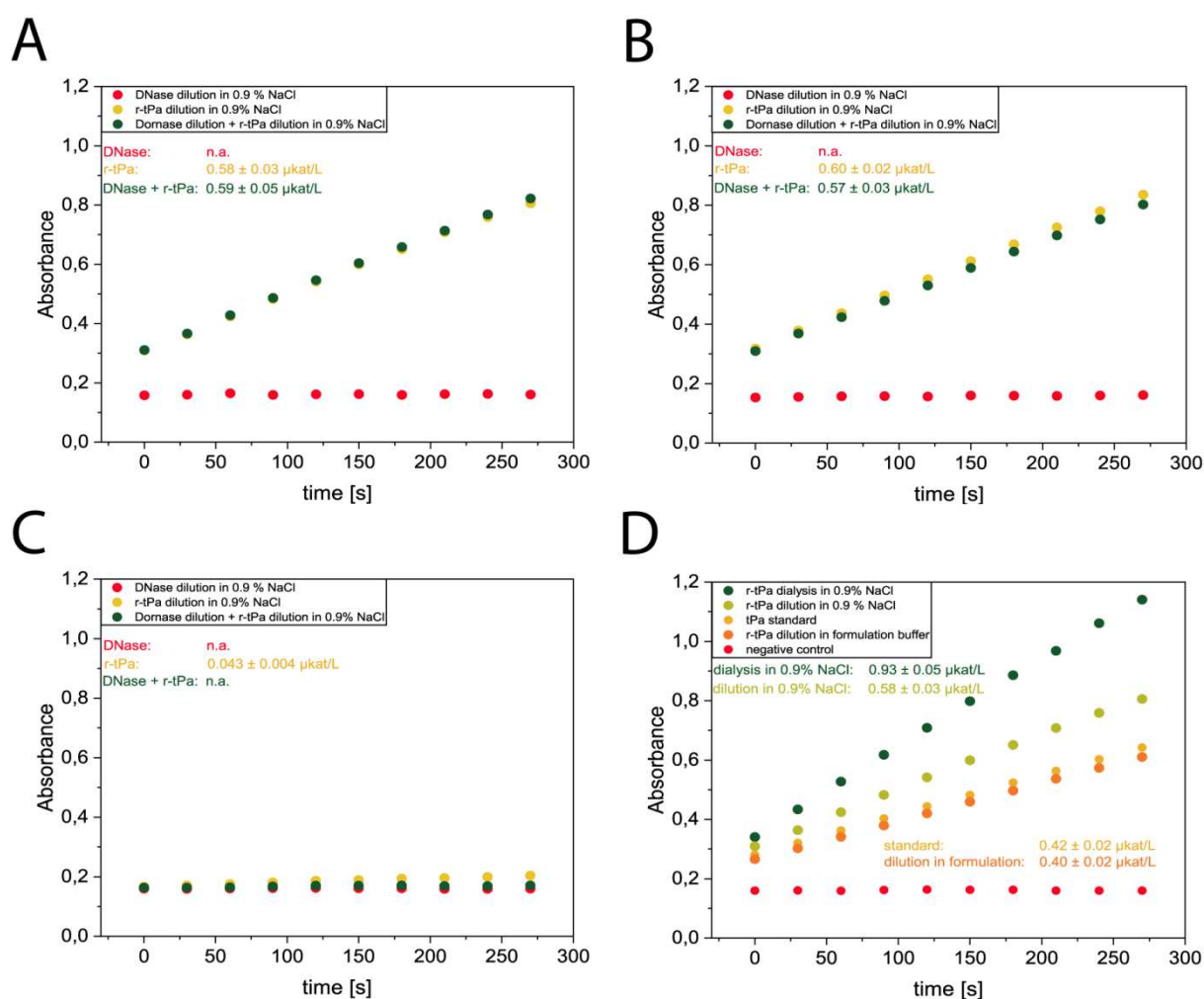


Figure VI.2. Amidolytic activity of BM 06.022 alone and in combination with DNase upon dilution in 0.9 % NaCl after mixing (A), after storage at 37 °C for 2 h (B) and after storage at 70 °C for 2 h (C). r-tPa activity of BM 06.022 after dialysis into 0.9 % NaCl, after dilution in 0.9 % NaCl, after dilution in the formulation buffer, and tPa activity of the tPa standard after dilution in the formulation buffer (D).

VI.3.3 Near-UV CD spectroscopy

Near-UV CD spectroscopy was applied to test for structural stability of both DNase and r-tPa upon dilution in 0.9 % NaCl alone and in combination. The obtained Near-UV CD spectra indicated native tertiary structures of DNase and r-tPa directly after dilution in 0.9 % NaCl and after storage at 37 °C for 2 h (See Figs. VI.3A and VI.3B).^{9,12} We can confirm that the tertiary structure of DNase was not affected by the absence of calcium, which was already reported by Chen *et al.*¹¹ Further, the Near-UV CD spectrum of the drug combination can be calculated by the arithmetic mean of the respective specific ellipticities.²⁸ The arithmetic mean of the single protein signals is equivalent to the measured Near-UV CD spectrum of the combination (See Fig. VI.3A). Thus, it is possible to predict the spectrum of the combination based on the mixing ratios of both proteins. Samples were also stored at 70 °C for 2 h to prove the ability of Near-UV CD spectroscopy to monitor changes in tertiary structure of the proteins alone and in mixtures (See Fig. VI.3D).

No structural changes were detected by Near-UV CD spectroscopy for DNase and r-tPa alone and in combined dilutions in 0.9 % NaCl, thus no enzymatic cleavage DNase by r-tPa was detected.

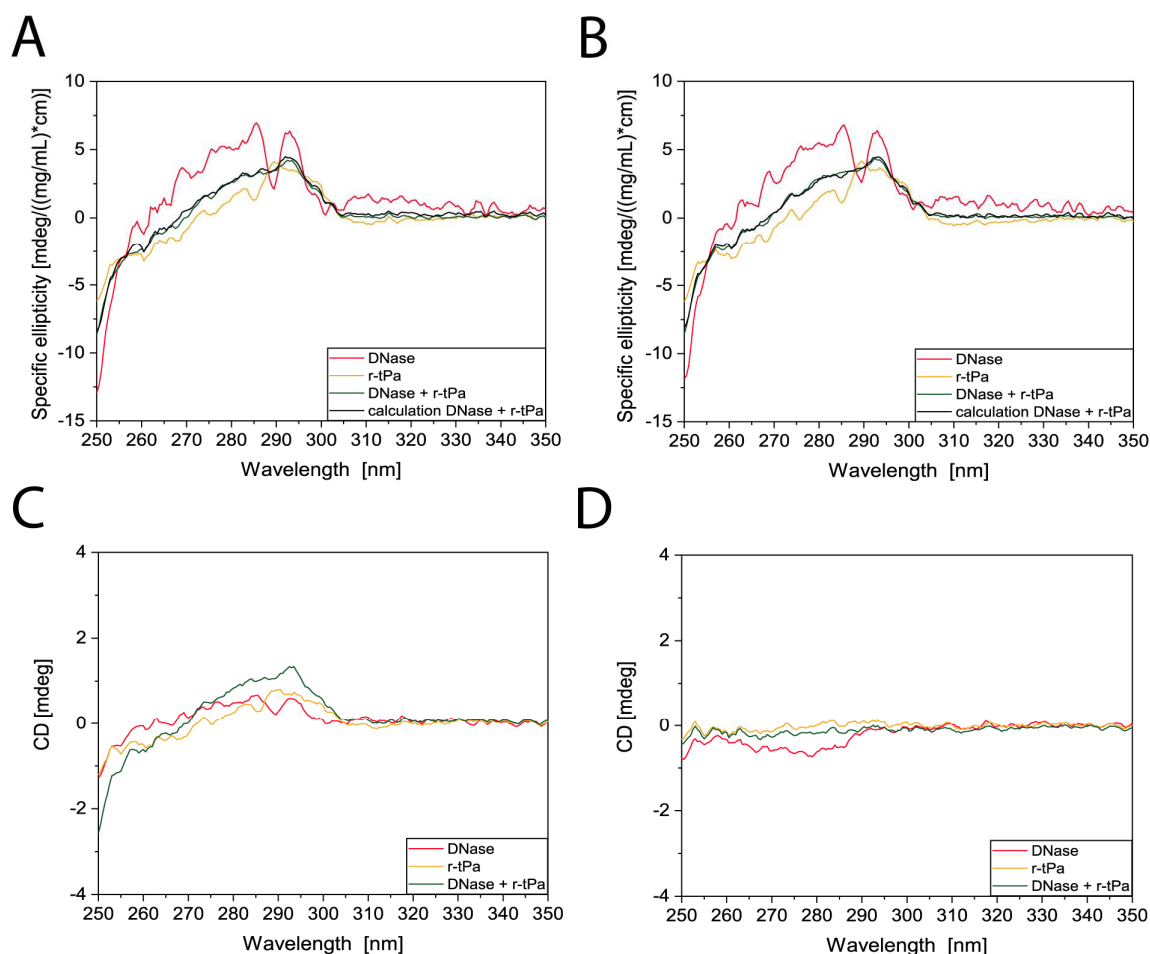


Figure VI.3. Near-UV CD spectra for DNase, r-tPa and the combination upon dilution in 0.9 % NaCl after mixing (A), after storage at 37 °C for 2 h (B), and after storage at 70 °C for 2 h (D). The calculation of the specific ellipticity is not appropriate for the samples that were stored at 70 °C based on insufficient protein concentration. Thus, the raw CD signal is presented for the samples after mixing (C) and after storage at 70°C for 2 h (D).

VI.3.4 Reversed-Phase High-Performance Liquid Chromatography (RP-HPLC)

A RP-HPLC method was developed to evaluate the chemical stability of DNase and r-tPa alone and in combination after dilution in 0.9 % NaCl. An example chromatogram is given in Fig. VI.4B and illustrates the separation of both proteins. Linearity for both proteins alone and in combination was shown (See Figs. VI.4C and VI.4D). The ability to monitor chemical degradation of both proteins was evaluated by analysis of samples that were stressed at 70 °C for 2 h (See Figs. VI.4E and VI.4F). The protein recovery after storage at 37 °C for 2 h was > 95 % for both single dilutions and the combined dilution, and no formation of chemical degradation products was detected by RP-HPLC. Interestingly, protein recovery was inferior

in the combination compared to the single dilutions upon storage at 70 °C for 2 h, which indicates that the combination is less stable compared to the single formulations (See Fig. VI.4F). However, the proteins do not face that severe stress in the context of co-administration.

VI.3.5 High-Performance Size Exclusion Chromatography (HP-SEC)

A HP-SEC method was developed to study protein aggregation of DNase and r-tPa alone and in combination after dilution in 0.9 % NaCl. An example chromatogram is given in Fig. VI.5B and illustrates the separation of both proteins. Linearity for both proteins alone and in combination was shown (See Figs. VI.5C and VI.5D). Linearity was the same in single formulations and combinations, despite the increased axial intercept in the combination based on the applied integration method and insufficient baseline separation. The ability to monitor protein aggregation of both proteins was evaluated by analysis of samples that were stressed at 70 °C for 2 h (See Figs. VI.5E and VI.5F). While DNase formed soluble aggregates that were well detected by HP-SEC, no soluble aggregates were detected for r-tPa, although the monomer peak intensity decreased. Most likely, this was caused by excessive protein aggregation of r-tPa that led to precipitation and formation of subvisible particles that did not appear in HP-SEC. The monomer recovery after storage at 37 °C for 2 h was > 95 % for both separate dilutions and the combined dilution. The monomer recovery was inferior for r-tPa in the combination compared to the single dilution upon storage at 70 °C for 2 h, which confirmed the results of RP-HPLC and also indicated that the combination was less stable compared to the single formulations when extensive stress was applied (See Fig. VI.5F). For DNase, the peak intensity of the soluble aggregates was decreased in the combination, which indicated a shift towards insoluble particle formation.

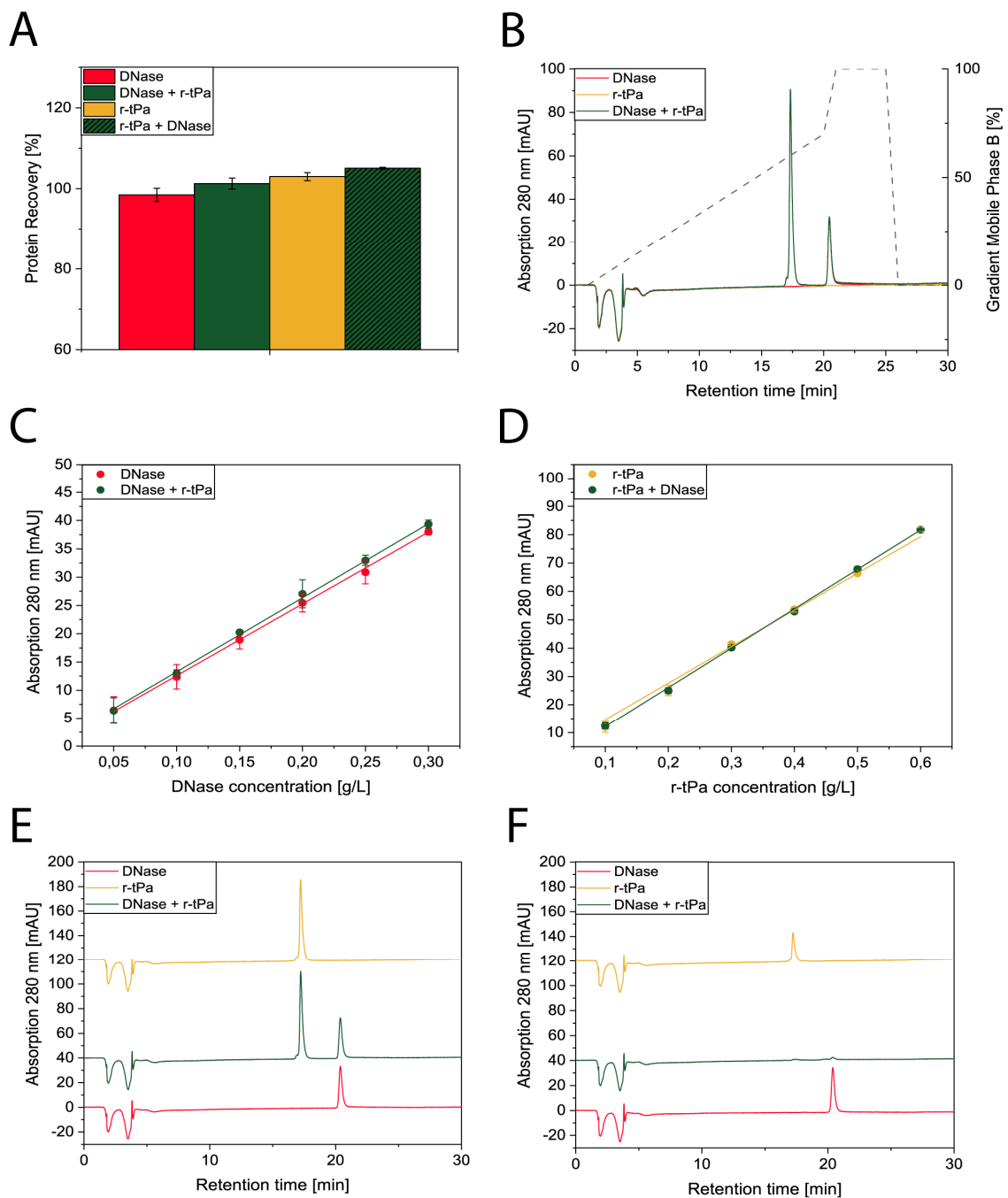


Figure VI.4. Protein recovery in RP-HPLC for DNase, r-tPa and the combination upon dilution in 0.9 % NaCl after storage at 37 °C for 2 h (A). Separation of both proteins alone and in combination by RP-HPLC (B). Linearity in RP-HPLC for DNase (C) and r-tPa (D) alone and in combination. Chromatograms for DNase and r-tPa alone and in combination after mixing (E) and after storage at 70 °C for 2 h (F).

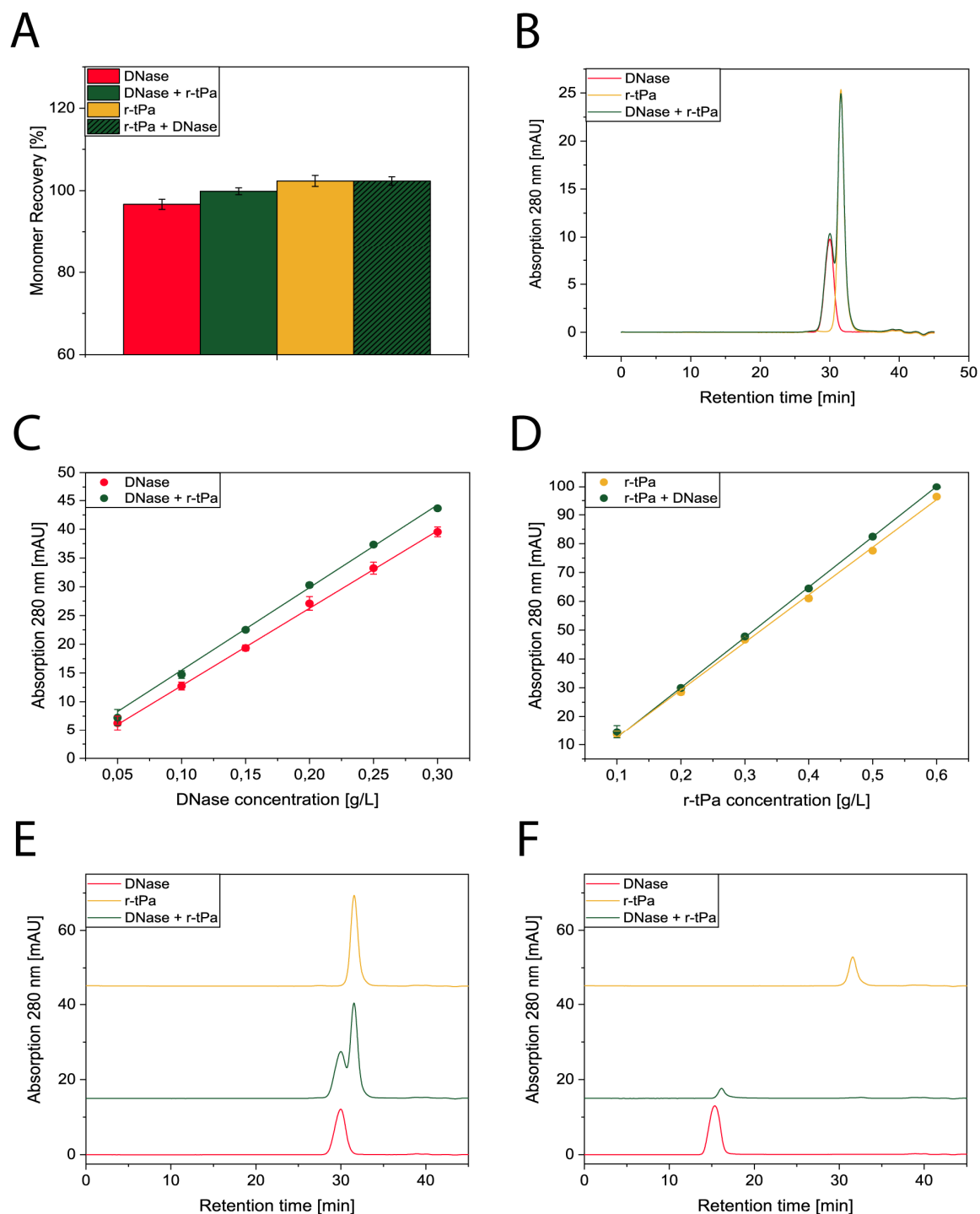


Figure VI.5. Monomer recovery in HP-SEC for DNase, r-tPa and the combination upon dilution in 0.9 % NaCl after storage at 37 °C for 2 h (A). Separation of both proteins alone and in combination by HP-SEC (B). Linearity in HP-SEC for DNase (C) and r-tPa (D) alone and in combination. Chromatograms for DNase and r-tPa alone and in combination after mixing (E) and after storage at 70 °C for 2 h (F).

VI.3.6 Flow Imaging Microscopy

Subvisible particle formation upon dilution of the single formulations of DNase and r-tPa and the combined dilution of both formulations in 0.9 % NaCl was studied by Flow Imaging Microscopy. Immediately after dilution subvisible particles, which also included large protein fibers, were detected in formulations that contained r-tPa (See Fig. VI.6A). This was surprising, because preliminary solubility experiments by HP-SEC and UV-spectrometry did not indicate any loss of soluble protein after dilution of the stock solution in 0.9 % NaCl compared to equal dilutions in the formulation buffer. After storage at 37 °C for 2 h, the particle count did not increase further (See Fig. VI.6B). Most likely, the precipitation of r-tPa was caused by excessive dilution of the solubilizing excipients arginine and polysorbate 80, although the dilution is in accordance with the patient information of Actilyse[®], that limits the dilution of r-tPa to 0.2 g/L to avoid precipitation,²⁹ and it has been previously suggested that r-tPa remains both physically and chemically stable in saline solution at a concentration of 0.2 g/L.³⁰ However, precipitation of r-tPa upon dilution to concentrations lower than 0.5 g/L has also been reported.³¹ While Semba *et al.* presented preserved bioactivity of r-tPa in the clot lysis assay upon dilution to 0.01 g/L in saline solution for up to 24 hours,³² the protein recovery measured by ELISA was reduced to less than 50 % immediately after dilution, which was assigned to adsorption, but may also be consequence of precipitation. Further, the non-glycosylated r-tPa variant BM 06.022 showed a very low water solubility of 0.07 g/L in previous studies,⁹ that could be increased to only 0.66 g/L by addition of 1 M NaCl. Still, the results presented by Tischer *et al.* indicated that 154 mM NaCl (which equals 0.9 % NaCl) increased the solubility of BM 06.022 sufficiently to reach the targeted concentration of 0.2 g/L upon dilution of the stock formulation in 0.9 % NaCl, especially as an arginine concentration of > 30 mM was still achieved in the dilution of the stock formulation.⁹

Although the subvisible particle formation was severe in dilutions of r-tPa, it is interesting to note that the measured r-tPa activity and the peak areas in the applied HPLC-methods remained the same in dilutions of the r-tPa stock formulation in either 0.9 % NaCl or the formulation buffer. Thus, the dilution in 0.9 % NaCl did neither alter the amidolytic activity, nor the recovery in HP-SEC and RP-HPLC, nor the tertiary structure in Near-UV CD spectroscopy. In the context of the treatment of pleural infection and administration into the pleural space, the detected particle formation might not be as critical as for intravenous injections. However, even if this excessive particle formation cannot be tolerated to ensure patient safety, in-line filtration during drug administration or addition of surfactants like polysorbate to the diluting agent offer viable strategies to reduce the particle formation.^{6,7,33}

No significant loss of protein content or soluble r-tPa is indicated by the activity assay, UV-spectrometry or HPLC-methods. Thus, the particle formation can be assigned to a small fraction of protein and the removal of small protein fraction that is responsible for particle formation by inline filtration is not expected to significantly impact efficacy or safety of the therapy.

The combined dilution of DNase and r-tPa in 0.9 % NaCl did not cause additional particle formation compared to the dilution of r-tPa alone (See Fig. VI.6A). Thus, no precipitation of calcium phosphate in the mixture was evident. Placebo formulations of DNase and r-tPa were prepared and diluted accordingly in 0.9 % NaCl to confirm these results. Again, no subvisible particle formation based on calcium phosphate precipitation is detected by Flow Imaging Microscopy after dilution and after storage at 37 °C for 2 h (See Figs. VI.6C and VI.6D).

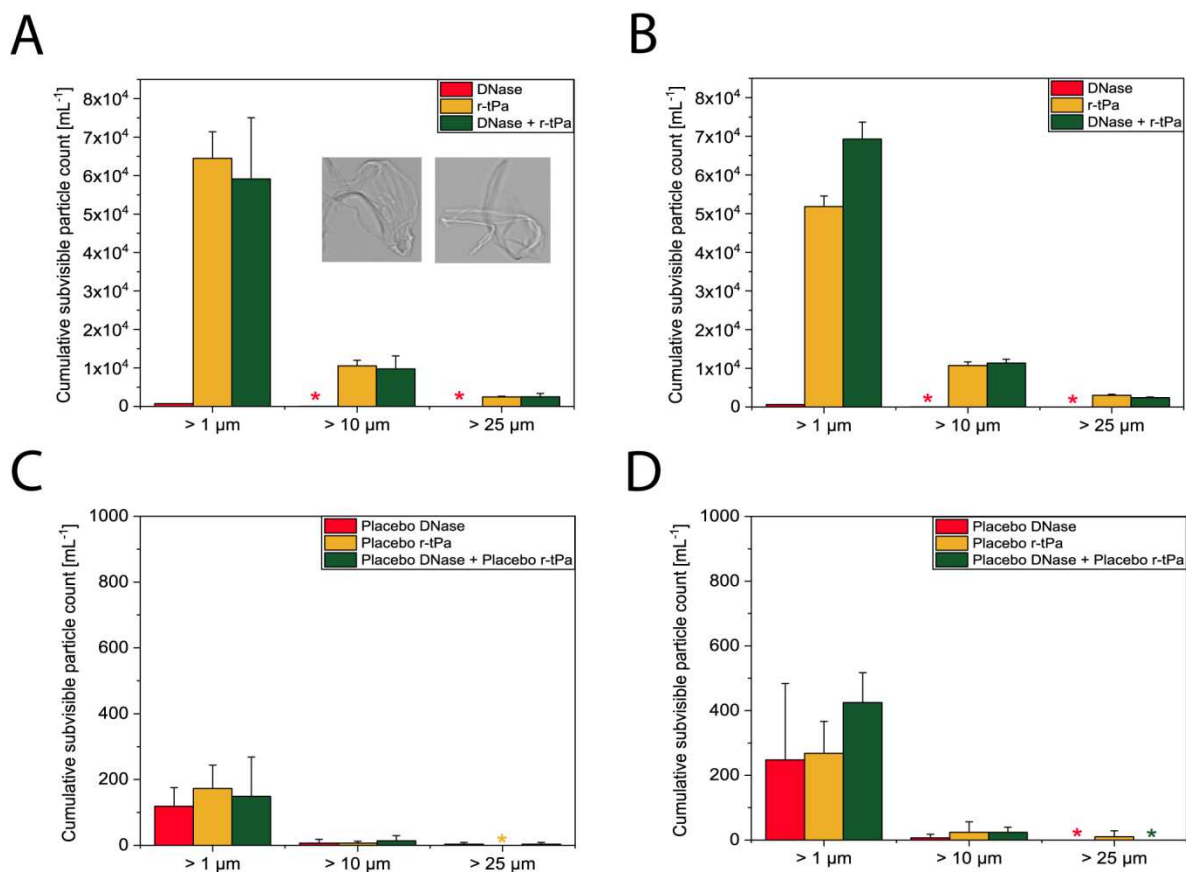


Figure VI.6. Subvisible particle formation in Flow Imaging Microscopy for DNase, r-tPa and the combination upon dilution in 0.9 % NaCl after mixing (A) and after storage at 37 °C for 2 h (B). Subvisible particle formation in placebo formulations upon dilution in 0.9 % NaCl after mixing (A) and after storage at 37 °C for 2 h. Transparent fiber formation in r-tPa dilutions is illustrated by two pictures of representative particles detected in Flow Imaging Microscopy (A).

VI.4 Conclusion

We evaluated the compatibility to DNase and r-tPa for concurrent administration upon combined dilution of the respective protein formulations in 0.9 % NaCl. Although both drugs seem to be compatible for co-administration based on the presented *in vitro* results, the formulations of the respective drug products are incompatible. A significant reduction of the *in vitro* DNase activity upon addition of phosphate impedes a co-administration of the respective drug products. To the best of our knowledge, all available r-tPa drug products on the market contain phosphate (See Table VI.1). Thus, we suggest that concurrent administration of DNase and r-tPa drug products is performed according to Kheir *et al.*,⁵ where different syringes and subsequent saline flushes are used. However, as the drug product incompatibility is only caused by the excipients, a co-formulation of both drugs could still allow concurrent administration. The presented methods and stability data can guide the rational development of a co-formulation of DNase and r-tPa. The most promising approaches for co-formulation are (1) co-lyophilization of both enzymes in arginine hydrochloride or (2) the use of other buffer systems than phosphate. The commonly known TAPS formulation contains tranexamic acid and polysorbate 80 as solubility enhancers (see Table VI.1), and the phosphate buffer could be replaced by tartrate or maleate, as already proposed by Kohnert *et al.*³⁴

However, future work has to elucidate the synergistic pharmacological effect of both drugs on a molecular level to enable a rational development of a co-formulation. Up to date, the lack of understanding of the combined pharmacodynamics, optimal dosing scheme and possible interactions of both drugs with inflammatory cells,² bacteria or body fluids impedes the development of a feasible co-formulation of both drugs. Further, the observed severe particle formation of r-tPa has to be significantly reduced to provide a drug product with high safety and quality. Most likely, the particle formation is a result of poorly selected formulation conditions, which can be solved in future study by appropriate excipient selection and co-formulation development.

VI.5 References

- (1) Hassan, M. *et al.* The microbiology of pleural infection in adults: A systematic review. *Eur. Respir. J.* **2019**, *54* (3). <https://doi.org/10.1183/13993003.00542-2019>.
- (2) Bedawi, E. O.; Hassan, M. & Rahman, N. M. Recent developments in the management of pleural infection: A comprehensive review. *Clin. Respir. J.* **2018**, *12* (8), 2309–2320. <https://doi.org/10.1111/crj.12941>.
- (3) Piccolo, F. *et al.* Intrapleural tissue plasminogen activator and deoxyribonuclease therapy for pleural infection. *J. Thorac. Dis.* **2015**, *7* (6), 999–1008. <https://doi.org/10.3978/j.issn.2072-1439.2015.01.30>.

- (4) Rahman, N. M. *et al.* Intrapleural use of tissue plasminogen activator and DNase in pleural infection. *N. Engl. J. Med.* **2011**, *365* (6), 518–526. <https://doi.org/10.1056/NEJMoa1012740>.
- (5) Kheir, F. *et al.* Concurrent versus sequential intrapleural instillation of tissue plasminogen activator and deoxyribonuclease for pleural infection. *J. Bronchol. Interv. Pulmonol.* **2018**, *25* (2), 125–131. <https://doi.org/10.1097/LBR.0000000000000461>.
- (6) Zheng, S.; Adams, M. & Mantri, R. V. An approach to mitigate particle formation on the dilution of a monoclonal antibody drug product in an iv administration fluid. *J. Pharm. Sci.* **2016**, *105* (3), 1349–1350. <https://doi.org/10.1016/j.xphs.2015.12.013>.
- (7) Kumru, O. S. *et al.* Compatibility, physical stability, and characterization of an IgG4 monoclonal antibody after dilution into different Intravenous administration bags. *J. Pharm. Sci.* **2012**, *101* (10), 3636–3650. <https://doi.org/10.1002/jps.23224>.
- (8) Nguyen, T. H. & Ward, C. Stability, characterization and formulation development of alteplase, a recombinant tissue plasminogen activator. In: Wang Y.J. & Pearlman R. (eds). *Stability and Characterization of Protein and Peptide Drugs: Case Histories*. Springer, Boston, MA, USA, **1993**, 91–134. https://doi.org/10.1007/978-1-4899-1236-7_3.
- (9) Tischer, A. *et al.* L-arginine hydrochloride increases the solubility of folded and unfolded recombinant plasminogen activator rPA. *Protein Sci.* **2010**, *19* (9), 1783–1795. <https://doi.org/10.1002/pro.465>.
- (10) Shire, S. J. Stability, characterization and formulation development of recombinant human deoxyribonuclease I [Pulmozyme, (Dornase Alpha)]. *Pharm. Biotechnol.* **1996**, *9*, 393–426. https://doi.org/10.1007/0-306-47452-2_11.
- (11) Chen, B. *et al.* Influence of calcium ions on the structure and stability of recombinant human deoxyribonuclease I in the aqueous and lyophilized states. *J. Pharm. Sci.* **1999**, *88* (4), 477–482. <https://doi.org/10.1021/js980273g>.
- (12) Cipolla, D. C. *et al.* Formulation and aerosol delivery of recombinant deoxyribonucleic acid derived human deoxyribonuclease I. **1994**, 322–342. <https://doi.org/10.1021/bk-1994-0567.ch019>.
- (13) Newton, D. W. Drug incompatibility chemistry. *Am. J. Heal. Pharm.* **2009**, *66* (4), 348–357. <https://doi.org/10.2146/ajhp080059>.
- (14) Madison, E. L.; Coombs, G. S. & Corey, D. R. Substrate specificity of tissue type plasminogen activator. *J. Biol. Chem.* **1995**, *270* (13), 7558–7562.
- (15) Ding, L. *et al.* Origins of the specificity of tissue-type plasminogen activator. *Proc. Natl. Acad. Sci. U. S. A.* **1995**, *92* (17), 7627–7631. <https://doi.org/10.1073/pnas.92.17.7627>.
- (16) Coombs, G. S. *et al.* Distinct mechanisms contribute to stringent substrate specificity of tissue-type plasminogen activator. *J. Biol. Chem.* **1996**, *271* (8), 4461–4467. <https://doi.org/10.1074/jbc.271.8.4461>.
- (17) Butenas, S.; Kalafatis, M. & Mann, K. G. Analysis of tissue plasminogen activator specificity using peptidyl fluorogenic substrates. *Biochemistry* **1997**, *36* (8), 2123–2131. <https://doi.org/10.1021/bi9617670>.
- (18) Calciumphosphat Trocken EMPROVE® ESSENTIAL Ph Eur, BP, E341 (iii), Material Safety Datasheet, Article No. 102143, Merck KGaA, Darmstadt, Germany, **2015**.
- (19) Majid, A. *et al.* Concurrent intrapleural instillation of tissue plasminogen activator and DNase for pleural infection a single-center experience. *Ann. Am. Thorac. Soc.* **2016**, *13* (9), 1512–1518. <https://doi.org/10.1513/AnnalsATS.201602-127OC>.
- (20) Sinicropi, D. *et al.* Colorimetric determination of DNase I activity with a DNA-methyl green substrate. *Analytical Biochemistry.* **1994**, *222* (8), 351–358. <https://doi.org/10.1006/abio.1994.1502>.

- (21) Kohnert, U. *et al.* Biochemical properties of the kringle 2 and protease domains are maintained in the refolded t-Pa deletion variant BM 06.022. *Protein Eng. Des. Sel.* **1992**, *5* (1), 93–100. <https://doi.org/10.1093/protein/5.1.93>.
- (22) Data sheet of the Biovision DNase I Activity Assay Kit, Biovision Inc., Milpitas, USA. <https://www.biovision.com/dnase-i-activity-assay-kit-fluorometric.html>. Accessed on 29.01.2021.
- (23) S-2288 tPa protocol for the microplate method, ML-00-00230Rev01, Diapharma Group, West Chester, USA.
- (24) Home Page Chromogenic Substrates University - Theoretical Basis for Calculation, Diapharma Group, West Chester, USA. http://chromogenicsubstrates.com/tech/chromogenic_substrates_calculation.htm. Accessed on 29.01.2021.
- (25) Savitzky, A. & Golay, M. J. E. Smoothing and differentiation of data by simplified least squares procedures. *Anal. Chem.* **1964**, *36* (8), 1627–1639. <https://doi.org/10.1021/ac60214a047>.
- (26) Hovest, A. S. & Horne, M. K. The effect of arginine on coagulation and fibrinolysis in vitro. *Fibrinolysis and Proteolysis* **1999**, *13* (1), 31–34. [https://doi.org/10.1016/S0268-9499\(99\)90013-9](https://doi.org/10.1016/S0268-9499(99)90013-9).
- (27) Cellai, A. P. *et al.* Assessment of fibrinolytic activity by measuring the lysis time of a tissue factor-induced clot: A feasibility evaluation. *Clin. Appl. Thromb.* **2010**, *16* (3), 337–344. <https://doi.org/10.1177/1076029608325542>.
- (28) Krieg, D. *et al.* Overcoming challenges in co-formulation of proteins with contradicting stability profiles - EPO plus G-CSF. *Eur. J. Pharm. Sci.* **2020**, *141*, 105073. <https://doi.org/10.1016/j.ejps.2019.105073>.
- (29) Professional Information (Fachinformation) Actilyse,[®] Boehringer Ingelheim GmbH & Co. KG, Ingelheim, Gemany, **2020**.
- (30) Israel, E. N. & Blackmer, A. B. Tissue plasminogen activator for the treatment of parapneumonic effusions in pediatric patients. *Pharmacotherapy* **2014**, *34* (5), 521–532. <https://doi.org/10.1002/phar.1392>.
- (31) Ward, C. & Weck, S. Dilution and storage of recombinant tissue plasminogen activator (Activase) in balanced salt solutions. *Am. J. Ophthalmol.* **1990**, *109* (1), 98–99. [https://doi.org/10.1016/s0002-9394\(14\)75593-x](https://doi.org/10.1016/s0002-9394(14)75593-x).
- (32) Semba, C. P.; Weck, S. & Patapoff, T. Alteplase: Stability and bioactivity after dilution in normal saline solution. *J. Vasc. Interv. Radiol.* **2003**, *14* (1), 99–102. <https://doi.org/10.1097/01.RVI.0000052297.26939.05>.
- (33) Werner, B. & Winter, G. Particle contamination of parenteralia and in-line filtration of proteinaceous drugs. *Int. J. Pharm.* **2015**, *496*. <https://doi.org/10.1016/j.ijpharm.2015.10.082>.
- (34) Kohnert, U. *et al.* Pharmaceutical preparation containing plasminogen activators (US5747030), **1998**.

Chapter VII Summary of the thesis

Protein co-formulations represent valuable additional tools for the treatment of severe diseases, if the clinical efficacy, safety and pharmacokinetic compatibility of the individual drugs can be shown and additional benefits such as improved clinical outcome, higher patient compliance or reduced costs can be provided by the fixed-dose combinations. However, the stabilization of protein co-formulations can be hindered by general analytical challenges, contradicting stability profiles, potential cross-interactions, and the incompatibility of excipients that may be essential to maintain the individual protein stability.

In Chapter I, an extensive overview on the clinical, regulatory, analytical and formulation challenges and opportunities for developing protein co-formulations was provided.

In Chapter II, EPO and G-CSF were co-formulated to identify formulation conditions that provide sufficient protein stability for two model protein drugs with considerably different physicochemical properties. Stability-indicating methods were developed to study the individual protein stability in co-formulations and accelerated stability studies were conducted for a wide range of liquid and lyophilized formulations. We developed a stable lyophilized co-formulation for EPO and G-CSF and showed the stability for both proteins in this co-formulation after storage at 4 °C for up to 12 months. The successful formulation strategy involved a pH-shift upon reconstitution of the lyophilized product that enabled the stabilization of both drugs in one single formulation. Moreover, this case study showed that a first protein drug can be stabilized in the solid state by co-formulation with a second protein drug. Although the optimal formulation conditions for the individual proteins cannot be provided by the co-formulation, intermediate formulation conditions were identified to achieve a sufficient stability for both proteins over the targeted shelf life.

Based on the results of Chapter II, we characterized the protein cross-interactions between EPO and G-CSF in different formulation conditions in more detail in Chapter III. The results indicate that the applied methods such as DLS and nanoDSF can detect changes of the individual protein aggregation in the co-formulations depending on the respective formulation conditions. We identified these methods as valuable tools for early formulation development, because detrimental cross-interactions can be rapidly identified with very low protein consumption. Further, the presented results indicate that protein co-formulations can offer both stabilizing and destabilizing effects on the individual proteins. The stability-compromising interactions were linked to the net surface charge of the individual proteins.

Long-range electrostatic attractive interactions between the oppositely charged proteins were detected at low pH values which favored aggregation, while long-range electrostatic repulsive cross-interactions at neutral pH values reduced aggregation. Thus, the cross-interactions can be limited by a rationale selection of the formulation parameters that avoid opposite surface charges of the proteins. Thus, it was demonstrated how changes in pH and ionic strength can affect the protein aggregation pathway in co-formulations. The results support and explain some of the findings during the accelerated stability studies in Chapter II. In addition, the presented analytical approach can be applied to the pre-clinical characterization of other protein co-formulations.

In Chapter IV, six clinically established mAbs that differ in net charge, charge distribution and CDR composition were selected and a biophysical characterization of all possible binary mixtures of these mAbs was performed. We compared the colloidal and conformational stability of the proteins alone and in combination in a wide range of formulation conditions. In contrast to the electrostatic cross-interactions between EPO and G-CSF that were detected in Chapter III and which promoted protein aggregation in specific formulation conditions, no stability-compromising cross-interactions between different mAbs were detected in a wide range of relevant formulation conditions. The excess scattering of the binary mixture resembled the sum of the excess scattering signals of the individual mAbs with the same concentration, which indicated that the individual mAbs followed the same individual aggregation pattern in the mixture as in the respective single formulations. Unfortunately, we cannot provide a framework or guideline on different mAb properties that could support formulation scientists to identify mAb properties that may be critical for protein co-formulation. The presented results indicate that mAbs which exhibit sufficient drug-like properties to enter the clinics can be co-formulated in a straight-forward manner as no stability-compromising cross-interactions must be expected. However, the presented dataset is limited to six clinically established, well-characterized and biophysically well behaving mAbs. The presented approach has to be applied to a higher number of proteins with different colloidal, conformational and chemical stabilities to identify drug properties and formulation parameters that are critical for the development of stable mAb co-formulations.

In Chapter V, trastuzumab and rituximab were selected as model proteins for a more detailed analysis of the protein stability in mAb co-formulations. Different ratios of both proteins in co-formulations were analyzed by DLS and nanoDSF to differentiate between self- and cross-interactions of the mAbs. The absence of critical protein cross-interactions between the mAbs was further confirmed by viscosity measurements and forced degradation studies by

HP-SEC and WCX-HPLC. The results confirm that the individual mAbs behave similarly in binary mixtures compared to the respective single formulations, and the stability of both mAbs was not negatively affected in the presence of different amounts of the second mAb. The findings in this chapter can aid the analytical development for antibody co-formulations, but the absence of stability-compromising cross-interactions in mAb co-formulations cannot be generalized and additional investigations have to be performed on a larger set of different mAb co-formulations.

In Chapter VI, the in-use stability of DNase and r-tPa was studied after dilution in standard saline solution. The subsequent application of both enzymes is an established clinical procedure for the treatment of pleural infections. However, the compatibility of both enzymes and in-use stability upon concurrent administration to facilitate the clinical treatment remained unclear. Analytical techniques were developed to investigate if the degradation of DNase or r-tPa is affected by the presence of the second protein. The presented results on the colloidal, chemical, and conformational stabilities and activities of both proteins after combined dilution in saline or after dialysis into saline indicated that the proteins are compatible. However, the incompatibility of the excipients impedes a concurrent administration because the lowered concentration of Ca^{2+} ions in the mixture caused a reduced *in vitro* activity of DNase. This chapter demonstrates a case where a co-formulation can be created at the patient bedside, but the necessary in-use protein stability should be demonstrated. The co-formulation of protein drugs can require the substitution of excipients that have been selected for the stabilization of the single proteins and require a re-formulation from scratch to meet the targeted stability requirements for both proteins.

In summary, this thesis provides an analysis on the rational development of protein co-formulations, the arising protein cross-interactions, the potential impact of these interactions on the individual protein stabilities and how the stability-compromising interactions that may arise during formulation development can be limited by a rational selection of feasible formulation conditions. The results confirm recently published studies on the stability of protein co-formulations and indicate that different protein entities in a co-formulation are not susceptible to stability-compromising cross-interactions as long as long-range electrostatic forces are avoided by a rationale selection of pH and ionic strength. It appears that especially mAbs with drug-like properties can be co-formulated in a straight-forward manner. Critical cross-interactions in mAb co-formulations are likely limited to mAbs with unfavorable physicochemical properties, which are not likely to become drugs. Future studies have to

confirm these results for a larger set of different mAb co-formulations to identify general protein properties that are critical for the development of protein co-formulations. Finally, it was also demonstrated that even proteins with significantly different physicochemical properties can be stabilized in a tailor-made co-formulation which overcomes the initially observed incompatibility. Although these results are highly specific for the tested proteins, they present successful pharmaceutical strategies which can support formulation scientists to stabilize challenging protein co-formulations.

Appendix 1: Publications associated with this thesis

Peer-reviewed publications:

Krieg, D.; Svilenov, H.; Gitter, J. H.; Winter, G. Overcoming challenges in co-formulation of proteins with contradicting stability profiles - EPO plus G-CSF. *Eur. J. Pharm. Sci.* 2020, 141, 105073. <https://doi.org/10.1016/j.ejps.2019.105073>

Krieg, D.; Berner, C.; Winter, G.; Svilenov, H. L. Biophysical characterization of binary therapeutic monoclonal antibody mixtures. *Mol. Pharm.* 2020, 17 (8), 2971–2986. <https://doi.org/10.1021/acs.molpharmaceut.0c00370>

Non Peer-reviewed publications:

Krieg, D.; Svilenov, H.; Gitter, J. H.; Winter, G. Analytische Methoden für Coformulierungen therapeutischer Proteine. *PZ Prisma* 2020, 27, 245-251.

Appendix 2: Presentations associated with this thesis

Oral presentations:

***Krieg, D.; Svilenov, H.; Gitter, J. H.; Winter, G.** Overcoming challenges in co-formulation of therapeutic proteins with contradicting stability profiles. PEGS Boston Virtual Conference, 2020, Boston, USA

Poster presentations:

^Δ**Krieg D., Svilenov H.L., Gitter, J.H., Winter G.** Overcoming challenges in co-formulation of proteins with excluding stability profiles – EPO plus G-CSF, Colorado Protein Stability Conference, July 29 – August 01, 2019, Breckenridge, Colorado, USA

Krieg D., Svilenov H.L. & Winter G. Co-lyophilization of EPO & G-CSF: formulation and process design, Freeze-Drying of Pharmaceuticals & Biologicals, September 18 – 21, 2018, Garmisch-Partenkirchen, Germany

Krieg D., Svilenov H.L. & Winter G. Lyophilized co-formulations of EPO & G-CSF 11th PBP World Meeting, March 19 – 22, 2018, Granada, Spain

* Invited talk

^Δ 2nd Prize in the Timasheff Award competition.